Charles University, Faculty of Science
Univerzita Karlova, Přírodovědecká fakulta

PhD study programme: Parasitology
PhD studijní obor: Parazitologie

Mgr. Vojtěch Vacek

Iron-Sulfur cluster assembly in *Monocercomonoides exilis*

Syntéza železo-sirných center v *Monocercomonoides exilis*

Ph.D. Thesis

Thesis supervisor: doc. Mgr. Vladimír Hampl, Ph.D.

Prague 2020

Declaration of the author

I hereby declare that presented thesis was written by me independently. And I also proclaim that the literary sources were cited properly and that neither this work nor its substantial part have been utilised to achieve the same or any other academic degree.

Prohlašuji, že jsem tuto práci zpracoval samostatně. Dále prohlašuji, že jsem řádně uvedl všechny použité zdroje a literaturu a že tato práce ani žádná její část nebyla použita k získání jiného nebo stejného akademického titulu.

……

Mgr. Vojtěch Vacek

Declaration of the supervisor

Data presented in this thesis resulted from team collaboration at the Evolutionary protistology group and from collaboration with our research partners.
I declare that the involvement of Mgr. Vojtěch Vacek in this work was substantial and that he contributed significantly to obtain the results.

……...
Doc. Mgr. Vladimír Hampl, Ph.D.
Thesis supervisor

Acknowledgements

I would like to thank my supervisor Vladimír Hampl for introducing me to protistology and for his kind guidance and support through my studies (as it was certainly hard work for him). I would also thank Beatrice Py and her lab for kindly hosting me during my internship in Marseille.

Special thanks belong to my colleagues form the Laboratory of evolutionary protistology for their support and friendly atmosphere in the lab.
Especially I would like to thank my family, for their support, encouragement, patience and understanding.

Table of Contents

Abstract

In the search for the mitochondrion of oxymonads, DNA of *Monocercomonoides exilis* – an oxymonad isolated from the gut of *Chinchilla*, was isolated and its genome was sequenced. Sequencing resulted in a fairly complete genome which was extensively searched or genes for mitochondrion related proteins, but no reliable candidate for such gene was identified. Even genes for the ISC pathway, which is responsible for Fe-S cluster assembly and considered to be the only essential function of reduced mitochondrion-like organelles (MROs), were absent. Instead, we were able to detect the presence of a SUF pathway which functionally replaced the ISC pathway.

Closer examination of the SUF pathway based on heterologous localisation revealed that this pathway localised in the cytosol. *In silico* analysis showed that SUF genes are highly conserved at the level of secondary and tertiary structure and most catalytic residues and motifs are present in their sequences. The functionality of these proteins was further indirectly confirmed by complementation experiments in *Escherichia coli* where SUF proteins of *M. exilis* were able to restore at least partially Fe-S cluster assembly of strains deficient in the SUF and ISC pathways. We also proved by bacterial adenylate cyclase two-hybrid system that SufB and SufC can form complex.

SUF genes were also found in transcriptomes and genomes of nine other Preaxostyla species (a group of anaerobic protists that belong to Metamonada), while the ISC pathway was consistently absent. Interestingly, in most Preaxostyla, we were able to identify at least partial fusions of SufD, S, and U, which is a unique situation. In a phylogenetic analysis of concatenated genes SufB, C, D, and S, Preaxostyla formed a well-supported clade nested inside of bacteria. The resulting clade is clearly distinct from that of the SUF pathways known from plastids and previously described SufBC systems of *Blastocystis hominis*, *Pygsuia biforma*, and related protists.

These results strongly suggest that the SUF pathway was acquired from bacteria by the last common ancestor of Preaxostyla, where it functionally replaced the mitochondrial ISC pathway. Based on these results it was proposed that *M. exilis* has completely lost its MRO and therefore it is the first described amitochondriate organism. The loss of MRO in the case of *M. exilis* was probably allowed by a combination of an anaerobic and endobiotic lifestyle of this organism, together with the replacement of the mitochondrial ISC pathway by cytosolically - localised SUF pathway which rendered the MRO expendable.

Abstrakt

Při hledání mitochondrií u oxymonád jsme osekvenovali genom *Monocercomonoides exilis* — oxymonády izolované ze střeva činčily. Sekvenování poskytlo relativně kompletní genom, který byl důkladně prohledán na geny proteinů asociovaých s mitochondriální organelou, ale ani po intenzivním hledání se nám nepodařilo odhalit žádné věrohodné mitochondriální geny. Nepodařilo se nalézt ani geny pro ISC dráhu, která je zodpovědná za syntézu Fe-S center a je považována za esenciální funkci organel mitochondriálního původu (MRO). Namísto ní se nám podařilo najít geny pro SUF dráhu, která ji zřejmě funkčně nahradila.

Bližší zkoumání SUF dráhy pomocí heterologních lokalizací naznačilo, že tato dráha je pravděpodobně lokalizována v cytosolu. *In silico* analýza prokázala, že proteiny SUF dráhy jsou konzervovány na úrovni sekundární a terciální struktury a že většina katalyticky významných aminokyselin a motivů je v nich přítomna. Funkčnost těchto proteinů byla nepřímo prokázána pomocí komplementací v *Escherichia coli* s mutovanou SUF a ISC drahou.

SUF dráhu se podařilo nalézt také v transkriptomech a genomech dalších devíti zástupců skupiny Preaxostyla (anaerobních protist patřících do skupiny Metamonada). U většiny preaxostyl se nám podařilo nalézt alespoň částečnou fúzi genů pro SufD, SufS a SufU. Tato fúze je unikátní pro tuto skupinu protist. V konkatenované fylogenetické analýze SUF proteinů utvořila Preaxostyla dobře podpořený klád umístěný mezi bakteriálními sekvencemi. Pozice tohoto kládu zřetelně ukazuje, že SUF systém preaxostyl je fylogeneticky odlišného původu od SUF dráhy známé z plastidů a SUF dráhy popsané u *Blastocystis hominis*, *Pygsuia biforma* a dalších protist.

Tyto výsledky silně poukazují na to, že Preaxotyla získala SUF dráhu od blíže neurčené skupiny bakterií a že k tomu došlo už u posledního společného předka preaxostyl. Na základě těchto výsledků jsme formulovali hypotézu, že minimálně v případě *M. exilis*, byla ztráta mitochondrie umožněna nahrazením mitochondriální ISC dráhy SUF dráhou lokalizovanou v cytosolu. Tato změna umožnila převést tvorbu Fe-S center do cytosolu a mitochondrie tak ztratila svou jedinou esenciální funkci, což umožnilo její postupnou ztrátu.

1 Introduction

Iron-Sulfur (Fe-S) clusters are one of the evolutionary oldest known inorganic cofactors of enzymes. They are virtually ubiquitous across all three domains of life — Bacteria, Archaea and Eukaryotes and are among the most versatile inorganic cofactors, which have many functions in the cell (Beinert 2000). They were discovered in early 1960 by electron paramagnetic resonance on membranes (Beinert and Sands 1960) and closely after that first soluble Fe-S proteins, clostridial ferredoxins, were isolated (Mortenson et al. 1962; Tagawa and Arnon 1962). More than 200 types of proteins were reported to harbour Fe-S clusters (Bandyopadhyay, Chandramouli, et al. 2008).

Fe-S clusters exist in a variety of forms (**Fig. 1**) from single Fe ion coordinated by four cysteines in active site of rubredoxin to a very complex 8Fe-7S cluster (so-called P-cluster) and Mo-7Fe-9S (FeMo-co) cluster, which is present in nitrogenase. However, most frequently they are found in 2Fe-2S (rhombic), 3Fe-4S and 4Fe-4S (cubane) forms (Beinert 1997; Beinert 2000).

Due to their unique structural features, Fe-S clusters can delocalise electrons over Fe and S atoms (Noodleman and Case 1992; Glaser et al. 2000), which makes them ideal candidates for their primary role in the cell, mediators of electron transport. Fe-S clusters can accept electron from one

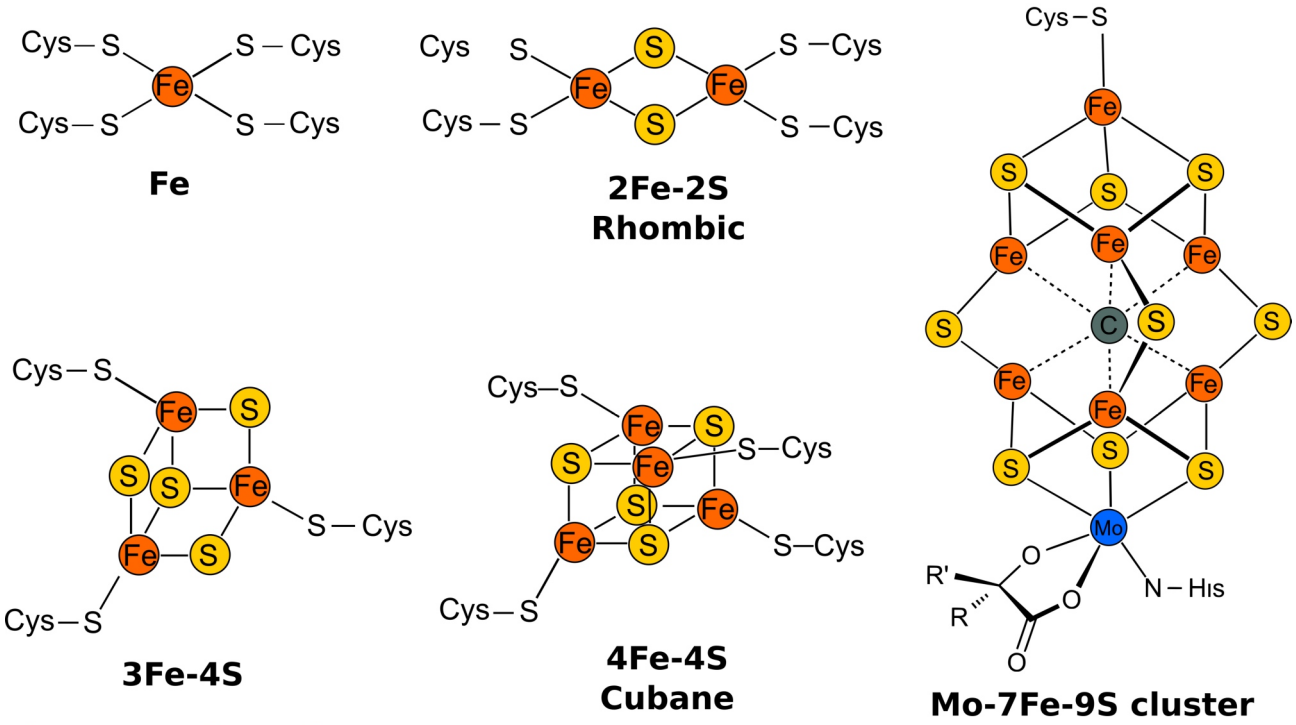

Fig. 1: Types of Fe-S clusters
Scheme showing structure of the most common types of clusters Fe-S cluster together with Mo-7Fe-9S cluster for comparison of complexity. Based on Fontecave et al. (2006).

species and transfer it to another, during electron transfer reactions (Brzóska et al. 2006). In protein, Fe-S clusters are typically coordinated by ligation of iron to Cys, second most frequent ligands are His residues. However, other amino acids like Asp, Arg, Ser, Glu, or Tyr were also described as potential coordinating ligands Fe-S clusters. Furthermore, alternative ligand can tune redox potential of Fe-S cluster which range from -600 mV to +450 mV (Bak and Elliott 2014). Most common 2Fe-2S and 4Fe-4S clusters can transfer 1 electron. However, complex clusters like P-cluster can transfer 2 electrons.

Thanks to their ability to transport electrons, Fe-S clusters are mainly involved in processes which involve electron transport like energy metabolism, where they are present in the mitochondrial respiration (complexes I-III), citric acid cycle (aconitase), and photosynthesis (cytochrome b6f complex, PSI and ferredoxins). Fe-S clusters have also an important structural function as they were shown to change and control protein structure in its vicinity (Plank et al. 1989; Golinelli et al. 1998; Mulholland et al. 1998). Third role is a sensory function, in which Fe-S clusters serve as indicators of oxidative stress and low intracellular levels of iron. Finally, important function often associated with Fe-S clusters is a substrate activation, which is represented by widespread Fe-S proteins called radical-SAM enzymes. These proteins catalyse the reductive cleavage of *S*-adenosylmethionine to generate a 5′-deoxyadenosyl radical which subsequently activates the substrate by abstracting a hydrogen atom.

Thanks to their variable functions, Fe-S cluster proteins are represented in many important cellular processes such as redox reactions, regulation of gene expression, DNA synthesis and repair, RNA modifications, iron homeostasis and ribosome biogenesis. Recently, they were also shown to be involved in antiviral defence (Upadhyay et al. 2014; Upadhyay et al. 2017) and they also regulate chromokinesin KIF4A during mitosis (Ben-Shimon et al. 2018). Some Fe-S proteins, like ferredoxin of *Clostridium* or polyferredoxin of methanogenic archaea, play a role in iron storage (Reeve et al. 1989; Hedderich et al. 1992).

The number of Fe-S clusters proteins in the cell varies greatly and is dependent on the genome size and living conditions of an organism. A non-photosynthetic eukaryotic cells contain approximately 50 to 80 Fe-S proteins, which is a lower number than in prokaryotes (Andreini et al. 2016). For example, *E. coli* contains approximately 150 experimentally confirmed Fe-S cluster proteins (Py and Barras 2010).

The clusters may form spontaneously *in vitro*, when the apoprotein is exposed to inorganic iron and sulfur sources under anaerobic conditions (Malkin and Rabinowitz 1966). However, the concentration of Fe and S necessary for this reaction may reach toxic levels, hence i*n vivo* Fe-S clusters are synthesized by relatively complex pathways. In Bacteria and Archaea four distinct pathways for the synthesis of Fe-S clusters have evolved — the ISC pathway (**I**ron-**S**ulfur **C**luster assembly) (Zheng et al. 1998), the NIF system (**NI**trogen **F**ixation) (Zheng et al. 1993), the SUF pathway (**S**ulfur **U**tilisation **F**actor) (Takahashi and Tokumoto 2002) and the CSD pathway (**C**ysteine **S**ulfinate **D**esulfinase) (Loiseau et al. 2005). In eukaryotic organisms, Fe-S clusters are synthesised usually by the mitochondrial ISC in combination with the cytosolic CIA (**C**ytosolic **I**ron-Sulfur cluster **A**ssembly) and eukaryotes with plastids possess in addition to that a SUF pathway localised in these organelles (Balk and Pilon 2011).

2 Fe-S clusters and origin of life.

The ubiquity of Fe-S clusters in living organisms and the fact that under ideal conditions Fe-S clusters may form spontaneously, are the main arguments for the “Iron-Sulfur world” hypothesis. Günter Wächtershäuser in a series of papers proposed that the ancestral pathway of CO_2 fixation was the reverse citric acid cycle (or reverse Krebs cycle) and the synthesis of pyrite (FeS_2) from FeS (pyrrhotite) and H_2S provided reducing electrons (Wächtershäuser 1988; Wachtershauser 1990; Wächtershäuser 1992). Originally this was proposed to happen in conditions similar to those in deep hydrothermal vents in the ocean, the so-called “Black Smokers”**.** This theory was criticized mainly because it depended on high pressure, temperature and unlikely high starting concentrations of compounds (Orgel 2008; Ross 2008; Rivas et al. 2011).

However, Russell and collaborators (Russell and Hall 1997) elaborated on the “Iron-Sulfur world” theory and managed to solve several of its most criticized aspects. They suggested that the origin of life happened on iron-monosulphide bubbles. These bubbles comprised of a semipermeable membrane consisting of FeS interlaced with nickel. Such membrane would act as a semipermeable catalytic boundary between two environments allowing for compartmentalization of the primitive cells. This would promote synthesis of organic anions by hydrogenation and carboxylation. Furthermore, Martin and Russell suggested that the ancestral way of CO_2 fixation was not the reverse TCA but rather an acetyl-CoA (or Wood-Ljungdahl) pathway (Martin and Russell 2003). As

the source of electrons they proposed H_2 (Martin and Russell 2007), which is produced by reduction of H_2O to H_2 by Fe^{2+}, this reactions results in Fe^{3+}. Released H_2 is used to exergonic reduction of CO_2 to acetate and/or methane while generating ATP via chemiosmosis. The H_2 required to push the equilibrium toward the accumulation of reduced organic compounds probably came from a geochemical process called serpentinization (Martin and Russell 2003; Martin and Russell 2007; Russell et al. 2010), which allowed to move these processes from hot vents to relatively low-temperature alkaline hydrothermal vents.

3 Differences between 2Fe-2S and 4Fe-4S clusters and their origin.

Although they may be found in a wide spectrum of forms, 2Fe-2S and 4Fe-4S clusters are the most abundant and represent 90% of all Fe-S clusters (Andreini et al. 2017). Distribution of these clusters differs as they have slightly different properties and characteristics (Beinert 1997; Johnson et al. 2005; Meyer 2008).

While 4Fe-4S can be produced by a simple reaction system *in vitro* (Herskovitz et al. 1972; Venkateswara and Holm 2004), 2Fe-2S clusters need more complicated reaction settings (Mayerle et al. 1973). 4Fe-4S clusters are more versatile and can be stabilised by only three thiolated ligands, meanwhile 2Fe-2S clusters require more ligands and complicated tertiary structure of proteins to be stabilised. Therefore 4Fe-4S clusters are considered evolutionary older and were probably preferred in anaerobic conditions of a primordial world. Later, circa 3.4 to 2.3 billion years ago (Rosing and Frei 2004; Kirschvink and Kopp 2008; Cardona et al. 2019), cyanobacteria evolved type II photosystems and started oxygen-producing photosynthesis ultimately resulting in the oxidation of the atmosphere between 2.4 and 2.1 billion years ago, an event known as the Great Oxidation Event (GOE) (Holland 2002). The oceans remained, however, anoxic until approximately 0.8 billion years (Canfield 1998; Lyons et al. 2014). Generally, all Fe-S clusters are very vulnerable to oxidation by O_2, ROS (reactive oxygen species) (Imlay 2006; Jang and Imlay 2007; Imlay 2013), NO and other reactive nitrogen species (RNS) (Vanin 2009). 4Fe-4S clusters are more susceptible to ROS, particularly to superoxide, than 2Fe-2S clusters (Touati 2000; Bruska et al. 2013; Bruska et al. 2015), hence 2Fe-2S clusters should have been preferred after the GOE by organisms living in aerobic conditions. Indeed, a large comparative study of more than 400 prokaryotic genomes showed that anaerobic species use mostly 4Fe-4S clusters, while aerobes tend to bear mainly 2Fe-

2S clusters (Andreini et al. 2017). The same study also revealed that anaerobic species tend to use more Fe-S cluster proteins than aerobes. Anaerobes and aerobes also share a common core of protein families containing Fe-S, which mostly harbour 4Fe-4S clusters. This core set is involved in ATP generation, amino acid metabolism, nucleotide and co-enzyme metabolism, and Fe-S biogenesis (Andreini et al. 2017), indicating the ancient origin of these pathways and their 4Fe-4S clusters.

The majority of mitochondrial Fe-S proteins was inherited from aerobic prokaryotes, which is consistent with the α-proteobacterial origin of the mitochondrial ISC system (Gray 2014), whereas some nuclear and cytoplasmic Fe-S proteins were inherited from anaerobic prokaryotes (Andreini et al. 2016). It was shown that 2Fe-2S cluster proteins regardless of their function are approximately two times enriched in the mitochondrion while the 4Fe-4S containing proteins are enriched in the nucleus (Andreini et al. 2016).

4 Functions of Fe-S cluster proteins

Fe-S clusters perform a wide variety of functions, which will be briefly reviewed in this section.

4.1 Regulation of gene expression

Fe-S proteins are involved in regulation of certain genes in both prokaryotes and eukaryotes. In Bacteria, this regulation occurs on transcription level and in eukaryotes on the post-translational level (Mettert and Kiley 2015). Regulatory Fe-S proteins usually also have sensory functions as they regulate adaptive responses. These proteins usually sense oxidative stress, low level of Fe or reduced activity Fe-S clusters biogenesis through integrity of their clusters. In prokaryotes, these proteins are represented by FNR, SoxR, IscR and SufR. In Eukaryotes, they are represented by Fra2 and Irp1 (Iron Response Protein 1).

4.1.1 Fumarate nitrate reductase

FNR (fumarate nitrate reductase) mediates the adaptive response to O_2. In *E. coli*, it regulates expression of more than 200 genes. Phylogenetic studies showed that FNR is widely distributed among many facultative anaerobes (Körner et al. 2003; Dufour et al. 2010). 4Fe-4S cluster of FNR

changes to 2Fe-2S when it comes in contact with O_2 and FNR is then inactivated. In *E. coli*, FNR was also shown to play a role in NO sensing; NO damages 4Fe-4S clusters of FNR resulting in lower DNA binding ability of this protein (Cruz-Ramos et al. 2002; Crack et al. 2013).

4.1.2 SoxR

SoxR is widespread among Proteobacteria and Actinobacteria, and mediates general stress response by activating expression of SoxS, which controls transcription of more than 100 genes including SOD, DNA repair nucleases, and efflux pumps (Chiang and Schellhorn 2012; Kobayashi et al. 2014). SoxR is activated by the oxidation of its 2Fe-2S cluster (Demple et al. 2002) to $[2Fe\text{-}2S]^{2+}$ state, allowing RNAP (RNA polymerase) to activate transcription (Chiang and Schellhorn 2012; Kobayashi et al. 2014).

4.1.3 IscR

IscR uses its 2Fe-2S cluster to sense the activity of cellular Fe-S biogenesis and regulate transcription of genes accordingly. Originally, IscR was described as a repressor of the *iscRSUAhscABfdx* operon. Upon acquisition of a 2Fe-2S cluster, IscR binds to the *iscR* promoter to repress transcription of the isc operon (Schwartz et al. 2001; Giel et al. 2013). IscR is expected to work on homeostatic model → apo-IscR competes with other Fe-S apoproteins for Fe-S clusters. O_2 and ROS-mediated Fe-S clusters damage increases the demand for Fe-S clusters, leading to an increased level of apo-IscR, hence de-repressing the *isc* operon. Some *in vitro* and *in vivo* experiments showed that the 2Fe-2S cluster of IscR is not needed to activate *sufABCDSE* operon in *E. coli*. This differential regulation is given by the ability of IscR to recognize two different DNA motifs, called Type 1 and Type 2 (Schwartz et al. 2001; Nesbit et al. 2009). Type 1 motif strictly requires holo-IscR. However, promoters with type 2 motif bind equally to both apo- and holo- form as the Fe-S cluster is not necessary for binding to type 2 motif (Nesbit et al. 2009). Apo-IscR uses the conserved E43 residue as selective filter to discriminate against type-1 DNA motifs after binding of Fe-S cluster, the negative effect of the E43 residue is diminished and holo-IscR can bind type-1 motif leading to repression of associated genes (Rajagopalan et al. 2013; Santos et al. 2014). Both oxidative stress and iron starvation will cause loss of Fe-S cluster and accumulation of apo-IscR that is then able to interact with type-2 promoter sequences and activate the expression of *suf* operon (Yeo et al. 2006). IscR also regulates expression of some other Fe-S assembly factors, Fe-S

enzymes, superoxide dismutase (SOD), ribonucleotide reductase, RNA metabolism and several other enzymes (Kim 2009; Otsuka et al. 2010). In some bacteria it also plays a role in pathogenicity and virulence (Lim and Choi 2014; Miller et al. 2014).

4.1.4 SufR

SufR is a 4Fe-4S cluster-containing protein which negatively regulates expression of the *suf*BCDS operon in Cyanobacteria (Wang et al. 2004; Shen et al. 2007). It was proved experimentally that SufR binding to DNA depends on the presence and oxidative state of its Fe-S cluster. Only SufR with bound $[4Fe\text{-}4S]^{2+}$ cluster binds to the promoter regions of *suf*B and *suf*R (Shen et al. 2007). A SufR homologue was also found in *Mycobacterium tuberculosis* and other mycobacteria (Willemse et al., 2018).

4.1.5 Fra2

In *Saccharomyces cerevisiae*, iron homeostasis is maintained by the paralogous transcription factors Aft1 (activator of ferrous transport) and Aft2. When iron is limited, Aft1 (and probably also Aft2) accumulates in the nucleus and activates transcription of genes responsible for storage and uptake of iron. When iron is not limited, Aft1 and Aft2 polymerizes, promoting their export from the nucleus and therefore inhibiting regulation mediated by Aft1 and Aft2. Activation of Aft1 and Aft2 depends on mitochondrial Fe-S cluster assembly and interaction of cytosolic monothiol glutaredoxins (Grx3 and Grx4) with Fra2 (BolA2). Grx3 or Grx4 forms dimers with Fra2, and the 2Fe-2S cluster is then transferred to Aft2 (Li et al. 2011; Li and Outten 2012). After acquisition of the 2Fe-2S cluster, Aft 2 dimerizes which lowers its DNA binding ability (Poor et al. 2014).

4.1.6 Irp1

Another example of a eukaryotic Fe-S protein with regulatory function is IRP1 (Iron regulatory protein 1). It has been studied extensively in mammals where it contains 4Fe-4S cluster and works as cytosolic aconitase. Its cluster is modulated by only three cysteinyl residues. This conformation makes one Fe ion labile and thus susceptible to oxidative damage mediated by O_2, ROS or RNS. This leads to the loss of the Fe ion and thus changing the 4Fe-4S cluster to and 3Fe-4S cluster which is then degraded resulting in apo-IRP1. The same effect can be also caused by low level of

intra-cellular iron. Apo-IRP1 binds with high affinity to the IRE (iron responsible elements) stem-loop structure on mRNA (Anderson et al. 2012).

4.2 DNA repair and replication

Iron-Sulfur proteins play an important role in DNA metabolism in both prokaryotes and eukaryotes (Wu and Brosh 2012). Endonuclease III was identified as the first DNA processing enzyme and it contains a 4Fe-4S cluster (Cunningham et al. 1989; Kuo et al. 1992). To the present date, many DNA processing enzymes have been shown to contain 4Fe-4S clusters, such as DNA glycosylases, DNA helicase XPD (Fuss et al. 2015), and all nuclear replicative DNA polymerases family (Netz, Sith et al. 2012). The presence of Fe-S clusters in so many DNA processing proteins was surprising, as the presence of Fe-S clusters near DNA can produce reactive oxygen species (ROS) *via* Fenton reaction. ROS can damage adjacent DNA bases implying a potential harmful effect on the integrity of DNA and genome stability (Imlay 2013).

The biological reasons for the persistent role of Fe-S clusters in DNA metabolism are unknown, but an interesting model proposes that iron participates in a DNA charge transport (DNA CT), which electrochemically probes DNA integrity. The ability of DNA to transfer electrical charges over large distances through its system of π-stacked nucleobases was discovered in the early 1990s (Murphy et al. 1993; Murphy et al. 1994). From that time it has attracted a lot of attention as it is useful for detection of structural changes in DNA resulting from alterations of the regular π-π stacking (Sontz et al. 2012; Zwang et al. 2018). It was shown that many different lesions, modifications and mutations of DNA can be detected electrochemically *via* their disruption of DNA CT (Boon et al. 2000; Boal and Barton 2005; Derosa et al. 2005).

It was shown that proteins which bind and kink the DNA, such as the TATA-binding protein, can turn off DNA CT, but there are also proteins such as histones that can bind to DNA without affecting it (Rajski and Barton 2001; Boon et al. 2002; Núñez et al. 2002).

The oxidative state of a 4Fe-4S cluster affects the DNA-binding capacity of proteins. Proteins carrying $[4Fe\text{-}4S]^{3+}$ clusters bind to DNA 550 times more tightly than those with $[4Fe\text{-}4S]^{2+}$ clusters (Tse et al. 2017). Hence it was proposed that the resting state of a cluster in DNA-associated proteins is that of a $[4Fe\text{-}4S]^{2+}$. Protein with this cluster is freely diffused and upon association of with dsDNA, it can be activated by oxidation of cluster to the $[4Fe\text{-}4S]^{3+}$ form which is tightly binds to DNA. This tightly bound $[4Fe\text{-}4S]^{3+}$ form can be reduced by electron transfer to

weakly binding $[4Fe\text{-}4S]^{2+}$ form, which allows its dissociation from dsDNA. Guanine radicals, which are products of oxidative stress, can also generate $[4Fe\text{-}4S]^{3+}$ species by DNA CT. Proteins with $[4Fe\text{-}4S]^{3+}$ would stay bound to dsDNA allowing precise localization of damaged DNA. Iterations of this scanning can occur throughout the cell and localising any DNA CT damage by interruption of signalling between the cluster protein which leads to both proteins tightly bound to DNA in oxidized $[4Fe\text{-}4S]^{3+}$ form (Barton et al. 2019). This may explain why so many proteins associated with the DNA metabolism contain 4Fe-4S clusters although these are potentially extremely dangerous for the DNA as potential source of damaging radicals.

4.2.1 DNA polymerases

In eukaryotic cells, nuclear genome replication is achieved through the coordinated action of three class B family of DNA polymerases (Pol): Pol α, Pol δ and Pol ε (Johansson and MacNeill 2010). All polymerases contain two conserved cysteine-rich metal-binding motifs (CysA (MBS1) and CysB (MBS2)) in the C-terminal domain of their catalytic subunits that coordinate either zinc or iron, respectively, and are required for the accessory subunit recruitment and replisome stability (Netz, Sith et al. 2012). Pols α, δ, ε, and ζ contain a 4Fe-4S cluster in their CysB motif; this motif is localised in a P-cluster and has a structural role essential for the stability of the holoenzyme. In the absence of the Fe-S cluster, Pol δ becomes unstable. Thus, the replication function is strongly dependent on Fe-S clusters (Netz, Sith et al. 2012). Rev3 (the catalytic subunit of Polζ) has 5’ ➔ 3’ polymerase activity and coordinates a critical [4Fe-4S] cluster in CysB (Baranovskiy et al. 2018).

4.2.2 DNA primase

A structural and redox Fe-S cluster was also identified in the large subunit of human DNA primase (O’Brien et al., 2017). DNA primase is associated with DNA Polα (Weiner et al. 2007). In addition to its catalytic role in DNA replication, it also regulates replication by physically interacting with other proteins involved in replication; mediates response to DNA damage; works as a molecular brake of the replication fork preventing the leading strand from outpacing the lagging strand (Lee et al. 2006); and plays a role in telomere maintenance (Weiner et al. 2007). The presence of a structurally-important 4Fe-4S cluster in DNA primase was revealed by crystallography (Baranovskiy et al. 2018). DNA primase contains three metal binding sites: one Zn^{+2}-binding site

with a proposed structural role and two Mg^{2+} (or Mn^{2+}) binding sites responsible for primase catalytic activity, and a 4Fe-4S binding site. The Fe-S binding site is composed from four conserved cysteines: Cys287, Cys367, Cys384, and Cys424. The cluster is fully-buried and is in a stable $[4Fe\text{-}4S]^{+2}$ state (Liu and Huang 2015). Substitutions of Fe-S coordinating cysteines resulted in the structural disruption of the p58 and p48 domains (Baranovskiy et al., 2018). The Fe-S cluster highly affects the stability of DNA primase, resulting in stalling of initiation of replication. Substitution of one conserved cysteine by alanine leads to the loss of cluster and reduction of both primase and polymerase activity. This indicates that the cluster is essential for the correct activity of the enzyme (Weiner et al. 2007; Baranovskiy et al. 2018).

4.2.3 DNA helicase XPD

DNA helicases have an important role in nucleic acid metabolism as they unwind dsDNA and allow access of single-stranded DNA (ssDNA) to various cellular machineries in DNA replication, repair, recombination, and transcription (Tuteja and Tuteja 2004). The first DNA helicase described to contain an Fe-S cluster was the XPD helicase isolated from the archaea *Sulfolobus acidocaldarius* (Rudolf et al. 2006)**.** Later, Fe-S clusters were identified in numerous helicases in the superfamily 2 (SF2) group. In eukaryotic cells, XPD is a part of the transcription factor II H (TFIIH) machinery that is involved both in nucleotide excision repair (NER) and initiation of transcription (Vashisht et al. 2015). The presence of the cluster is essential for the interaction of XPD with TFIIH. In fact, the XPD protein functions as a sensor of DNA damage as it unwinds DNA through the redox activity of its cluster (Rudolf et al. 2006; Fan et al. 2008). The XPD protein contains a 4Fe-4S cluster in the helicase domain at the N-terminus of the protein (Wolski et al. 2008). The XPD structure shows the 4Fe-4S cluster in the core helicase domain containing a central hole that allows the passage of ssDNA upon unwinding (Fan et al. 2008; Liu et al. 2008; Wolski et al. 2008). Both, structural (Fan et al. 2008; Wolski et al. 2008) and biochemical (Pugh et al. 2008) analyses confirmed the presence of the Fe-S cluster near the dsDNA strand separation site. In the yeast homologue of XPD helicase Rad3 was shown that the Fe-S cluster is essential for excision repair (Rudolf et al. 2006).

The mitochondrial helicase from *Drosophila melanogaster* contains additional 2Fe-2S cluster in its N-terminal domain. This cluster is supposed to be responsible for recruiting and binding DNA in the replication fork (Shutt and Gray 2006).

4.2.4 Dna2 nuclease/helicase

Dna2 nuclease/helicase is a multifunctional enzyme conserved in eukaryotic organisms consisting of a nuclease and a helicase domains fused together. It is involved in several important processes: processing of Okazaki fragments during replication, repairing of DNA double-strand break (DSB), maintenance of telomeres, processing and restarting reversed replication forks, and activation of checkpoint response of the cell cycle (Budd and Campbell 2009; Cejka et al. 2010; Nimonkar et al. 2011). It is also essential for mtDNA stability and base excision repair (BER) (Zheng et al. 2008; Duxin et al. 2009). Dna2 contains a 4Fe-4S cluster coordinated by 4 conserved cysteines ($CX_{248}CX_2CX_5C$ motif). Mutations in the Fe-S coordinating cysteines did not affect DNA binding activity, but affected the way in which the enzyme bound to DNA, as well as terminated its DNA-dependent ATPase and helicase activity (Pokharel and Campbell 2012). Resulting mutants had defective DNA replication and repair *in vivo,* confirming an essential role of the Fe-S cluster in Dna2 activity (Pokharel and Campbell 2012).

4.2.5 Glycosylases

Base Excision Repair (BER) is initiated by DNA glycosylases which cleave bonds between damaged nitrogen bases and the pentose. Endonuclease III (Cunningham et al. 1989; Kuo et al. 1992), adenine glycosylase (MutY) (Fromme et al. 2004) and uracil DNA glycosylases (family IV - VI) (Schormann et al. 2014) are Fe-S cluster containing proteins (Kuo et al., 1992). Some studies suggest that the Fe-S containing domain of glycosylases is involved in binding of DNA and that 4Fe-4S clusters use DNA CT to detect DNA lesions (Boon et al. 2003; Romano et al. 2011). These studies suggest that 4Fe-4S clusters of DNA glycosylases undergo oxidation when they get in contact with DNA. When the cluster undergoes oxidation, it transfers an electron via DNA CT probably to another glycosylase. In damaged DNA, the electron is not transported, cluster remains and the glycosylase stays bound to DNA and initiates repair (Boon et al. 2003).

4.3 Radical SAM enzymes

Radical SAM superfamily (RSS) consists of more than 100 000 enzymes, which utilize S-adenosylmethionine (SAM) as a cofactor to generate radicals (Sofia 2001; Holliday et al. 2018). RSS are present in all three kingdoms of life and generally are supposed to be evolutionary very old (Holliday et al. 2018).

All RSS enzymes contain a 4Fe-4S cluster which is coordinated by three cysteines (conserved CX_3CX_2C motif) (Sofia 2001) leaving one Fe atom labile. A subset of radical SAM enzymes contains one or more additional Fe-S clusters (Sofia 2001). Unligated Fe binds to α-amino and α-carboxylate groups of SAM, which results in cleavage of SAM to methionine and 5'-deoxyadenosyl radical. 5'-deoxyadenosyl radical is an oxidant which extracts hydrogen atoms from target substrates (Lanz and Booker 2012; Lanz and Booker 2015) in broad spectra of reactions, some of which are mentioned below.

Radical SAM proteins are involved in the synthesis of various cofactors like biotin or lipoyl catalysed by biotin synthase (BioB) (Frey and Booker 2001) and lipoyl synthase (LipA) (Lotierzo et al. 2005), respectively**.** Another functions of RSS include the synthesis of vitamin K (menaquinone) (Miller et al. 2000; Cicchillo, Iwig, et al. 2004; Cicchillo, Lee, et al. 2004), activation of pyruvate formate lyase (Buis and Broderick, 2005) and activation of glycyl radical enzymes (Buis and Broderick 2005). Maturation of complex cofactors such as metallocofactor of Fe-Fe hydrogenase is also associated with radical SAM enzymes. Fe-Fe hydrogenase cofactor (or H-cluster) composes of 4Fe-4S cluster connected via cysteine thiolate to a modified 2Fe-2S cluster with unique non-protein ligands (Shisler and Broderick 2014). H-cluster is synthesised by three maturases HydG (Peters 1998), HydE (Pilet et al. 2009) and HydF (Nicolet et al. 2008). HydG and HydE are RSS enzymes and HydF is a GTPase. Another complex cofactor synthesised with help of RSS enzymes is molybdopterin cofactor (MoCo). MoCo cofactor is essential for the activity of xanthine dehydrogenase, aldehyde oxidase and sulfite oxidase. The first step of MoCo synthesis is catalysed by MoaA which is a RSS enzyme (Shepard et al. 2016). Synthesis of complex heterocycles like in the tRNA specific base wybutosin is also catalysed by RSS enzymes (Hänzelmann and Schindelin 2004). Another RSS protein family enzyme RimO is involved in the methylthiolation of 12 ribosomal subunits and MiaB which methylthiolatiates tRNAs (Young and Bandarian 2011)**.** RSS also play roles in formation of some complex metabolic products like antibiotics (Anton et al. 2008) and anti-viral defence in the case of Viperin (RSADII) (Panayiotou et al., 2018; Upadhyay et al., 2017, 2014).

4.4 Ribosome biogenesis

Diphthamide is an unique post-translationally modified histidine-based residue found only in archaeal and eukaryotic translation elongation factor 2 (EF2) (Gomez-Lorenzo et al. 2000; Ortiz et

al. 2006), which is a GTPase required for translation (Gomez-Lorenzo et al. 2000). Dipthamide is synthesized in four steps by a specialised pathway consisting of at least seven proteins. The first step is catalysed by at least four proteins Dph1-Dph4 (Su et al. 2013). Dph1-Dph2 heterodimer in eukaryotes (Dong et al. 2018) or Dph2 homodimer in Archaea (Zhang et al. 2010). Dph1 and Dph2 are non-canonical 4Fe-4S cluster-containing radical SAM proteins. Archaeal Dph2 homodimer needs only one 4Fe-4S cluster for *in vitro* activity (Zhang et al. 2010; Zhu et al. 2011). The eukaryotic Dph1-Dph2 heterodimer needs the 4Fe-4S cluster-binding cysteine residues in both subunits for diphthamide biosynthesis to occur *in vivo* (Dong et al., 2019).

RNase L inhibitor (Rli1 or ABCE1 in human and mouse) is a multifunctional ABC-family protein involved in ribosome biogenesis and maturation (Kispal et al., 2005; Yarunin et al., 2005), translation initiation (Dong et al. 2004; Chen et al. 2006), translation termination (Khoshnevis et al. 2010), and ribosome recycling (Becker et al. 2012). Rli1 contains a unique N-terminal Fe-S cluster domain which binds two $[4Fe\text{-}4S]^{2+}$ clusters (Barthelme et al. 2007). The Fe-S cluster domain is connected to a twin-ATPase body formed by two nucleotide binding domains (NBS) bound by a flexible linker. After ATP binding NBDs change overall conformation of Rli1 in tweezer like motion and Fe-S domain splits ribosome complex to 30S and 70S subunits mechanically (Barthelme et al. 2011; Becker et al. 2012; Nürenberg-Goloub et al. 2018).

4.5 RNA modifications

RNAs are often post-transcriptionally modified, a necessary addition for proper function of RNA. All modifications are performed by specific RNA-modifying enzymes. There are about 100 different types of RNA modifications; some performed by a single enzyme, some require complex pathways (Machnicka et al. 2013). Several of these modifications are performed by the activity of Fe-S proteins.

4.5.1 Methylation of RNAs

Methylation of adenosine to 2-methyladenosine at position 2503 in the 23S rRNA in *E. coli* (Sergiev et al. 2011), and on position 37 in a subset of tRNAs (Jühling et al. 2009) is catalysed by the radical SAM dependent enzyme RlmN (Toh et al. 2008; Yan et al. 2010). Methylation of 23S rRNA regulates elongation of translation by interacting with nascent peptides and is also involved in resistance to several antibiotics that target the large ribosomal subunit. The enzyme *Cfr*

(chloramphenicol resistance) isolated from *Staphylococcus sciuri* is similar to RlmN, but catalyses the formation of 8-methyladenosine at position 2503 of the 23S rRNA and has been shown to play a role in resistance to chloramphenicol in *E. coli* and *Staphylococcus* spp. (Kehrenberg et al. 2005; Long et al. 2006). RlmN and Cfr share the same target residue in rRNA and their methylations occur independently. Therefore 2-, 8-dimethyladenosine can be produced at position 2503 by the serial action of the two enzymes.

4.5.2 Methylthioltransferases (MTTs)

Atoms of sulfur are often incorporated into tRNAs as post-translational modifications (Shigi 2014). A subset of tRNAs that decode U-starting codons and A-starting codons was reported to harbour 2-methylthio-N6-isopentenyladenosine (ms^2i^6A) and 2-methylthio-N6-threonylcarbamoyladenosine (ms^2ct^6A), respectively, at position 37. Methylthiol group of ms^2i^6A37 stabilises codon-anticodon interactions by in the decoding centre of ribosome and facilitating precise decoding of tRNA (Jenner et al. 2010). Methylthiol modification of 2-methylthio-N6-isopentenyladenosine is also involved in reading-frame maintenance and is required for the attenuation activity of some operons involved in amino acid biosynthesis (Urbonavicius et al. 2001). Methylthiotransferases (MTTase) are involved in methylthiolation of RNAs and proteins. MTTases belong to a subset of radical SAM enzymes that contain two 4Fe-4S clusters (Buck and Griffiths 1982). RNA MTTases are classified into two types, MiaB and MtaB, which are responsible for 2-methylthio-N6-isopentenyladenosine and 2-methylthio-N6-threonylcarbamoyladenosine formation, respectively (Hernández et al. 2007). Another MTTase RimO catalyses methylthiolation of an Asp residue in ribosome protein S12 (Arragain et al. 2010).

4.5.3 Wybutosine synthesis

Wybutosine (yW) and derived bases are fluorescent nucleosides found at position 37 of tRNAs of eukaryotes and archaea (Blobstein et al. 1973; Zhou et al. 2004). Wybutosine and hydroxywybutosine are present in Phe tRNA of yeast and mammals, respectively. Wyosine, isowyosine, and methylwyosine are present in archaeal tRNAs. Wybutosine confers conformational rigidity on the anticodon loop of tRNA. On the ribosome, yW stabilizes the codon-anticodon interaction and maintains the reading frame by preventing a frameshift (Waas et al. 2007). Five enzymes, TRM5 and TYW1-4, participate in the biosynthesis of wybutosine in yeast. Only TYW1

contains an Fe-S cluster . TYW1 contains a canonical radical SAM motif with three conserved Cys residues that coordinate an Fe-S cluster (Noma et al. 2006). The functional importance of these Cys residues for yW formation was confirmed by *in vivo* complementation studies in yeast (Suzuki et al. 2007). Structural analysis revealed that archaeal TYW1 harbours two 4Fe-4S clusters (Young and Bandarian 2011; Young and Bandarian 2013).

4.6 Elongator complex

The elongator complex (Elp) is associated with actively transcribing RNA polymerase II (RNAPII). It is comprised of six components Elp1- Elp6, with the main catalytic activity carried out by Elp3, but all six subunits are necessary for the complete function of the complex in eukaryotes (Dauden et al., 2017; Huang, Johansson, & Byström, 2005). Elp3 is a radical SAM protein, contains a 4Fe-4S cluster coordinated by a conserved CxxxxCxxC motif on the N-terminus, and a histone/lysine acetyltransferase domain (KAT) on the C-terminus (Wittschieben et al. 1999; Lin et al. 2019). Elp3 is also present in Archaea, some Bacteria and viruses (Selvadurai et al. 2014).

4.7 Regulation of cytokinesis

The knockdowns of MMS19 and CIA2B (proteins of CIA pathway delivery complex) led to a poor alignment of chromosomes in metaphase and improper localization of key mitotic factors resulting defects of mitosis (Ito et al., 2010; Stehling et al., 2012). As the cause of this phenotype was suggested KIF4A, an Fe-S protein essential for the formation of the midzone and midbody during telophase and cytokinesis (Hu et al. 2011). Recently, spectroscopic analyses detected that chromosome-associated kinesin KIF4A is coordinating a 4Fe-4S cluster in its C-terminal cysteine rich domain (CRD) (Ben-Shimon et al. 2018). This cluster is localised in the conserved cysteine-rich domain CRD at the C-terminus of KIF4A and contains 9 cysteine motifs, similar to the 8 cysteine conserved Fe-S binding motif of eukaryotic polymerases (Netz, Sith et al. 2012).

4.8 Catalytic function

4.8.1 Aconitase

Aconitases are highly conserved bifunctional Fe-S proteins present in eukaryotes, Bacteria and some Archaea and belong to the family of Fe-S-containing dehydratases (Beinert et al. 1996; Gruer et al. 1997). Mitochondrial form of these enzymes catalyses the reversible isomerization of citrate to isocitrate in Krebs cycle (TCA), while the cytosolic form (Irp1) bears a function in regulation of iron metabolism in humans (Anderson et al., 2012; Farooq et al. 2013). For both functions, an Fe-S cluster undergoes degradation from 4Fe-4S to 3Fe-4S (Rose and O'Connell 1967; Flint et al. 1993). Aconitase contains a 4Fe-4S cluster coordinated by three conserved cysteines, this conformation leaves one Fe atom free and susceptible to loss and oxidation. In the isomerisation reaction, labile Fe acts as a Lewis acid and assists a dehydration reaction, removing a water molecule from the substrate.

The other function of aconitase is sensing oxidative stress and the level of intracellular iron, hence regulating iron metabolism. In this case, the Fe-S cluster of aconitase undergoes oxidation and changes from a 4Fe-4S to 3Fe-4S after being exposed to ROS or low iron levels (Haile et al. 1992). This oxidised form of aconitase then binds to IRE (Iron Responsive Element) and regulates expression of associated genes (Hentze and Kühn 1996). IREs are stem-loop structures located in the 5' UTR or 3' UTR of mRNA. The location of the IRE dictates the effect of the binding of IRP-1 on the mRNA transcript, hence if the IRE is located on 5' UTR it will decrease protein production and binding to the 3' UTR will have the opposite effect (Eisenstein 2000; Muckenthaler et al. 2008). It was shown that frataxin interacts with mitochondrial aconitase in a citrate-dependent fashion, decreasing the intensity of oxidant-induced inactivation, and converting the cluster from inactive $[3Fe\text{-}4S]^{+}$ back to the active $[4Fe\text{-}4S]^{2+}$ form (Bulteau et al. 2004).

In bacteria, aconitase is a bifunctional protein and was demonstrated to possess both enzymatic activity in the TCA cycle as well as mRNA-binding activity through recognition of IRE-like sequences thus regulating gene expression (Serio et al. 2006; Michta et al. 2014; Austin et al. 2015).

4.8.2 Pyruvate:ferredoxin oxidoreductase

Pyruvate:ferredoxin oxidoreductase (PFO or also PFOR) catalyses the reversible thiamine pyrophosphate (TPP)-dependent oxidative decarboxylation of pyruvate to form acetyl-CoA and CO_2. Because this reaction is reversible, PFO is also called pyruvate synthase. PFO is one of the core enzymes of anaerobic metabolism and oxidation of pyruvate by this enzyme is required to

connect glycolysis (Embden- Meyerhof) and the Wood-Ljungdahl pathway (Drake et al. 1981; Ljungdahl 1986; Menon and Ragsdale 1996; Furdui and Ragsdale 2000). PFO is also involved in three prokaryotic autotrophic pathways as a CO_2-fixing enzyme by reductive carboxylation of acetyl-CoA: 1) reverse tricarboxylic acid (rTCA) cycle, originally discovered in anaerobic photosynthetic green sulfur bacteria (Evans et al. 1966), 2) the reductive acetyl-CoA (rAcCoA) pathway of acetogenic eubacteria and methanogenic archaea, 3) the archaeal dicarboxylate/hydroxybutyrate (DC/HB) cycle (Fuchs 2011).

All members of the Archaea kingdom appear to contain PFO; it is also widely distributed among Bacteria and anaerobic protists (Horner et al. 1999; Leger et al. 2017). In protists, PFO is considered the hallmark protein of hydrogenosomes, but may also be localised in cytosol or may have a dual localisation (Meza-Cervantez et al. 2011). PFO has been found in the following groups of protists: Metamonada, Fornicata, Jakobida, Heterolobosea, Breviatea, Stramenopila, Rhizaria, Amoebozoa and Alveolata (Horner et al. 1999; Leger et al. 2017).

Phylogenetic analysis suggests that all known eukaryotic PFOs are monophyletic (Leger et al. 2016). However, the identity of the relative bacterial group remains unclear. There are only two crystal structures of PFO up to date: one from *Desulfovibrio africanus* (Charon et al. 1999; Chabrière et al. 2001) and another one from *Sulfolobus tokodaii* (Yan et al. 2016). Another related crystal structure is that of oxalate oxidoreductase (member of OFOR superfamily) from *Moorella thermoacetica*, which shares a very similar structure to PFO (Gibson et al., 2015, 2016). PFOs have seven structural domains, with domains I and VI forming the TPP binding site which is close to domain VI which binds one 4Fe-4S cluster. Domain V contains two additional 4Fe-4S clusters which transfer electrons to a ferredoxin, the terminal electron acceptor for PFO.

4.8.3 Hydrogenases

Hydrogenases are enzymes which catalyses conversion of protons and electrons to H_2. They are widespread in prokaryotes and protists and represent a diverse group of metalloenzymes. By presence of specific type of metallocluster they can be divided into three groups: 1) nickel-iron containing [NiFe] hydrogenases, 2) diiron containing [FeFe] hydrogenases and 3) Fe only containing [Fe] hydrogenases (Vignais et al. 2001; Vignais and Billoud 2007; Greening et al. 2016). [Fe] hydrogenases do not have an Fe-S cluster hence they will not be discussed here.

The [NiFe] hydrogenases are the most studied group of hydrogenases, mostly used in binding and oxidation of H_2. Phylogenetic studies divide [NiFe] hydrogenase into four groups (which can be further divided into 22 functional sub-groups) (Greening et al. 2016) based on their different functions: (1) membrane-bound H_2-uptake [NiFe]-hydrogenases; (2) cytosolic H_2-uptake [NiFe]-hydrogenases; (3) cytosolic bidirectional [NiFe]-hydrogenases; and (4) membrane-bound H_2 evolving hydrogenases. [NiFe] hydrogenases usually contain three auxiliary Fe-S clusters and dinuclear Ni-Fe cluster responsible for H_2 activation (Vignais and Billoud 2007). The standard [NiFe] site consists of an Fe centre that coordinates one carbon monoxide (CO) and two cyanide (CN) ligands and a Ni centre bound by two terminal Cys ligands (Fontecilla-Camps et al. 2007).

[FeFe] hydrogenases can be based on their function and phylogeny divided into three main groups: (A) — fermentative and bifurcating hydrogenases; (B) — ancestral group of unknown function; group (C) —putative sensory hydrogenases. The group A can be further subdivided in to four groups based on their function (Greening et al. 2016). The group A1 of [FeFe]-hydrogenases mediates ferredoxin-dependent H_2 production. Hydrogenases of this group are usually found in anaerobic prokaryotes and protists, where they are often localised in hydrogenosomes or chloroplasts. The number of auxiliary FeS clusters associated with the electron transport chain in [FeFe] hydrogenase can differ between organisms (Moser et al. 1995; Peters 1998; Nicolet et al. 1999; Page et al. 1999; Mulder et al. 2010; Greening et al. 2016). The different Fe-S clusters present in [FeFe] hydrogenases reflect the cellular environments and physiological electron donors/acceptors that interface with these proteins. The key feature common to all [FeFe] hydrogenases is the highly conserved active-site domain, which houses a unique H-cluster. The H-cluster consists of a canonical cubane 4Fe-4S cluster, covalently bound to a unique diiron complex [2Fe]. The atypical diiron unit consists of proximal and distal Fe (Fep & Fed) metal centres that are each coordinated by a CO and CN ligand (Fontecilla-Camps et al. 2007; Lubitz et al. 2007).

4.8.4 Nitrogenase

Nitrogenase is a multifunctional enzyme, which is best known for the catalysis of biological fixation of atmospheric nitrogen into ammonia, an essential process for the global nitrogen cycle. Phylogenomic studies suggest that nitrogenase evolved in anaerobic methanogens and spread to various other organisms (Boyd et al. 2011; Dos Santos et al. 2012). It has been identified in a diversity of microorganisms, including obligate aerobes and oxygenic phototrophs, however, it has never been reported in eukaryotes.

There are three different nitrogenases — molybdenum dependent (Nif), vanadium dependent (Vnf), and Fe-only nitrogenase (Anf). Mo-nitrogenase is the most abundant and has the highest activity; the other two nitrogenases are also called alternative nitrogenases and due to their lower activity (Fontecilla-Camps et al. 2007; Lubitz et al. 2007) are considered to be “backup enzymes” which are used in cases when Mo-nitrogenase is not available.

Mo-nitrogenase works as a complex of two proteins —nitrogenase, encoded by the *nifDK* and the nitrogenase reductase encoded by *nifH* gene (Eady and Robson 1984). NifDK is a heterotetrameric ($\alpha_2\beta_2$) protein formed by two αβ dimers. Crystal structure of the nitrogenase complex revealed that NifDK contains two Fe-S clusters, a P-cluster, which is a formation of 8Fe-7S cluster that transports electrons to the FeMo-cofactor, and a Mo-7Fe-9S-homocitrate cluster that provides the substrate reduction site and which is buried under the surface of NifDK complex (Bulen and LeComte 1966). NifH contains a 4Fe-4S cluster and an ATP hydrolysis site. NifH acts as a tail-to-tail homodimer which is bridged by one 4Fe-4S cluster (Kim and Rees 1992; Schindelin et al. 1997). NifH is essential for the function of nitrogenase and was shown to be involved in the formation of the P-cluster, the insertion of FeMo-cofactor and the transfer of electrons for nitrogenase catalysis. Furthermore, it has been shown to act on its own as carbon monoxide dehydrogenase (Georgiadis et al. 1992).

The V-nitrogenase similarly to Mo-nitrogenase consists of two component proteins: a homodimeric iron protein (VnfH) which contains bridging 4Fe-4S cluster and an ATP-binding site per subunit (Rohde et al. 2018), and an octameric vanadium-iron protein (VnfDGK) that contains a P^V-cluster at each α/β-subunit interface and a V-cluster V-7Fe-8S-C-homocitrate within each α-subunit (Rohde et al. 2018).

Fe-only nitrogenase is the least studied nitrogenase. There is no reported crystal structure of of this protein, although it is anticipated that the protein would have structure similar to Mo- and V-dependent nitrogenases as they are highly conserved.

One of the Fe-S cluster biosynthesis pathways, the NIF pathway, is usually dedicated to maturation of nitrogenase and FeMo-cofactor (Zheng and Dean 1994; D.C.C. Johnson et al. 2005; Zhao et al. 2007) with notable exception for NIF pathway of *Entamoeba histolytica* and *Mastigamoeba balamuthi*.

5 Basic mechanism of Fe-S cluster synthesis

Regardless of the simplicity of the synthesis of Fe-S clusters and the possibility of their spontaneous formation on apoproteins in *vitro* in the presence of iron-salts and sulfide under anaerobic conditions (Malkin and Rabinowitz 1966; Herskovitz et al. 1972; Hagen et al. 1981), *in vivo* this possibility is reduced due to the toxicity of Fe (Touati 2000) and S (Munday 1989). Therefore, in living organisms, several dedicated pathways have evolved to perform this task. The main pathways are NIF (**NI**trogen **F**ixation) (Dean et al. 1993; Zheng and Dean 1994), ISC (**I**ron-**S**ulfur **C**luster assembly) (Zheng et al. 1998), SUF (**S**ulfur **U**tilisation **F**actor) (Takahashi and Tokumoto 2002) and CSD (**C**ysteine **S**ulfinate **D**esulfinase) (Loiseau et al. 2005). However physiological importance of CSD pathway is yet to be elucidated.

Although the pathways differ in composition, distribution and physiological functions, they share a similar three-module organisation: 1) sulfur is mobilised from cysteine by the activity of a cysteine desulfurase, 2) the Fe-S cluster is formed *de novo* on a scaffold protein, 3) the newly formed Fe-S cluster is transferred to the target apoprotein **(Fig. 2).**

5.1 Source of sulfur

L-cysteine is the most common source of sulfur for the Fe-S cluster assembly. Sulfur is released by the catalytic activity of a pyridoxal 5′-phosphate (PLP) depending enzymes called cysteine desulfurases. Cysteine desulfurases belongs to the group of class V fold-type I amino-transferases (Grishin et al. 1995) and can be divided into two specific groups. Group I in which NifS and IscS belong, and group II where SufS and CsdA may be found (Mihara et al. 1997). These enzymes act as homodimers and decompose L-cysteine to L-alanine to release sulfur in a form of persulfide, which is later used by biosynthetic pathways (Mueller 2006).

The catalytic mechanism of cysteine desulfurases can be divided into two steps. The first step is a desulfurase reaction in which the sulfur atom from L-cysteine is transferred into the side chain of the catalytic cysteine residue forming a persulfide-bound intermediate. The second step is a transpersulfurase reaction, in which the persulfide intermediate is transferred from the cysteine desulfurase to acceptor proteins.

PLP plays an important role as it starts the reaction by forming an external cysteine-aldimine then a subtracted proton generates a cysteine-ketimine PLP intermediate. The cysteine residue of PLP

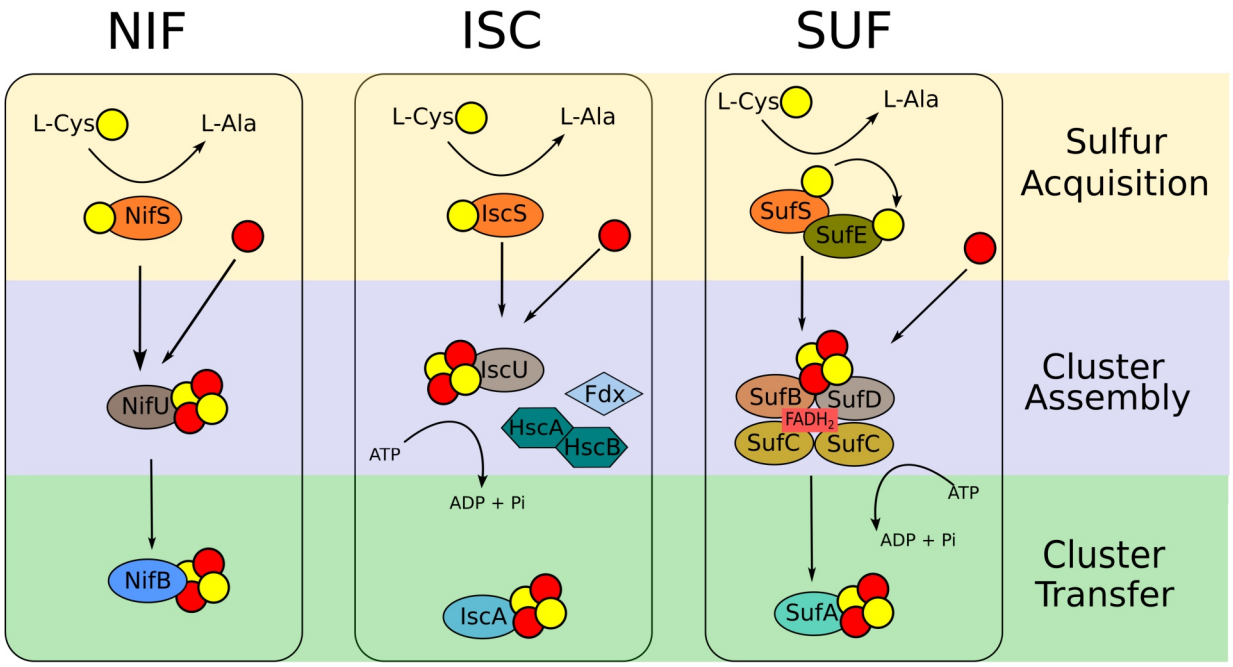

Fig. 2: Basic scheme of Fe-S cluster assembly pathways
Scheme showing essential steps in Fe-S cluster assembly which are common for all three main pathways. In the first step, cysteine is released from L-cysteine by cysteine desulfurase. In contrast to sulfur, the source of iron is unknown or at least disputable for all systems. The second step involves the assembly of Fe-S cluster on a scaffold protein. Newly synthesised cluster is in the third step transferred to recipient apoproteins. Based on Roche et al. (2015)

cysteine-ketiminidin intermediate attacks nucleophilically the sulfur of L-cysteine breaking the C-S bond and forming a covalent persulfide intermediate. Then, after deprotonation of the ketimine PLP intermediate and re-protonation of the α-carbon, alanine is released (Zheng et al. 1994; Mihara et al. 2000; Behshad et al. 2004; Tirupati, Vey, Catherine L. Drennan, et al. 2004a).

Crystal structures of cysteine desulfurases have been solved for both groups: NifS from *Termotoga. maritima and* IscS from *E. coli* are representatives of group I, while SufS from *E. coli* and *Synechocystis* sp. PCC6803 (Mihara et al. 2002; Tirupati et al. 2004a) are representatives of group II. Structures for both groups show remarkable similarity although conservation on sequence level is not so high. However, the group I has a conserved motif containing a catalytic Cys localised on a flexible loop which is often distorted in crystal structures, whereas, in group II this loop is shorter and more structurally defined. In *E. coli* the SufS has an 11-residue deletion compared to that of IscS leading to a restricted flexibility of its Cys364-containing loop (Mihara et al. 2002; Tirupati et al. 2004b; Blauenburg et al. 2016). Thanks to this difference, group II cysteine desulfurases have lower activity on their own, requiring an enhancer protein to be fully active (Loiseau et al. 2003;

Ollagnier-de-Choudens et al. 2003; Outten et al. 2003; Layer et al. 2007). Additionally, group II enzymes have a 19-residue insertion that forms a β-hairpin motif. The hairpin of one monomer reaches across the interface of the dimer and interacts with the active site of the second monomer (Lima 2002).

Some archaea like *Methanococcus maripaludis*, a methanogenic mesophyllic archaeon isolated from salt-marsh sediment, lacks cysteine desulfurase and instead acquires sulfur from sulfide which is abundant in its environment (Liu et al. 2010).

5.2 Source of iron

The source of iron for Fe-S cluster synthesis remains enigmatic. In eukaryotes, frataxin is believed to be the source of iron for the mitochondrial ISC pathway. However, in Bacteria and Archaea the source of iron for Fe-S cluster assembly remains elusive.

5.2.1 Frataxin

Frataxin (Fxn) is a small acidic protein (Gibson et al. 1996) which is conserved in most eukaryotes and in some bacteria, namely Alpha-, Beta-, Delta-, Gammaproteobacteria and Acidobacteria species, as well as in one representative of the Chlorobi phylum (Roche, Agrebi, et al. 2015). In humans, frataxin is associated with serious neurodegenerative disease called Friedreich's Ataxia (Koeppen 2011) and therefore is extensively studied. When it was first discovered, frataxin was believed to be associated with mitochondrial iron homeostasis, as its deletion in yeast caused accumulation of iron in the organelle (Babcock et al. 1997). Later, it was shown that it was probably associated with Fe-S cluster synthesis, as frataxin can form a complex with Nfs1, Isu1 and Isd11 and affects the synthesis of Fe-S clusters (Gerber and Lill 2002). The role of iron donor for mitochondrial Fe-S cluster assembly was suggested as it was experimentally shown that frataxin can bind Fe^{2+} and Fe^{3+} on its acidic ridge residues (Gerber et al. 2003; Yoon and Cowan 2003; Layer et al. 2006). Nuclear magnetic resonance (NMR) of human frataxin revealed that His86 in the N-terminal part acts as another iron binding site. This site is independent of the Fe binding sites localised on the acidic ridge (Gentry et al. 2013).

Later this hypothesis was also supported by the ability of frataxin to transfer iron *in vitro* onto the reduced 3Fe-4S cluster of aconitase and restore it back to the 4Fe-4S form. Lately, experiments combining NMR spectroscopy with isothermal titration calorimetry revealed that the frataxin bound

Fe^{2+} interacts weakly with NFS1-ISD11-ACP complex *in vitro* and, if ISCU, L-cysteine and ferredoxin are present, this interactions improves the dissociation of Fe^{2+} from frataxin. These experiments suggest that frataxin might be a proximal source of iron for ISC (Cai, Frederick, Tonelli, et al. 2018).

On the other hand, the recently published cryo-EM structure of the human NFS1-ISD11-ACP1-ISCU2-FXN complex suggests that the iron binding site of frataxin is not in proximity of the active site of 2Fe-2S cluster synthesis of ISCU2. This leaves open the question about what the iron-binding ability of frataxin is used for in biological processes and whether it has a direct role in iron acquisition (Fox et al. 2019).

Frataxin also plays an important role as a regulator of the mitochondrial ISC pathway. It was shown that, in eukaryotes, frataxin binds to ISCU-NFS1-ISD11 complex to stabilize it and to activate the cysteine desulfurase, as well as to control the entry of iron into the complex (Tsai and Barondeau 2010; Bridwell-Rabb et al. 2012). Interestingly, in bacteria, CyaY (bacterial homologue of frataxin) acts as inhibitor of cysteine desulfurase activity (Adinolfi et al. 2009). It was shown that regulation activity is not dependent on the type of Fxn but rather on the type of cysteine desulfurase (Bridwell-Rabb et al. 2012). Lately, it was shown that in humans this activation happens on the mobile S-transfer loop of NFS1 and that it helps to release the persufide from NFS1, acting as a Sulfur delivery agens for ISCU2 (Patraa & Barondeaua, 2019).

In *E. coli* and *Salmonella enterica*, deletion of CyaY did not produce any remarkable phenotype (Li et al. 1999; Pohl et al. 2007; Velayudhan et al. 2014; Roche, Huguenot, et al. 2015) showing that, in contrast to eukaryotes, frataxin is not essential for Fe-S cluster assembly in these species. This is due to the difference in IscU sequences. Sequencing of the fast growing Δ*yfh1* (yeast frataxin homologue) in a *S. cerevisiae* strain revealed that the cause for frataxin dependency in yeast is a methionine at position 141 in ISU1 (Yoon et al. 2015). When this Met was mutated to Cys, Ile, Leu, or Val, yeasts showed improved growth phenotype in the absence of frataxin (Yoon et al. 2012). Also, a mutation of Ile108 (equivalent of met 141 in *S. cerevisiae*) to Met in *E. coli* IscU, made it CyaA-dependent (Roche, Agrebi, et al. 2015). Remarkably, the only group of prokaryotes where methionine is conserved at this position are *Rickettsiae* suggesting that frataxin dependency of eukaryotes was inherited together with the ISC pathway from α-proteobacteria (Roche, Agrebi, et al. 2015).

5.2.2 Donor of iron in the SUF system

Up to date, there is no direct evidence which would pin-point the donor of Fe for the SUF system. However, during years of explorations, two possible Fe donor candidates have been pointed out, SufA and SufD.

SufD was proposed to play a role in iron acquisition since a detailed comparison of EPR spectra of the isolated $SufB_2C_2$ and $SufBC_2D$ complexes revealed depletion of iron in the $SufB_2C_2$ sub-complex (Saini et al. 2010). Some studies showed connection between SufD and iron metabolism (Nachin et al. 2003; Expert et al. 2008). However, up to date there is no in vitro evidence for SufD binding to any form of iron.

SufA was suggested as a possible Fe donor protein for the SUF system as it has Fe binding activity in *E. coli* and cyanobacteria (Wollenberg et al. 2003; Ding et al. 2004; Lu et al. 2008; Landry et al. 2013). However, all these studies were carried out *in vitro*. Also, the analysis of the phenotype under standard growth conditions did not show any strong evidence which would support a role for IscA/SufA in cellular Fe homeostasis (Seidler et al. 2001; Djaman et al. 2004; Balasubramanian et al. 2006). Therefore, IscA/SufA may only be carrier proteins which transfer Fe or Fe-S cluster to target apoproteins.

5.3 Scaffold

Iron and Sulfur are assembled into an Fe-S cluster on a scaffold protein. In ISC and NIF pathways, the proteins IscU and NifU serve as scaffolds, respectively. In the case of the SUF pathway, the scaffold is formed by a $SufBC_2D$ complex. CSD was proposed to interact with $SufBC_2D$ complex

5.3.1 NifU

NifU, the first one discovered, is a modular scaffold containing three distinct domains (Fu et al. 1994; Agar, Yuvaniyama, et al. 2000; Yuvaniyama et al. 2000). A central ferredoxin-like domain contains a stable 2Fe-2S cluster which cannot be transferred to an apoprotein and was proposed to play a role in redox processes during cluster assembly. The N-terminal domain of NifU is highly similar to IscU and forms both 2Fe-2S and 4Fe-4S clusters that can be transferred to apoproteins or to the C-terminal Fe-S cluster-binding from where it is transferred to an apoprotein (Smith et al. 2005). *In vivo* studies indicate that the two scaffold domains have somewhat redundant functions

and that the N-terminal IscU-like domain is the most important for nitrogenase Fe-S cluster assembly (Dos Santos et al. 2004).

5.3.2 IscU

IscU is similar to NifU and was also shown to form both 2Fe-2S and 4Fe-4S clusters *in vitro*, which can be both transferred to apoproteins. Firstly, two 2Fe-2S clusters are assembled on an IscU homodimer one by one and are thought to be adjacent to one another at the dimer interface. Then, they undergo rapid coupling to produce a single bridging 4Fe-4S cluster on the IscU homodimerya (Agar, Krebs, et al. 2000; Chandramouli et al. 2007). The 2Fe-2S clusters and may. The donor of electrons for this coupling was shown to be ferredoxin (Kim et al. 2013; Yan et al. 2015). Ferredoxin was also proposed to be the donor of electrons for the reduction of S^0 to S^{2-} (the redox state of S in the cluster) (Cai, Frederick, Tonelli, et al. 2018). The conversion of 2Fe-2S clusters to a 4Fe-4S cluster is irreversible, however, 4Fe-4S can be reduced to a single 2Fe-2S upon exposition to oxygen (Chandramouli et al. 2007).

5.3.3 SufBCD

In the SUF pathway, an Fe-S cluster is assembled on a $SufBC_2D$ complex. The interface between the SufD and SufB heterodimer was proposed as the actual place where the Fe-S cluster assembly occurs (Yuda et al. 2017). SufC is an ATPase and was proposed to change the conformation of the $SufBC_2D$ complex, allowing delivery of S and Fe, and otherwise assisting with assembly of the cluster (Hirabayashi et al. 2015). As SufC monomers form a transient dimer after binding of ATP, they change the conformation of the BCD complex and it exposes the cluster assembly site, otherwise buried inside the complex.

The $SufBC_2D$ complex was shown to bind $FADH_2$ (Wollers et al. 2010), a molecule proposed to play a role in the reduction of Fe-S cluster assembly by reducing iron. It was also proposed that flavin might be the source of electrons for the cleavage of persulfide (Yuda et al. 2017). Other possible complexes - $SufB_2C_2$, $SufD_2C_2$ have been reported (Wada et al. 2009; Chahal and Outten 2012) these alternative complexes were proposed to represent different stages of the biosynthetic process of Fe-S cluster assembly which enable the transfer of Sulfur from SufE to SufB, the recruitment of iron from SufD, and the assembly of clusters on the SufBD interface (Chahal and Outten 2012). However, their physiological importance is unknown.

The mechanisms and form of the Fe-S cluster assembled on the $SufBC_2D$ complex is still a matter of discussion. Early *in vitro* reconstitution studies of the SUF pathway established that SufB of *E. coli* assembles a 4Fe-4S cluster which can be changed to a 2Fe-2S cluster when exposed to O_2 (Layer et al. 2007; Tsaousis et al. 2012) and 4Fe-4S and 3Fe-4S clusters were also observed on purified His-SufB after *in vivo* co-expression with *sufCDSE* genes (Saini et al. 2010). Later, *in vitro* reconstitution of apo-SufB under anaerobic conditions showed that SufB can stabilize a 2Fe-2S cluster and that it is more stable than the 2Fe-2S cluster on IscU. The 2Fe-2S cluster on SufB could be converted to a 4Fe-4S cluster under reducing conditions when needed (Blanc et al. 2014).

5.4 Transport to apoproteins

The last step in Fe-S cluster biosynthesis is the transfer of the assembled cluster onto the target protein. This step can be done in several ways: 1) direct transfer of the cluster via scaffold, 2) transfer by chaperones and, 3) transporting the Fe-S cluster by a specialised carrier.

5.4.1 HscA/HscB

In the ISC system, chaperone HscB (in eukaryotes HSC20) and its co-chaperone HscA interact with IscU enhancing the transfer of the cluster to apoprotein 20 times (Chandramouli and Johnson 2006). HscA interacts with IscU via a conserved LPPVK motif (Hae Kim et al. 2012). HscB recognizes the LYR motif in the sequence of some proteins and transfers the Fe-S cluster directly from IscU to the apoprotein (Maio et al. 2014; Maio and Rouault 2015; Maio et al. 2017). HscB was also shown to interact with monothiol glutaredoxin GLRX5 which was proposed to be an intermediate Fe-S cluster carrier (Ye et al. 2010).

5.4.2 A-type carriers

SufA, IscA and ErpA belong to the family of A-type carriers (ATC) (Vinella et al. 2009). All ATCs contain three conserved cysteine residues Cys50, Cys114 and Cys 116 (*E. coli* SufA numeration). These residues are binding sites for the transient cluster. ATC proteins can be phylogenetically divided into three groups. Proteins belonging to ATC-I family were predicted to connect to apo-targets, whereas the ATC-II members were proposed to be associated with scaffolds (Vinella et al.

2009). These were originally proposed to be alternative scaffolds for Fe-S cluster assembly (Ollagnier-De-Choudens et al. 2001; Ollagnier-de-Choudens et al. 2004), however, this hypothesis was rejected and they are now considered as carriers or iron donors. The main reasons for this are following. Firstly, *in vitro* studies showed that IscA can accept a cluster from IscU (Ollagnier-de Choudens et al. 2003), but cannot transfer a cluster to IscU, similarly, SufA can receive a cluster from the $SufBC_2D$ complex, but not in opposite direction (Chahal et al. 2009). Secondly, Fe-S clusters are preferentially assembled on IscU, not on IscA in presence of IscS (Yang et al. 2006). And thirdly, Fe-S clusters are transferred from $SufBC_2D$ or $SufB_2C_2$ complexes to aconitase *via* a SufA intermediate, only if apo-SufA is present (Chahal and Outten 2012). It was also shown that IscA/SufA are important for the maturation of 4Fe-4S proteins under aerobic conditions (Tan et al. 2009). In *E. coli*, SufA and IscA have a partially redundant functions, as the deletion of either IscA or SufA had only a mild effect on the cell growth, while deletion of both IscA and SufA was lethal for the cells (Lu et al. 2008).

Genes belonging to ATC-III family are spread among various bacterial phyla, which suggest that they spread by horizontal gene transfer. Also ATC-III group genes are usually surrounded by NIF genes suggesting that they are involved in the maturation of nitrogenases (Vinella et al. 2009).

5.4.3 Nfu

Other Fe-S carrier proteins are the Nfus. They belong to the U-type family of proteins and contain a domain which resembles the C-terminal Nfu domain of NifU (Angelini et al. 2008). All proteins from this family contain highly conserved CXXC motif in the Nfu domain which coordinates the Fe-S cluster. They can transiently bind an Fe-S cluster and transfer it onto apoproteins *in vitro* (Bandyopadhyay, Naik, et al. 2008). NfuA in *E. coli* has an N-terminal domain structurally similar to that of the ATC protein, however, the conserved three cysteine motif proposed to bind an Fe-S cluster in ATCs is missing. It was shown that NfuA can receive Fe-S clusters from IscU/HscB/HscA or SufBCD scaffolds and eventually transfer them to the ATCs IscA and SufA. Alternatively, it can transfer a 4Fe-4S cluster directly to apo-aconitase (AcnB) (Py et al. 2012). Recently, it was shown, that in *E. coli* NfuA and ErpA can form a carrier complex which is resistant to oxidative stress. NfuA was shown to accept Fe-S clusters from scaffold proteins and transfer them to ErpA which delivers them to target proteins (Py et al. 2018).

5.4.4 GLRX

Monothiol glutaredoxins (Grx) can bind Fe-S clusters (Herrero and De La Torre-Ruiz 2007) and have been suggested to play a role in Fe homeostasis and Fe-S trafficking. They are capable of binding 2Fe-2S clusters and transferring them to A-type carriers (Mühlenhoff et al. 2010; Mapolelo, Zhang, Randeniya, A.-N. Albetel, et al. 2013). The crystal structure showed Grxs function as dimers containing one 2Fe-2S cluster coordinated Cys ligand from conserved CGFS site of both monomers (Abdalla et al. 2016). Proteins from *Azotobacter vinelandii* were demonstrated to preform unidirectional 2Fe-2S cluster transfer in *vitro* from the IscU to the general-purpose monothiol CGFS Grx5 only in the presence of the dedicated HscA/HscB co-chaperone. Additionally, 2Fe-2S cluster-containing Grx5 was shown to be competent for the maturation of apo-Isc-ferredoxin at a much faster rate than 2Fe-2S cluster-loaded IscU in the presence of the HscA/HscB co-chaperone system (Shakamuri et al. 2012). In yeast, cytosolic monothiol Grxs (Grx3/4) interact with Fra2 (yeast BolA homolog) to form a heterodimeric complex with a bound 2Fe-2S cluster and play important role in Fe homeostasis (Poor et al. 2014). Also, mitochondrial Grx5 facilitates the transfer of Fe-S clusters from the mitochondrial Isu1 (IscU) scaffold protein to the acceptor protein and is believed to serve as an intermediate Fe-S cluster carrier (Mühlenhoff et al. 2003).

In vivo experiments showed that other monothiol CGFS Grxs from prokaryotes or eukaryotes can complement *S. cerevisiae* G*rx5* mutants, suggesting that this function is conserved in this class of proteins throughout evolution (Molina-Navarro et al. 2006; Bandyopadhyay, Gama, et al. 2008).

6 Bacterial systems for Fe-S cluster assembly.

Four distinctive pathways for Fe-S cluster assembly have evolved in prokaryotic organisms, although physiological role of CDS pathway in not fully understood. Most bacteria contain more than one pathway. In this chapter, each of them will be discussed briefly.

6.1 NIF pathway

NIF was the first discovered Fe-S cluster assembly pathway. It was originally discovered in *A. vinelandii* in 1992 (Zheng et al. 1993) and later was found in all nitrogen-fixing bacteria (Boyd, Hamilton et al. 2011; Dos Santos et al. 2012). The pathway seems to be dedicated to the synthesis of the P-cluster and the FeMo-cluster of nitrogenase and cannot replace other pathways in

maturation of other Fe-S cluster proteins (Dos Santos et al. 2007; Zhao et al. 2007). Its distribution is limited to nitrogen-fixing bacteria but has been found also in some anaerobic protists, where it replaced mitochondrial pathways.

The composition of the NIF pathway varies greatly between species, however, six genes (NifH, D, K, E, N and B) have been found in most (Dos Santos et al. 2012). In *A. vinelandii* (model organism for study of nitrogenase) it consists of more than 20 genes, divided into two main operons (Jacobson et al. 1989; Rodriguez-Quinones et al. 1993). Sixteen of these genes — *nifH, D, K, Y, T, E, N, X, U, S, V, Z, W, M, B, Q* are probably essential for the biosynthesis of nitrogenase (Rubio and Ludden 2008). However, in Fe-S cluster synthesis, only three of them — NifS, NifU and NifB — are involved (Zhao et al. 2007). NifS belongs to the group I of PLP-dependent cysteine desulfurases and its crystal structure has shown that it works as a homodimer (Zheng et al. 1993; Zheng et al. 1994). During Fe-S cluster assembly, NifS forms a transient heterotetramer with NifU, and synthesis is mediated by the activity of NifS (Yuvaniyama et al. 2000; Smith et al. 2005). NifU acts as a scaffold protein and its N-terminal domain is structurally similar to that of IscU. In contrast to

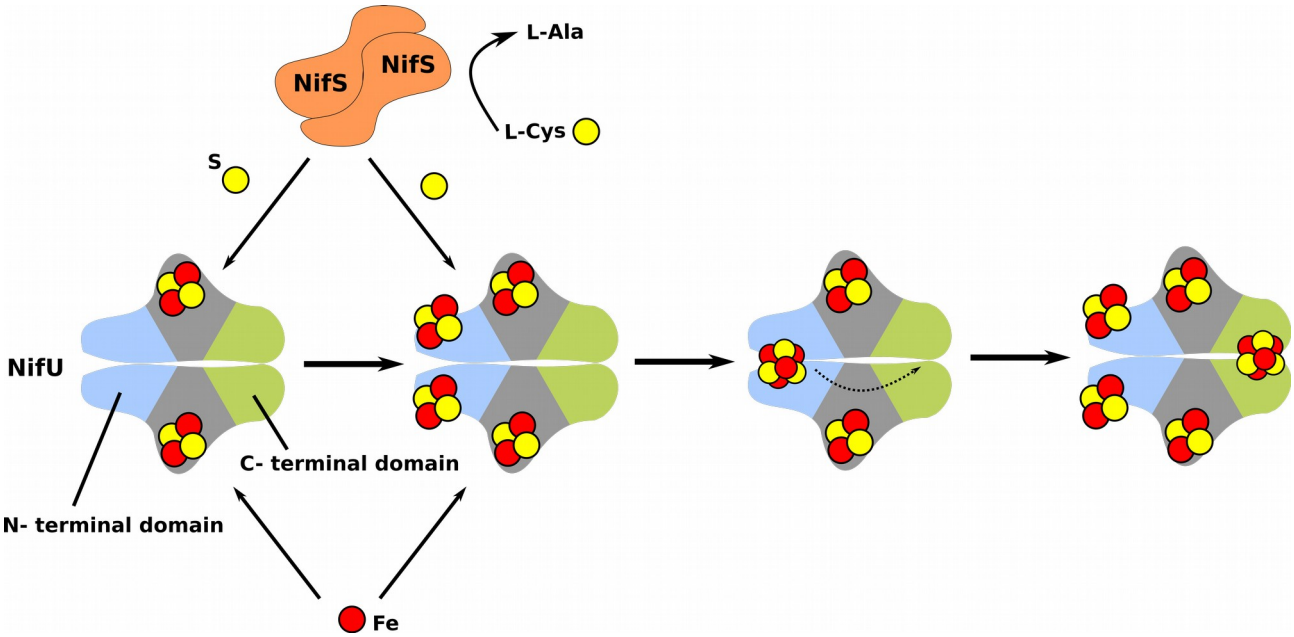

Fig. 3: Proposed Fe-S cluster assembly on NifU
First, sulfur is released from L-cysteine by NifS and transferred to NifU where Fe-S cluster is assembled. Source of iron is unknown. Then two 2Fe-2S clusters are assembled on N-terminal domain of the NifU. In the next step, two 2Fe-2S clusters are fused together to form a 4Fe-4S cluster which is then transferred to the C-terminal (Nfu) domain from where it is transferred to recipient proteins. *In vitro* experiments showed that two 4Fe-4S clusters per dimer of NifU can be formed (Smith et al., 2005). The middle domain of NifU contains permanently bound 2Fe-2S cluster for which exact role is unknown. However, it was proposed to have redox function in 4Fe-4S cluster synthesis. Based on Smith et al. (2005)
IscU, it displays three Fe-S cluster binding domains. The N- and C-terminal domains contain

transient Fe-S clusters which will be further delivered to target apoproteins, the middle domain contains a permanent 2Fe-2S cluster (Fu et al. 1994), that has been proposed to have a redox function (Olson et al. 2000). NifU is also able to form two 2Fe-2S clusters which are later fused into one 4Fe-4S cluster (**Fig. 3**). The assembled 4Fe-4S cluster is transferred to NifB (Curatti et al. 2006), a radical SAM enzyme containing three 4Fe-4S clusters, one coordinated by a conserved RSS cysteine motif that has catalytic function, and two other clusters that probably serve as precursors for synthesis of the NifB-cofactor (8Fe-9S-C cluster) (Wilcoxen et al. 2016).

6.2 ISC pathway

The core of the ISC pathway consists of five proteins — IscS, IscU, ferredoxin (Fdx) and two chaperones HscA and HscB. IscS is a PLP-dependent, group I cysteine desulfurase which acts as homodimer (Mihara and Esaki 2003). IscU is a scaffold protein on which the assembly of Fe-S cluster takes place.

Crystal structures of the *E. coli* apo-IscU-IscS complex have shown that it forms heterotetramer consisting of an IscS dimer and two IscU monomers, with each subunit of IscU interacting with one subunit of the IscS dimer (Shi et al. 2010; Marinoni et al. 2012). Both subunits of IscU bind to IscS close to the catalytic centre of IscS, but they are not in direct contact. During cysteine desulfurase activity, IscS flexible loop-containing cysteine is believed to move towards IscU and transfer persulfide onto IscU.

IscU was shown to assemble two 2Fe-2S clusters which later undergo fusion into a 4Fe-4S cluster *in vitro* (Chandramouli et al. 2007). It was shown to interact directly with apoproteins and transfer 2Fe-2S or 4Fe-4S clusters to them (Agar, Krebs, et al. 2000; Chandramouli et al. 2007; Unciuleac et al. 2007). For some apoproteins, the transfer of the Fe-S cluster is mediated by chaperones HscA and HscB. HscA is an Hsp70 (DnaK) family member with ATPase activity, meanwhile HscB is a member of the Hsc20 (DnaJ) family (Vickery and Cupp-Vickery 2007). HscA interacts with IscU through a conserved LPPVK motif (Cupp-Vickery, Peterson, et al. 2004; Tapley and Vickery 2004; Li et al. 2009) and the Fe-S cluster is released from IscU in an ATP-dependent manner (Bonomi et al. 2008). HscB also shows weak interaction with IscS (Puglisi et al. 2016). HscB was proposed to play the role of a scaffold, facilitating the binding of the substrate and regulating ATPpase activity of HscA (Cupp-Vickery and Vickery 2000). HscB/HscA chaperones can enhance the transfer of the cluster from IscU to apoprotein up to 20 times (Chandramouli and Johnson 2006). It was proposed

that the chaperone complex stabilizes IscU and allows transfer of the Fe-S cluster to apoproteins (Bonomi et al. 2011).

Ferredoxin (Fdx) is a 12-kDa protein which contains a stable 2Fe-2S cluster (Kakuta et al. 2001). Fdx is essential for Fe-S cluster assembly and its deletion has similar effect as the deletion of IscS or IscU (Tokumoto and Takahashi 2001). In Fe-S cluster assembly it acts as a donor of electrons for coupling 2Fe-2S clusters into 4Fe-4S cluster on IscU (Chandramouli et al. 2007; Kim et al. 2013; Yan et al. 2015). It has been speculated that Fdx could also perform the persulfide reduction step (S^0-S^{-2}) on IscS during the initial stages of Fe-S cluster assembly (Lange, Kaut, Kispal, & Lill, 2000).

IscA is a small protein (12-kDa) member of the A-type protein family (Vinella et al. 2009). Crystal structures of IscA have shown that it can exist as a dimer or tetramer and that it contains three cysteines that form a cysteine-binding pocket. This pocket can bind either a mononuclear iron atom or an Fe-S cluster (Bilder et al. 2004; Cupp-Vickery, Silberg, et al. 2004). It was shown that IscA can bind a 2Fe-2S and a 4Fe-4S cluster under anaerobic conditions, both *in vitro* (Krebs et al. 2001; Ollagnier-De-Choudens et al. 2001) and *in vivo* (Morimoto et al. 2006; Zeng et al. 2007). Under aerobic conditions, IscA is also capable of binding Fe (Ding and Clark 2004; Wang et al. 2010; Mapolelo et al. 2012).

IscX (YfhJ) is a small acidic protein encoded by the last gene in the ISC operon of *E. coli* (Tokumoto and Takahashi 2001). IscX is highly conserved and is present only in prokaryotes and Apicomplexa (Pastore et al., 2006). *In vitro* studies have shown that it can bind Fe although with weaker affinity than CyaY (Pastore et al. 2006) and that it forms a complex with IscS. Based on this results it was proposed that it may play a role of Fe donor or regulatory protein (Pastore et al. 2006). Recently, experiments combining nuclear magnetic resonance with small angle scattering and biochemical methods, showed that IscX competes with CyaY for the binding site on IscS, and modulates the inhibitory effects of CyaY, in this case rescuing the rates of enzymatic cluster formation inhibited by CyaY. The modulatory effect of IscX is stronger at low iron concentrations. These results strongly suggest a mechanism of dual regulation of iron Sulfur cluster assembly under the control of iron as an effector (Pastore et al. 2006; Kim et al. 2014).

CyaY (bacterial frataxin) also plays an important role as regulatory protein, which inhibits Fe-S cluster assembly on the ISC pathway (Adinolfi et al. 2018) as it was discussed in previous chapters.

6.3 SUF pathway

The SUF pathway is considered to be oldest of all the Fe-S cluster assembly pathways. It is present in all three kingdoms of life and is widely distributed among Bacteria and Archaea (Takahashi and Tokumoto 2002; Boyd et al. 2014). For some organisms, it is the only system for Fe-S cluster assembly, while other organisms possess more than one pathway. In *E. coli*, the SUF pathway is upregulated under conditions of oxidative stress and Fe limitations (Nachin et al. 2003; Outten et al. 2004).

SufS is PLP-dependent cysteine desulfurase belonging to the group II. Its basal activity is very low when compared to group I cysteine desulfurases, but increases greatly in the presence of SufE or SufU (Loiseau et al., 2003; Outten et al., 2003; Selbach et al., 2014). SufS mobilizes Sulfur from L-cysteine and the released Sulfur is bound in form of persulfide to Cys364 (*E. coli* numeration) from which it is transferred to SufE Cys51 residue (Ollagnier-de-Choudens, Lascoux et al. 2003). This transfer takes place via a ping-pong mechanism and under oxidative conditions it is more effective and robust than IscS - IscU transfer (Dai and Outten 2012; Selbach et al. 2013). There are three published crystal structures of SufS up to date (Fujii et al. 2000; Tirupati et al. 2004b; Blauenburg et al. 2016). They show that the catalytic cysteine Cys364 is localised on the extended loop, but this loop has an 11-residue deletion when compared with that of IscS leading to its restricted flexibility.

SufE is an enhancer (activator) of SufS activity, which forms with the SufS dimer a complex with S_2E_2 stoichiometry (Loiseau et al. 2003; Outten et al. 2003). It was shown to transfer Sulfur from SufS to SufB. Cys51 was identified as critical residue for this reaction. Study of structural dynamics of the SufS-SufE complex revealed, that SufS changes structure slightly after interaction with SufE at its catalytic centre. This structural change enhances cysteine desulfurase activity. Structural studies of SufE from *E. coli* showed that the active Cys51, is localised on the tip of the loop and its side chain is deep in the hydrophobic cavity where it is protected from solvents (Goldsmith-Fischman et al. 2004). For the transfer of persulfide, Cys51 of SufE must come into close proximity to the active Cys364 of SufS. To achieve this, SufE undergoes a structural change which allows flexibility of its Cys51 loop. It was shown that Asp74 is the key player for keeping the loop inside of SufE structure. Mutation of SufE Asp74 to Arg increased accessibility of Cys51 to the solvent and enhanced flexibility of the active site loop eventually leading to enhanced cysteine desulfurase activity of SufS (Dai et al. 2015).

SufU is similar to IscU on the sequence level, however, it acts as enhancer/activator of SufS analogically to SufE and not as scaffold (Albrecht et al. 2010; Selbach et al. 2014). SufU is present in various bacteria including Bacilli, Actinobacteria, Spirochaetes and Thermotogae (Tokumoto et al. 2004; Huet et al. 2005; Boyd et al. 2014; Wayne Outten 2015). Interestingly, phylogenetic studies showed that SufU and SufE do not occur together, hence most organisms encode only SufU or SufE in the *suf* operon, yet many organisms encode SufE separately, outside of the *suf* operon. Although SufU and SufE are not similar at the sequence level, they share similar tertiary structure. SufU was shown to be essential in *B. subtilis*. The three conserved cysteine residues of *B. subtilis* SufU (Cys41, Cys66, Cys128) together with Asp43 constitute the binding site for Zn, which is essential for the interaction with SufS (Albrecht et al. 2010; Selbach et al. 2010). Swapping of the Zn ligand between SufU and SufS frees Cys41 of SufU and allows the transfer of persulfide from Cys364 of SufS (Selbach et al. 2014; Fujishiro et al. 2017). Recently, it was shown that SufS and SufU from *B. subtilis* can functionally replace SufS and SufE in *E. coli* and vice versa, but SufU or SufE alone were not capable replacing each other (Fujishiro et al. 2017).

SufB serves as scaffold protein, however, the type of cluster which it assembles remains uncertain. *In vitro r*econstitutions showed the production of 2Fe-2S and 4Fe-4S clusters (Layer et al. 2007; Blanc et al. 2014). It was also proved that SufB is capable of transferring both 2Fe-2S and 4Fe-4S to acceptor proteins *in vitro* (Chahal et al. 2009; Wollers et al. 2010; Chahal and Outten 2012). *In vivo*, however, only 4Fe-4S and 3Fe-4S clusters have been identified to be present on SufB (Saini et al. 2010). Up to the date, there is no crystal structure of SufB alone, with the only published being the one from the $SufBC_2D$ complex (PDB: 5AWF) (Hirabayashi et al. 2015; Yuda et al. 2017). The N-terminal part of SufB contains a conserved cysteine motif CxxCxxxC which was proposed to bind an Fe-S cluster (Layer et al. 2007). However, recent studies showed that this is not exactly accurate (Yuda et al. 2017). The same study showed that Fe-S ligands are most probably Cys405, Glu434, His433 and Glu432 residues (Yuda et al. 2017). SufB also contains FAD binding motifs and the $SufBC_2D$ complex was shown to contain $FADH_2$ after isolation in native conditions (Wollers et al. 2010). The exact role of $FADH_2$ in the $SufBC_2D$ complex and Fe-S cluster assembly is unknown. SufB interacts with the SufSE complex and acquires S from SufS *via* SufE, yet this interaction can only take place if SufC is present **(Fig. 4)**. Cysteines at positions 254 and 405 of SufB from *E. coli* were identified as probable acceptors of S from SufE, with Cys254 being critical for the occurrence of this interaction (Yuda et al. 2017).

SufC is a member of the ABC ATPase superfamily and contains all the characteristic motifs (Nachin et al. 2001; Nachin et al. 2003; Kitaoka et al. 2006). The basal activity of SufC is relatively low but it increases significantly when it is in complex with SufB or SufD (Petrovic et al. 2008). The ATPase activity of SufC is not essential for Fe-S cluster assembly *in vitro*, however *in vivo*, mutations in the ATP binding site disrupted the activity of the SUF pathway (Nachin et al. 2003; Saini et al. 2010). The crystal structure of the $SufBC_2D$ complex has shown that SufC forms a head-to-tail dimer. After binding of ATP, SufC changes the structure of the $SufBC_2D$ complex, leading to the exposure of Cys405 of SufB and His360 of SufD, which are normally buried inside of the complex (Hirabayashi et al. 2015). It was also shown that mutations in the Walker A motif of SufC reduced eightfold the Fe content on the isolated $SufBC_2D$ complex, strongly suggesting that the ATPase activity of SufC is necessary for Fe acquisition (Saini et al. 2010).

SufD is a paralog of SufB and the *E. coli* proteins have 17% identity and 37% similarity. Sequence homology suggests that this protein originated as a duplicate of SufB. This is in accordance with phylogenetic analyses, where the earliest forms of the SUF pathway consist of SufB and SufC only (Takahashi and Tokumoto 2002). SufD from *E. coli* has a sequence with no known predicted motifs and after purification it does not contain any cofactors nor prosthetic groups, and after incubation with an excess of iron and Sulfur, it does not harbour any Fe-S cluster. Although SufD was proposed to be involved in acquisition of iron (Nachin et al. 2003; Expert et al. 2008), there is no direct evidence that SufD binds iron in any form.

SufA belongs to the A-type family of Fe-S cluster carriers (Yokoyama et al. 2018) and it can bind 2Fe-2S and 4Fe-4S clusters after *in vitro* reconstitution (Ollagnier-de-Choudens et al. 2004; Ollagnier-de-Choudens, Nachin et al., 2003). *In vivo*, it contains a 2Fe-2S cluster under anaerobic conditions. SufA contains three strictly conserved cysteine residues Cys50, Cys114 and Cys116 (*E. coli* SufA numbering) which are present in almost all ATCs and were proposed to bind an Fe-S cluster (Ollagnier-de-Choudens, Nachin et al. 2003; Ollagnier-de-Choudens et al. 2004). SufA is important for the maturation of 4Fe-4S proteins under physiological conditions (Vinella et al. 2009) and was demonstrated to transfer an Fe-S cluster to apoproteins such as aconitase (4Fe-4S enzymes) or Fdx (2Fe-2S protein) (Tan et al. 2009).

6.4 The CSD system (Cysteine sulfinate desulfinase)

CSD pathway is the third system for Fe-S cluster assembly in *E. coli*. It composes of cysteine sulfinate desulfinase encoded by CsdA and its enhancer (activator) CsdE (Loiseau et al. 2005). CsdA is group II cystein desulfurase, but in contrast to SufS, CsdA is not specific to L-cysteine and is capable of releasing of Sulfur and selenium from L-cysteine sulfinate, L-cysteine and L-selenocysteine respectively (Mihara et al. 2000). Interaction of CsdE with CsdA enhances cysteine

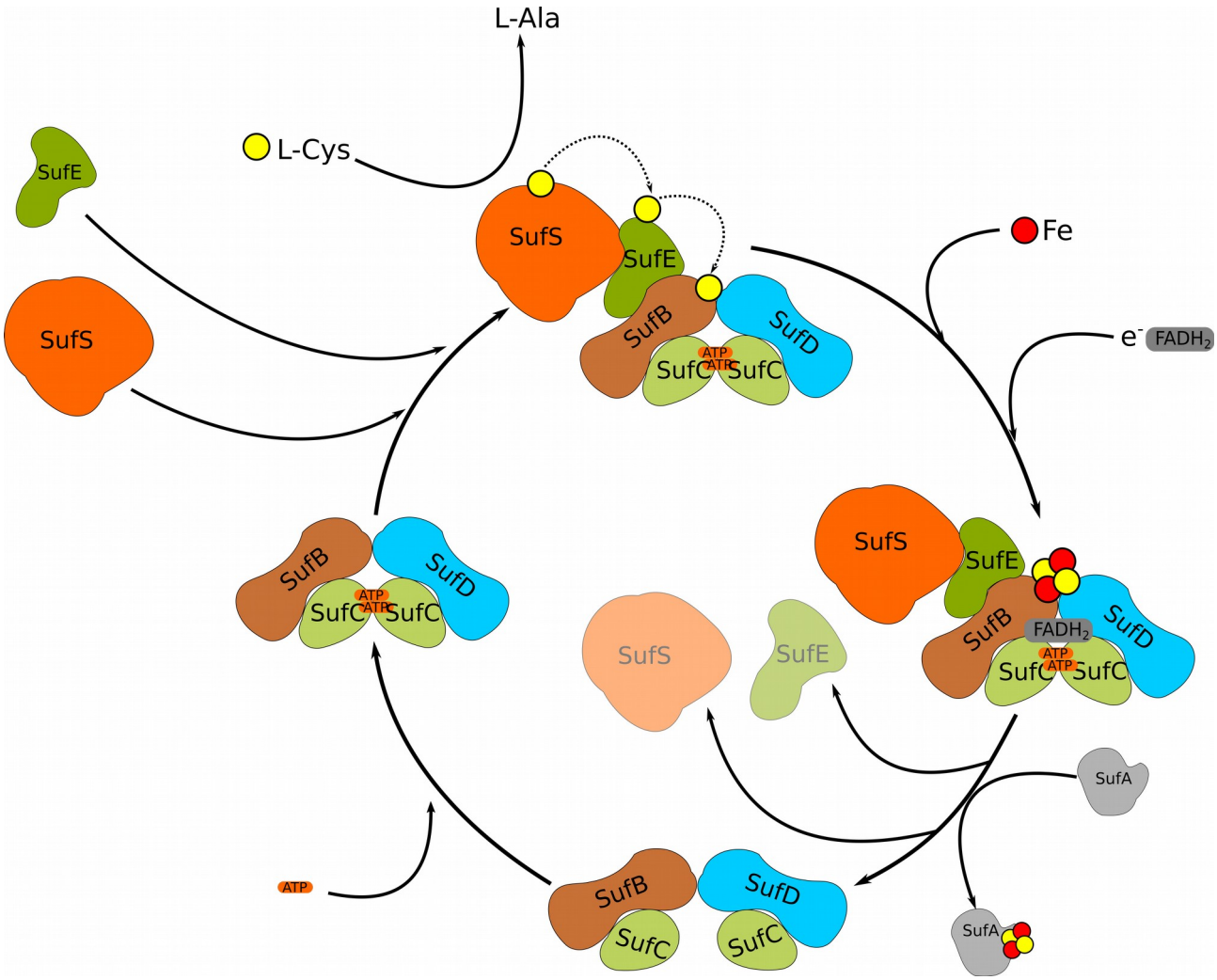

Fig. 4: Proposed mechanism of Fe-S cluster assembly on SufBC$_2$D complex

The figure shows the proposed mechanism of Fe-S cluster assembly in *E. coli*, therefore SufE, and is depicted although the mechanism for SufU should be the same. Fe-S cluster assembly by SUF pathway is initiated by the ATPase activity of SufC. Upon hydrolysis of ATP, SufC dimerises and significantly changes the structure of SufBC$_2$D complex, this change exposes Cys405 of SufB and His360 of SufD to surface. This complex can interact with SufSE complex. Then cysteine desulfurase activity of SufS generates persulfide, which is transferred via Cys51 of SufE, to SufB and Fe-S cluster is synthesised on SufB-SufD interface. Source of iron and electrons is unknown although $FADH_2$ was proposed to be the source of electrons. In next step SufSE dissociates from complex and cluster is transferred to SufA which can maturate 4Fe-4S proteins. After that SufBC$_2$D complex is regenerated. Based on Hirabayashi et. al. (2015).

desulfurase activity two folds and results in persulfide bound to Cys61 of CsdE (Loiseau et al. 2005; Trotter et al. 2009). Multicopy expression of C*sdA* restored activity of all Fe-S enzymes tested in an *iscS sufS* double mutant (Trotter et al. 2009).

CsdA shares 45% identity to SufS and CsdE has 35% identity to SufE. Which suggest that CsdAE and SufSE complexes are closely related to each other. Furthermore crystal structure of CsdAE complex revealed similarity SufSE complex (Kim and Park 2013; Fernández et al. 2016). Crystal structures of SufE (Goldsmith-Fischman et al. 2004) and CsdE (Liu et al. 2009; Kenne et al. 2016) showed structural similarity between these two enzymes. Structures of free SufE and CsdE have reactive thiol group is in hydrophobic cavity, where it is protected from exposition to solvent. During transfer of Sulfur, CsdE undergoes major transformation to allow connection of catalytic thiol group with CsdA (Kim and Park 2013). This is similar to mechanism of SufSE persulfide transfer.

In *E. coli* CsdAE complex has been proposed to interact with SufBCD complex and to act as Fe-S cluster assembly pathway (Trotter et al. 2009). This is in concord with interactome study, which showed that CsdE interacts with some Fe-S cluster proteins (Bolstad et al. 2010). However, exact conditions in which CsdAE-SufBCD complex serves as Fe-S cluster assembly pathway are yet to be elucitated.

CsdAE also forms transient interactions with CsdL and transfer Sulfur to it (Trotter et al. 2009; López-Estepa et al. 2015). CsdL is E1-like (or ubiquitin-activating-like) protein which is also known as TcdA (tRNA threonylcarbamoyladenosine dehydratase A) and is responsible for N6-threonylcarbamoyladenosine (ct^6A) synthesis (tRNA modification which has a crucial role in maintaining accuracy of translation during protein synthesis). *In E. coli*, ct^6A synthesis *in vivo* is dependent on the presence of a functional CsdA-CsdE system. However, ct^6A is non-thiolated modification and its synthesis can be reconstituted *in vitro* with just CsdL and ATP (Miyauchi et al. 2013).

7 Fe-S cluster assembly in eukaryotes

Eukaryotes typically contain an ISC pathway for Fe-S cluster assembly in mitochondrion and a cytosolic CIA pathway, involved in the maturation of cytosolic and nuclear Fe-S cluster proteins.

Plastid-containing eukaryotes furthermore contain a SUF pathway localised inside plastids. However, there are also exceptions to this general rule.

7.1 Mitochondrial ISC pathway

The mitochondrion synthesises Fe-S clusters via the ISC pathway. This pathway was most likely inherited from α-proteobacteria (Richards and Van Der Giezen 2006). It reflects its bacterial origin, and the mechanisms and protein functions are generally like those described in bacteria. However, in contrast to bacteria, where the core ISC pathway contains five proteins, in *S. cerevisiae* and *Homo sapiens* the ISC pathway consists of 18 proteins. The mitochondrial pathway also produces uncharacterised sulfur or iron-sulfur intermediate (X-S) which is transported via the Atm1 (ABCB7) transporter to the cytosol, where it is utilised by the CIA pathway (Kispal et al. 1999; Pandey et al. 2019).

The mitochondrial Fe-S cluster assembly can be divided into three phases: i) a 2Fe-2S cluster is formed on ISCU2, ii) it is transported in a HSP70 mediated fashion to GLRX5 and in some cases to target apoproteins, and iii) finally but not always it is converted to 4Fe-4S cluster and delivered to target apoproteins **(Fig. 5)**. For description of ISC mechanism human (mammalian) nomenclature will be used if not stated otherwise.

The 2Fe-2S cluster assembly is catalysed by seven proteins, six of them forming a complex (also called core ISC complex) which consists of cysteine desulfurase (NFS1), the scaffold (ISCU2), acyl carrier protein (ACP1), ISD11, ferredoxin (FDX2) and frataxin (FXN). For overview of 2Fe-2S cluster assembly by ISC pathway see **Fig. 6**.

NFS1 is a PLP-dependent group I cysteine desulfurase which works as a dimer (Mihara et al. 2000), determining the overall symmetric shape of the core ISC complex (Boniecki et al. 2017; Cai, Frederick, Dashti, et al. 2018; Fox et al. 2019). The dimer is stabilised by interaction with two ISD11 proteins, small acidic proteins exclusive of eukaryotes (Richards and Van Der Giezen 2006). Each ISD11 binds one ACP1 (acyl carrier protein), shown to have a regulatory function on NFS1 activity (Van Vranken et al. 2016). The catalytic Cys residue of NFS1 is localised on a flexible loop with similar structure and function as the flexible loop of the bacterial IscS (Fujishiro et al. 2017; Blahut et al. 2019). The persulfide is transferred from NFS1 to a Cys138 on the scaffold protein ISCU2 which is analogous to bacterial IscU (Fujishiro et al. 2017; Blahut et al. 2019). Crystal structures revealed that ISCU2 binds near the flexible loop of NFS1 together with FXN (Boniecki et

al., 2017; Fox et al., 2019). The *in vitro* reconstitution of purified ISC components produced a homodimer of ISCU2 with one 2Fe-2S cluster bridging two ISCU2 monomers (Webert et al., 2014). However, it is unknown how relevant this product is *in vivo.* The exact mechanism of how holo-ISCU2 is produced remains unknown. A recent study showed that the binding of Fe^{2+} to ISCU2 is essential for the transfer of sulfur (Gervason et al. 2019), yet the source of iron for ISC remains

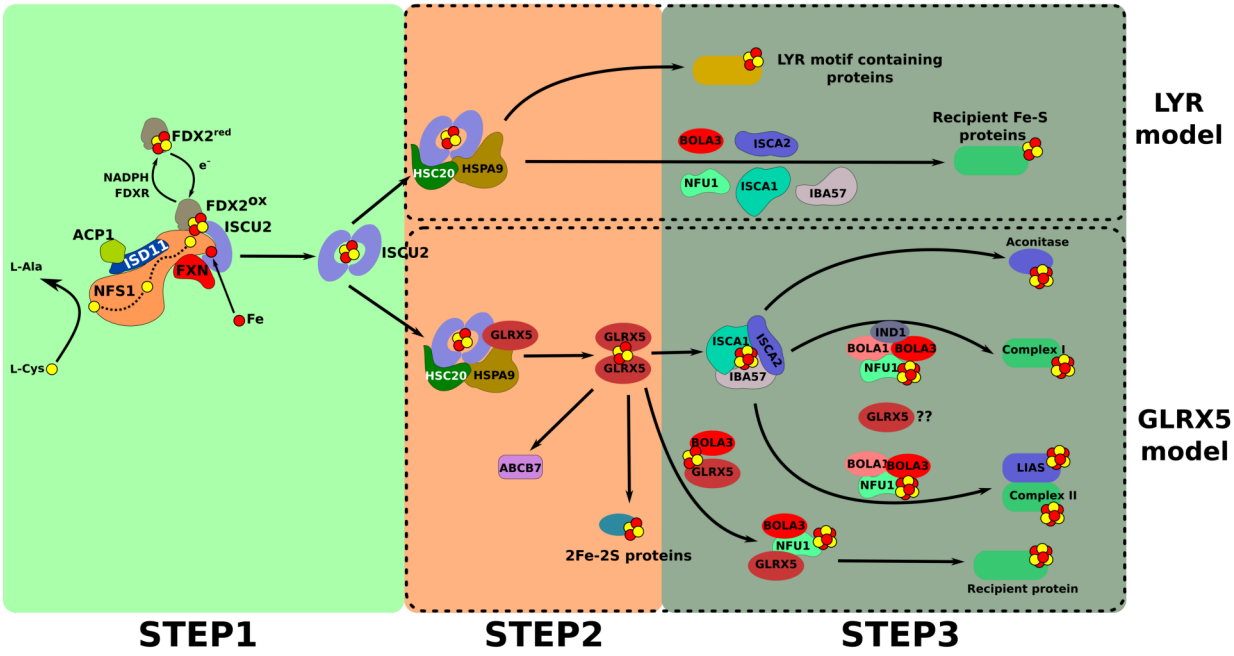

Fig. 5: Overview of mitochondrial ISC pathway.
Mitochondrial Fe-S cluster assembly can be divided into three steps. In the first step, the 2Fe-2S cluster is assembled on core the ISC complex. Firstly sulfur is released from L-cysteine by NFS1 and transferred to ISCU. In the second step, is the nascent 2Fe-2S cluster transferred from ISCU2 dimer to recipient protein. Or unknown sulfur-containing compound is transferred by ABCB7 to the cytosol. There are two proposed models for this step – the first model does not involve GLRX5 and 2Fe-2S cluster is transferred from ISCU2 dimer directly (without GLRX5) to target LYR motif-containing apoprotein. This is mediated by HSC20/HSPA9 complex which was proposed release ISCU2 from ISC core complex and HSC20 serves as guide molecule which recognizes and binds LYR motif on target recipient proteins, or can be by HSC20 mediated transfer transferred to specific carriers which will then transfer clusters to specific target apoproteins. The second model involves HSC20/HSPA9 mediated transfer of cluster from ISCU2 to GLRX5 dimer from where it is further distributed. Mitochondrial 2Fe-2S proteins will receive cluster probably directly from GLRX5. The third step involves the synthesis of a 4Fe-4S cluster by specialised ISCA1-ISCA2-IBA57 complex and its delivery to target recipient proteins. Insertion of 4Fe-4S to some proteins like aconitase does not need any additional proteins (in mammals, yeast most likely needs NFU1). However, maturation of some proteins needs specialised targeting machinery, like Complex I which for which IND1-NFU1 complex is necessary. Alternatively, 4Fe-4S cluster can be assembled on NFU1 by a combination of two 2Fe-2S clusters received from GLRX5-BOLA3 complex. Based on Braymer and Lill (2017) and Maio et al. (2014).

unknown. Furthermore, it was shown that the apo-form of ISCU2 does not have high Fe binding affinity.

The transfer of persulfide from NFS1 to ISCU2 is enhanced in the presence of FXN. In the light of this, FXN was proposed to work as an allosteric regulator of the persulfide transfer process (Tsai and Barondeau 2010; Fox et al. 2015; Gervason et al. 2019). FXN was also considered to be donor of iron for the ISC pathway thanks to its ability to bind Fe (Gerber et al. 2003; Yoon and Cowan 2003; Stemmler et al. 2010; Gentry et al. 2013; Cai, Frederick, Tonelli, et al. 2018). However, this

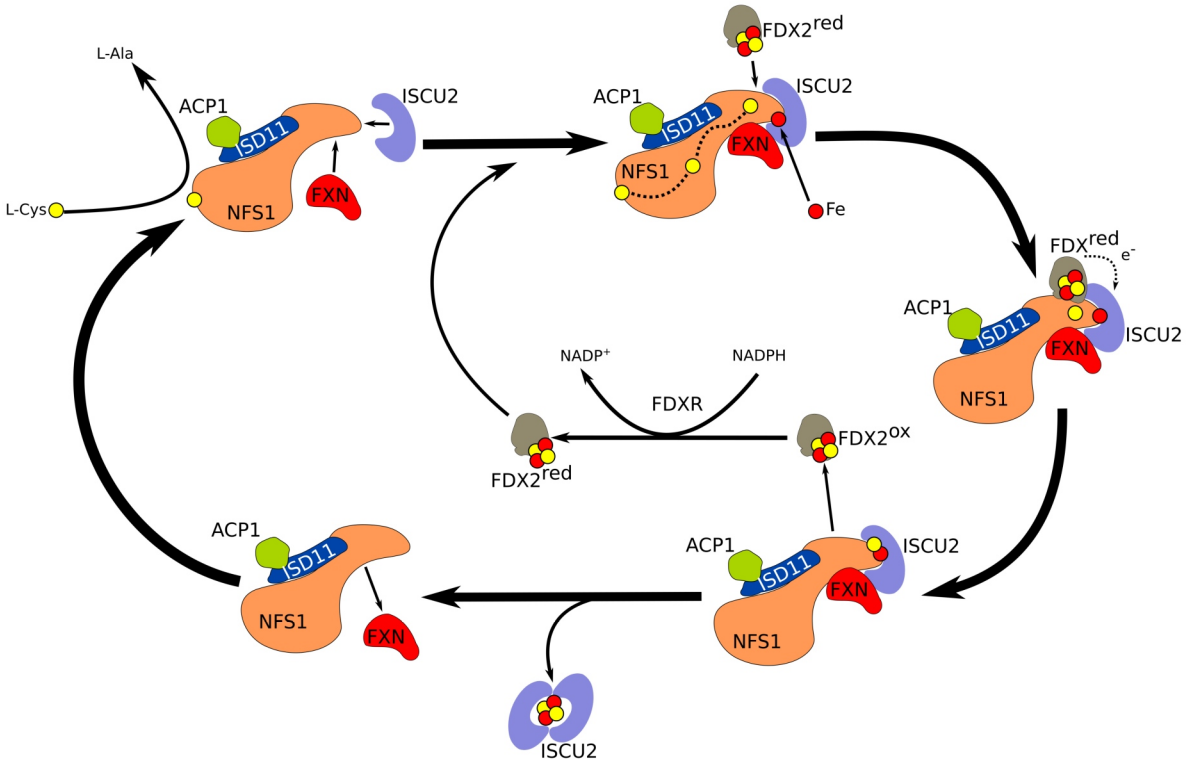

Fig. 6: Proposed mechanism of 2Fe-2S cluster assembly by ISC pathway
Proposed model for 2Fe-2S cluster assembly on core ISC complex. For better comprehensibility, only half of the complex is shown. In the first step, NFS1 converts cysteine to alanine and generates persulfide on its active site cysteine. Then persulfide is transferred to the flexible loop cysteine with the assistance of Frataxin (FXN). Upon binding of Fe to ISCU2, the NFS1 bound persulfide sulphur is transferred to one of the conserved cysteine residues of the ISCU2. Role of FXN in this reaction is not fully understood. However, it was proposed to facilitate the transfer of persulfide or provide Fe to ISU2. Reduced ferredoxin (FDX2) is the donor of electrons for reduction of persulfide to sulfide (S^{2-}) which is needed for Fe-S cluster assembly reaction. The exact mechanism of the 2Fe-2S cluster remains a mystery. After the donation of electron oxidized FDX2 dissociates from complex and is recycled to reduced form by ferredoxin oxidoreductase (FDXR). Dimer of ISCU2 with one bridging 2Fe-2S cluster is likely the final product of reaction as it shown to be the product of *in vitro* reconstitution. Based on Blanc et al. (2015).

function of FXN has been recently questioned as the N-terminal α-helix responsible for Fe^{2+} binding is not in the vicinity of the Fe-S assembly site in the cryo-EM structure of the core ISC complex (Fox et al. 2019). Ferredoxin is the donor of electrons for reduction of S^0 to S^{-2}. This is supported by fact that the 2Fe-2S cluster of FDX2 is close to the cluster synthesis site in the core ISC complex (Boniecki et al. 2017). FDX2 has higher affinity for ISCU2 when it is in reduced rather than in oxidized form, a possible explanation for the fast cycling of FDX2 between the core ISC and FAD-dependent ferredoxin reductase (Webert et al. 2014).

In the second phase, the newly synthesized cluster is released from ISCU2 by a dedicated Hsp70 chaperone system which consists of HSPA9 and HSC20 and transferred to the monothiol glutaredoxin 5 (GRX5) (Uzarska et al. 2013; Dutkiewicz and Nowak 2018) or directly to target apo-protein without involvement of GLRX5 (Maio et al. 2014). In both cases, HSPA9 binds to ISCU2 by a conserved LPPVK motif in ISCU2 and changes its conformation to loosen the binding of 2Fe-2S cluster and facilitate its transfer. However, the LPPVK motif overlaps with the binding site for FXN (Manicki et al. 2014; Boniecki et al. 2017; Fox et al. 2019) suggesting that ISCU2 must dissociate from the core ISC complex to interact with HSC20/HSPA9 complex.

In the model, which does not involve GLRX5, HSC20 was shown to bind to the LYR motif of SDHB -succinate dehydrogenase B (Fe-S cluster containing subunit of complex II) and to LYRM7 (LYR motif containing protein 7) also known as Complex III assembly factor. Similar results were also shown for respiratory complexes I and III (Maio et al. 2014; Maio and Rouault 2015; Maio and Rouault 2016; Maio et al. 2017). It was proposed that GLRX5 may act as alternative scaffold to deliver Fe-S cluster to apoprotein (Maio et al. 2014). Based on these results, it was proposed that the LYR motif may be a general motif used by HSC20 to recognize target Fe-S proteins, because also some other LYRM proteins were shown to contain Fe-S clusters (Angerer 2013; Rouault 2019). However, this model is critically reviewed by some authors as LYR motif tends to be buried deep inside of natively folded protein and therefore not accessible by HSC20. Also, in recent interactome study no interaction between HSC20 and SDHB or ACD1 was observed (Dibley et al. 2020).

The second model (studied predominantly in yeast) involves GLRX5 which belongs to the family of Fe-S clusters binding monothiol glutaredoxins (Herrero and De La Torre-Ruiz 2007; Bandyopadhyay, Gama, et al. 2008). GLRX5 binds to HSPA9/HSC20/ISCU2 complex in ATP dependent manner and Fe-S cluster is transferred to GLRX5 dimer (Banci et al. 2014; Ciofi-Baffoni et al. 2018). On the GLRX5 dimer, Fe-S cluster is bound by a conserved Cys residue (Cys 67) and a

Cys of non-covalently bound glutathione (Johansson et al. 2011). After acquisition of 2Fe-2S cluster GLRX5 transfers it to recipient proteins.

The third phase involves the conversion of the GRX5-bound 2Fe-2S cluster to a 4Fe-4S cluster and its transfer to the recipient proteins, such as respiratory complexes I and II. This step is catalysed by the set of specialised ISC proteins — Isca1, Isca2 and Iba57— for 4Fe-4S cluster synthesis, and Nfu1, Bol1, Bol3 and Ind1 for 4Fe-4S cluster delivery and insertion. ISCA1 and ISCA2, along with IBA57, form the ISA complex that has been proposed to act as a scaffold for the assembly of 4Fe-4S clusters from 2Fe-2S clusters and the delivery of the nascent 4Fe-4S cluster into a range of mitochondrial proteins (Mühlenhoff et al. 2011; Sheftel et al. 2012b).

ISCA1 and ISCA2 can physically interact with GLRX5 and their interaction leads to the transfer of 2Fe-2S cluster from GLRX5 to ISCA1 and ISCA2 (Kim et al. 2010; Mapolelo et al. 2013). *In vitro* studies in anaerobic conditions confirmed that GLRX5 can transfer a 2Fe-2S cluster to the ISCA protein, however, the formation of 4Fe-4S clusters was observed only on the ISCA1-ISCA2 heterodimer and not on individual proteins (Brancaccio et al. 2014). Alternatively, homodimeric ISCA2 can form a single 4Fe-4S cluster from 2Fe-2S clusters donated by GLRX5 (Brancaccio et al. 2017).

The crystal structure of IBA57 revealed that it forms a complex with ISCA2 but not with ISCA1, and that the IBA57-ISCA2 complex binds one 2Fe-2S cluster on its interface (Gourdoupis et al. 2018; Nasta et al. 2019). The holo IBA57-ISCA2 complex can maturate cytosolic apo-aconitase *in vitro* when DTT is present. However, ISCA1-ISCA2 complex was also shown to maturate apo-aconitase without the presence of IBA57 (Beilschmidt et al. 2017). The IBA57-ISCA2 heterocomplex is involved in formation or repairing 4Fe-4S clusters under aerobic conditions and transfer 2Fe-2S clusters to mitochondrial recipient proteins. It has been proposed that there may be two distinct ISCA1-ISCA2 and IBA57-ISCA2 pathways which work under specific conditions (Nasta et al. 2019).

NFU1 works as a homodimer which coordinates a 4Fe-4S cluster and functions in mitochondria, cytosol and plastids (Léon et al. 2003; Tong et al. 2003; Gao et al. 2013; Wachnowsky et al. 2016). Originally it was considered as an alternative scaffold protein for the ISC pathway (Tong et al. 2003) but later it was characterised as the late acting carrier required for the maturation of specific 4Fe-4S clusters proteins (Cameron et al. 2011; Navarro-Sastre et al. 2011) and was shown to deliver a 4Fe-4S cluster directly to apo-aconitase *in vitro* (Cai et al. 2016). NFU1 has a high target

specificity and is responsible for the maturation of lipoyl synthase and complex I and II of the mitochondrial respiratory chain (Cameron et al. 2011; Navarro-Sastre et al. 2011). Recently, it was also described that NFU1 can interact with 2Fe-2S carrying GLRX5-BOLA3 complex and form 4Fe-4S cluster (Nasta et al. 2020) representing alternative to ISCA1-ISCA2-IBA57 complex described from yeast.

IND1 is a p-loop ATPase responsible for the highly specific maturation of respiratory complex I (Bych, Kerscher, et al. 2008; Sheftel et al. 2009). Thanks to its high specificity, IND1 is conserved only in organisms which have complex I (Bych, Kerscher, et al. 2008). IND1 is a functional paralog of the cytosolic CFD1 and NBP35 scaffolds, harbouring a C-terminal domain containing a conserved CXXC motif which transiently binds an Fe-S cluster (Netz et al. 2007).

Involvement of the proteins from BOLA family in the ISC pathway was discovered relatively recently (Melber et al. 2016; Uzarska et al. 2016) in human and yeast. Three homologs of these proteins display different subcellular localisation. BOLA1 and BOLA3 are localised in mitochondrion whereas BOLA2 is present in the cytosol. BOLA1 and BOLA3 were shown to physically interact *in vitro* with human NFU1 and GLRX5 (Nasta et al. 2017; Gourdoupis et al. 2018), forming a heterodimer with GLRX5 that contains a 2Fe-2S cluster. Mutants of BOLA1 and BOLA3 showed mild respiratory defect caused by the lower activity of LIAS (lipoyl synthase), all of which require 4Fe-4S clusters (Melber et al. 2016; Uzarska et al. 2016; Nasta et al. 2017). The exact function of BOLA proteins is not yet fully understood.

7.2 CIA

The CIA pathway is an eukaryotic novelty present in all studied eukaryotes, with two exceptions of Nbp35 and Cia2B which actually have prokaryotic homologs (Boyd et al. 2009; Tsaousis et al. 2014). The cytosolic Fe-S cluster pathway is dependent on the mitochondrial ISC pathway (Kispal et al. 1999), which exports an unknown sulfur or iron-sulfur compound (X-S) (Biederbick et al. 2006; Pandey et al. 2019). This compound is transported by the ABC transporter Atm1 localised in the inner mitochondrial membrane (Biederbick et al. 2006; Pondarré et al. 2006). Transfer of this compound is assisted by glutathione (GSH) (Sipos et al. 2002) and Erv1 (Lange et al. 2001; Allen et al. 2005; Mesecke et al. 2005; Banci et al. 2012). *In vitro* experiments provided evidence that a 2Fe-2S cluster can be coordinated by the cysteine residue of GSH and the resulting 2Fe-2S $(GSH)_4$ complex can be transported via Atm1 to the cytosol (Li and Cowan 2015). A recent study with ^{35}S

and ^{55}Fe labelling showed that the yeast mitochondrion exports two different intermediates named by authors $(Fe\text{-}S)_{int}$ and $(S)_{int}$. $(Fe\text{-}S)_{int}$ is used for cytosolic Fe-S cluster assembly whereas $(S)_{int}$ is used for thiolation of tRNAs (Pandey et al. 2019).

The number of proteins involved in the CIA pathway differ significantly from 11 proteins (Paul and Lill 2015) in humans down to four in *Giardia intestinalis* (Pyrih et al. 2016). The CIA pathway may be divided into two steps - early acting, which assembles a 4Fe-4S cluster, and late acting involved in delivering cluster to recipient proteins in the cytosol and nucleus (**Fig. 7**).

In yeast and humans, the 4Fe-4S cluster is assembled on a Cfd1-Nbp35 heterodimer scaffold. Cfd1 and Nbp35 are P-loop NTPases which share significant similarity (Hausmann et al. 2005; Netz et al. 2007). The Nbp35-Cfd1 complex works as a heterotetramer and coordinates four 4Fe-4S clusters. Clusters in complex can be divided into two groups — labile 4Fe-4S clusters (or bridging clusters) which are bound on the C-terminus of the Cfd1-Nbp35 heterodimer interface and coordinated by conserved CXXC motifs, and stable 4Fe-4S clusters permanently bound on the conserved ferredoxin-like $CX_{13}CX_2CX_5C$ motif on the N-terminus of Nbp35. A stable 4Fe-4S cluster is

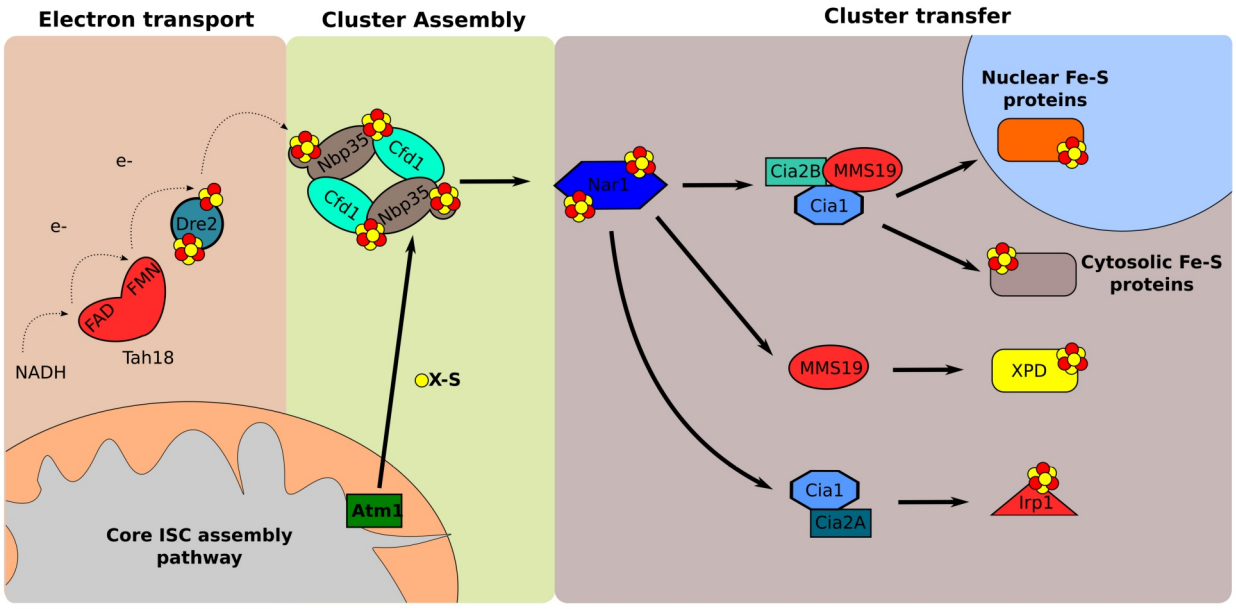

Fig. 7: Scheme of CIA pathway
The maturation of cytosolic and nuclear Fe-S proteins depends on the core ISC pathway providing sulphur compound X-S. Transporter Atm1 exports X-S into the cytosol in a glutathione-dependent way. CIA pathway then uses X-S for 4Fe-4S cluster synthesis on Cfd1-Nbp35 scaffold complex. Electrons necessary for the reaction are provided by electron transport chain consisting of flavin-oxidoreductase Tah18 and Dre2. After assembly, Cfd1-Nbp35 bound 4Fe-4S cluster is released from complex and transferred with help of Nar1 to specific targeting complexes consisting of various combination of Cia1, Cia2B, Cia2A and MMS19. Composition of targeting complexes varies for different recipient proteins. Based on Paul and Lill (2015)

essential for the function of Cfd1-Nbp35 complex (Hausmann et al. 2005; Netz et al. 2007; Netz, Pierik et al. 2012). The bridging Fe-S cluster binding is labile facilitating the rapid transfer to apoproteins. Both, Nbp35 and Cfd1 possess an ATPase domain essential but with a not yet fully understood role (Hausmann et al. 2005; Netz et al. 2007). It was shown that the Cdf1 homodimer has no measurable activity, although all domains required for NTPase activity are well conserved. The Nbp35 homodimer and Cfd1-Nbp35 heterodimer both possess ATPase activity, yet the K_m of Cdf1-Nbp35 is 10 times higher than that of Nbp35 homodimer (Camire et al. 2015). Although Cfd1 has no ATPase activity it still binds ATP with a high affinity comparable to that of Nbp35, which led to the proposal that Cfd1 may be responsible for binding of ATP, meanwhile Nbp35 activates nucleotide hydrolysis (Grossman et al., 2019). Nbp35 is present in all known eukaryotes, but Cfd1 is missing in plants and some anaerobic protists (Bych, Netz, et al. 2008; Tsaousis et al. 2014; Pyrih et al. 2016). In the case of plants, Nbp35 was shown to perform Fe-S cluster assembly without Cfd1 (Bych, Netz, et al. 2008).

Assembly of 4Fe-4S clusters on the Cfd1-Nbp35 complex is dependent on the supply of electrons, which are provided by Tah18 and Dre2 electron transfer complex (Netz et al. 2010; Brancaccio et al. 2014). Tah18 contains NADPH, FAD and FMN binding domains (Vernis et al. 2009) and transfers electrons from NADPH through the FAD and FMN to the 2Fe-2S cluster of Dre2. Dre2 has C-terminal Fe-S domain which harbours one 2Fe-2S and one 4Fe-4S cluster (Zhang et al. 2008; Netz et al. 2010; Netz et al. 2016) and an *S*-adenosylmethionine methyltransferase-like domain with an unknown function.

After assembly on the Cfd1-Nbp35 scaffold the cluster is transferred onto Nar1, an iron-only hydrogenase-like Fe-S protein, which acts as intermediate transfer protein and delivers 4Fe-4S cluster to the CIA targeting complexes (Balk et al. 2004; Urzica et al. 2009) or delivers them directly to recipient proteins.

Proteins Cia1, Cia2A, Cia2B and MMS19 act during the late targeting phase of cytosolic Fe-S cluster assembly. These four proteins interact together to form various targeting complexes, which deliver Fe-S clusters to target recipient proteins (Srinivasan et al. 2007; Gari et al. 2012; Stehling et al. 2012; Stehling et al. 2013; Odermatt and Gari 2017).

Cia1 is WD40-repeat containing protein which interacts with Nar1 and receives an Fe-S cluster from it (Balk et al. 2005). MMS19 contains nine HEAT repeats distributed through the whole protein. The HEAT repeats on C-terminus were shown to be responsible for the interaction with

Cia2B, and Cia1 bind to the C-terminus of MMS19, resulting in a complex that has a binding site for Fe-S clusters on the connecting interface between subunits (Odermatt and Gari 2017). MMS19 was shown to interact with nuclease Dna2 and Rli1 and its downregulation affected proteins involved in DNA metabolism such as XPD and a number of DNA polymerases and helicases (Gari et al. 2012; Stehling et al. 2012). The presence of three subunits Cia1, Cia2B and MMS19 was necessary for the binding of most recipient Fe-S proteins, with exception of XPD, for which just MMS19 is sufficient (Odermatt and Gari 2017). Therefore, Cia2B and MMS19 were proposed to form a docking site for Fe-S proteins. Cia1-Cia2B-MMS19 complex was shown to be involved in the maturation of most nuclear Fe-S cluster proteins and the second complex Cia1-Cia2A seems to be dedicated to the maturation of Irp1 and the stabilisation of Irp2 which are responsible for maintaining iron homeostasis in cell (Stehling et al., 2013).

7.3 Fe-S cluster assembly in anaerobic protists

Fe-S cluster assembly is mostly studied in model organisms in eukaryotes represented by humans and yeast, both of which represent opisthokonts with aerobic lifestyle. However, very little is known about Fe-S cluster assembly in anaerobic protists, which contain reduced mitochondrion related organelles (MROs). MROs are generally divided into 5 groups (Muller et al. 2012) based on their energetic metabolism. However, this classification is artificial, and many MROs blur boundaries between the established classes creating a continuum of organelles without clear borders between types (Leger et al. 2017). Almost all MROs contain the ISC pathway including the hydrogenosomes of *Trichomonas vaginalis* (Tachezy et al. 2001; Sutak et al. 2004), and those of anaerobic ciliates (Lewis et al. 2019) and anaerobic fungi (Kameshwar and Qin 2018); as well as mitosomes of *Giardia intestinalis* (Tovar et al. 2003), *Cryptosporidium* spp. (Miller et al. 2018a) and some *Microsporidia* (Katinka et al. 2001; Goldberg et al. 2008; Freibert et al. 2017). The ISC pathway has been proposed to be the only essential pathway of these organelles and the only reason for their retention (Williams et al., 2002).

Most of the data on Fe-S cluster assembly pathways is known from genomic projects and most of the organisms have not been assessed by biochemical or molecular biology methods. In this chapter, the Fe-S cluster assembly in anaerobic protists will be briefly reviewed (Table 1).

7.3.1 Fe-S cluster assembly in MROs of anaerobic parasites and symbionts

Hydrogenosomes and mitosomes are anaerobic forms of mitochondria which have evolved several times independently from aerobic ancestors (Stehling et al. 2013; Roger et al. 2017) and are therefore of α-proteobacterial origin (Embley et al. 1995; Yarlett and Hackstein 2005; Lewis et al. 2019). Virtually all known hydrogenosomes and mitosomes, with few notable exceptions, contain version of ISC pathway, which consistently of α-proteobacterial origin as well (Gray 2012; Wang and Wu 2015).

Trichomonas vaginalis

Hydrogenosomes were first described in *Tritrichomonas foetus* (Lindmark & Müller, 1973) and since then they have been described in several other lineages of protists. They have been mostly studied in parabasalids, especially trichomonads, as these organisms are of great medical and veterinary importance. Hydrogenosomes are characteristic by their production of H_2 and contain pathways involved in energy metabolism. There is relatively little known about the Fe-S cluster assembly in these organelles. The genome of *T. vaginalis* harbours IscU, two copies of IscS, Isd11 and Fxn, seven copies of 2Fe-2S Fdx, three copies of IscA2, four copies of Nfu and two homologs of HscB (Tachezy et al. 2001; Sutak et al. 2004; Dolezal et al. 2007; Schneider et al. 2011; Beltrán et al. 2013). Frataxin of *T. vaginalis* was shown to be targeted to the hydrogenosome and partially complements its homolog in *S. cerevisiae* (Dolezal et al. 2007). The hydrogenosomal localisation of IscS was confirmed by immunofluorescence microscopy (Sutak et al. 2004). Concerning CIA pathway it lacks the Tah18/Dre2 complex and Mms19, and contains Cfd1, Nbp35, Nar1, Cia1 and Cia2B (Pyrih et al. 2016).

Spironucleus salmonicida

Spironucleus salmonicida bears hydrogenosome with reduced ISC pathway. So far IscS, IscU, Nfu, Fxn, two Fdxs and HscB, have been identified to contain N-terminal targeting sequence and were localised to this hydrogenosome by immunofluorescence microscopy (Jerlström-Hultqvist et al. 2013). Sequence of selenophosphate synthetase fused with NifS was also found in its genome (Xu et al. 2014). However, localisation and function of this protein remains unknown. Components of the CIA pathway — Nbp35, Nar1, Cia1, and Cia2 were also found in the *S. salmonicida* genome (Pyrih et al. 2016).

Giardia intestinalis

Giardia intestinalis mitosomes contain the essential components of the ISC pathway. IscU and IscS were localised to the mitosome by immunofluorescence and immunoelectron microscopy (Tovar et al. 2003). Later, 2Fe-2S ferredoxin was localised into the mitosome of *G. intestinalis* followed by IscA, Nfu, Hsp70 (HscA), and Jac1 (HscB) (Jedelský et al. 2011). *G. intestinalis* CIA pathway consists of only four proteins, Nbp35 (three copies), Cia1, Cia2 and Nar1, with the mitochondrial transporter Atm1 missing together with associated protein Erv1, as well as electron transport chain components Dre2/Tah18. Interestingly Cia2 was shown to have a dual localisation between the cytosol and the intermembrane space of the mitosome, with the majority of the protein localised in the intermembrane space. It has been hypothesized that this protein may be involved in the transport of X-S to cytosol. Nbp35 was also shown to have dual localisation - two copies are associated with outer mitochondrial membrane (Nbp35-1 and Nbp35-2) and third copy displays cytosolic localisation (Pyrih et al. 2016). Recently Bol-A like proteins were also identified in *G. intestinalis* (Xu et al. 2020), as well as a novel mitosomal NADPH-dependent diflavin oxidoreductase termed GiOR-1. The original hypothesis was that this protein utilizes NADPH for the reduction of mitosomal ferredoxin; however, it was shown that it can reduce various other electron acceptors like cytochrome b_5 but not the ferredoxin (Jedelský et al. 2011).

Anaerobic ciliates

Anaerobic ciliates also contain hydrogen producing MROs which are often associated with endosymbiotic methanogenic bacteria (Fenchel and Finlay 1991; Embley et al. 1992; Finlay and Fenchel 1996). Organelles of these organisms are much less studied than MROs of trichomonads or anaerobic fungi. Study of partial genome of and mtDNA genome of *N. ovalis* revealed presence of mitochondrial ferredoxin, but no other component of ISC pathway was detected due to limited data availability (de Graaf et al. 2011). Recent study detected almost complete ISC pathways in single-cell transcriptomes of *Cyclidium porcatum*, *Metopus contortus* and *Plagiopyla frontata* (Lewis et al. 2019). Also some mitochondrial Fe-S proteins including ferredoxin, SdhB, and several subunits of complex I were detected. Atm1 is also present in all three species (for complete list of identified ISC proteins see Table 1).

Anaerobic fungi

Anaerobic fungi like *Neocallimastix* and *Piromyces* from the gastrointestinal tract of many herbivorous mammals also contain hydrogenosomes (de Graaf et al. 2011). ISC proteins IscU, IscA, IscS, ferredoxin and chaperones Hsp70, Hsp60, Hsp10 were found in genomes of *Anaeromyces robustus, Neocallimastix californiae* G1, *Orpinomyces* sp., *Piromyces finnis* and *Piromyces* sp. E2 (Kameshwar and Qin 2018). The genome of *Orpinomyces* sp. C1A contains the ISC pathway genes IscS, IscU, IscA, Isa1, Isa2, Fxn, ferredoxin, Hsp70 (HscA), Jac1 (HscB), Grx4 and Atm1 and Erv1 from export machinery. Also, four genes of CIA pathway (Nbp35, Cfd1, Cia1, and Nar1) were accounted in this genome (Youssef et al. 2013).

Microsporidia

Analysis of genome sequences of microsporidian parasites *Encephalitozoon cuniculi* (Katinka et al. 2001) and *Trachipleistophora hominis* (Heinz et al. 2012) revealed that the core ISC machinery is conserved in these organisms. The mitosomal localization of ISC proteins was confirmed by immunofluorescent microscopy of IscS, IscU, and frataxin in *E. cuniculi*. However, parallel experiments with *T. hominis* confirmed IscS localisation in mitosomes while IscU and frataxin localized to the cytosol (Goldberg et al. 2008). Later experiments showed mitosomal localisation for all these proteins, which were further confirmed by biochemical analysis of mitosome-enriched fractions isolated from *T. hominis* infected rabbit kidney cells (Freibert et al. 2017). Complementation experiments in yeast showed that *T. hominis* IscU and Isd11 were able to fully complement its homologs in yeast (Freibert et al. 2017). From the export machinery, three candidates for Atm1, sulfhydryl oxidase (Erv) as well as two genes for enzymes of glutathione synthesis pathway were identified in the genome of *T. hominis*. Identified Erv is most likely Erv2, which is associated with endoplasmic reticulum, while mitochondrial Erv1 seems to be missing. *In vitro* experiments revealed that *T. hominis* IscS-Isd11, IscU, Fdx and Fxn with human recombinant FdxR were able to create 2Fe-2S cluster on IscU (Freibert et al. 2017).

The CIA pathway of microsporidia is rather complete in *T. hominis* and *E. cuniculi*. It consists of eight proteins: Cfd1, Nbp35, Nar1, Grx3, Cia1, Cia2 and Dre2/Tah18 complex (Freibert et al. 2017). Both *E. cuniculi* and *T. hominis* Cfd1-Nbp35 contain the conserved cysteine residues shown to coordinate the Fe-S clusters of this complex. Genes for Cfd1, Nbp35, Nar1 and Cia1 of *T. hominis* were tested for their ability to rescue the growth of the respective yeast CIA depletion mutants. However, none of the tested genes showed any positive results (Freibert et al. 2017).

***Cryptosporidium* spp.**

Cryptosporidium parvum was shown to contain a double membrane organelle of mitochondrial origin that lacks genome (Šlapeta and Keithly 2004). Mitosomes from the most studied cryptosporidium species, *Cryptosporidium parvum*, contain IscS, IscU, Fxn, HscA, HscB, Fdx, Ind1, Grx5 and Atm1 (Miller et al. 2018b). Heterologous localisation of GFP with N-terminal targeting sequences from *C. parvum* IscS and IscU were shown to localise to the mitochondrion of yeast (LaGier et al. 2003). This was further confirmed by localisation with specific antibodies, hence demonstrating mitosomal localisation of IscU, IscS and Fxn in *C. parvum* sporozoites and merozoites. The same study also showed that *C. parvum* IscS can functionally replace its yeast homolog. Interestingly, the immunofluorescent localisation experiments were inconsistent in the localization pattern of the ISC proteins during the different life cycle stages of *C. parvum* infection. Authors of the study offered two potential explanations for this phenomenon: either the ISC machinery is translocated to the cytosol in various life cycle stages of *Cryptosporidium*, or there are morphological changes of *Cryptosporidium* mitosomes in later stages of parasites (Miller et al. 2018a). From the CIA pathway, four genes were identified in *C. parvum* — Nar1, Nbp35, Cfd1, and Cia1 (Stejskal et al. 2003; Ali and Nozaki 2013), yet no other functional data are available.

Mikrocytos mackini

Mikrocytos mackini is a parasite of oysters belonging to Rhizaria. It was initially proposed to be an amitochondriate organism, as transmission electron microscopy did not reveal any MRO (Hine et al. 2001). However, analysis of *M. mackini* partial transcriptome revealed four ISC candidates, IscU, IscS, mtHsp70 (HscA), and FdxR all of which contain predictable N-terminal sequences (Burki et al. 2013). No other mitochondrial components were identified. Based on this analysis, it has been hypothesised that *M. mackini* possess mitosomes. Although more experimental data and genomic or transcriptomic sequences will be required for the precise characterisation of this organelle.

7.3.2 Fe-S cluster assembly in MROs of free-living anaerobes

In the chapters above, MROs of parasitic organisms were discussed due to the intense studies on these species, owing to their medical and economical importance. In the following paragraphs free-living anaerobes will be briefly discussed as there is less information available about their Fe-S cluster assembly.

The free-living members of Fornicata contain MROs morphologically similar to the hydrogenosomes of *T. vaginalis* (Park et al. 2009; Kolisko et al. 2010; Park et al. 2010; Yubuki et al. 2013; Yubuki et al. 2016). Several members of Fornicata have been examined for the presence of ISC pathway, namely *Carpediemonas membranifera*, *Chilomastix cuspidata*, *Dysnectes brevis*, *Ergobibamus cyprinoides*, and *Trepomonas* PC1, and have been shown to contain IscS, IscU and mtHsp70 in their genomes or transcriptomes (Leger et al. 2017). A little bit more is known about *Kipferlia bialata* whose genome contains IscS, IscU, IscA, Fxn, HscB, HscA and GrpE (nucleotide exchange factor which enhances activity of HscA/HscB). Furthermore IscU, IscS, HscA and GrpE bear predicted mitochondrial N-terminal targeting sequences (Tanifuji et al. 2018). The CIA pathway has been studied only in Metamonada where it seems to be reduced to four proteins: Cia1 (with the exception of *Spironucleus vortens*), Nar1, Cia2 and Nbp35 (Pyrih et al. 2016).

Some anaerobically living members of Heterolobosea like *Sawyeria marylandensis* (O'Kelly et al. 2003), *Psalteriomonas lanterna*, *Monopylocystis visvesvarai* (O'Kelly et al. 2003) and *Creneis carolina* (Pánek et al. 2014), are found mostly in low oxygen conditions and carry the MROs morphologically resembling hydrogenosomes. There are almost no studies of these organisms which would go beyond light or electron microscopy. Therefore, there is very little information about their Fe-S cluster assembly. Two exceptions to this are *Sawyeria marylandensis* and *Psalteriemonas lanterna* which were reported to contain hydrogenosomes. In ESTs (expressed sequence tags) of *S. marylandensis*, the ISC pathway genes IscS, IscU and frataxin were found, meanwhile in *P. lanterna* only IscS has been reported (Barberà et al., 2010). Nothing is known about the CIA pathway in these organisms as all studies have been focused on MROs.

Microaerophilic cercomonad (Rhizaria) *Brevimastigomonas motovehiculus* contains a metabolically versatile MRO which is probably in transitional state between mitochondrion and hydrogenosome. In *B. motovehiculus*, a fairly complete set of ISC genes has been found, and based on the presence of N-terminal targeting sequence on them, they are believed to be localised to the MRO (Gawryluk et al., 2016).

In the free-living anaerobic stramenopile *Cantina marsupialis*, transcripts for the components of the Fe-S cluster assembly machinery, IscS, IscU, Isa2, Fxn, Grx, HscB and Ind1 were identified and proposed to be localised in its MRO (Noguchi et al. 2015). Another free-living stramenopile *Lenisia limosa* (Hamann et al. 2016) also contains genes coding for ISC components in its genome assembly (NCBI BioProject PRJNA277740).

7.3.3 FeS cluster assembly in *Entamoeba histolytica* and *Mastigamoeba balamuthi*

In Archamoebae the canonical ISC machinery was replaced by the NIF system. This was first described in the human parasite *Entamoeba histolytica* (Ali et al. 2004), however, later it was found also in other species of genus *Entamoeba* such as *Entamoeba invadens*, *Entamoeba moshkovski* and *Entamoeba nuttalli*. It is also present in the free-living *Mastigamoeba balamuthi* (Nyvltova et al. 2013), which is closely related to *Entamoeba histolytica*.

It was shown that this system consists of two proteins NifS and NifU and both proteins were shown to complement their homologs in bacteria (Ali et al. 2004). Phylogenetic analysis showed that the NIF pathway of *Archamoebae* was acquired by lateral gene transfer from ε -proteobacteria (Gill et al. 2007). Analysis of NifS and NifU sequences from *E. histolytica* did not reveal any recognisable N-terminal targeting sequences (Van Der Giezen et al. 2004) rising questions about localisation of this pathway in *E. histolytica*. The first experiments with localisation of the NIF pathway suggested a dual localisation between cytosol and mitosome (Maralikova et al. 2010). However, dual localisation was not confirmed neither by proteomic analysis (Mi-ichi et al. 2009) nor other studies (Dolezal et al. 2010; Nyvltova et al. 2013). The genome of *M. balamuthi* contains two sets of NIF components from which one was localised to cytosol and the second one to the MRO (Nyvltova et al. 2013).

Entamoeba histolytica contains five CIA components, namely Cfd1, Nbp35, Nar1, Dre2 and Cia1 (Ali and Nozaki 2013). Similarly, the genome of *Mastigamoeba balamuthi* contains genes for Cfd1, Nbp35, Nar1 and Cia1 of the CIA pathway (Nyvltova et al., 2013). The genomes of both *E. histolytica* and *M. balamuthi* also contain Cia2, however, it was not reported by the previously mentioned studies. It was demonstrated that Cfd1 and Nbp35 of *E. histolytica* can form a complex both *in vivo* and *in vitro,* and it was proposed that CIA may interact with the cytosolic NIF system to maturate cytosolic Fe-S proteins (Anwar et al. 2014) yet there is no direct evidence for this hypothesis.

7.3.4 SUF system in protists without plastids

In recent years, the SUF system was discovered in protists which apparently have not possessed plastids during their evolution. The first such organism is *Blastocystis hominis* (Tsaousis et al.

2012). This obligatory anaerobic stramenopile living in intestines contains anaerobic mitochondria together with the ISC pathway (Stechmann et al. 2008). However, additional proteins for the Fe-S cluster assembly belonging to SUF pathway were found. Identified proteins SufB and SufC, appeared to be fused into one protein. Localisation of these proteins by specific antibodies showed that they localise to the cytosol. Functional characterization of SufCB of *B. hominis* showed that the protein displays ATPase activity and may bind a 4Fe-4S cluster. Furthermore, it is upregulated under oxidative stress (Tsaousis et al. 2012). The CIA pathway of *B. hominis* consists of Cia1, Cia2, MMS19, Nbp35, Nar1, and also a divergent putative Tah18 (Tsaousis et al. 2014).

Another fusion of SufB and SufC genes was also found in the free-living anaerobic breviate *Pygsuia biforma* (Stairs et al. 2014). *P. biforma* contains two versions of SufCB, one localised in the mitochondrion and a second one in cytosol. In contrast to *B. hominis*, the only components of the ISC found in *P. biforma* were Nfu1 and Ind1. Interestingly, the cysteine desulfurase is missing from this organism. Although an IscS-like domain is fused with a 4-thiouridine biosynthesis protein was found in *P. biforma*, the lack of mitochondrial targeting sequence and its evolutionary origin, which differs from that of the from mitochondrial IscS, suggests that it is not involved in Fe-S cluster assembly in the MRO of *P. biforma*. Therefore, the source of sulfur for Fe-S cluster assembly in *P. biforma* remains a mystery (Stairs et al. 2014). From the CIA pathway genes, Nbp35, Cfd1, Nar1, Cia1, Cia2, and Met18 were identified in the transcriptome of *P. biforma* (Stairs et al. 2014).

A fusion gene SufCB was also found in the jakobid *Stygiella incarcerata* (Leger et al. 2016). It lacks any recognisable mitochondrial N-terminal targeting sequence and was therefore proposed to be localised to the cytosol. *S. incarcerata* also contains an ISC pathway localised in its MRO. The genes for IscS, IscU, Isa1 and Isa2, Fxn, Fdx, Grx5, HscA, Nfu and Atm1 were accounted in this transcriptome. The same fusion of SUF genes were also found in the transcriptome of the closely related *Velundella trypanoides* (Leger et al. 2016) Lastly, a SufCB fusion gene was found in the transcriptome of *Proteromonas lacertae,* a stramenopile closely related to *Blastocystis* (Tsaousis 2019).

Several phylogenetic analyses of SufB and SufC genes showed that *P. biforma*, *S. incarcerata* and *B. hominis* genes form a strongly supported clade sister to Methanomicrobiales (Tsaousis et al. 2012; Stairs et al. 2014; Leger et al. 2016). This suggests that these Suf genes were acquired from this group of Archaea independently from the SUF system found in plastids, which is of cyanobacterial origin. The patchy distribution of this novel pathway in the eukaryotic tree gave origin to three possible theories: 1) SufCB fusion was acquired independently by each organism or

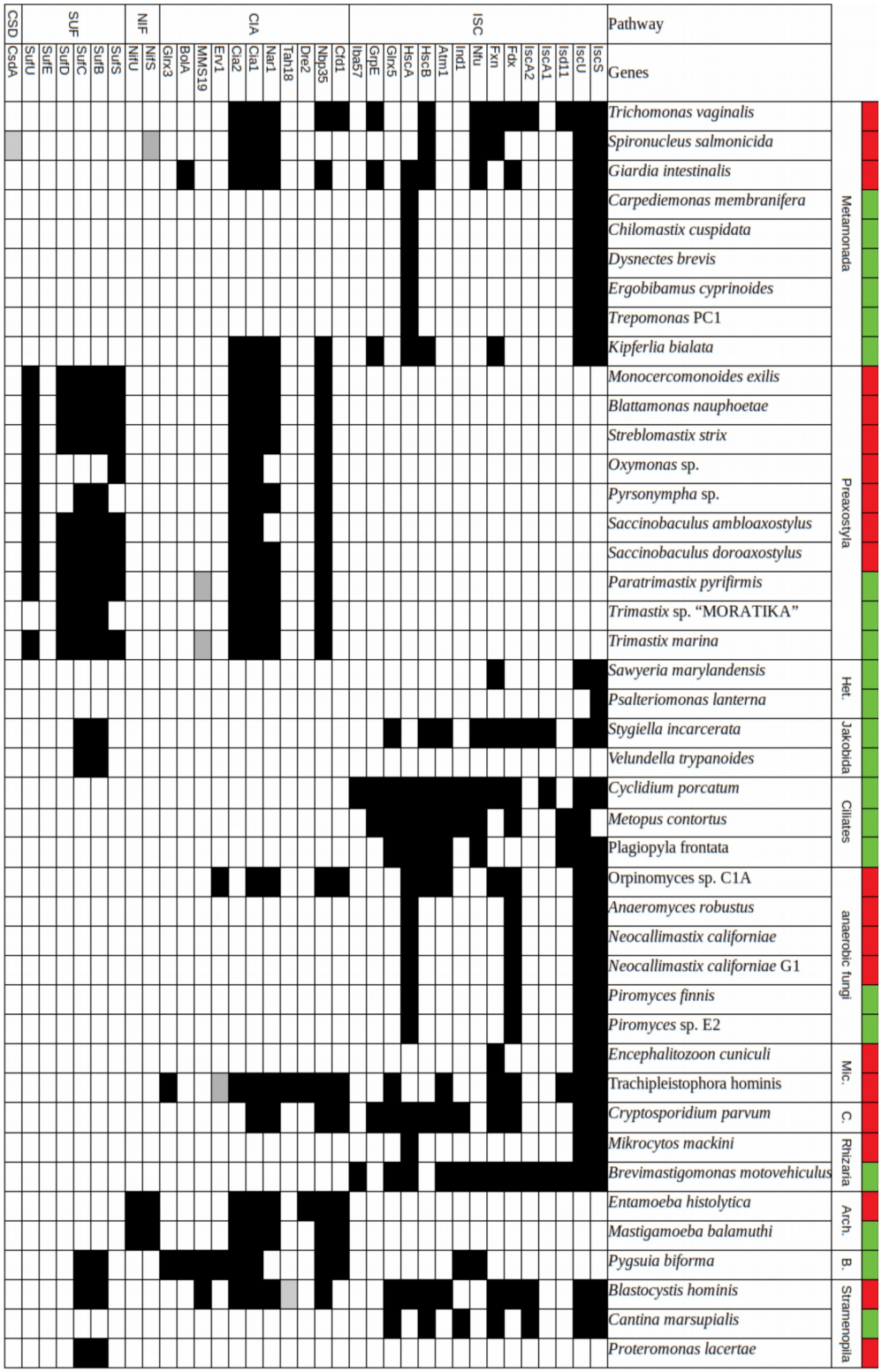

Table 1: Inventory of Fe-S cluster assembly genes in anaerobic protists
Genes identified in organism are marked in black. Grey indicates divergent genes with unknown function. Free-living organisms have green bar over their name and endobiotic have red bar. Het. = Heterolobosea, Mic. = Microsporidia, C. = Cryptosporidium, Arch. = Archamoebae, B. = Breviatea

its ancestor (at least three independent acquisitions); 2) SufCB was acquired once by one of these eukaryotes and then was transferred laterally to other species; and 3) SUF pathway was present already in LECA and then was lost in the majority of other organisms (Tsaousis 2019).

8 Preaxostyla

Preaxostyla are a group of anaerobic flagellates protists which are part of Metamonada (Hampl et al. 2009; Adl et al. 2019). They are named after preaxostyle - lattice-like cytoskeleton structure connecting two pairs of basal bodies. Preaxostyla are a sister group to Parabasalia and Fornicata and consists of three monophyletic groups — free-living Trimastigidae and Paratrimastigidae and endobiotic Oxymonadida (Zhang et al. 2015).

There is relatively little information available about this group of protists. Before the paper published as a part of this thesis, most of the studies of Preaxostyla were aimed to the description of new species, or phylogeny and morphology, and there are only a few studies which deal with molecular biology of these organisms (Keeling and Leander 2003; Liapounova et al. 2006; Slamovits and Keeling 2006a; Slamovits and Keeling 2006b).

8.1 Free-living Preaxostyla

Trimastigidae and Paratrimastigidae are free-living anaerobic or microaerophilic flagellates living in freshwater or seawater sediments. They bear a classical excavate morphology — four flagella and *a* feeding groove on the ventral side of the cell. In contrast to oxymonads, the Golgi apparatus is well-developed and they contain MROs resembling hydrogenosomes (Simpson 2003; Zhang et al. 2015). Little was known about these organelles before publishing papers that compose this thesis. 19 genes possibly associated with MROs were found in ESTs of *Paratrimastix pyriformis* (Hampl et al. 2008), of which three — Tom40, Cpn60, and MPP subunit α were part of the mitochondrial import machinery. No genes associated with Fe-S cluster assembly were found.

8.2 Oxymonadida

Oxymonads are endobiotic, typically inhabiting the gut of insects, with the largest diversity found in lower termites and wood-eating cockroaches of the genus *Cryptocercus* (Hampl 2017). Alternatively, some species of oxymonads may also be found in the intestines of vertebrates.

Recently, several new species were described including first potentially free-living species of oxymonads (Treitli et al. 2018). The morphology of oxymonads, in contrast to that of free-living Preaxostyla, does not bear all the typical excavate features and it differs greatly between species (Simpson et al. 2002). Despite being intensively studied by TEM microscopy, neither stacked Golgi, peroxisomes nor MROs were found, with the possible exception of *Saccinobaculus doroaxostylus*, where a large, probably double-membrane-bounded organelle resembling hydrogenosomes, has been reported (Carpenter et al. 2008).

Oxymonads are often involved in symbiosis with bacteria either on their surface (Noda et al. 2006), in their cytoplasm (Stingl et al. 2005; Yang et al. 2005) or in their nucleus (Sato et al. 2014). In some cases they even evolved distinct structures proposed facilitate attachment of prokaryotes on the surface of protists (Leander and Keeling 2004). They have been proposed to have a mutualistic relationship with their termite host and are probably involved in the digestion of cellulose, like parabasalids (Li et al. 2005; Brune and Ohkuma 2010; Ohkuma and Brune 2011). Large oxymonads such as *Pyrsonympha*, *Oxymonas* and *Microrhopalodina* have been shown to ingest and degrade wood (Carpenter et al. 2013), yet the production of cellulolytic enzymes has not been experimentally confirmed in oxymonads so far. Smaller oxymonads may not necessarily be involved in cellulose digestion (Radek 1999).

Recently single cell metagenomics revealed that *Streblomastix strix* is indirectly involved in digestion of cellulose in the hindgut of the termite *Zootermopsis angusticollis* (Treitli et al. 2019). S. *strix* itself does not produce any glycosyl hydrolases, however, its associated Bacteroidetes ectosymbionts were shown to express a wide range of these enzymes (Treitli et al. 2019).

Little was known about the molecular biology of these protists before papers incorporated in this thesis, except for the study of the glycolytic pathway of *Monocercomonoides* sp. (Liapounova et al., 2006) and two works identifying proteolytic enzymes in *S. strix* and *Monocercomonoides* sp. (Dacks et al., 2008). Also, oxymonads *S. strix* (Keeling and Leander 2003) and an unidentified oxymonad from the family *Polymastigidae* (de Koning et al. 2007) were shown to use non-canonical genetic code, in which only TGA serves as a stop codon, while the other two canonical stop-codons encode glutamine. *S. strix* was also shown to have a relatively high density of spliceosomal introns (Slamovits and Keeling 2006a).

9 Aims of thesis

- Search for mitochondrion related genes in the genomic and transcriptomic data of *Monocercomonoides exilis*.
- Localize SUF pathway of *Monocercomonoides exilis* in heterologous systems.
- Find and characterize Fe-S cluster assembly proteins in available genomes and transcriptomes of Preaxostyla and resolve their evolutionary history.
- Predict and annotate Fe-S cluster proteins in *M. exilis* and compare them to other closely related protists to elucidate if change of Fe-S cluster pathway influenced inventory of Fe-S cluster proteins.
- Confirm functionality of SUF proteins of *M. exilis* by complementation experiments in *E. coli.*

10 Summary

Oxymonads are the last large group of protists which no MRO was identified, despite the fact that they were studied quite intensively by TEM in the past. Also, more recent studies of *M. exilis* did not identify any morphological traces of MRO including thorough search with the use of classical TEM and FIB-SEM Tomography (focused ion beam scanning electron microscopy) (Treitli et al. 2018; Karnkowska et al. 2019)

10.1 *Monocercomonoides exilis* genome

To definitely answer the question “Does oxymonads have mitochondrion or not?” we sequenced genome of *Monocercomonoides exilis* by 454 whole genome shotgun method (Karnkowska et al. 2016). Sequencing resulted in fairly complete genome consisting of 2095 scaffolds giving together approximately 75 Mb with average coverage 35x. Completeness of the genome was estimated by CEGMA (Core Eukaryotic Genes Mapping Approach) (Parra et al. 2007) which identified presence 63.3% of core eukaryotic genes and after removing of mitochondrial genes and using manually curated *M. exilis* gene model estimated completeness increased to 90%. Furthermore we were able to identify 77 out of 78 conserved families of cytosolic eukaryotic ribosomal proteins (Lecompte et al. 2002). Automatic gene prediction resulted in 16 629 predicted proteins. Genes contain surprisingly high number of introns compared to genomes of other sequenced metamonads - more than 67% genes contain introns and average intron content is 1.9 per gene. As expected, we were not able to identify any mtDNA in the assembly, which is in concordance with the results from other metamonads whose MROs lacks mtDNA.

10.2 Search for mitochondrion related genes

Search for the mitochondrion related genes was performed by BLAST and HMMER with MitoMiner (Smith et al. 2012) based reference set containing 12,925 proteins taken from 11 eukaryotic mitochondrial proteomes, which was further enriched with MRO localised proteins of *E. histolytica*, *G. intestinalis*, *P. biforma*, *S. salmonicida*, *T. vaginalis*, and *P. pyriformis.* However, we were not able to identify any specifically mitochondrial genes in the genome including translocases of inner (TIM) and outer (TOM) membrane, which are otherwise present in all known MROs including highly reduced mitosomes of *G. intestinalis* and *E. histolytica* (Dolezal et al. 2010;

Zarsky et al. 2012). Also, we were not able to identify any components of mitochondrial ISC pathway which is considered to be the only essential function of MROs and is present in virtually all known MROs, with few previously described exceptions.

10.3 Fe-S cluster assembly in *M. exilis*

Instead of the ISC pathway, which is missing, we were able to identify genes of SUF pathway for Fe-S cluster assembly. In eukaryotes, the SUF pathway is limited to plastids and few protists like *P. biforma, S. incarcerata* (Stairs et al. 2014) or *B. hominis* (Tsaousis et al. 2012). *The* SUF pathway of *M. exilis* consists from five genes SufB, SufC, SufD, SufS, and SufU. Interestingly, last three genes are fused into one SufDSU gene. Up to the date, this fusion is unique and is known only from Preaxostyla. SUFs are *bona fide* genes of *M. exilis* and not the bacterial contamination, as we have

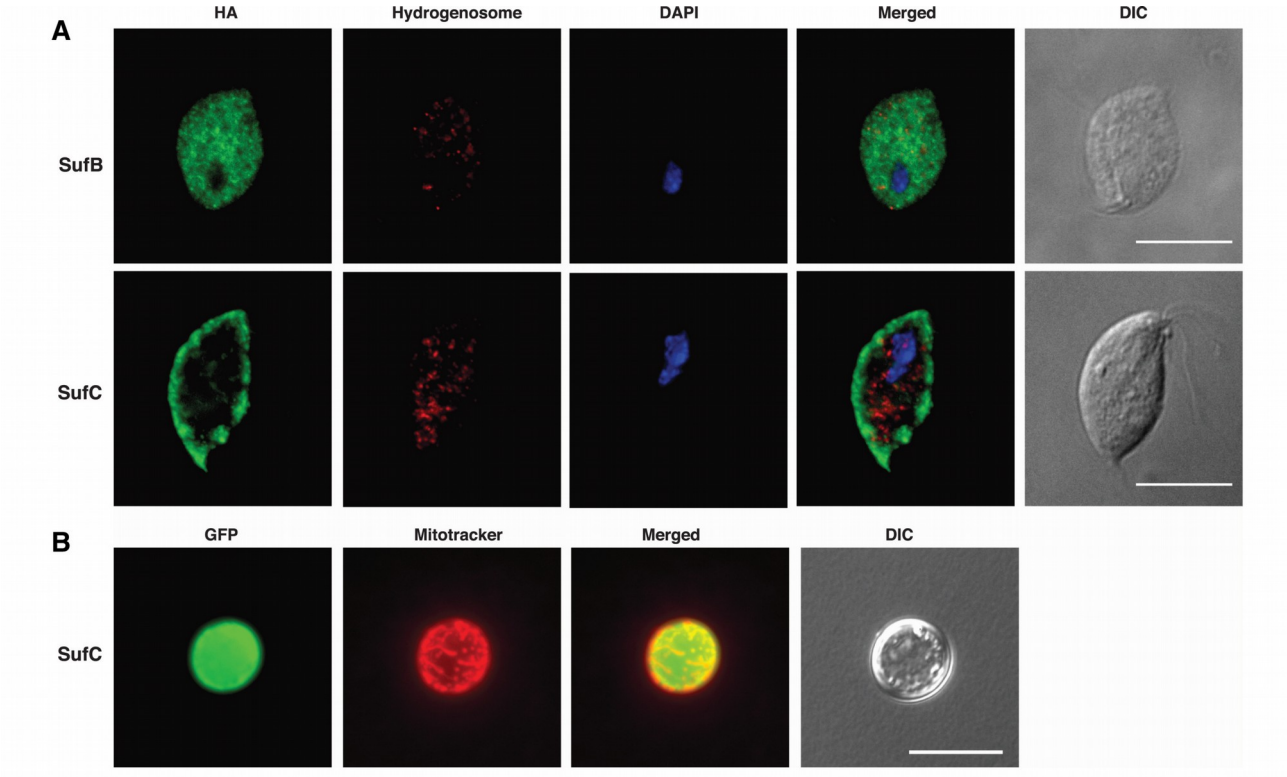

Fig. 8: Heterologous localisation of SufB and SufC
(**A**) Heterologous expression of *M. exilis* SufB and SufC proteins in *T. vaginalis*. *M. exilis* proteins with a C-terminal HA tag were expressed in T. vaginalis and visualised by an anti-HA antibody (GREEN). The signal of the anti-HA antibody does not co-localise with hydrogenosomes stained using an anti-malic enzyme antibody (RED). The nucleus was stained using DAPI (BLUE). Scale bar, 10 nm. (**B**) Heterologous expression of *M. exilis* SufC protein in *S. cerevisiae*. *M. exilis* proteins tagged with GFP were expressed in *S. cerevisiae* (GREEN). The GFP signal does not co-localise with the yeast mitochondria stained by Mitotracker (RED). Scale bar, 10 nm (Karnkowska et al. 2016).

shown that FISH probes, which localised genes for SufB, SufC and SufDSU, to the nucleus of *M. exilis*. None of the SUF genes has any recognisable N-terminal targeting sequence and heterologous localisation of SufC in *S. cerevisiae* and SufB and SufC in *T. vaginalis* showed cytosolic localisation **(Fig. 8)** indicating that SUF pathway has most likely have cytosolic localisation in the *M. exilis* cell.

The genome also contains genes for CIA pathway. We were able to identify four genes - Nbp35, Cia1, Cia2b (two copies) and Nar1. This minimalistic set of proteins is comparable with other members of Metamonada (Pyrih et al. 2016). CIA pathway cannot synthesise Fe-S clusters on its own but needs an unknown sulfur or iron-sulfur compound (usually termed X-S) produced by ISC pathway (Kispal et al. 1999; Pandey et al. 2019). Consistently with the loss of MRO genes for proteins involved in the transport of X-S from MRO like Atm1 or Erv1 are also missing. Similarly to other Metamonada, electron transport chain proteins (Tah18 and Dre2) are not present (Pyrih et al. 2016). The absence of Dre2 is not surprising as it is often missing in anaerobes (Basu et al. 2014; Tsaousis et al. 2014). From this we can conclude that the cytosolic and nuclear Fe-S proteins are most likely maturated by the unique combination of SUF and CIA pathway and that whole system is localised in cytosol.

To check if the change of Fe-S cluster assembly pathway changed the content of Fe-S protein genes we *in silico* predicted Fe-S cluster containing proteins in the genome of *M. exilis*. Prediction was based on the MetalPredator software (Valasatava et al. 2016). 70 proteins were predicted to potentially contain Fe-S clusters and this number is comparable to other anaerobically living eukaryotes (Karnkowska et al. 2019). For list of predicted Fe-S proteins see Table 2. Therefore, we conclude that the switch from the ISC to SUF pathway did not affected number Fe-S cluster proteins in *M. exilis.* All predicted proteins seem to contain 4Fe-4S clusters with the only exception of xanthine dehydrogenase which is predicted to contain 2Fe-2S cluster. This is in concord with the bioinformatic studies which showed that anaerobically living organisms tends to have more 4Fe-4S clusters (Andreini et al. 2017).

10.4 Characterisation of SUF genes

In silico analysis of SufB protein sequence revealed that all residues predicted to be responsible for the Fe-S cluster formation (Arg226, Asp228 Cys254, Gln285, Trp287, Lys303, numbering from *E. coli*) (Hirabayashi et al. 2015; Yuda et al. 2017) are present in *M. exilis* SufB as well as are the residues reported to form the interface with SufD (Cys405 and Glu434 in *E. coli*) (Yuda et al.

2017). From the four described $FADH_2$ binding sites (Wollers et al. 2010), only two are present in *M. exilis* SufB. In many organisms, however, the $FADH_2$ binding sites are not conserved at all and the exact role of $FADH_2$ for Fe-S cluster assembly is unknown. SufD of *M. exilis* contains His360 (*E. coli* numbering) one of the two amino acids proposed to be essential for forming an interface between SufB and SufD (Yuda et al., 2017). The second residue reported for forming interface with SufB - Cys358, is substituted to alanine in *M. exilis*. However, this substitution seems to be common in Gram positive bacteria.

SufC of *M. exilis* contains all the characteristic conserved motives of ABC ATPases such as the Walker A, Walker B, ABC signature motif, the Q-loop, the P-loop and the H-motif. All amino acids (Lys40, Lys152, Glu171, Asp173 and His203) identified in *E. coli* SufC as potentially important for the ATPase activity (Kitaoka et al. 2006; Hirabayashi et al. 2015) are also conserved in the sequence of *M. exilis* SufC. Predicted model of SufC of *M. exilis* shows high resemblance to the structure of *E. coli* SufC. Also, recent experiments in our lab confirmed that the SufC is a functional ATPase *in vitro* (Zelena, 2020).

M. exilis SufS has a well conserved active site cysteine (Cys361 in *B. subtilis*) and adjacent residues show a high level of similarity to the sequences of SufS from *B. subtilis*, *E. coli* and other organisms (Blauenburg et al. 2016). Also the lysine residue responsible for the binding of PLP (Lys 224 in *B. subtilis*) is conserved (Selbach et al. 2010; Selbach et al. 2014). Although PLP binding site is seemingly perturbed by three insertions when compared to SufS sequences of *B. subtilis and E. coli*, the PLP binding pocket is undisturbed in the predicted model. Also His342, which was reported to interact with SufU in Gram positive bacteria (Fujishiro et al. 2017) and to enhance transfer of persulfide, is conserved.

M. exilis SufU lacks, as others members of this protein family, the LPVVK motif which is present in IscU (Riboldi et al. 2009), and 19 amino acid long insert conserved is elongated to 27 amino acids in *M. exilis. Z*inc binding residues - Cys98, Cys136, Cys206 and Asp100 (*M. exilis* numbering) are well conserved in the sequence protein (Selbach et al. 2014; Fujishiro et al. 2017).

Another evidence for the functionality of the SUF pathway in *M. exilis* was obtained using the BACTH assay (Bacterial Adenylate Cyclase Two Hybrid system) (Battesti and Bouveret 2012) that proved interaction between *M. exilis* SufB and SufC. These results corroborate the *in vitro* experiments of Zelena (2020) with recombinant proteins.

10.5 Bacterial complementation

To test the functionality of SUF system of *M. exilis*, we performed complementation experiments in *E. coli*. Two types of experiments were done - 1) complementation of a single gene mutants of *E. coli*, where deficient gene was replaced by the gene from *M. exilis* cloned into pTrc99a vector and growth phenotype under conditions of oxidative stress and iron starvation were observed. 2) Complementation in *E. coli* strains deficient in ISC pathway and the examined gene. In these experiments ability of the gene to complement its *E. coli* homologue was measured by β-galactosidase assay. Genes for SufB, SufC, and parts of the SufDSU - SufS and SufSU were tested. None of the tested genes was able to fully restore the Fe-S cluster assembly in *E. coli* in the first type of experiments. However, genes for SufB, SufS and SufSU showed significantly higher production of Fe-S clusters than negative control in the β-galactosidase assay (**Fig. 9**). These experiments showed that SUF of *M. exilis* is capable of a partial restoration of Fe-S assembly in *E. coli*. However, the effect is not strong enough to restore viability of *E. coli* cells.

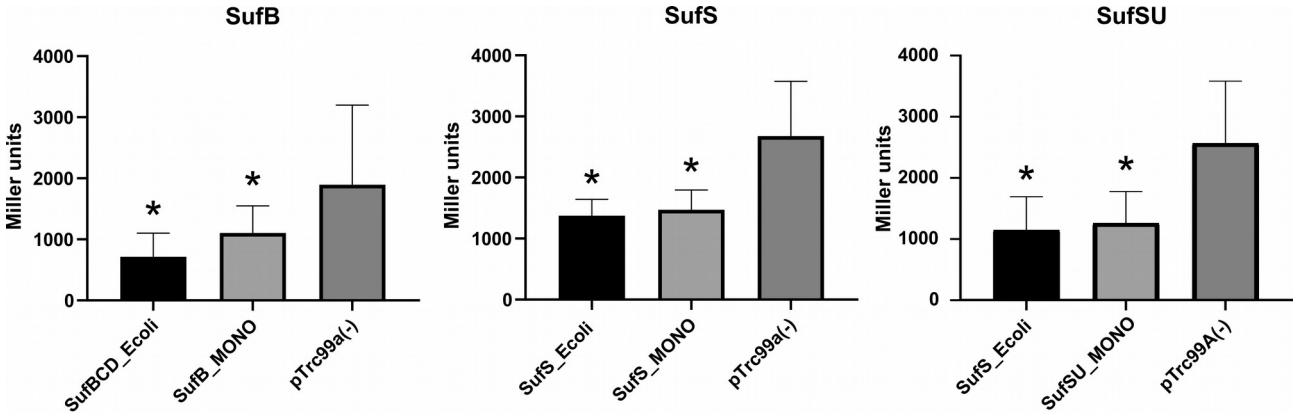

Fig. 9: Complementation in *E. coli* – β-galactosidase assay

Charts show readings of β-galactosidase cloned under IscR promoter which is inhibited by holo-IscR. Lesser the activity of β-galactosidase means higher Fe-S cluster assembly rates. Columns with asterisk are significantly different from negative control (P-test < 0.05). As negative control empty pTrc99A vector was used (dark grey columns). Positive control SufS is the of *E. coli* and SufBCD of *E. coli* were used respectively(black columns). Genotypes of strains used for comlementation are as follows: SufB - ΔlacZ PiscR(trans)::lacZ mev ΔiscAU ΔsufB ::kan Tn10, SufS and SufSU - ΔlacZ PiscR(trans)::lacZ MEV+ ΔiscS::cat ΔsufS::kan Tn10. All strains were based on *E. coli* MG1655 strain.

Loci	Best hit NCBI (blastp)	Organism of best hit (blastp)	Interproscan result	Fe-S cluster	Homologue in yeast	KEGG orthology
MONOS_248	Dihydropyrimidine dehydrogenase [NADP(+)]-like	Lingula anatina	Dihyropyrimidine dehydrogenase	4Fe-4S	Glt1P Ura1p	k00207
MONOS_405	Fanconi anemia group J protein homolog	Harpegnathos saltator	Helicase	4Fe-4S		K15362
MONOS_994	Radical SAM protein	Planctomycetes bacterium SM23_32	Radical SAM/MiaB	4Fe-4S		K04069
MONOS_1240	Fe-hydrogenase	Paratrimastix pyriformis	Fe hydrogenase	4Fe-4S	YLR455W-like	
MONOS_1242	SufB	Paratrimastix pyriformis	Iron-sulfur cluster assembly scaffold protein, partial			K09014
MONOS_1904	DNA repair helicase rad15	Grifola frondosa	DNA repair DEAD helicase RAD3/XP-D subfamily member	4Fe-4S?	Rad3-like	K10844
MONOS_1914	2-hydroxyglutaryl-CoA dehydratase	Treponema phagedenis	ATPase/CoA_activase	4Fe-4S		
MONOS_1920	Fe-hydrogenase large subunit family protein/Ferredoxin hydrogenase	Treponema putidum	Fe-only hydrogenase	4Fe-4S		
MONOS_2176	4Fe-4S ferredoxin iron-sulfur binding domain protein	Desulfatibacillum alkenivorans AK-01	Flavoproteins/4Fe-4S ferredoxin	4Fe-4S		
MONOS_2420	DNA-directed RNA polymerase II	Coccidioides immitis RS	DNA-directed RNA polymerase		Rbp11p	K03008
MONOS_2602	Choline transporter-like protein 1	Tribolium castaneum	Choline transporter like protein		Pns1p	K15377
MONOS_2675	L-serine dehydratase	Bacteroidales bacterium CF	L-serine dehydratase			K01752
MONOS_3322	Thioredoxin	Aotus nancymaae	Thioredoxin		Trx2p	K03671
MONOS_3835	2-hydroxyglutaryl-CoA dehydratase	Treponema putidum	ATPase/CoA_activase			
MONOS_3869	L-serine dehydratase	Bacteroidales bacterium CF	L-serine dehydratase			K01752
MONOS_4141	DNA polymerase alpha catalytic subunit	Lichtheimia corymbifera JMRC:FSU:9682	DNA polymerase		Pol1	K02320
MONOS_4172	Fe-S binding protein/ferredoxin	Clostridium tyrobutyricum	Flavoproteins/4Fe-4S ferredoxin	4Fe-4S	Irc3p	
MONOS_4180	Xanthine dehydrogenase	Aspergillus ruber CBS 135680	Xanthine dehydrogenase	2Fe-2S		K00106
MONOS_4520	Pyruvate:ferredoxin oxidoreductase	Paratrimastix pyriformis	Pyruvate -flavodoxin oxidoreductase-related	4Fe-4S	Met5p, Ecm17p	K03737
MONOS_5000	DNA polymerase alpha catalytic subunit	Lichtheimia corymbifera JMRC:FSU:9682	DNA polymerase B	4Fe-4S	Pol1	K02320
MONOS_5443	DNA polymerase delta catalytic subunit	Tomocerus sp. E-82	DNA polymerase delta catalytic subunit	4Fe-4S	Cdc2p	K02327
MONOS_6059	putative ferredoxin 2 [4Fe-4S]	Mastigamoeba balamuthi	4Fe-4S ferredoxins	4Fe-4S		
MONOS_6460	radical SAM/SPASM domain-containing protein	Methanocella arvoryzae	Aldolase_TIM/Radical SAM domain protein	4Fe-4S		
MONOS_6512	PREDICTED: thioredoxin	Aotus nancymaae	Thioredoxin		Trx2p	K03671
MONOS_6566	Dihydropyrimidine dehydrogenase	Polysphondylium pallidum PN500	FAD:NADPH dehydrogenase/oxidoreductase	4Fe-4S	Glt1	K00266
MONOS_6709	Pyruvate:ferredoxin (flavodoxin) oxidoreductase, homodimeric	Halothermothrix orenii	Pyruvate-flavodoxin oxdoreductase-related	4Fe-4S	Met5p	K00169
MONOS_7045	ATP-binding cassette sub-family E member 1	Exaiptasia pallida	ATP-binding transport protein-related/ 4Fe-4S ferredoxin	4Fe-4S	Rli1p	K06174
MONOS_7086	Radical SAM and acetyltransferase domains containing protein	Spraguea lophii 42_110	Radical_SAM/MiaB/histone acetyl transferase		Elp3	K07739
MONOS_7180	2-hydroxyglutaryl-CoA dehydratase	Carnobacterium divergens	CoA_activase_DUF2229			
MONOS_7280	RNA polymerase II core subunit	Dictyostelium fasciculatum	DNA-directed RNA polymerease II subunit RPB3		Rpb3	K03011
MONOS_7884	MiaB-like tRNA modifying enzyme, archaeal-type	Allomyces macrogynus ATCC 38327	MiaB/ Methylthiotransferase_N			K15865
MONOS_8067	ATP-dependent RNA helicase chl1	Rhizophagus irregularis DAOM 197198w	ATP-dep_Helicase_C	4Fe-4S	Chl1p	K11273
MONOS_8203	RNA polymerase Rpb3/Rpb11 dimerization domain containing protein	Acanthamoeba castellanii str. Neff	DNA-dir_RNA_pol_RpoA/D/Rpb3		Rpc40p	K03027
MONOS_8398	Cytosolic Fe-S cluster assembly factor nubp1 (Nbp35)	Oxytricha trifallax	Cytosolic Fe-S cluster assembly factor NUBP2	4Fe-4S	Nbp35p	
MONOS_8913	Dihydropyrimidine dehydrogenase [NADP(+)]-like	Octopus bimaculoides	Dihydropyrimidine dehydrogenase [NADP(+)]	4Fe-4S		
MONOS_9109	Serine/threonine-protein kinase, putative	Oxytricha trifallax	DNA repair DEAD helicase RAD3/XPD subfamily member		Kic1	K11136
MONOS_9203	SufSU	Prevotella nigrescens	Cystein desulfurase			K11717
MONOS_9530	Pyruvate: ferredoxin (flavodoxin) oxidoreductase	Thermoanaerobacter siderophilus SR4	Pyruvate -flavodoxin oxidoreductase-related	4Fe-4S	Met5p, Ecm17	K00169
MONOS_10117	DNA-directed RNA polymerases I and III subunit RPAC2-like	Lingula anatina	RBP11-like subunits of RNA polymerase		Rpc19p	K03020
MONOS_11341	DNA polymerase delta catalytic subunit	Tomocerus sp. E-82	DNA polymerase delta catalytic subunit			K02327
MONOS_11732	Hydroxylamine reductase	Desulfonatronospira thiodismutans	Hydroxylamine reductase/ prismane protein-like			K05601
MONOS_12154	Pyruvate:ferredoxin (flavodoxin) oxidoreductase, homodimeric	Thermoanaerobacter siderophilus SR4	Pyruvate -flavodoxin oxidoreductase-related	4Fe-4S	Met10p, Ecm17p	K00169
MONOS_13001	26S proteasome nonATPase regulatory subunit 7, putative	Acanthamoeba castellanii str. Neff	Eukaryotic translation initiation factor 3 subunit f-related		Yor261C, Rpn8p	K03038
MONOS_13381	Fe-hydrogenase large subunit family protein	Treponema putidum	26S proteasome non-ATPase regulatory subunit 7	4Fe-4S		
MONOS_14435	Xanthine dehydrogenase	Aspergillus ruber CBS 135680	Xanthine dehydrogenase	2Fe-2S		K00106
MONOS_15091	DNA primase large subunit	Clupea harengus	DNA primase large subunit	4Fe-4S	Pri2p	K02685
MONOS_15232	Cytosolic Fe-S cluster assembly factor NARFL	Fundulus heteroclitus	Cytosolic fe-s cluster assembly factor NARFL	*4Fe-4S?*	Nar1p	
MONOS_15936	4Fe-4S ferredoxin	Peptostreptococcaceae bacterium AS15	4Fe-4S ferredoxins	4Fe-4S		
MONOS_16338	N/A	N/A				
MONOS_16551	N/A	N/A				
MONOS_16811	Rubrerythrin					
MONOS_130	Xanthine dehydrogenase		Xanthine dehydrogenase	2Fe-2S		K00106
MONOS_16812	Ferredoxin	Aneurinibacillus terranovensis	4Fe-4S ferredoxins	4Fe-4S	Uip5p	
MONOS_2737	DSBA oxidoreductase	Stemphylium lycopersici	Thioredoxin-like fold			
MONOS_742	Hypothetical protein DAPPUDRAFT_105663	Daphnia pulex	Metallodependent phosphatase/ Ser/Thr-sp_prot-phosphatase		Cna1p	K04348
MONOS_1638	Putative Protein disulfide isomerase	Zostera marina	Thioredoxin/Thioredoxin-like fold		Mpd1p	
MONOS_875	FAT domain-containing protein	Colletotrichum gloeosporioides Cg-14			YJR066Wp-like, Tor2-like	K07203
MONOS_405	Fanconi anemia group J protein homolog	Harpegnathos saltator	DEAD helicase		Rad3p	K15362
MONOS_885	PREDICTED: probable protein disulfide-isomerase A6	Pyrus x bretschneideri	Thioredoxin/ Thioredoxin-like fold/ protein disulfide isomerase		PDI1-like	K09584
MONOS_4572	Putative Protein disulfide isomerase	Penicillium brasilianum	thioredoxin2/ thioredoxin6 / protein disulfide isomerase		PDI1-like	K01829
MONOS_12039	DNA polymerase zeta catalytic subunit	Papilio polytes	DNA-dir_DNA_pol_B	4Fe-4S	Rev3p	
MONOS_11341	DNA polymerase delta catalytic subunit	Orchesella cincta	DNA polymerase delta catalytic subunit/ DNA polymerase B	4Fe-4S	Pol3	K02327
MONOS_8934	Protein disulfide isomerase	Grosmannia clavigera kw1407	Thioredoxin2 /thioredoxin6 /protein disulfide isomerase		Pdi1p	K09580
MONOS_7901	Endonuclease III-like protein 1	Blastocystis sp. Subtype 4	A/G-specific adenine glycosylase/endonuclease III	4Fe-4S	Ntg1p	K10773
MONOS_5248	PREDICTED: DNA polymerase epsilon catalytic subunit A-like	Acropora digitifera	DNA polymerase epsilon catalytic subunit A		Pol2	K02324
MONOS_5759	PREDICTED: protein disulfide-isomerase like 2-1	Beta vulgaris subsp. Vulgaris	Thioredoxin1/thioredoxin2/Erp29C-domain		PDI1-like	K09584
MONOS_7654	PREDICTED: probable protein disulfide-isomerase A6	Pyrus x bretschneideri	Thioredoxin2/protein disulfide isomerase		PDI1-like	K09584
MONOS_9857	PREDICTED: TPR repeat-containing thioredoxin TDX isoform X2	Capsicum annuum	Thioredoxin/TPR region		Trx1	
MONOS_5719	Thioredoxin domain-containing protein	Toxoplasma gondii ARI	Thioredoxin/protein disulfide isomerase		Grx4p	K03671
MONOS_12201	TPA: Chaperone protein DnaJ/thioredoxin domain-containing protein	Neospora caninum Liverpool	Thioredoxin2/protein disulfide isomerase		Grx4p	K03671

Table 2: List of predicted Fe-S proteins of *M. exilis.* (Karnkowska et al. 2019)

10.6 Fe-S cluster assembly in other Preaxostyla

To verify the presence of SUF pathway in other members of Preaxostyla we examined available genomes and transcriptomes of several members of this group - namely - *Blattamonas nauphoetae* (strain Nau3), *P. pyriformis* strain ATCC 50935, *Streblomastix strix* (single-cell genome assembly), *Saccinobaculus doroaxostylus* (single cell transcriptomes), *Saccinobaculus ambloaxostylus* (three single cell transcriptomes), *Oxymonas* sp. (Single cell transcriptome), two single cell transcriptome assemblies of *Streblomastix* sp. (Streblo-1, Streblo-4), one single cell transcriptome assembly of *Pyrsonympha* sp., transcriptome assembly of *Trimastix marina* strain PCT (Leger et al. 2017), and a transcriptome assembly of trimastigid "MORAITIKA".

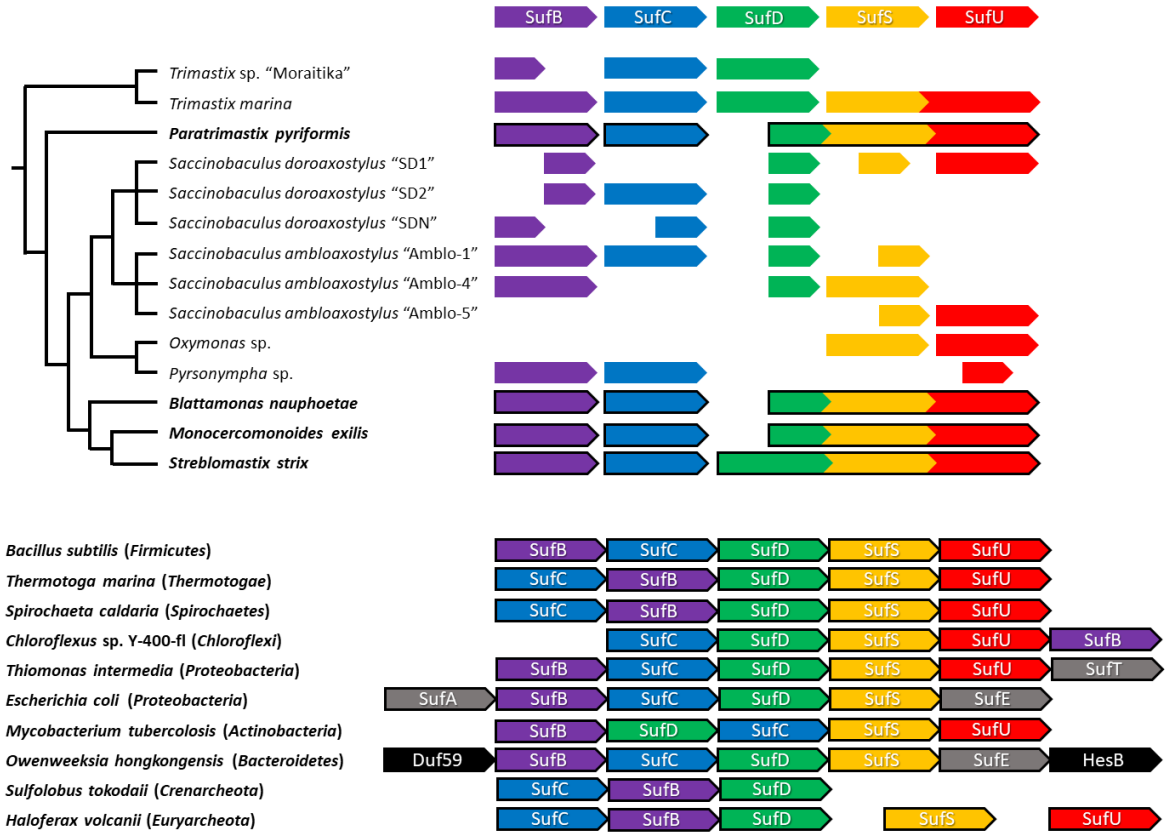

Fig. 10: Inventory of SUF genes in Preaxostyla.
The scheme shows SUF genes/transcripts identified in the members of Preaxostyla. The relationship within this group is indicated by the tree. For organisms in bold, genomic data were investigated, in others transcriptomic or single-cell transcriptomic data sets were used. Completeness of a gene/transcript is indicated by the length of the arrow. The order of Preaxostyla genes does not reflect their order in the genome. Gene fusions are marked by fused arrows. At the bottom are given schemes of typical SUF gene operons in representatives of prokaryotic groups (Vacek et al. 2018)

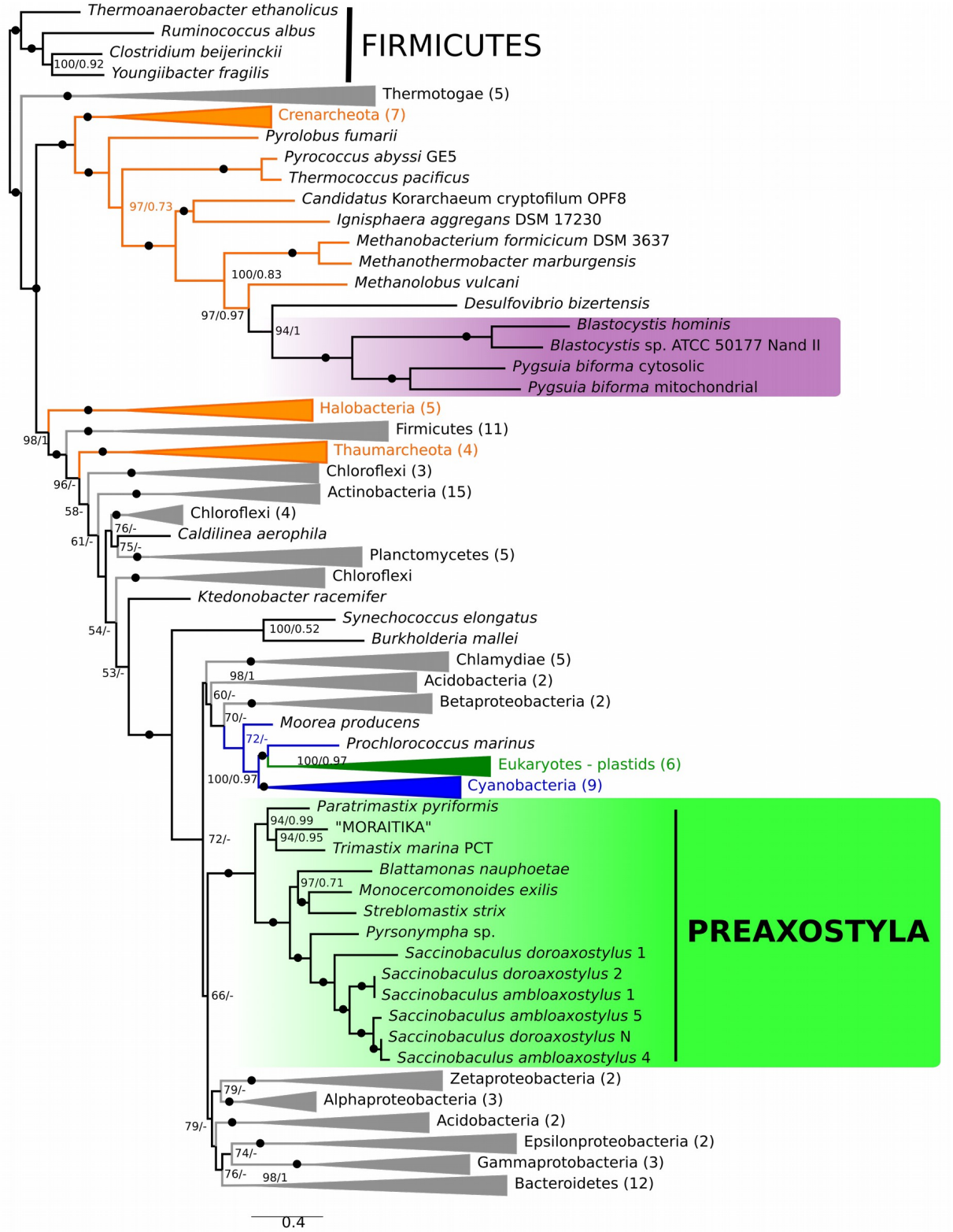

Fig. 11: Phylogenetic analysis of concatenated SufB, C, D, and S.

The topology of the tree was calculated by ML in IQ-TREE (Nguyen et al. 2015) using partition specific models. Numbers at nodes represent statistical support in regular ML bootstraps/Bayesian posterior probabilities. The support 99/0.99 and higher is indicated by filled circles, values <50 and 0.5 are not shown (Vacek et al. 2018).

We were able to find genes for the SUF pathway in all Preaxostyla (**Fig. 10**) and ISC pathway seems to be missing in all of them. Although there is possibility that some genes might be missing due to the incompleteness of the transcriptomes. Interestingly, we were able to detect fusion gene SufDSU in all Preaxostyla with sequenced genomes and at least partial fusion of SufS and SufU in *T. marina* transcriptome. Free-living trimastigids represent a nice comparison as they contain MRO resembling hydrogenosomes (Hampl et al. 2008; Zubáčová et al. 2013), however, like Oxymonadida, they lack ISC system and have SUF system instead. Localisation of the SUF pathway in these organisms is unknown, however, SUF genes of *P. pyriformis* lack any recognisable N-terminal targeting sequences suggesting cytosolic localisation of this pathway.

Phylogenetic analysis of concatenated SufB, SufC, SufD and SufS genes (**Fig. 11**) showed that Preaxostyla forms a well-supported clade nested inside of bacteria. This clade is clearly distinct to clades of SUF system known from plastids (which is of cyanobacterial origin) and SUF system reported from *Blastocystis*, *Pygsuia*, *Stygiela* and other protists, which was acquired from methanogenic archaea (Tsaousis et al. 2012; Stairs et al. 2014; Tsaousis 2019). These results suggest that the last common ancestor of Preaxostyla acquired SUF pathway by lateral gene transfer from

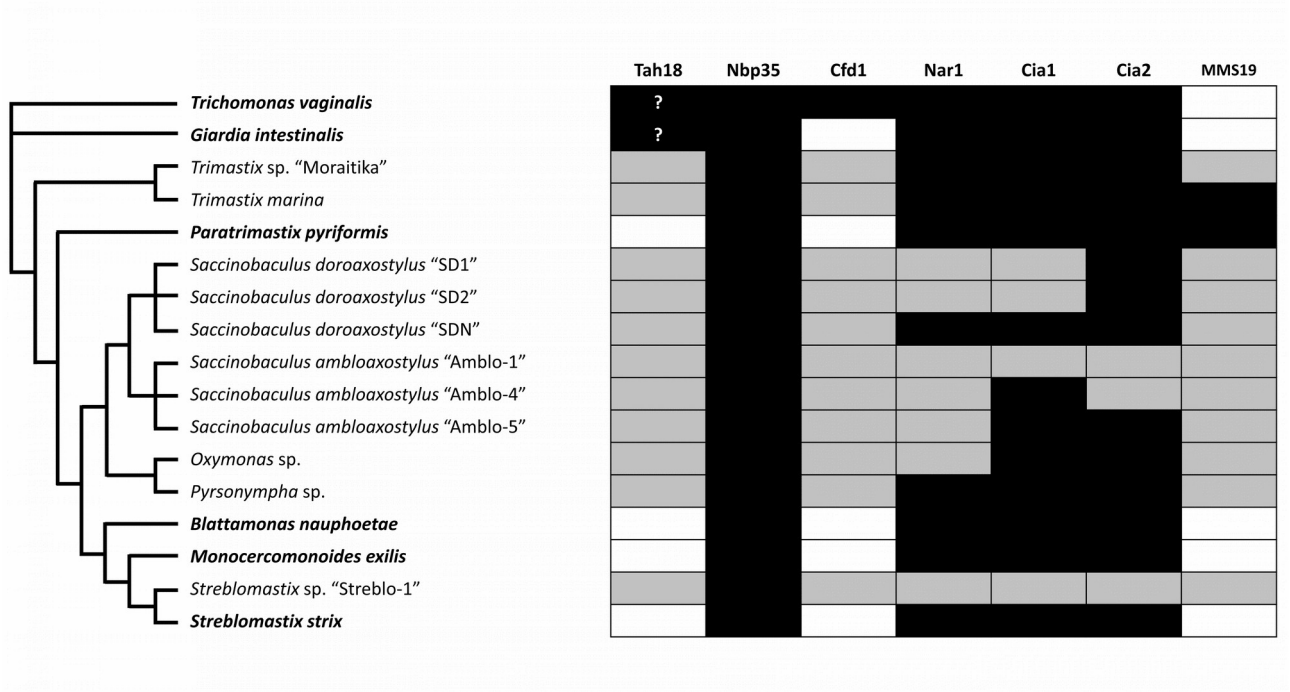

Fig. 12: Inventory of CIA genes in Preaxostyla.
The scheme shows the presence (black) or absence (white/grey) of CIA genes/transcripts in Preaxostyla with reference to Metamonada represented by *G. intestinalis* and *T. vaginalis*. White/grey shading indicates that the gene was not identified in available genome/transcriptome, respectively. The gene inventory of *T. vaginalis* and *G. intestinalis* was taken from (Pyrih et al. 2016). Question marks indicate uncertain orthology to Tah18 (Vacek et al. 2018).

unknown bacteria (Vacek et al. 2018) and that the acquisition of SUF system preceded the loss of MRO as trimastigids has both SUF system and an MRO. CIA pathway of all examined Preaxostyla is similar to that reported from *G. intestinalis* (Pyrih et al. 2016) and consists of four genes - Cia1, Cia2, Nar1 and Nbp35 (**Fig. 12**).

10.7 SUF pathway and mitochondrial loss

Presence of SUF system in all examined Preaxostyla indicates that it was present in their last common ancestor. It is highly probable that the acquisition of the SUF pathway was one of the important prerequisites necessary for the loss of mitochondrion. Localisation of the SUF pathway in the cytosol allowed to bypass mitochondrial ISC pathway which lead to subsequent redundancy of the only essential function of MRO. Once MRO has lost it indispensability for the cell, it was probably lost completely.

It is difficult to say, when this event happened, however, there is a hint from the fossils of oxymonads which were discovered in the gut of *Kalotermes* sp. termite isolated from a Burmese amber (Poinar 2009). These fossils highly resembling current oxymonad species indicate that oxymonads were probably fully diversified already in the Early Cretaceous period (~145 - 105.5 million years ago) and therefore the SUF pathway which is widespread among Preaxostyla must have been acquired before this date.

11 References

Abdalla M, Dai YN, Chi CB, Cheng W, Cao DD, Zhou K, Ali W, Chen Y, Zhou CZ. 2016. Crystal structure of yeast monothiol glutaredoxin Grx6 in complex with a glutathione-coordinated [2Fe-2S] cluster. Acta Crystallogr Sect Struct Biol Commun. 72(10):732–737. doi:10.1107/S2053230X16013418.

Adinolfi S, Iannuzzi C, Prischi F, Pastore C, Iametti S, Martin SR, Bonomi F, Pastore A. 2009. Bacterial frataxin CyaY is the gatekeeper of iron-sulfur cluster formation catalyzed by IscS. Nat Struct Mol Biol. 16(4):390–396. doi:10.1038/nsmb.1579.

Adinolfi S, Puglisi R, Crack JC, Iannuzzi C, Dal Piaz F, Konarev P V., Svergun DI, Martin S, Le Brun NE, Pastore A. 2018. The Molecular Bases of the Dual Regulation of Bacterial Iron Sulfur Cluster Biogenesis by CyaY and IscX. Front Mol Biosci. 4(FEB):97. doi:10.3389/fmolb.2017.00097.

Adl SM, Bass D, Lane CE, Lukeš J, Schoch CL, Smirnov A, Agatha S, Berney C, Brown MW, Burki F, et al. 2019. Revisions to the Classification, Nomenclature, and Diversity of Eukaryotes. J Eukaryot Microbiol. 66(1):4–119. doi:10.1111/jeu.12691.

Agar JN, Krebs C, Frazzon J, Huynh BH, Dean DR, Johnson MK. 2000. IscU as a scaffold for iron-sulfur cluster biosynthesis: Sequential assembly of [2Fe-2S] and [4Fe-4S] clusters in IscU. Biochemistry. 39(27):7856–7862. doi:10.1021/bi000931n.

Agar JN, Yuvaniyama P, Jack RF, Cash VL, Smith AD, Dean DR, Johnson MK. 2000. Modular organization and identification of a mononuclear iron-binding site within the NifU protein. J Biol Inorg Chem. 5(2):167–177. doi:10.1007/s007750050361.

Albrecht AG, Netz DJA, Miethke M, Pierik AJ, Burghaus O, Peuckert F, Lill R, Marahiel MA. 2010. SufU is an essential iron-sulfur cluster scaffold protein in Bacillus subtilis. J Bacteriol. 192(6):1643–1651. doi:10.1128/JB.01536-09.

Ali V, Nozaki T. 2013. Iron-Sulfur clusters, their biosynthesis, and biological functions in protozoan parasites. In: Advances in Parasitology. Vol. 83. Academic Press. p. 1–92.

Ali V, Shigeta Y, Tokumoto U, Takahashi Y, Nozaki T. 2004. An Intestinal Parasitic Protist, Entamoeba histolytica, Possesses a Non-redundant Nitrogen Fixation-like System for Iron-Sulfur Cluster Assembly under Anaerobic Conditions. J Biol Chem. 279(16):16863–16874. doi:10.1074/jbc.M313314200.

Allen S, Balabanidou V, Sideris DP, Lisowsky T, Tokatlidis K. 2005. Erv1 mediates the Mia40-dependent protein import pathway and provides a functional link to the respiratory chain by shuttling electrons to cytochrome c. J Mol Biol. 353(5):937–944. doi:10.1016/j.jmb.2005.08.049.

Anderson CP, Shen M, Eisenstein RS, Leibold EA. 2012. Mammalian iron metabolism and its control by iron regulatory proteins. Biochim Biophys Acta - Mol Cell Res. 1823(9):1468–1483. doi:10.1016/j.bbamcr.2012.05.010.

Andreini C, Banci L, Rosato A. 2016. Exploiting Bacterial Operons to Illuminate Human Iron-Sulfur Proteins. J Proteome Res. 15(4):1308–1322. doi:10.1021/acs.jproteome.6b00045.

Andreini C, Rosato A, Banci L. 2017. The Relationship between Environmental Dioxygen and Iron-Sulfur Proteins Explored at the Genome Level. Missirlis F, editor. PLoS One. 12(1):e0171279. doi:10.1371/journal.pone.0171279.

Angelini S, Gerez C, Ollagnier-de Choudens S, Sanakis Y, Fontecave M, Barras F, Py B. 2008. NfuA, a new factor required for maturing Fe/S proteins in Escherichia coli under oxidative stress and iron starvation conditions. J Biol Chem. 283(20):14084–91. doi:10.1074/jbc.M709405200.

Angerer H. 2013. The superfamily of mitochondrial Complex1-LYR motif-containing (LYRM) proteins. Biochem Soc Trans. 41(5):1335–1341. doi:10.1042/BST20130116.

Anton BP, Saleh L, Benner JS, Raleigh EA, Kasif S, Roberts RJ. 2008. RimO, a MiaB-like enzyme, methylthiolates the universally conserved Asp88 residue of ribosomal protein S12 in Escherichia coli. Proc Natl Acad Sci U S A. 105(6):1826–1831. doi:10.1073/pnas.0708608105.

Anwar S, Dikhit MR, Singh KP, Kar RK, Zaidi A, Sahoo GC, Roy AK, Nozaki T, Das P, Ali V. 2014. Interaction between Nbp35 and Cfd1 proteins of cytosolic Fe-S cluster assembly reveals a stable complex formation in Entamoeba histolytica. PLoS One. 9(10). doi:10.1371/journal.pone.0108971.

Arragain S, Handelman SK, Forouhar F, Wei FY, Tomizawa K, Hunt JF, Douki T, Fontecave M, Mulliez E, Atta M. 2010. Identification of eukaryotic and prokaryotic methylthiotransferase for biosynthesis of 2-methylthio-N6-threonylcarbamoyladenosine in tRNA. J Biol Chem. 285(37):28425–28433. doi:10.1074/jbc.M110.106831.

Austin CM, Wang G, Maier RJ. 2015. Aconitase functions as a pleiotropic posttranscriptional regulator in Helicobacter pylori. J Bacteriol. 197(19):3076–3086. doi:10.1128/JB.00529-15.

Babcock M, De Silva D, Oaks R, Davis-Kaplan S, Jiralerspong S, Montermini L, Pandolfo M, Kaplan J. 1997. Regulation of mitochondrial iron accumulation by Yfh1p, a putative homolog of frataxin. Science (80-). 276(5319):1709–1712. doi:10.1126/science.276.5319.1709.

Bak DW, Elliott SJ. 2014. Alternative fes cluster ligands: Tuning redox potentials and chemistry. Curr Opin Chem Biol. 19(1):50–58. doi:10.1016/j.cbpa.2013.12.015.

Balasubramanian R, Shen G, Bryant DA, Golbeck JH. 2006. Regulatory roles for IscA and SufA in iron homeostasis and redox stress responses in the cyanobacterium Synechococcus sp. strain PCC 7002. J Bacteriol. 188(9):3182–3191. doi:10.1128/JB.188.9.3182-3191.2006.

Balk J, Aguilar Netz DJ, Tepper K, Pierik AJ, Lill R. 2005. The Essential WD40 Protein Cia1 Is Involved in a Late Step of Cytosolic and Nuclear Iron-Sulfur Protein Assembly. Mol Cell Biol. 25(24):10833–10841. doi:10.1128/mcb.25.24.10833-10841.2005.

Balk J, Pierik AJ, Aguilar Netz DJ, Mühlenhoff U, Lill R. 2004. The hydrogenase-like Nar1p is essential for maturation of cytosolic and nuclear iron-Sulfur proteins. EMBO J. 23(10):2105–2115. doi:10.1038/sj.emboj.7600216.

Balk J, Pilon M. 2011. Ancient and essential: The assembly of iron-sulfur clusters in plants. Trends Plant Sci. 16(4):218–226. doi:10.1016/j.tplants.2010.12.006. http://dx.doi.org/10.1016/j.tplants.2010.12.006.

Banci L, Bertini I, Calderone V, Cefaro C, Ciofi-Baffoni S, Gallo A, Tokatlidis K. 2012. An Electron-Transfer Path through an Extended Disulfide Relay System: The Case of the Redox Protein ALR. J Am Chem Soc. 134(3):1442–1445. doi:10.1021/ja209881f.

Banci L, Brancaccio D, Ciofi-Baffoni S, Del Conte R, Gadepalli R, Mikolajczyk M, Neri S, Piccioli M, Winkelmann J. 2014. [2Fe-2S] cluster transfer in iron-sulfur protein biogenesis. Proc Natl Acad Sci U S A. 111(17):6203–8. doi:10.1073/pnas.1400102111.

Bandyopadhyay S, Gama F, Molina-Navarro MM, Gualberto JM, Claxton R, Naik SG, Huynh BH, Herrero E, Jacquot JP, Johnson MK, et al. 2008. Chloroplast monothiol glutaredoxins as scaffold proteins for the assembly and delivery of [2Fe-2S] clusters. EMBO J. 27(7):1122–1133. doi:10.1038/emboj.2008.50.

Bandyopadhyay S, Chandramouli K, Johnson MK. 2008. Iron-sulfur cluster biosynthesis. Biochem Soc Trans. 36(6):1112–1119. doi:10.1042/BST0361112.

Bandyopadhyay S, Naik SG, O'Carroll IP, Huynh BH, Dean DR, Johnson MK, Dos Santos PC. 2008. A proposed role for the Azotobacter vinelandii nfua protein as an intermediate iron-sulfur cluster carrier. J Biol Chem. 283(20):14092–14099. doi:10.1074/jbc.M709161200.

Baranovskiy AG, Siebler HM, Pavlov YI, Tahirov TH. 2018. Iron–Sulfur Clusters in DNA Polymerases and Primases of Eukaryotes. In: Methods in Enzymology. Vol. 599. Academic Press Inc. p. 1–20.

Barberà MJ, Ruiz-Trillo I, Tufts JYA, Bery A, Silberman JD, Roger AJ. 2010. Sawyeria marylandensis (heterolobosea) has a hydrogenosome with novel metabolic properties. Eukaryot Cell. 9(12):1913–1924. doi:10.1128/EC.00122-10.

Barthelme D, Dinkelaker S, Albers SV, Londei P, Ermler U, Tampé R. 2011. Ribosome recycling depends on a mechanistic link between the FeS cluster domain and a conformational switch of the twin-ATPase ABCE1. Proc Natl Acad Sci U S A. 108(8):3228–3233. doi:10.1073/pnas.1015953108.

Barthelme D, Scheele U, Dinkelaker S, Janoschka A, MacMillan F, Albers SV, Driessen AJM, Stagni MS, Bill E, Meyer-Klaucke W, et al. 2007. Structural organization of essential iron-sulfur clusters in the evolutionarily highly conserved ATP-binding cassette protein ABCE1. J Biol Chem. 282(19):14598–14607. doi:10.1074/jbc.M700825200.

Barton JK, Silva RMB, O'Brien E. 2019. Redox Chemistry in the Genome: Emergence of the [4Fe4S] Cofactor in Repair and Replication. Annu Rev Biochem. 88(1):163–190. doi:10.1146/annurev-biochem-013118-110644.

Basu S, Netz DJ, Haindrich AC, Herlerth N, Lagny TJ, Pierik AJ, Lill R, Lukeš J. 2014. Cytosolic iron-Sulfur protein assembly is functionally conserved and essential in procyclic and bloodstream Trypanosoma brucei. Mol Microbiol. 93(5):897–910. doi:10.1111/mmi.12706.

Battesti A, Bouveret E. 2012. The bacterial two-hybrid system based on adenylate cyclase reconstitution in Escherichia coli. Methods. 58(4):325–334. doi:10.1016/j.ymeth.2012.07.018.

Becker T, Franckenberg S, Wickles S, Shoemaker CJ, Anger AM, Armache JP, Sieber H, Ungewickell C, Berninghausen O, Daberkow I, et al. 2012. Structural basis of highly conserved ribosome recycling in eukaryotes and archaea. Nature. 482(7386):501–506. doi:10.1038/nature10829.

Behshad E, Parkin SE, Bollinger JM. 2004. Mechanism of cysteine desulfurase Slr0387 from Synechocystis sp. PCC 6803: kinetic analysis of cleavage of the persulfide intermediate by chemical reductants. Biochemistry. 43(38):12220–6. doi:10.1021/bi049143e.

Beilschmidt LK, De Choudens SO, Fournier M, Sanakis I, Hograindleur MA, Clémancey M, Blondin G, Schmucker S, Eisenmann A, Weiss A, et al. 2017. ISCA1 is essential for mitochondrial Fe4S4 biogenesis in vivo. Nat Commun. 8. doi:10.1038/ncomms15124.

Beinert H. 1997. Iron-Sulfur Clusters: Nature's Modular, Multipurpose Structures. Science (80-). 277(5326):653–659. doi:10.1126/science.277.5326.653.

Beinert H. 2000. Iron-sulfur proteins: Ancient structures, still full of surprises. J Biol Inorg Chem. 5(1):2–15. doi:10.1007/s007750050002.

Beinert H, Kennedy MC, Stout CD. 1996. Aconitase as iron-sulfur protein, enzyme, and iron-regulatory protein. Chem Rev. 96(7):2335–2373. doi:10.1021/cr950040z.

Beinert H, Sands RH. 1960. Studies on succinic and DPNH dehydrogenase preparations by paramagnetic resonance (EPR) spectroscopy. Biochem Biophys Res Commun. 3(1):41–46. doi:10.1016/0006-291X(60)90100-5.

Beltrán NC, Horváthová L, Jedelský PL, Šedinová M, Rada P, Marcinčiková M, Hrdý I, Tachezy J. 2013. Iron-Induced Changes in the Proteome of Trichomonas vaginalis Hydrogenosomes. PLoS One. 8(5). doi:10.1371/journal.pone.0065148.

Ben-Shimon L, Paul VD, David-Kadoch G, Volpe M, Stümpfig M, Bill E, Mühlenhoff U, Lill R, Ben-Aroya S. 2018. Fe-S cluster coordination of the chromokinesin KIF4A alters its subcellular localization during mitosis. J Cell Sci. 131(12):jcs211433. doi:10.1242/jcs.211433.

Benjdia A, Balty C, Berteau O. 2017. Radical SAM enzymes in the biosynthesis of ribosomally synthesized and post-translationally modified peptides (RiPPs). Front Chem. 5(NOV):87. doi:10.3389/fchem.2017.00087.

Biederbick A, Stehling O, Rosser R, Niggemeyer B, Nakai Y, Elsasser H-P, Lill R. 2006. Role of Human Mitochondrial Nfs1 in Cytosolic Iron-Sulfur Protein Biogenesis and Iron Regulation. Mol Cell Biol. 26(15):5675–5687. doi:10.1128/MCB.00112-06.

Bilder PW, Ding H, Newcomer ME. 2004. Crystal Structure of the Ancient, Fe-S Scaffold IscA Reveals a Novel Protein Fold. Biochemistry. 43(1):133–139. doi:10.1021/bi035440s.

Blahut M, Wise CE, Bruno MR, Dong G, Makris TM, Frantom PA, Dunkle JA, Outten FW. 2019. Direct observation of intermediates in the SufS cysteine desulfurase reaction reveals functional roles of conserved active-site residues. J Biol Chem. 294(33):12444–12458. doi:10.1074/jbc.RA119.009471.

Blanc B, Clémancey M, Latour JM, Fontecave M, Ollagnier De Choudens S. 2014. Molecular investigation of iron-sulfur cluster assembly scaffolds under stress. Biochemistry. 53(50):7867–7869. doi:10.1021/bi5012496.

Blauenburg B, Mielcarek A, Altegoer F, Fage CD, Linne U, Bange G, Marahiel MA. 2016. Crystal Structure of Bacillus subtilis Cysteine Desulfurase SufS and Its Dynamic Interaction with Frataxin and Scaffold Protein SufU. Rouault T, editor. PLoS One. 11(7):e0158749. doi:10.1371/journal.pone.0158749.

Blobstein SH, Grunberger D, Weinstein IB, Nakanishi K. 1973. Isolation and Structure Determination of the Fluorescent Base from Bovine Liver Phenylalanine Transfer Ribonucleic Acid. Biochemistry. 12(2):188–193. doi:10.1021/bi00726a002.

Boal AK, Barton JK. 2005. Electrochemical detection of lesions in DNA. Bioconjug Chem. 16(2):312–321. doi:10.1021/bc0497362.

Bolstad HM, Botelho DJ, Wood MJ. 2010. Proteomic analysis of protein-protein interactions within the cysteine sulfinate desulfinase Fe-S cluster biogenesis system. J Proteome Res. 9(10):5358–5369. doi:10.1021/pr1006087.

Boniecki MT, Freibert SA, Mühlenhoff U, Lill R, Cygler M. 2017. Structure and functional dynamics of the mitochondrial Fe/S cluster synthesis complex. Nat Commun. 8(1):1287. doi:10.1038/s41467-017-01497-1.

Bonomi F, Iametti S, Morleo A, Ta D, Vickery LE. 2008. Studies on the mechanism of catalysis of iron-sulfur cluster transfer from IscU[2Fe2S] by HscA/HscB chaperones. Biochemistry. 47(48):12795–801. doi:10.1021/bi801565j.

Bonomi F, Iametti S, Morleo A, Ta D, Vickery LE. 2011. Facilitated transfer of IscU-[2Fe2S] clusters by chaperone-mediated ligand exchange. Biochemistry. 50(44):9641–9650. doi:10.1021/bi201123z.

Boon EM, Ceres DM, Drummond TG, Hill MG, Barton JK. 2000. Mutation detection by electro catalysis at DNA-modified electrodes. Nat Biotechnol. 18(10 SUPPL.):1096–1100. doi:10.1038/80301.

Boon EM, Livingston AL, Chmiel NH, David SS, Barton JK. 2003. DNA-mediated charge transport for DNA repair. Proc Natl Acad Sci. 100(22):12543–12547. doi:10.1073/pnas.2035257100.

Boon EM, Salas JE, Barton JK. 2002. An electrical probe of protein-DNA interactions on DNA-modified surfaces. Nat Biotechnol. 20(3):282–286. doi:10.1038/nbt0302-282.

Boyd E. S., Anbar AD, Miller S, Hamilton TL, Lavin M, Peters JW. 2011. A late methanogen origin for molybdenum-dependent nitrogenase. Geobiology. 9(3):221–232. doi:10.1111/j.1472-4669.2011.00278.x.

Boyd Eric S., Hamilton TL, Peters JW. 2011. An alternative path for the evolution of biological nitrogen fixation. Front Microbiol. 2(OCT). doi:10.3389/fmicb.2011.00205.

Boyd ES, Thomas KM, Dai Y, Boyd JM, Outten FW. 2014. Interplay between Oxygen and Fe-S Cluster Biogenesis: Insights from the Suf Pathway. Biochemistry. 53(37):5834–5847. doi:10.1021/bi500488r.

Boyd JM, Drevland RM, Downs DM, Graham DE. 2009. Archaeal ApbC/Nbp35 homologs function as iron-sulfur cluster carrier proteins. J Bacteriol. 191(5):1490–1497. doi:10.1128/JB.01469-08.

Brancaccio D, Gallo A, Mikolajczyk M, Zovo K, Palumaa P, Novellino E, Piccioli M, Ciofi-Baffoni S, Banci L. 2014. Formation of [4Fe-4S] clusters in the mitochondrial iron-sulfur cluster assembly machinery. J Am Chem Soc. 136(46):16240–16250. doi:10.1021/ja507822j.

Brancaccio D, Gallo A, Piccioli M, Novellino E, Ciofi-Baffoni S, Banci L. 2017. [4Fe-4S] cluster assembly in mitochondria and its impairment by copper. J Am Chem Soc. 139(2):719–730. doi:10.1021/jacs.6b09567.

Bridwell-Rabb J, Iannuzzi C, Pastore A, Barondeau DP. 2012. Effector role reversal during evolution: The case of frataxin in Fe-S cluster biosynthesis. Biochemistry. 51(12):2506–2514. doi:10.1021/bi201628j.

Brugerolle G, Patterson D. 1997. Ultrastructure of Trimastix convexa hollande, an amitochondriate anaerobic flagellate with a previously undescribed organization. Eur J Protistol. 33(2):121–130. doi:10.1016/S0932-4739(97)80029-6.

Brune A, Ohkuma M. 2010. Role of the Termite Gut Microbiota in Symbiotic Digestion. In: Biology of Termites: a Modern Synthesis. Dordrecht: Springer Netherlands. p. 439–475.

Bruska MK, Stiebritz MT, Reiher M. 2013. Analysis of differences in oxygen sensitivity of Fe–S clusters. Dalt Trans. 42(24):8729. doi:10.1039/c3dt50763g.

Bruska MK, Stiebritz MT, Reiher M. 2015. Binding of Reactive Oxygen Species at Fe- S Cubane Clusters. Chem - A Eur J. 21(52):19081–19089. doi:10.1002/chem.201503008.

Brzóska K, Męczyńska S, Kruszewski M. 2006. Iron-sulfur cluster proteins: Electron transfer and beyond. In: Acta Biochimica Polonica. Vol. 53. p. 685–691.

Buck M, Griffiths E. 1982. Iron mediated methylthiolation of tRNA as a regulator of operon expression in Escherichia coli. Nucleic Acids Res. 10(8):2609–24. doi:10.1093/nar/10.8.2609.

Budd ME, Campbell JL. 2009. Interplay of Mre11 Nuclease with Dna2 plus Sgs1 in Rad51-Dependent Recombinational Repair. Lichten M, editor. PLoS One. 4(1):e4267. doi:10.1371/journal.pone.0004267.

Buis JM, Broderick JB. 2005. Pyruvate formate-lyase activating enzyme: Elucidation of a novel mechanism for glycyl radical formation. Arch Biochem Biophys. 433(1):288–296. doi:10.1016/j.abb.2004.09.028.

Bulen WA, LeComte JR. 1966. The nitrogenase system from Azotobacter: two-enzyme requirement for N2 reduction, ATP-dependent H2 evolution, and ATP hydrolysis. Proc Natl Acad Sci U S A. 56(3):979–986. doi:10.1073/pnas.56.3.979.

Bulteau AL, O'Neill HA, Kennedy MC, Ikeda-Saito M, Isaya G, Szweda LI. 2004. Frataxin acts as an iron chaperone protein to modulate mitochondrial aconitase activity. Science (80-). 305(5681):242–245. doi:10.1126/science.1098991.

Burki F, Corradi N, Sierra R, Pawlowski J, Meyer GR, Abbott CL, Keeling PJ. 2013. Phylogenomics of the intracellular parasite mikrocytos mackini reveals evidence for a mitosome in rhizaria. Curr Biol. 23(16):1541–1547. doi:10.1016/j.cub.2013.06.033.

Bych K, Kerscher S, Netz DJA, Pierik AJ, Zwicker K, Huynen MA, Lill R, Brandt U, Balk J. 2008. The iron-Sulfur protein Ind1 is required for effective complex I assembly. EMBO J. 27(12):1736–1746. doi:10.1038/emboj.2008.98.

Bych K, Netz DJAA, Vigani G, Bill E, Lill R, Pierik AJ, Balk J. 2008. The essential cytosolic iron-sulfur protein Nbp35 acts without Cfd1 partner in the green lineage. J Biol Chem. 283(51):35797–35804. doi:10.1074/jbc.M807303200.

Cai K, Frederick RO, Dashti H, Markley JL. 2018. Architectural Features of Human Mitochondrial Cysteine Desulfurase Complexes from Crosslinking Mass Spectrometry and Small-Angle X-Ray Scattering. Structure. 26(8):1127-1136.e4. doi:10.1016/j.str.2018.05.017.

Cai K, Frederick RO, Tonelli M, Markley JL. 2018. Interactions of iron-bound frataxin with ISCU and ferredoxin on the cysteine desulfurase complex leading to Fe-S cluster assembly. J Inorg Biochem. 183:107–116. doi:10.1016/j.jinorgbio.2018.03.007.

Cai K, Liu G, Frederick RO, Xiao R, Montelione GT, Markley JL. 2016. Structural/Functional Properties of Human NFU1, an Intermediate [4Fe-4S] Carrier in Human Mitochondrial Iron-Sulfur Cluster Biogenesis. Structure. 24(12):2080–2091. doi:10.1016/j.str.2016.08.020.

Cai K, Tonelli M, Frederick RO, Markley JL. 2017. Human Mitochondrial Ferredoxin 1 (FDX1) and Ferredoxin 2 (FDX2) Both Bind Cysteine Desulfurase and Donate Electrons for Iron-Sulfur Cluster Biosynthesis. Biochemistry. 56(3):487–499. doi:10.1021/acs.biochem.6b00447.

Cameron JM, Janer A, Levandovskiy V, MacKay N, Rouault TA, Tong WH, Ogilvie I, Shoubridge EA, Robinson BH. 2011. Mutations in iron-sulfur cluster scaffold genes NFU1 and BOLA3 cause a fatal deficiency of multiple respiratory chain and 2-oxoacid dehydrogenase enzymes. Am J Hum Genet. 89(4):486–495. doi:10.1016/j.ajhg.2011.08.011.

Camire EJ, Grossman JD, Thole GJ, Fleischman NM, Perlstein DL. 2015. The Yeast Nbp35-Cfd1 Cytosolic Iron-Sulfur Cluster Scaffold Is an ATPase. J Biol Chem. 290(39):23793–23802. doi:10.1074/jbc.M115.667022.

Canfield DE. 1998. A new model for Proterozoic ocean chemistry. Nature. 396(6710):450–453. doi:10.1038/24839.

Cardona T, Sánchez-Baracaldo P, Rutherford AW, Larkum AW. 2019. Early Archean origin of Photosystem II. Geobiology. 17(2):127–150. doi:10.1111/gbi.12322.

Carpenter KJ, Waller RF, Keeling PJ. 2008. Surface Morphology of Saccinobaculus (Oxymonadida): Implications for Character Evolution and Function in Oxymonads. Protist. 159(2):209–221. doi:10.1016/j.protis.2007.09.002.

Carpenter KJ, Weber PK, Davisson ML, Pett-Ridge J, Haverty MI, Keeling PJ. 2013. Correlated SEM, FIB-SEM, TEM, and NanoSIMS imaging of microbes from the hindgut of a lower termite: Methods for in situ functional and ecological studies of uncultivable microbes. Microsc Microanal. 19(6):1490–1501. doi:10.1017/S1431927613013482.

Cejka P, Cannavo E, Polaczek P, Masuda-Sasa T, Pokharel S, Campbell JL, Kowalczykowski SC. 2010. DNA end resection by Dna2-Sgs1-RPA and its stimulation by Top3-Rmi1 and Mre11-Rad50-Xrs2. Nature. 467(7311):112–116. doi:10.1038/nature09355.

Cicchillo RM, Iwig DF, Jones AD, Nesbitt NM, Baleanu-Gogonea C, Souder MG, Tu L, Booker SJ. 2004. Lipoyl synthase requires two equivalents of S-adenosyl-L-methionine to synthesize one equivalent of lipoic acid. Biochemistry. 43(21):6378–6386. doi:10.1021/bi049528x.

Cicchillo RM, Lee KH, Baleanu-Gogonea C, Nesbitt NM, Krebs C, Booker SJ. 2004. Escherichia coli lipoyl synthase binds two distinct [4Fe-4S] clusters per polypeptide. Biochemistry. 43(37):11770–11781. doi:10.1021/bi0488505.

Ciofi-Baffoni S, Nasta V, Banci L. 2018. Protein networks in the maturation of human iron-sulfur proteins. Metallomics. 10(1):49–72. doi:10.1039/c7mt00269f.

Crack JC, Stapleton MR, Green J, Thomson AJ, Le Brun NE. 2013. Mechanism of [4Fe-4S](Cys)4 cluster nitrosylation is conserved among NO-responsive regulators. J Biol Chem. 288(16):11492–11502. doi:10.1074/jbc.M112.439901.

Cruz-Ramos H, Crack J, Wu G, Hughes MN, Scott C, Thomson AJ, Green J, Poole RK. 2002. NO sensing by FNR: Regulation of the Escherichia coli NO-detoxifying flavohaemoglobin, Hmp. EMBO J. 21(13):3235–3244. doi:10.1093/emboj/cdf339.

Cunningham RP, Asahara H, Bank JF, Scholes CP, Salerno JC, Surerus K, Miinck E, McCracken J, Peisach J, Emptage MH. 1989. Endonuclease III Is an Iron-Sulfur Protein. Biochemistry. 28(10):4450–4455. doi:10.1021/bi00436a049.

Cupp-Vickery JR, Peterson JC, Ta DT, Vickery LE. 2004. Crystal structure of the molecular chaperone HscA substrate binding domain complexed with the IscU recognition peptide ELPPVKIHC. J Mol Biol. 342(4):1265–1278. doi:10.1016/j.jmb.2004.07.025.

Cupp-Vickery JR, Silberg JJ, Ta DT, Vickery LE. 2004. Crystal structure of IscA, an iron-sulfur cluster assembly protein from Escherichia coli. J Mol Biol. 338(1):127–137. doi:10.1016/j.jmb.2004.02.027.

Cupp-Vickery JR, Vickery LE. 2000. Crystal structure of Hsc20, a J-type co-chaperone from Escherichia coli. J Mol Biol. 304(5):835–845. doi:10.1006/jmbi.2000.4252.

Curatti L, Ludden PW, Rubio LM. 2006. NifB-dependent in vitro synthesis of the iron-molybdenum cofactor of nitrogenase. Proc Natl Acad Sci U S A. 103(14):5297–5301. doi:10.1073/pnas.0601115103.

Dai Y, Kim D, Dong G, Busenlehner LS, Frantom PA, Outten FW. 2015. SufE D74R Substitution Alters Active Site Loop Dynamics to Further Enhance SufE Interaction with the SufS Cysteine Desulfurase. Biochemistry. 54(31):4824–4833. doi:10.1021/acs.biochem.5b00663.

Dai Y, Outten FW. 2012. The E. coli SufS-SufE sulfur transfer system is more resistant to oxidative stress than IscS-IscU. FEBS Lett. 586(22):4016–4022. doi:10.1016/j.febslet.2012.10.001.

Dean DR, Bolin JT, Zheng L. 1993. Nitrogenase metalloclusters: structures, organization, and synthesis. J Bacteriol. 175(21):6737–6744. doi:10.1128/JB.175.21.6737-6744.1993.

Demple B, Ding H, Jorgensen M. 2002. Escherichia coli SoxR protein: Sensor/transducer of oxidative stress and nitric oxide. Methods Enzymol. 348:355–364. doi:10.1016/s0076-6879(02)48654-5.

Derosa MC, Sancar A, Barton JK. 2005. Electrically monitoring DNA repair by photolyase. Proc Natl Acad Sci U S A. 102(31):10788–10792. doi:10.1073/pnas.0503527102.

Dibley MG, Formosa LE, Lyu B, Reljic B, McGann D, Muellner-Wong L, Kraus F, Sharpe AJ, Stroud DA, Ryan MT. 2020. The mitochondrial acyl-carrier protein interaction network highlights important roles for LYRM family members in complex i and mitoribosome assembly. Mol Cell Proteomics. 19(1):65–77. doi:10.1074/mcp.RA119.001784.

Ding H, Clark RJ. 2004. Characterization of iron binding in IscA, an ancient iron-Sulfur cluster assembly protein. Biochem J. 379(2):433–440. doi:10.1042/BJ20031702.

Ding H, Clark RJ, Ding B. 2004. IscA mediates iron delivery for assembly of iron-sulfur clusters in IscU under the limited accessible free iron conditions. J Biol Chem. 279(36):37499–37504. doi:10.1074/jbc.M404533200.

Djaman O, Outten FW, Imlay JA. 2004. Repair of oxidized iron-sulfur clusters in Escherichia coli. J Biol Chem. 279(43):44590–44599. doi:10.1074/jbc.M406487200.

Dolezal P, Dagley MJ, Kono M, Wolynec P, Likić VA, Foo JH, Sedinová M, Tachezy J, Bachmann A, Bruchhaus I, et al. 2010. The Essentials of Protein Import in the Degenerate Mitochondrion of Entamoeba histolytica. Soldati-Favre D, editor. PLoS Pathog. 6(3):e1000812. doi:10.1371/journal.ppat.1000812.

Dolezal P, Dancis A, Lesuisse E, Sutak R, Hrdý I, Embley TM, Tachezy J. 2007. Frataxin, a conserved mitochondrial protein, in the hydrogenosome of Trichomonas vaginalis. Eukaryot Cell. 6(8):1431–1438. doi:10.1128/EC.00027-07.

Dong J, Lai R, Nielsen K, Fekete CA, Qiu H, Hinnebusch AG. 2004. The essential ATP-binding cassette protein RLI1 functions in translation by promoting preinitiation complex assembly. J Biol Chem. 279(40):42157–42168. doi:10.1074/jbc.M404502200.

Dong M, Dando EE, Kotliar I, Su X, Dzikovski B, Freed JH, Lin H. 2019. The asymmetric function of Dph1–Dph2 heterodimer in diphthamide biosynthesis. J Biol Inorg Chem. 24(6):777–782. doi:10.1007/s00775-019-01702-0

Dong M, Zhang Y, Lin H. 2018. Noncanonical Radical SAM Enzyme Chemistry Learned from Diphthamide Biosynthesis. Biochemistry. 57(25):3454–3459. doi:10.1021/acs.biochem.8b00287.

Drake HL, Hu SI, Wood HG. 1981. Purification of five components from Clostridium thermoaceticum which catalyze synthesis of acetate from pyruvate and methyltetrahydrofolate. Properties of phosphotransacetylase. J Biol Chem. 256(21):11137–11144.

Dufour YS, Kiley PJ, Donohue TJ. 2010. Reconstruction of the Core and Extended Regulons of Global Transcription Factors. Burkholder WF, editor. PLoS Genet. 6(7):e1001027. doi:10.1371/journal.pgen.1001027.

Dutkiewicz R, Nowak M. 2018. Molecular chaperones involved in mitochondrial iron–sulfur protein biogenesis. J Biol Inorg Chem. 23(4):569–579. doi:10.1007/s00775-017-1504-x.

Duxin JP, Dao B, Martinsson P, Rajala N, Guittat L, Campbell JL, Spelbrink JN, Stewart SA. 2009. Human Dna2 Is a Nuclear and Mitochondrial DNA Maintenance Protein. Mol Cell Biol. 29(15):4274–4282. doi:10.1128/mcb.01834-08.

Eady RR, Robson RL. 1984. Characteristics of N2 fixation in Mo-limited batch and continuous cultures of Azotobacter vinelandii. Biochem J. 224(3):853–862. doi:10.1042/bj2240853.

Eisenstein RS. 2000. Iron regulatory proteins and the molecular control of mammalian iron metabolism. Annu Rev Nutr. 20(1):627–662. doi:10.1146/annurev.nutr.20.1.627.

Embley TM, Finlay BJ, Dyal PL, Hirt RP, Wilkinson M, Williams AG. 1995. Multiple origins of anaerobic ciliates with hydrogenosomes within the radiation of aerobic ciliates. Proc R Soc London Ser B Biol Sci. 262(1363):87–93. doi:10.1098/rspb.1995.0180.

Embley TM, Finlay BJ, Thomas RH, Dyal PL. 1992. The use of rRNA sequences and fluorescent probes to investigate the phylogenetic positions of the anaerobic ciliate Metopus palaeformis and its archaeobacterial endosymbiont. J Gen Microbiol. 138(7):1479–1487. doi:10.1099/00221287-138-7-1479.

Evans MC, Buchanan BB, Arnon DI. 1966. A new ferredoxin-dependent carbon reduction cycle in a photosynthetic bacterium. Proc Natl Acad Sci U S A. 55(4):928–934. doi:10.1073/pnas.55.4.928.

Expert D, Boughammoura A, Franza T. 2008. Siderophore-controlled iron assimilation in the enterobacterium Erwinia chrysanthemi: Evidence for the involvement of bacterioferritin and the suf iron-sulfur cluster assembly machinery. J Biol Chem. 283(52):36564–36572. doi:10.1074/jbc.M807749200.

Ezraty B, Gennaris A, Barras F, Collet JF. 2017. Oxidative stress, protein damage and repair in bacteria. Nat Rev Microbiol. 15(7):385–396. doi:10.1038/nrmicro.2017.26.

Fan L, Fuss JO, Cheng QJ, Arvai AS, Hammel M, Roberts VA, Cooper PK, Tainer JA. 2008. XPD Helicase Structures and Activities: Insights into the Cancer and Aging Phenotypes from XPD Mutations. Cell. 133(5):789–800. doi:10.1016/j.cell.2008.04.030.

Farooq MA, Pracheil TM, Dong Z, Xiao F, Liu Z. 2013. Mitochondrial DNA instability in cells lacking aconitase correlates with iron citrate toxicity. Oxid Med Cell Longev. 2013:493536. doi:10.1155/2013/493536.

Fenchel T, Finlay BJ. 1991. Endosymbiotic Methanogenic Bacteria In Anaerobic Ciliates: Significance For the Growth Efficiency of the Host. J Protozool. 38(1):18–22. doi:10.1111/j.1550-7408.1991.tb04788.x.

Fernández FJ, Ardá A, López-Estepa M, Aranda J, Peña-Soler E, Garces F, Round A, Campos-Olivas R, Bruix M, Coll M, et al. 2016. Mechanism of sulfur transfer across protein-protein interfaces: The cysteine desulfurase model system. ACS Catal. 6(6):3975–3984. doi:10.1021/acscatal.6b00360.

Finlay T., Fenchel BJ. 1996. Ecology and Evolution in Anoxic Worlds. J Evol Biol. 9(2):259–260. doi:10.1046/j.1420-9101.1996.9020259.x.

Flint DH, Tuminello JF, Emptage MH. 1993. The inactivation of Fe-S cluster containing hydro-lyases by superoxide. J Biol Chem. 268(30):22369–22376.

Fontecave M. 2006. Iron-sulfur clusters: Ever-expanding roles. Nat Chem Biol. 2(4):171–174. doi:10.1038/nchembio0406-171.

Fontecilla-Camps JC, Volbeda A, Cavazza C, Nicolet Y. 2007. Structure/function relationships of [NiFe]- and [FeFe]-hydrogenases. Chem Rev. 107(10):4273–4303. doi:10.1021/cr050195z.

Fox NG, Das D, Chakrabarti M, Lindahl PA, Barondeau DP. 2015. Frataxin Accelerates [2Fe-2S] Cluster Formation on the Human Fe-S Assembly Complex. Biochemistry. 54(25):3880–3889. doi:10.1021/bi5014497.

Fox NG, Yu X, Feng X, Bailey HJ, Martelli A, Nabhan JF, Strain-Damerell C, Bulawa C, Yue WW, Han S. 2019. Structure of the human frataxin-bound iron-sulfur cluster assembly complex provides insight into its activation mechanism. Nat Commun. 10(1). doi:10.1038/s41467-019-09989-y.

Freibert SA, Goldberg A V., Hacker C, Molik S, Dean P, Williams TA, Nakjang S, Long S, Sendra K, Bill E, et al. 2017. Evolutionary conservation and in vitro reconstitution of microsporidian iron-sulfur cluster biosynthesis. Nat Commun. 8. doi:10.1038/ncomms13932.

Frey PA, Booker SJ. 2001. Radical mechanisms of S-adenosylmethionine-dependent enzymes. Adv Protein Chem. 58:1–45. doi:10.1016/s0065-3233(01)58001-8.

Fromme JC, Banerjee A, Huang SJ, Verdine GL. 2004. Structural basis for removal of adenine mispaired with 8-oxoguanine by MutY adenine DNA glycosylase. Nat Mater. 427(6975):652–656. doi:10.1038/nature02306.

Fu W, Jack RF, Morgan TV, Dean DR, Johnson MK. 1994. nifU Gene Product from Azotobacter vinelandii Is a Homodimer That Contains Two Identical [2Fe-2S] Clusters. Biochemistry. 33(45):13455–13463. doi:10.1021/bi00249a034.

Fuchs G. 2011. Alternative Pathways of Carbon Dioxide Fixation: Insights into the Early Evolution of Life? Annu Rev Microbiol. 65(1):631–658. doi:10.1146/annurev-micro-090110-102801.

Fujii T, Maeda M, Mihara H, Kurihara T, Esaki N, Hata Y. 2000. Structure of a NifS homologue: X-ray structure analysis of CsdB, an Escherichia coli counterpart of mammalian selenocysteine lyase. Biochemistry. 39(6):1263–1273. doi:10.1021/bi991732a.

Fujishiro T, Terahata T, Kunichika K, Yokoyama N, Maruyama C, Asai K, Takahashi Y. 2017. Zinc-Ligand Swapping Mediated Complex Formation and Sulfur Transfer between SufS and SufU for Iron-Sulfur Cluster Biogenesis in Bacillus subtilis. J Am Chem Soc. 139(51):18464–18467. doi:10.1021/jacs.7b11307.

Furdui C, Ragsdale SW. 2000. The role of pyruvate ferredoxin oxidoreductase in pyruvate synthesis during autotrophic growth by the Wood-Ljungdahl pathway. J Biol Chem. 275(37):28494–28499. doi:10.1074/jbc.M003291200.

Fuss JO, Tsai CL, Ishida JP, Tainer JA. 2015. Emerging critical roles of Fe-S clusters in DNA replication and repair. Biochim Biophys Acta - Mol Cell Res. 1853(6):1253–1271. doi:10.1016/j.bbamcr.2015.01.018.

Gao H, Subramanian S, Couturier J, Naik SG, Kim S-K, Leustek T, Knaff DB, Wu H-C, Vignols F, Huynh BH, et al. 2013. Arabidopsis thaliana Nfu2 Accommodates [2Fe-2S] or [4Fe-4S] Clusters and Is Competent for in Vitro

Maturation of Chloroplast [2Fe-2S] and [4Fe-4S] Cluster-Containing Proteins. Biochemistry. 52(38):6633–6645. doi:10.1021/bi4007622.

Gari K, Ortiz AML, Borel V, Flynn H, Skehel JM, Boulton SJ, Leon Ortiz AM, Borel V, Flynn H, Skehel JM, et al. 2012. MMS19 links cytoplasmic iron-sulfur cluster assembly to DNA metabolism. Science (80-). 337(6091):243–245. doi:10.1126/science.1219664.

Gentry LE, Thacker MA, Doughty R, Timkovich R, Busenlehner LS. 2013. His86 from the N-terminus of frataxin coordinates iron and is required for Fe-S cluster synthesis. Biochemistry. 52(35):6085–6096. doi:10.1021/bi400443n.

Georgiadis MM, Komiya H, Chakrabarti P, Woo D, Kornuc JJ, Rees DC. 1992. Crystallographic structure of the nitrogenase iron protein from Azotobacter vinelandii. Science (80-). 257(5077):1653–1659. doi:10.1126/science.1529353.

Gerber J, Lill R. 2002. Biogenesis of iron-sulfur proteins in eukaryotes: Components, mechanism and pathology. Mitochondrion. 2(1–2):71–86. doi:10.1016/S1567-7249(02)00041-7.

Gerber J, Mühlenhoff U, Lill R. 2003. An interaction between frataxin and Isu1/Nfs1 that is crucial for Fe/S cluster synthesis on Isu1. EMBO Rep. 4(9):906–911. doi:10.1038/sj.embor.embor918.

Gervason S, Larkem D, Mansour A Ben, Botzanowski T, Müller CS, Pecqueur L, Le Pavec G, Delaunay-Moisan A, Brun O, Agramunt J, et al. 2019. Physiologically relevant reconstitution of iron-sulfur cluster biosynthesis uncovers persulfide-processing functions of ferredoxin-2 and frataxin. Nat Commun. 10(1):3566. doi:10.1038/s41467-019-11470-9.

Gibson TJ, Koonin E V., Musco G, Pastore A, Bork P. 1996. Friedreich's ataxia protein: Phylogenetic evidence for mitochondrial dysfunction. Trends Neurosci. 19(11):465–468. doi:10.1016/S0166-2236(96)20054-2.

Giel JL, Nesbit AD, Mettert EL, Fleischhacker AS, Wanta BT, Kiley PJ. 2013. Regulation of iron-Sulfur cluster homeostasis through transcriptional control of the Isc pathway by [2Fe-2S]-IscR in Escherichia coli. Mol Microbiol. 87(3):478–492. doi:10.1111/mmi.12052.

Van Der Giezen M, Cox S, Tovar J. 2004. The iron-sulfur cluster assembly genes iscS and iscU of Entamoeba histolytica were acquired by horizontal gene transfer. BMC Evol Biol. 4:7. doi:10.1186/1471-2148-4-7.

Gill EE, Diaz-Triviño S, Barberà MJ, Silberman JD, Stechmann A, Gaston D, Tamas I, Roger AJ. 2007. Novel mitochondrion-related organelles in the anaerobic amoeba Mastigamoeba balamuthi. Mol Microbiol. 66(6):1306–1320. doi:10.1111/j.1365-2958.2007.05979.x.

Glaser T, Hedman B, Hodgson KO, Solomon EI. 2000. Ligand K-edge X-ray absorption spectroscopy: A direct probe of ligand - Metal covalency. Acc Chem Res. 33(12):859–868. doi:10.1021/ar990125c.

Goldberg A V., Molik S, Tsaousis AD, Neumann K, Kuhnke G, Delbac F, Vivares CP, Hirt RP, Lill R, Embley TM. 2008. Localization and functionality of microsporidian iron-Sulfur cluster assembly proteins. Nature. 452(7187):624–628. doi:10.1038/nature06606.

Goldsmith-Fischman S, Kuzin A, Edstrom WC, Benach J, Shastry R, Xiao R, Acton TB, Honig B, Montelione GT, Hunt JF. 2004. The SufE sulfur-acceptor protein contains a conserved core structure that mediates interdomain interactions in a variety of redox protein complexes. J Mol Biol. 344(2):549–565. doi:10.1016/j.jmb.2004.08.074.

Golinelli M-P, Chatelet C, Duin EC, Johnson MK, Meyer J. 1998. Extensive Ligand Rearrangements around the [2Fe-2S] Cluster of Clostridium pasteurianum Ferredoxin †. Biochemistry. 37(29):10429–10437. doi:10.1021/bi9806394.

Gomez-Lorenzo MG, Spahn CM, Agrawal RK, Grassucci RA, Penczek P, Chakraburtty K, Ballesta JP, Lavandera JL, Garcia-Bustos JF, Frank J. 2000. Three-dimensional cryo-electron microscopy localization of EF2 in the Saccharomyces cerevisiae 80S ribosome at 17.5 A resolution. EMBO J. 19(11):2710–8. doi:10.1093/emboj/19.11.2710.

Gourdoupis S, Nasta V, Calderone V, Ciofi-Baffoni S, Banci L. 2018. IBA57 Recruits ISCA2 to Form a [2Fe-2S] Cluster-Mediated Complex. J Am Chem Soc. 140(43). doi:10.1021/jacs.8b09061.

de Graaf RM, Ricard G, van Alen TA, Duarte I, Dutilh BE, Burgtorf C, Kuiper JWP, van der Staay GWM, Tielens AGM, Huynen MA, et al. 2011. The Organellar Genome and Metabolic Potential of the Hydrogen-Producing Mitochondrion of Nyctotherus ovalis. Mol Biol Evol. 28(8):2379–2391. doi:10.1093/molbev/msr059. https://doi.org/10.1093/molbev/msr059.

Gray MW. 2012. Mitochondrial evolution. Cold Spring Harb Perspect Biol. 4(9). doi:10.1101/cshperspect.a011403.

Gray MW. 2014. The pre-endosymbiont hypothesis: A new perspective on the origin and evolution of mitochondria. Cold Spring Harb Perspect Biol. 6(3). doi:10.1101/cshperspect.a016097.

Greening C, Biswas A, Carere CR, Jackson CJ, Taylor MC, Stott MB, Cook GM, Morales SE. 2016. Genomic and metagenomic surveys of hydrogenase distribution indicate H 2 is a widely utilised energy source for microbial growth and survival. ISME J. 10(3):761–777. doi:10.1038/ismej.2015.153.

Grishin N V., Phillips MA, Goldsmith EJ. 1995. Modeling of the spatial structure of eukaryotic ornithine decarboxylases. Protein Sci. 4(7):1291–1304. doi:10.1002/pro.5560040705.

Gruer MJ, Artymiuk PJ, Guest JR. 1997. The aconitase family: three structural variations on a common theme. Trends Biochem Sci. 22(1):3–6. doi:10.1016/s0968-0004(96)10069-4.

Hae Kim J, Tonelli M, Kim T, Markley JL. 2012. Three-dimensional structure and determinants of stability of the iron-sulfur cluster scaffold protein IscU from escherichia coli. Biochemistry. 51(28):5557–5563. doi:10.1021/bi300579p.

Hagen KS, Reynolds JG, Holm RH. 1981. Definition of reaction sequences resulting in self-assembly of [Fe4S4(SR)4]2- clusters from simple reactants. J Am Chem Soc. 103(14):4054–4063. doi:10.1021/ja00404a013.

Haile DJ, Rouault TA, Harford JB, Kennedy MC, Blondin GA, Beinert H, Klausner RD. 1992. Cellular regulation of the iron-responsive element binding protein: Disassembly of the cubane iron-sulfur cluster results in high-affinity RNA binding. Proc Natl Acad Sci U S A. 89(24):11735–11739. doi:10.1073/pnas.89.24.11735.

Hamann E, Gruber-Vodicka H, Kleiner M, Tegetmeyer HE, Riedel D, Littmann S, Chen J, Milucka J, Viehweger B, Becker KW, et al. 2016. Environmental Breviatea harbour mutualistic Arcobacter epibionts. Nature. 534(7606):254–258. doi:10.1038/nature18297.

Hampl V. 2017. Preaxostyla. In: Handbook of the Protists. Cham: Springer International Publishing. p. 1139–1174.

Hampl V, Hug L, Leigh JW, Dacks JB, Lang BF, Simpson AGB, Roger AJ. 2009. Phylogenomic analyses support the monophyly of Excavata and resolve relationships among eukaryotic ‘supergroups’. Proc Natl Acad Sci. 106(10):3859–3864. doi:10.1073/pnas.0807880106.

Hänzelmann P, Schindelin H. 2004. Crystal structure of the S-adenosylmethionine-dependent enzyme MoaA and its implications for molybdenum cofactor deficiency in humans. Proc Natl Acad Sci U S A. 101(35):12870–12875. doi:10.1073/pnas.0404624101.

Hausmann A, Aguilar Netz DJ, Balk J, Pierik AJ, Muhlenhoff U, Lill R. 2005. The eukaryotic P loop NTPase Nbp35: An essential component of the cytosolic and nuclear iron-sulfur protein assembly machinery. Proc Natl Acad Sci. 102(9):3266–3271. doi:10.1073/pnas.0406447102.

Hedderich R, Albracht SPJ, Linder D, Koch J, Thauer RK. 1992. Isolation and characterization of polyferredoxin from Methanobacterium thermoautotrophicum The mvhb gene product of the methylviologen-reducing hydrogenase operon. FEBS Lett. 298(1):65–68. doi:10.1016/0014-5793(92)80023-A.

Heinz E, Williams TA, Nakjang S, Noël CJ, Swan DC, Goldberg A V., Harris SR, Weinmaier T, Markert S, Becher D, et al. 2012. The Genome of the Obligate Intracellular Parasite Trachipleistophora hominis: New Insights into Microsporidian Genome Dynamics and Reductive Evolution. PLoS Pathog. 8(10). doi:10.1371/journal.ppat.1002979.

Hentze MW, Kühn LC. 1996. Molecular control of vertebrate iron metabolism: mRNA-based regulatory circuits operated by iron, nitric oxide, and oxidative stress. Proc Natl Acad Sci U S A. 93(16):8175–8182. doi:10.1073/pnas.93.16.8175.

Hernández HL, Pierrel F, Elleingand E, García-Serres R, Huynh BH, Johnson MK, Fontecave M, Atta M. 2007. MiaB, a Bifunctional Radical- S- Adenosylmethionine Enzyme Involved in the Thiolation and Methylation of tRNA, Contains Two Essential [4Fe-4S] Clusters †. Biochemistry. 46(17):5140–5147. doi:10.1021/bi7000449.

Herrero E, De La Torre-Ruiz MA. 2007. Monothiol glutaredoxins: A common domain for multiple functions. Cell Mol Life Sci. 64(12):1518–1530. doi:10.1007/s00018-007-6554-8.

Herskovitz T, Averill BA, Holm RH, Ibers JA, Phillips WD, Weiher JF. 1972. Structure and properties of a synthetic analogue of bacterial iron--sulfur proteins. Proc Natl Acad Sci U S A. 69(9):2437–2441. doi:10.1073/pnas.69.9.2437.

Hine PM, Bower SM, Meyer GR, Cochennec-Laureau N, Berthe FCJ. 2001. Ultrastructure of Mikrocytos mackini, the cause of Denman Island disease in oysters Crassostrea spp. and Ostrea spp. in British Columbia, Canada. Dis Aquat Organ. 45(3):215–227. doi:10.3354/dao045215.

Hirabayashi K, Yuda E, Tanaka N, Katayama S, Iwasaki K, Matsumoto T, Kurisu G, Outten FW, Fukuyama K, Takahashi Y, et al. 2015. Functional dynamics revealed by the structure of the SufBCD Complex, a novel ATP-binding cassette (ABC) protein that serves as a scaffold for iron-sulfur cluster biogenesis. J Biol Chem. 290(50):29717–29731. doi:10.1074/jbc.M115.680934.

Hiratsuka T, Furihata K, Ishikawa J, Yamashita H, Itoh N, Seto H, Dairi T. 2008. An alternative menaquinone biosynthetic pathway operating in microorganisms. Science (80-). 321(5896):1670–1673. doi:10.1126/science.1160446.

Holland HD. 2002. Volcanic gases, black smokers, and the great oxidation event. Geochim Cosmochim Acta. 66(21):3811–3826. doi:10.1016/S0016-7037(02)00950-X.

Holliday GL, Akiva E, Meng EC, Brown SD, Calhoun S, Pieper U, Sali A, Booker SJ, Babbitt PC. 2018. Atlas of the Radical SAM Superfamily: Divergent Evolution of Function Using a “Plug and Play” Domain. In: Methods in Enzymology. Vol. 606. Academic Press Inc. p. 1–71.

Holliday GL, Thornton JM, Marquet A, Smith AG, Rébeillé F, Mendel R, Schubert HL, Lawrence AD, Warren MJ. 2007. Evolution of enzymes and pathways for the biosynthesis of cofactors. Nat Prod Rep. 24(5):972–987. doi:10.1039/b703107f.

Horner DS, Hirt RP, Embley TM. 1999. A single eubacterial origin of eukaryotic pyruvate:ferredoxin oxidoreductase genes: Implications for the evolution of anaerobic eukaryotes. Mol Biol Evol. 16(9):1280–1291. doi:10.1093/oxfordjournals.molbev.a026218.

Hu CK, Coughlin M, Field CM, Mitchison TJ. 2011. KIF4 regulates midzone length during cytokinesis. Curr Biol. 21(10):815–824. doi:10.1016/j.cub.2011.04.019.

Huet G, Daffé M, Saves I. 2005. Identification of the Mycobacterium tuberculosis SUF machinery as the exclusive mycobacterial system of [Fe-S] cluster assembly: Evidence for its implication in the pathogen’s survival. J Bacteriol. 187(17):6137–6146. doi:10.1128/JB.187.17.6137-6146.2005.

Chabrière E, Vernède X, Guigliarelli B, Charon MH, Hatchikian EC, Fontecilla-Camps JC. 2001. Crystal structure of the free radical intermediate of pyruvate:ferredoxin oxidoreductase. Science (80-). 294(5551):2559–2563. doi:10.1126/science.1066198.

Chahal H, Dai Y, Saini A. 2009. The SufBCD Fe− S scaffold complex interacts with SufA for Fe− S cluster transfer. Biochemistry. 48(44):10644–10653. doi:10.1021/bi901518y.The. http://pubs.acs.org/doi/abs/10.1021/bi901518y.

Chahal HK, Outten FW. 2012. Separate FeS scaffold and carrier functions for SufB2C 2 and SufA during in vitro maturation of [2Fe2S] Fdx. J Inorg Biochem. 116:126–134. doi:10.1016/j.jinorgbio.2012.06.008.

Chandramouli K, Johnson MK. 2006. HscA and HscB stimulate [2Fe-2S] cluster transfer from IscU to apoferredoxin in an ATP-dependent reaction. Biochemistry. 45(37):11087–11095. doi:10.1021/bi061237w.

Chandramouli K, Unciuleac MC, Naik S, Dean DR, Boi HH, Johnson MK. 2007. Formation and properties of [4Fe-4S] clusters on the IscU scaffold protein. Biochemistry. 46(23):6804–6811. doi:10.1021/bi6026659.

Charon MH, Volbeda A, Chabriere E, Pieulle L, Fontecilla-Camps JC. 1999. Structure and electron transfer mechanism of pyruvate:ferredoxin oxidoreductase. Curr Opin Struct Biol. 9(6):663–669. doi:10.1016/S0959-440X(99)00027-5.

Chen XJ, Wang X, Butow RA. 2007. Yeast aconitase binds and provides metabolically coupled protection to mitochondrial DNA. Proc Natl Acad Sci U S A. 104(34):13738–13743. doi:10.1073/pnas.0703078104.

Chen ZQ, Dong J, Ishimura A, Daar I, Hinnebusch AG, Dean M. 2006. The essential vertebrate ABCE1 protein interacts with eukaryotic initiation factors. J Biol Chem. 281(11):7452–7457. doi:10.1074/jbc.M510603200.

Chiang SM, Schellhorn HE. 2012. Regulators of oxidative stress response genes in Escherichia coli and their functional conservation in bacteria. Arch Biochem Biophys. 525(2):161–169. doi:10.1016/j.abb.2012.02.007.

Imlay JA. 2006. Iron-Sulfur clusters and the problem with oxygen. Mol Microbiol. 59(4):1073–1082. doi:10.1111/j.1365-2958.2006.05028.x.

Imlay JA. 2013. The molecular mechanisms and physiological consequences of oxidative stress: Lessons from a model bacterium. Nat Rev Microbiol. 11(7):443–454. doi:10.1038/nrmicro3032.

Ito S, Tan LJ, Andoh D, Narita T, Seki M, Hirano Y, Narita K, Kuraoka I, Hiraoka Y, Tanaka K. 2010. MMXD, a TFIIH-Independent XPD-MMS19 Protein Complex Involved in Chromosome Segregation. Mol Cell. 39(4):632–640. doi:10.1016/j.molcel.2010.07.029.

Jacobson MR, Brigle KE, Bennett LT, Setterquist RA, Wilson MS, Cash VL, Beynon J, Newton WE, Dean DR. 1989. Physical and genetic map of the major nif gene cluster from Azotobacter vinelandii. J Bacteriol. 171(2):1017–1027. doi:10.1128/jb.171.2.1017-1027.1989.

Jang S, Imlay JA. 2007. Micromolar intracellular hydrogen peroxide disrupts metabolism by damaging iron-sulfur enzymes. J Biol Chem. 282(2):929–37. doi:10.1074/jbc.M607646200.

Jedelský PL, Doležal P, Rada P, Pyrih J, Šmíd O, Hrdý I, Šedinová M, Marcinčiková M, Voleman L, Perry AJ, et al. 2011. The minimal proteome in the reduced mitochondrion of the parasitic protist Giardia intestinalis. Lightowlers B, editor. PLoS One. 6(2):e17285. doi:10.1371/journal.pone.0017285.

Jenner LB, Demeshkina N, Yusupova G, Yusupov M. 2010. Structural aspects of messenger RNA reading frame maintenance by the ribosome. Nat Struct Mol Biol. 17(5):555–560. doi:10.1038/nsmb.1790.

Jerlström-Hultqvist J, Einarsson E, Xu F, Hjort K, Ek B, Steinhauf D, Hultenby K, Bergquist J, Andersson JO, Svärd SG. 2013. Hydrogenosomes in the diplomonad Spironucleus salmonicida. Nat Commun. 4:1–9. doi:10.1038/ncomms3493.

Johansson C, Roos AK, Montano SJ, Sengupta R, Filippakopoulos P, Guo K, Von Delft F, Holmgren A, Oppermann U, Kavanagh KL. 2011. The crystal structure of human GLRX5: Iron-sulfur cluster co-ordination, tetrameric assembly and monomer activity. Biochem J. 433(2):303–311. doi:10.1042/BJ20101286.

Johansson E, MacNeill SA. 2010. The eukaryotic replicative DNA polymerases take shape. Trends Biochem Sci. 35(6):339–347. doi:10.1016/j.tibs.2010.01.004.

Johnson DC, Dean DR, Smith AD, Johnson MK. 2005. Structure, Function, and Formation of Biological Iron-Sulfur Clusters. Annu Rev Biochem. 74(1):247–281. doi:10.1146/annurev.biochem.74.082803.133518.

Johnson DCC, Dos Santos PCC, Dean DRR. 2005. NifU and NifS are required for the maturation of nitrogenase and cannot replace the function of isc -gene products in Azotobacter vinelandii. Biochem Soc Trans. 33(1):90–93. doi:10.1042/BST0330090.

Jühling F, Mörl M, Hartmann RK, Sprinzl M, Stadler PF, Pütz J. 2009. tRNAdb 2009: compilation of tRNA sequences and tRNA genes. Nucleic Acids Res. 37(Database issue):D159-62. doi:10.1093/nar/gkn772.

Kakuta Y, Horio T, Takahashi Y, Fukuyama K. 2001. Crystal structure of Escherichia coli Fdx, an adrenodoxin-type ferredoxin involved in the assembly of iron-sulfur clusters. Biochemistry. 40(37):11007–11012. doi:10.1021/bi010544t.

Kameshwar AKS, Qin W. 2018. Genome Wide Analysis Reveals the Extrinsic Cellulolytic and Biohydrogen Generating Abilities of Neocallimastigomycota Fungi . J Genomics. 6:74–87. doi:10.7150/jgen.25648.

Karnkowska A, Treitli SCSC, Brzoň O, Novák L, Vacek V, Soukal P, Barlow LDLD, Herman EKEK, Pipaliya SVSV, Pánek T, et al. 2019. The Oxymonad Genome Displays Canonical Eukaryotic Complexity in the Absence of a Mitochondrion. Mol Biol Evol. 36(10):2292–2312. doi:10.1093/molbev/msz147.

Karnkowska A, Vacek V, Zubáčová Z, Treitli SCSC, Petrželková R, Eme L, Novák L, Žárský V, Barlow LDLD, Herman EKEK, et al. 2016. A eukaryote without a mitochondrial organelle. Curr Biol. 26(10):1274–1284. doi:10.1016/j.cub.2016.03.053.

Katinka MD, Duprat S, Cornillott E, Méténler G, Thomarat F, Prensier G, Barbe V, Peyretaillade E, Brottier P, Wincker P, et al. 2001. Genome sequence and gene compaction of the eukaryote parasite Encephalitozoon cuniculi. Nature. 414(6862):450–453. doi:10.1038/35106579.

Keeling PJ, Leander BS. 2003. Characterisation of a Non-canonical genetic code in the oxymonad Streblomastix strix. J Mol Biol. 326(5):1337–1349. doi:10.1016/S0022-2836(03)00057-3.

Kehrenberg C, Schwarz S, Jacobsen L, Hansen LH, Vester B. 2005. A new mechanism for chloramphenicol, florfenicol and clindamycin resistance: Methylation of 23S ribosomal RNA at A2503. Mol Microbiol. 57(4):1064–1073. doi:10.1111/j.1365-2958.2005.04754.x.

Kenne AN, Kim S, Park SY. 2016. The crystal structure of Escherichia coli CsdE. Int J Biol Macromol. 87:317–321. doi:10.1016/j.ijbiomac.2016.02.071.

Khoshnevis S, Gross T, Rotte C, Baierlein C, Ficner R, Krebber H. 2010. The iron-Sulfur protein RNase L inhibitor functions in translation termination. EMBO Rep. 11(3):214–219. doi:10.1038/embor.2009.272.

Kim J, Rees DC. 1992. Structural models for the metal centers in the nitrogenase molybdenum-iron protein. Science (80-). 257(5077):1677–1682. doi:10.1126/science.1529354.

Kim JH, Bothe JR, Frederick RO, Holder JC, Markley JL. 2014. Role of IscX in iron-sulfur cluster biogenesis in Escherichia coli. J Am Chem Soc. 136(22):7933–7942. doi:10.1021/ja501260h.

Kim JH, Frederick RO, Reinen NM, Troupis AT, Markley JL. 2013. [2Fe-2S]-Ferredoxin binds directly to cysteine desulfurase and supplies an electron for iron-sulfur cluster assembly but is displaced by the scaffold protein or bacterial frataxin. J Am Chem Soc. 135(22):8117–8120. doi:10.1021/ja401950a.

Kim KD, Chung WH, Kim HJ, Lee KC, Roe JH. 2010. Monothiol glutaredoxin Grx5 interacts with Fe-S scaffold proteins Isa1 and Isa2 and supports Fe-S assembly and DNA integrity in mitochondria of fission yeast. Biochem Biophys Res Commun. 392(3):467–472. doi:10.1016/j.bbrc.2010.01.051.

Kim S-H. 2009. IscR Modulates Catalase A (KatA) Activity, Peroxide Resistance, and Full Virulence of Pseudomonas aeruginosa PA14. J Microbiol Biotechnol. 19(12):1520–1526. doi:10.4014/jmb.0906.06028.

Kim S, Park SY. 2013. Structural changes during cysteine desulfurase CsdA and sulfur acceptor CsdE interactions provide insight into the trans-persulfuration. J Biol Chem. 288(38):27172–27180. doi:10.1074/jbc.M113.480277.

Kirschvink JL, Kopp RE. 2008. Palaeoproterozoic ice houses and the evolution of oxygen-mediating enzymes: The case for a late origin of photosystem II. In: Philosophical Transactions of the Royal Society B: Biological Sciences. Vol. 363. Royal Society. p. 2755–2765.

Kispal G, Csere P, Prohl C, Lill R. 1999. The mitochondrial proteins Atm1p and Nfs1p are essential for biogenesis of cytosolic Fe/S proteins. EMBO J. 18(14):3981–3989. doi:10.1093/emboj/18.14.3981.

Kitaoka S, Wada K, Hasegawa Y, Minami Y, Fukuyama K, Takahashi Y. 2006. Crystal structure of Escherichia coli SufC, an ABC-type ATPase component of the SUF iron-sulfur cluster assembly machinery. FEBS Lett. 580(1):137–143. doi:10.1016/j.febslet.2005.11.058.

Kobayashi K, Fujikawa M, Kozawa T. 2014. Oxidative stress sensing by the iron-sulfur cluster in the transcription factor, SoxR. J Inorg Biochem. 133:87–91. doi:10.1016/j.jinorgbio.2013.11.008.

Koeppen AH. 2011. Friedreich's ataxia: Pathology, pathogenesis, and molecular genetics. J Neurol Sci. 303(1–2):1–12. doi:10.1016/j.jns.2011.01.010.

Kolisko M, Silberman JD, Cepicka I, Yubuki N, Takishita K, Yabuki A, Leander BS, Inouye I, Inagaki Y, Roger AJ, et al. 2010. A wide diversity of previously undetected free-living relatives of diplomonads isolated from marine/saline habitats. Environ Microbiol. 12(10):2700–2710. doi:10.1111/j.1462-2920.2010.02239.x.

de Koning AP, Noble GP, Heiss AA, Wong J, Keeling PJ. 2007. Environmental PCR survey to determine the distribution of a non-canonical genetic code in uncultivable oxymonads. Environ Microbiol. 0(0):070907020408002-??? doi:10.1111/j.1462-2920.2007.01430.x.

Körner H, Sofia HJ, Zumft WG. 2003. Phylogeny of the bacterial superfamily of Crp-Fnr transcription regulators: Exploiting the metabolic spectrum by controlling alternative gene programs. FEMS Microbiol Rev. 27(5):559–592. doi:10.1016/S0168-6445(03)00066-4.

Krebs C, Agar JN, Smith AD, Frazzon J, Dean DR, Huynh BH, Johnson MK. 2001. IscA, an alternate scaffold for Fe-S cluster biosynthesis. Biochemistry. 40(46):14069–14080. doi:10.1021/bi015656z.

Kuo CF, McRee DE, Fisher CL, O'Handley SF, Cunningham RP, Tainer JA. 1992. Atomic structure of the DNA repair [4Fe-4S] enzyme endonuclease III. Science (80-). 258(5081):434–440. doi:10.1126/science.1411536.

LaGier MJ, Tachezy J, Stejskal F, Kutisova K, Keithly JS. 2003. Mitochondrial-type iron-sulfur cluster biosynthesis genes (IscS and IscU) in the apicomplexan Cryptosporidium parvum. Microbiology. 149(12):3519–3530. doi:10.1099/mic.0.26365-0.

Landry AP, Cheng Z, Ding H. 2013. Iron binding activity is essential for the function of IscA in iron–Sulfur cluster biogenesis. Dalt Trans. 42(9):3100–3106. doi:10.1039/C2DT32000B. http://xlink.rsc.org/?DOI=C2DT32000B.

Lange H, Lisowsky T, Gerber J, Mühlenhoff U, Kispal G, Lill R. 2001. An essential function of the mitochondrial sulfhydryl oxidase Erv1p/ALR in the maturation of cytosolic Fe/S proteins. EMBO Rep. 2(8):715–720. doi:10.1093/embo-reports/kve161.

Lanz ND, Booker SJ. 2012. Identification and function of auxiliary iron-sulfur clusters in radical SAM enzymes. Biochim Biophys Acta - Proteins Proteomics. 1824(11):1196–1212. doi:10.1016/j.bbapap.2012.07.009.

Lanz ND, Booker SJ. 2015. Auxiliary iron-sulfur cofactors in radical SAM enzymes. Biochim Biophys Acta - Mol Cell Res. 1853(6):1316–1334. doi:10.1016/j.bbamcr.2015.01.002.

Layer G, Aparna Gaddam S, Ayala-Castro CN, Choudens SO De, Lascoux D, Fontecave M, Outten FW. 2007. SufE transfers sulfur from SufS to SufB for iron-sulfur cluster assembly. J Biol Chem. 282(18):13342–13350. doi:10.1074/jbc.M608555200.

Layer G, Ollagnier-De Choudens S, Sanakis Y, Fontecave M. 2006. Iron-sulfur cluster biosynthesis: Characterization of escherichia coli CYaY as an iron donor for the assembly of [2Fe-2S] clusters in the scaffold IscU. J Biol Chem. 281(24):16256–16263. doi:10.1074/jbc.M513569200.

Leander BS, Keeling PJ. 2004. Symbiotic innovation in the oxymonad Streblomastix strix. J Eukaryot Microbiol. 51(3):291–300. doi:10.1111/j.1550-7408.2004.tb00569.x.

Lecompte O, Ripp R, Thierry J-C, Moras D, Poch O. 2002. Comparative analysis of ribosomal proteins in complete genomes: an example of reductive evolution at the domain scale. Nucleic Acids Res. 30(24):5382–5390. doi:10.1093/nar/gkf693.

Lee JB, Hite RK, Hamdan SM, Xie XS, Richardson CC, Van Oijen AM. 2006. DNA primase acts as a molecular brake in DNA replication. Nature. 439(7076):621–624. doi:10.1038/nature04317.

Leger MM, Eme L, Hug LA, Roger AJ. 2016. Novel Hydrogenosomes in the Microaerophilic Jakobid Stygiella incarcerata. Mol Biol Evol. 33(9):2318–2336. doi:10.1093/molbev/msw103.

Leger MM, Kolisko M, Kamikawa R, Stairs CW, Kume K, Čepička I, Silberman JD, Andersson JO, Xu F, Yabuki A, et al. 2017. Organelles that illuminate the origins of Trichomonas hydrogenosomes and Giardia mitosomes. Nat Ecol Evol. 1(4):0092. doi:10.1038/s41559-017-0092.

Léon S, Touraine B, Ribot C, Briat JF, Lobréaux S. 2003. Iron-Sulfur cluster assembly in plants: Distinct NFU proteins in mitochondria and plastids from Arabidopsis thaliana. Biochem J. 371(3):823–830. doi:10.1042/BJ20021946.

Lewis WH, Lind AE, Sendra KM, Onsbring H, Williams TA, Esteban GF, Hirt RP, Ettema TJGG, Embley TM. 2019. Convergent Evolution of Hydrogenosomes from Mitochondria by Gene Transfer and Loss. Mol Biol Evol. 37(2):524–539. doi:10.1093/molbev/msz239.

Li DS, Ohshima K, Jiralerspong S, Bojanowski MW, Pandolfo M. 1999. Knock-out of the cyaY gene in Escherichia coli does not affect cellular iron content and sensitivity to oxidants. FEBS Lett. 456(1):13–16. doi:10.1016/S0014-5793(99)00896-0.

Li H, DT M, NN D, SG N, NS L, BM H, PJ R-G, BH H, MK J, CE O. 2009. The yeast iron regulatory proteins Grx3/4 and Fra2 form heterodimeric complexes containing a [2Fe-2S] cluster with cysteinyl and histidyl ligation. Biochemistry. 48(40):9569–9581.

Li H, Mapolelo DT, Dingra NN, Keller G, Riggs-Gelasco PJ, Winge DR, Johnson MK, Outten CE. 2011. Histidine 103 in Fra2 Is an Iron-Sulfur Cluster Ligand in the [2Fe-2S] Fra2-Grx3 Complex and Is Required for in Vivo Iron Signaling in Yeast. J Biol Chem. 286(1):867–876. doi:10.1074/jbc.M110.184176.

Li H, Outten CE. 2012. Monothiol CGFS Glutaredoxins and BolA-like Proteins: [2Fe-2S] Binding Partners in Iron Homeostasis. Biochemistry. 51(22):4377–4389. doi:10.1021/bi300393z.

Li J, Cowan JA. 2015. Glutathione-coordinated [2Fe-2S] cluster: A viable physiological substrate for mitochondrial ABCB7 transport. Chem Commun. 51(12):2253–2255. doi:10.1039/c4cc09175b.

Li L, Fröhlich J, König H. 2005. Cellulose Digestion in the Termite Gut. In: Intestinal Microorganisms of Termites and Other Invertebrates. Springer-Verlag. p. 221–241.

Liapounova NA, Hampl V, Gordon PMK, Sensen CW, Gedamu L, Dacks JB. 2006. Reconstructing the mosaic glycolytic pathway of the anaerobic eukaryote Monocercomonoides. Eukaryot Cell. 5(12):2138–2146. doi:10.1128/EC.00258-06.

Lim JG, Choi SH. 2014. IscR is a global regulator essential for pathogenesis of vibrio vulnificus and induced by host cells. Infect Immun. 82(2):569–578. doi:10.1128/IAI.01141-13.

Lima CD. 2002. Analysis of the E. coli NifS CsdB protein at 2.0 Å reveals the structural basis for perselenide and persulfide intermediate formation. J Mol Biol. 315(5):1199–1208. doi:10.1006/jmbi.2001.5308.

Lin TY, Abbassi NEH, Zakrzewski K, Chramiec-Głąbik A, Jemioła-Rzemińska M, Różycki J, Glatt S. 2019. The Elongator subunit Elp3 is a non-canonical tRNA acetyltransferase. Nat Commun. 10(1). doi:10.1038/s41467-019-08579-2.

Liu G, Li Z, Chiang Y, Acton T, Montelione GT, Murray D, Szyperski T. 2009. High-quality homology models derived from NMR and X-ray structures of E. coli proteins YgdK and Suf E suggest that all members of the YgdK/Suf E protein family are enhancers of cysteine desulfurases. Protein Sci. 14(6):1597–1608. doi:10.1110/ps.041322705.

Liu H, Rudolf J, Johnson KA, McMahon SA, Oke M, Carter L, McRobbie AM, Brown SE, Naismith JH, White MF. 2008. Structure of the DNA Repair Helicase XPD. Cell. 133(5):801–812. doi:10.1016/j.cell.2008.04.029.

Liu L, Huang M. 2015. Essential role of the iron-sulfur cluster binding domain of the primase regulatory subunit Pri2 in DNA replication initiation. Protein Cell. 6(3):194–210. doi:10.1007/s13238-015-0134-8.

Liu Y, Sieprawska-Lupa M, Whitman WB, White RH. 2010. Cysteine is not the sulfur source for iron-sulfur cluster and methionine biosynthesis in the methanogenic archaeon Methanococcus maripaludis. J Biol Chem. 285(42):31923–31929. doi:10.1074/jbc.M110.152447.

Ljungdahl L. 1986. The Autotrophic Pathway of Acetate Synthesis in Acetogenic Bacteria. Annu Rev Microbiol. 40(1):415–450. doi:10.1146/annurev.micro.40.1.415.

Loiseau L, Ollagnier-de-Choudens S, Nachin L, Fontecave M, Barras F. 2003. Biogenesis of Fe-S cluster by the bacterial suf system. SufS and SufE form a new type of cysteine desulfurase. J Biol Chem. 278(40):38352–38359. doi:10.1074/jbc.M305953200.

Loiseau L, Ollagnier-De Choudens S, Lascoux D, Forest E, Fontecave M, Barras F. 2005. Analysis of the heteromeric CsdA-CsdE cysteine desulfurase, assisting Fe-S cluster biogenesis in Escherichia coli. J Biol Chem. 280(29):26760–26769. doi:10.1074/jbc.M504067200.

Long KS, Poehlsgaard J, Kehrenberg C, Schwarz S, Vester B. 2006. The Cfr rRNA methyltransferase confers resistance to phenicols, lincosamides, oxazolidinones, pleuromutilins, and streptogramin A antibiotics. Antimicrob Agents Chemother. 50(7):2500–2505. doi:10.1128/AAC.00131-06.

López-Estepa M, Ardá A, Savko M, Round A, Shepard WE, Bruix M, Coll M, Fernández FJ, Jiménez-Barbero J, Vega MC. 2015. The crystal structure and small-angleX-ray analysis of CsdL/TcdA reveal a new tRNA binding motif in the MoeB/E1 superfamily. PLoS One. 10(4). doi:10.1371/journal.pone.0118606.

Lotierzo M, Tse Sum Bui B, Florentin D, Escalettes F, Marquet A. 2005. Biotin synthase mechanism: An overview. In: Biochemical Society Transactions. Vol. 33. p. 820–823.

Lu J, Yang J, Tan G, Ding H. 2008. Complementary roles of SufA and IscA in the biogenesis of iron-sulfur clusters in Escherichia coli. Biochem J. 409(2):535–543. doi:10.1042/BJ20071166.

Lubitz W, Reijerse E, van Gastel M. 2007. [NiFe] and [FeFe] hydrogenases studied by advanced magnetic resonance techniques. Chem Rev. 107(10):4331–4365. doi:10.1021/cr050186q.

Lushchak O V., Piroddi M, Galli F, Lushchak VI. 2014. Aconitase post-translational modification as a key in linkage between Krebs cycle, iron homeostasis, redox signaling, and metabolism of reactive oxygen species. Redox Rep. 19(1):8–15. doi:10.1179/1351000213Y.0000000073.

Lyons TW, Reinhard CT, Planavsky NJ. 2014. The rise of oxygen in Earth’s early ocean and atmosphere. Nature. 506(7488):307–315. doi:10.1038/nature13068.

Machnicka MA, Milanowska K, Oglou OO, Purta E, Kurkowska M, Olchowik A, Januszewski W, Kalinowski S, Dunin-Horkawicz S, Rother KM, et al. 2013. MODOMICS: A database of RNA modification pathways - 2013 update. Nucleic Acids Res. 41(D1). doi:10.1093/nar/gks1007.

Maio N, Kim KS, Singh A, Rouault TA. 2017. A Single Adaptable Cochaperone-Scaffold Complex Delivers Nascent Iron-Sulfur Clusters to Mammalian Respiratory Chain Complexes I–III. Cell Metab. 25(4):945-953.e6. doi:10.1016/j.cmet.2017.03.010.

Maio N, Rouault TA. 2015. Iron-sulfur cluster biogenesis in mammalian cells: New insights into the molecular mechanisms of cluster delivery. Biochim Biophys Acta - Mol Cell Res. 1853(6):1493–1512. doi:10.1016/j.bbamcr.2014.09.009.

Maio N, Rouault TA. 2016. Mammalian Fe-S proteins: Definition of a consensus motif recognized by the co-chaperone HSC20. Metallomics. 8(10):1032–1046. doi:10.1039/c6mt00167j.

Maio N, Singh A, Uhrigshardt H, Saxena N, Tong WH, Rouault TA. 2014. Cochaperone binding to LYR motifs confers specificity of iron sulfur cluster delivery. Cell Metab. 19(3):445–457. doi:10.1016/j.cmet.2014.01.015.

Malkin R, Rabinowitz JC. 1966. The reconstitution of clostridial ferredoxin. Biochem Biophys Res Commun. 23(6):822–827. doi:10.1016/0006-291X(66)90561-4.

Manicki M, Majewska J, Ciesielski S, Schilke B, Blenska A, Kominek J, Marszalek J, Craig EA, Dutkiewicz R. 2014. Overlapping binding sites of the frataxin homologue assembly factor and the heat shock protein 70 transfer factor on the Isu iron-sulfur cluster scaffold protein. J Biol Chem. 289(44):30268–30278. doi:10.1074/jbc.M114.596726.

Mapolelo DT, Zhang B, Naik SG, Huynh BH, Johnson MK. 2012. Spectroscopic and functional characterization of iron-sulfur cluster-bound forms of azotobacter vinelandii NifIscA. Biochemistry. 51(41):8071–8084. doi:10.1021/bi3006658.

Mapolelo DT, Zhang B, Randeniya S, Albetel A-N, Li H, Couturier J, Outten CE, Rouhier N, Johnson MK. 2013. Monothiol glutaredoxins and A-type proteins: partners in Fe–S cluster trafficking. Dalt Trans. 42(9):3107. doi:10.1039/c2dt32263c.

Mapolelo DT, Zhang B, Randeniya S, Albetel AN, Li H, Couturier J, Outten CE, Rouhier N, Johnson MK. 2013. Monothiol glutaredoxins and A-type proteins: Partners in Fe-S cluster trafficking. Dalt Trans. 42(9):3107–3115. doi:10.1039/c2dt32263c.

Maralikova B, Ali V, Nakada-Tsukui K, Nozaki T, van der Giezen M, Henze K, Tovar J. 2010. Bacterial-type oxygen detoxification and iron-sulfur cluster assembly in amoebal relict mitochondria. Cell Microbiol. 12(3):331–342. doi:10.1111/j.1462-5822.2009.01397.x.

Marinoni EN, Deoliveira JS, Nicolet Y, Raulfs EC, Amara P, Dean DR, Fontecilla-Camps JC. 2012. (IscS-IscU) 2 complex structures provide insights into Fe 2S 2 biogenesis and transfer. Angew Chemie - Int Ed. 51(22):5439–5442. doi:10.1002/anie.201201708.

Martin W, Russell MJ. 2003. On the origins of cells: a hypothesis for the evolutionary transitions from abiotic geochemistry to chemoautotrophic prokaryotes, and from prokaryotes to nucleated cells. Allen JF, Raven JA, editors. Philos Trans R Soc London Ser B Biol Sci. 358(1429):59–85. doi:10.1098/rstb.2002.1183.

Martin W, Russell MJ. 2007. On the origin of biochemistry at an alkaline hydrothermal vent. Philos Trans R Soc B Biol Sci. 362(1486):1887–1925. doi:10.1098/rstb.2006.1881.

Mayerle JJ, Frankel RB, Holm RH, Ibers JA, Phillips WD, Weiher JF. 1973. Synthetic analogs of the active sites of iron sulfur proteins. Structure and properties of bis[o xylyldithiolato μ 2 sulfidoferrate(III)], an analog of the 2Fe 2S proteins. Proc Natl Acad Sci U S A. 70(8):2429–2433. doi:10.1073/pnas.70.8.2429.

Melber A, Na U, Vashisht A, Weiler BD, Lill R, Wohlschlegel JA, Winge DR. 2016. Role of Nfu1 and Bol3 in iron-sulfur cluster transfer to mitochondrial clients. Elife. 5(AUGUST). doi:10.7554/eLife.15991.

Menon S, Ragsdale SW. 1996. Evidence that carbon monoxide is an obligatory intermediate in anaerobic acetyl-CoA synthesis. Biochemistry. 35(37):12119–12125. doi:10.1021/bi961014d.

Mesecke N, Terziyska N, Kozany C, Baumann F, Neupert W, Hell K, Herrmann JM. 2005. A disulfide relay system in the intermembrane space of mitochondria that mediates protein import. Cell. 121(7):1059–1069. doi:10.1016/j.cell.2005.04.011.

Mettert EL, Kiley PJ. 2015. Fe-S proteins that regulate gene expression. Biochim Biophys Acta. 1853(6):1284–1293. doi:10.1016/j.bbamcr.2014.11.018.

Meyer J. 2008. Iron-sulfur protein folds, iron-sulfur chemistry, and evolution. J Biol Inorg Chem. 13(2):157–170. doi:10.1007/s00775-007-0318-7.

Meza-Cervantez P, González-Robles A, Cárdenas-Guerra RE, Ortega-López J, Saavedra E, Pineda E, Arroyo R. 2011. Pyruvate: Ferredoxin oxidoreductase (PFO) is a surface-associated cell-binding protein in Trichomonas vaginalis and is involved in trichomonal adherence to host cells. Microbiology. 157(12):3469–3482. doi:10.1099/mic.0.053033-0.

Mi-ichi F, Yousuf MA, Nakada-Tsukui K, Nozaki T. 2009. Mitosomes in Entamoeba histolytica contain a sulfate activation pathway. Proc Natl Acad Sci. 106(51):21731–21736. doi:10.1073/pnas.0907106106.

Mihara H, Esaki N. 2003. Bacterial cysteine desulfurases: Their function and mechanisms. Appl Microbiol Biotechnol. 60(1–2):12–23. doi:10.1007/s00253-002-1107-4.

Mihara H, Fujii T, Kato S ichiro, Kurihara T, Hata Y, Esaki N. 2002. Structure of external aldimine of Escherichia coli CsdB, an IscS/NifS homolog: Implications for its specificity toward selenocysteine. J Biochem. 131(5):679–685. doi:10.1093/oxfordjournals.jbchem.a003151.

Mihara H, Kurihara T, Yoshimura T, Esaki N. 2000. Kinetic and mutational studies of three NifS homologs from Escherichia coli: mechanistic difference between L-cysteine desulfurase and L-selenocysteine lyase reactions. J Biochem. 127(4):559–67. doi:10.1093/oxfordjournals.jbchem.a022641.

Mihara H, Kurihara T, Yoshimura T, Soda K, Esaki N. 1997. Cysteine sulfinate desulfinase, a NIFS-like protein of Escherichia coli with selenocysteine lyase and cysteine desulfurase activities. Gene cloning, purification, and characterization of a novel pyridoxal enzyme. J Biol Chem. 272(36):22417–22424. doi:10.1074/jbc.272.36.22417.

Michta E, Ding W, Zhu S, Blin K, Ruan H, Wang R, Wohlleben W, Mast Y. 2014. Proteomic approach to reveal the regulatory function of aconitase AcnA in oxidative stress response in the antibiotic producer Streptomyces viridochromogenes Tü494. PLoS One. 9(2). doi:10.1371/journal.pone.0087905.

Miller CN, Jossé L, Tsaousis AD. 2018a. Localization of Fe-S Biosynthesis Machinery in Cryptosporidium parvum Mitosome. J Eukaryot Microbiol. 65(6):913–922. doi:10.1111/jeu.12663.

Miller CN, Jossé L, Tsaousis AD. 2018b. Localization of Fe-S Biosynthesis Machinery in Cryptosporidium parvum Mitosome. J Eukaryot Microbiol. 65(6):913–922. doi:10.1111/jeu.12663.

Miller HK, Kwuan L, Schwiesow L, Bernick DL, Mettert E, Ramirez HA, Ragle JM, Chan PP, Kiley PJ, Lowe TM, et al. 2014. IscR Is Essential for Yersinia pseudotuberculosis Type III Secretion and Virulence. PLoS Pathog. 10(6). doi:10.1371/journal.ppat.1004194.

Miller JR, Busby RW, Jordan SW, Cheek J, Henshaw TF, Ashley GW, Broderick JB, Cronan JE, Marletta MA. 2000. Escherichia coli lipA is a lipoyl synthase: In vitro biosynthesis of lipoylated pyruvate dehydrogenase complex from octanoyl-acyl carrier protein. Biochemistry. 39(49):15166–15178. doi:10.1021/bi002060n.

Miyauchi K, Kimura S, Suzuki T. 2013. A cyclic form of N 6-threonylcarbamoyladenosine as a widely distributed tRNA hypermodification. Nat Chem Biol. 9(2):105–111. doi:10.1038/nchembio.1137.

Molina-Navarro MM, Casas C, Piedrafita L, Bellí G, Herrero E. 2006. Prokaryotic and eukaryotic monothiol glutaredoxins are able to perform the functions of Grx5 in the biogenesis of Fe/S clusters in yeast mitochondria. FEBS Lett. 580(9):2273–2280. doi:10.1016/j.febslet.2006.03.037.

Morimoto K, Yamashita E, Kondou Y, Lee SJ, Arisaka F, Tsukihara T, Nakai M. 2006. The Asymmetric IscA Homodimer with an Exposed [2Fe-2S] Cluster Suggests the Structural Basis of the Fe-S Cluster Biosynthetic Scaffold. J Mol Biol. 360(1):117–132. doi:10.1016/j.jmb.2006.04.067.

Mortenson LE, Valentine RC, Carnahan JE. 1962. An electron transport factor from Clostridium pasteurianum. Biochem Biophys Res Commun. 7(6):448–452. doi:10.1016/0006-291X(62)90333-9.

Moser CC, Page CC, Farid R, Dutton PL. 1995. Biological electron transfer. J Bioenerg Biomembr. 27(3):263–274. doi:10.1007/BF02110096.

Muckenthaler MU, Galy B, Hentze MW. 2008. Systemic Iron Homeostasis and the Iron-Responsive Element/Iron-Regulatory Protein (IRE/IRP) Regulatory Network. Annu Rev Nutr. 28(1):197–213. doi:10.1146/annurev.nutr.28.061807.155521.

Mueller EG. 2006. Trafficking in persulfides: Delivering sulfur in biosynthetic pathways. Nat Chem Biol. 2(4):185–194. doi:10.1038/nchembio779.

Mühlenhoff U, Gerber J, Richhardt N, Lill R. 2003. Components involved in assembly and dislocation of iron-sulfur clusters on the scaffold protein Isu1p. EMBO J. 22(18):4815–4825. doi:10.1093/emboj/cdg446.

Mühlenhoff U, Molik S, Godoy JR, Uzarska MA, Richter N, Seubert A, Zhang Y, Stubbe J, Pierrel F, Herrero E, et al. 2010. Cytosolic monothiol glutaredoxins function in intracellular iron sensing and trafficking via their bound iron-sulfur cluster. Cell Metab. 12(4):373–385. doi:10.1016/j.cmet.2010.08.001.

Mühlenhoff U, Richter N, Pines O, Pierik AJ, Lill R. 2011. Specialized function of yeast Isa1 and Isa2 proteins in the maturation of mitochondrial [4Fe-4S] proteins. J Biol Chem. 286(48):41205–41216. doi:10.1074/jbc.M111.296152.

Mulder DW, Boyd ES, Sarma R, Lange RK, Endrizzi JA, Broderick JB, Peters JW. 2010. Stepwise FeFe-hydrogenase H-cluster assembly revealed in the structure of HydA ΔeFG. Nature. 465(7295):248–251. doi:10.1038/nature08993.

Mulholland SE, Gibney BR, Rabanal F, Dutton PL. 1998. Characterization of the Fundamental Protein Ligand Requirements of [4Fe-4S] $^{2+/+}$ Clusters with Sixteen Amino Acid Maquettes. J Am Chem Soc. 120(40):10296–10302. doi:10.1021/ja981279a.

Muller M, Mentel M, van Hellemond JJ, Henze K, Woehle C, Gould SB, Yu R-Y, van der Giezen M, Tielens AGM, Martin WF. 2012. Biochemistry and Evolution of Anaerobic Energy Metabolism in Eukaryotes. Microbiol Mol Biol Rev. 76(2):444–495. doi:10.1128/mmbr.05024-11.

Munday R. 1989. Toxicity of thiols and disulphides: Involvement of free-radical species. Free Radic Biol Med. 7(6):659–673. doi:10.1016/0891-5849(89)90147-0.

Murphy CJ, Arkin MR, Ghatlia ND, Bossmann S, Turro NJ, Barton JK. 1994. Fast photoinduced electron transfer through DNA intercalation. Proc Natl Acad Sci U S A. 91(12):5315–5319. doi:10.1073/pnas.91.12.5315.

Murphy CJ, Arkin MR, Jenkins Y, Ghatlia ND, Bossmann SH, Turro NJ, Barton JK. 1993. Long-range photoinduced electron transfer through a DNA helix. Science (80-). 262(5136):1025–1029. doi:10.1126/science.7802858.

Nachin L, El Hassouni M, Loiseau L, Expert D, Barras F. 2001. SoxR-dependent response to oxidative stress and virulence of Erwinia chrysanthemi: the key role of SufC, an orphan ABC ATPase. Mol Microbiol. 39(4):960–972. doi:10.1046/j.1365-2958.2001.02288.x.

Nachin L, Loiseau L, Expert D, Barras F. 2003. SufC: an unorthodox cytoplasmic ABC/ATPase required for [Fe-S] biogenesis under oxidative stress. EMBO J. 22(3):427–37. doi:10.1093/emboj/cdg061.

Nasta V, Giachetti A, Ciofi-Baffoni S, Banci L. 2017. Structural insights into the molecular function of human [2Fe-2S] BOLA1-GRX5 and [2Fe-2S] BOLA3-GRX5 complexes. Biochim Biophys Acta - Gen Subj. 1861(8):2119–2131. doi:10.1016/j.bbagen.2017.05.005.

Nasta V, Suraci D, Gourdoupis S, Ciofi-Baffoni S, Banci L. 2020. A pathway for assembling [4Fe-4S]2+ clusters in mitochondrial iron–sulfur protein biogenesis. FEBS J. 287(11):2312–2327. doi:10.1111/febs.15140.

Nasta V, Da Vela S, Gourdoupis S, Ciofi-Baffoni S, Svergun DI, Banci L. 2019. Structural properties of [2Fe-2S] ISCA2-IBA57: a complex of the mitochondrial iron-sulfur cluster assembly machinery. Sci Rep. 9(1). doi:10.1038/s41598-019-55313-5.

Navarro-Sastre A, Tort F, Stehling O, Uzarska MA, Arranz JA, Del Toro M, Labayru MT, Landa J, Font A, Garcia-Villoria J, et al. 2011. A fatal mitochondrial disease is associated with defective NFU1 function in the maturation of a subset of mitochondrial Fe-S proteins. Am J Hum Genet. 89(5):656–667. doi:10.1016/j.ajhg.2011.10.005.

Nesbit AD, Giel JL, Rose JC, Kiley PJ. 2009. Sequence-Specific Binding to a Subset of IscR-Regulated Promoters Does Not Require IscR Fe-S Cluster Ligation. J Mol Biol. 387(1):28–41. doi:10.1016/j.jmb.2009.01.055.

Netz DJA, Genau HM, Weiler BD, Bill E, Pierik AJ, Lill R. 2016. The conserved protein Dre2 uses essential [2Fe-2S] and [4Fe-4S] clusters for its function in cytosolic iron-sulfur protein assembly. Biochem J. 473(14):2073–2085. doi:10.1042/BCJ20160416.

Netz DJA, Pierik AJ, Stümpfig M, Mühlenhoff U, Lill R. 2007. The Cfd1-Nbp35 complex acts as a scaffold for iron-sulfur protein assembly in the yeast cytosol. Nat Chem Biol. 3(5):278–286. doi:10.1038/nchembio872.

Netz DJA, Stith CM, Stümpfig M, Köpf G, Vogel D, Genau HM, Stodola JL, Lill R, Burgers PMJ, Pierik AJ. 2012. Eukaryotic DNA polymerases require an iron-sulfur cluster for the formation of active complexes. Nat Chem Biol. 8(1):125–132. doi:10.1038/nchembio.721.

Netz DJA, Stümpfig M, Doré C, Mühlenhoff U, Pierik AJ, Lill R. 2010. Tah18 transfers electrons to Dre2 in cytosolic iron-sulfur protein biogenesis. Nat Chem Biol. 6(10):758–765. doi:10.1038/nchembio.432.

Netz DJA., Pierik AJ, Stümpfig M, Bill E, Sharma AK, Pallesen LJ, Walden WE, Lill R. 2012. A bridging [4Fe-4S] cluster and nucleotide binding are essential for function of the Cfd1-Nbp35 complex as a scaffold in iron-sulfur protein maturation. J Biol Chem. 287(15):12365–12378. doi:10.1074/jbc.M111.328914.

Nguyen LT, Schmidt HA, Von Haeseler A, Minh BQ. 2015. IQ-TREE: A fast and effective stochastic algorithm for estimating maximum-likelihood phylogenies. Mol Biol Evol. 32(1):268–274. doi:10.1093/molbev/msu300.

Nicolet Y, Piras C, Legrand P, Hatchikian CE, Fontecilla-Camps JC. 1999. Desulfovibrio desulfuricans iron hydrogenase: The structure shows unusual coordination to an active site Fe binuclear center. Structure. 7(1):13–23. doi:10.1016/S0969-2126(99)80005-7.

Nicolet Y, Rubach JK, Posewitz MC, Amara P, Mathevon C, Atta M, Fontecave M, Fontecilla-Camps JC. 2008. X-ray structure of the [FeFe]-hydrogenase maturase HydE from Thermotoga maritima. J Biol Chem. 283(27):18861–18872. doi:10.1074/jbc.M801161200.

Nimonkar A V., Genschel J, Kinoshita E, Polaczek P, Campbell JL, Wyman C, Modrich P, Kowalczykowski SC. 2011. BLM-DNA2-RPA-MRN and EXO1-BLM-RPA-MRN constitute two DNA end resection machineries for human DNA break repair. Genes Dev. 25(4):350–362. doi:10.1101/gad.2003811.

Noda S, Inoue T, Hongoh Y, Kawai M, Nalepa CA, Vongkaluang C, Kudo T, Ohkuma M. 2006. Identification and characterization of ectosymbionts of distinct lineages in Bacteroidales attached to flagellated protists in the gut of termites and a wood-feeding cockroach. Environ Microbiol. 8(1):11–20. doi:10.1111/j.1462-2920.2005.00860.x.

Noguchi F, Shimamura S, Nakayama T, Yazaki E, Yabuki A, Hashimoto T, Inagaki Y, Fujikura K, Takishita K. 2015. Metabolic Capacity of Mitochondrion-related Organelles in the Free-living Anaerobic Stramenopile Cantina marsupialis. Protist. 166(5):534–550. doi:10.1016/j.protis.2015.08.002.

Noma A, Kirino Y, Ikeuchi Y, Suzuki T. 2006. Biosynthesis of wybutosine, a hyper-modified nucleoside in eukaryotic phenylalanine tRNA. EMBO J. 25(10):2142–2154. doi:10.1038/sj.emboj.7601105.

Noodleman L, Case DA. 1992. Density-functional theory of spin polarization and spin coupling in iron—sulfur clusters. Adv Inorg Chem. 38(C):423–458. doi:10.1016/S0898-8838(08)60070-7.

Núñez ME, Noyes KT, Barton JK. 2002. Oxidative charge transport through DNA in nucleosome core particles. Chem Biol. 9(4):403–415. doi:10.1016/S1074-5521(02)00121-7.

Nürenberg-Goloub E, Heinemann H, Gerovac M, Tampé R. 2018. Ribosome recycling is coordinated by processive events in two asymmetric ATP sites of ABCE1. Life Sci Alliance. 1(3). doi:10.26508/lsa.201800095.

Nyvltova E, Sutak R, Harant K, Sedinova M, Hrdy I, Paces J, Vlcek C, Tachezy J, Nývltová E, Šuták R, et al. 2013. NIF-type iron-sulfur cluster assembly system is duplicated and distributed in the mitochondria and cytosol of Mastigamoeba balamuthi. Proc Natl Acad Sci. 110(18):7371–7376. doi:10.1073/pnas.1219590110.

O'Brien E, Holt ME, Thompson MK, Salay LE, Ehlinger AC, Chazin WJ, Barton JK. 2017. The [4Fe4S] cluster of human DNA primase functions as a redox switch using DNA charge transport. Science (80-). 355(6327). doi:10.1126/science.aag1789.

O'Brien E, Silva RMB, Barton JK. 2016. Redox Signaling through DNA. Isr J Chem. 56(9–10):705–723. doi:10.1002/ijch.201600022.

O'Kelly CJ, Farmer MA, Nerad TA. 1999. Ultrastructure of Trimastix pyriformis (Klebs) Bernard et al.: Similarities of Trimastix Species with Retortamonad and Jakobid Flagellates. Protist. 150(2):149–162. doi:10.1016/S1434-4610(99)70018-0.

O'Kelly CJ, Silberman JD, Amaral Zettler LA, Nerad TA, Sogin ML. 2003. Monopylocystis visvesvarai n. gen., n. sp. and Sawyeria marylandensis n. gen., n. sp.: Two new amitochondrial heterolobosean amoebae from anoxic environments. Protist. 154(2):281–290. doi:10.1078/143446103322166563.

Odermatt DC, Gari K. 2017. The CIA Targeting Complex Is Highly Regulated and Provides Two Distinct Binding Sites for Client Iron-Sulfur Proteins. Cell Rep. 18(6):1434–1443. doi:10.1016/j.celrep.2017.01.037.

Ohkuma M, Brune A. 2011. Diversity, structure, and evolution of the termite gut microbial community. In: Biology of Termites: A Modern Synthesis. Springer Netherlands. p. 413–438.

Ollagnier-de-Choudens S, Lascoux D, Loiseau L, Barras F, Forest E, Fontecave M. 2003. Mechanistic studies of the SufS-SufE cysteine desulfurase: evidence for sulfur transfer from SufS to SufE. FEBS Lett. 555(2):263–7.

Ollagnier-De-Choudens S, Mattioli T, Takahashi Y, Fontecave M. 2001. Iron-sulfur cluster assembly. Characterization of IscA and evidence for a specific and functional complex with ferredoxin. J Biol Chem. 276(25):22604–22607. doi:10.1074/jbc.M102902200.

Ollagnier-de-Choudens S, Sanakis Y, Fontecave M. 2004. SufA/IscA: reactivity studies of a class of scaffold proteins involved in [Fe-S] cluster assembly. JBIC J Biol Inorg Chem. 9(7):828–838. doi:10.1007/s00775-004-0581-9.

Ollagnier-de Choudens S, Nachin L, Sanakis Y, Loiseau L, Barras F, Fontecave M. 2003. SufA from Erwinia chrysanthemi. Characterization of a scaffold protein required for iron-sulfur cluster assembly. J Biol Chem. 278(20):17993–18001. doi:10.1074/jbc.M300285200.

Olson JW, Agar JN, Johnson MK, Maier RJ. 2000. Characterization of the NifU and NifS Fe-S cluster formation proteins essential for viability in Helicobacter pylori. Biochemistry. 39(51):16213–16219. doi:10.1021/bi001744s.

Orgel LE. 2008. The implausibility of metabolic cycles on the prebiotic earth. PLoS Biol. 6(1):0005–0013. doi:10.1371/journal.pbio.0060018.

Ortiz PA, Ulloque R, Kihara GK, Zheng H, Kinzy TG. 2006. Translation elongation factor 2 anticodon mimicry domain mutants affect fidelity and diphtheria toxin resistance. J Biol Chem. 281(43):32639–32648. doi:10.1074/jbc.M607076200.

Otsuka Y, Miki K, Koga M, Katayama N, Morimoto W, Takahashi Y, Yonesaki T. 2010. IscR regulates RNase LS activity by repressing rnlA transcription. Genetics. 185(3):823–830. doi:10.1534/genetics.110.114462.

Outten FW, Djaman O, Storz G. 2004. A suf operon requirement for Fe-S cluster assembly during iron starvation in Escherichia coli. Mol Microbiol. 52(3):861–872. doi:10.1111/j.1365-2958.2004.04025.x.

Outten FW, Wood MJ, Muñoz FM, Storz G, Munoz FM, Storz G. 2003. The SufE protein and the SufBCD complex enhance SufS cysteine desulfurase activity as part of a sulfur transfer pathway for Fe-S cluster assembly in Escherichia coli. J Biol Chem. 278(46):45713–9. doi:10.1074/jbc.M308004200.

Page CC, Moser CC, Chen X, Dutton PL. 1999. Natural engineering principles of electron tunnelling in biological oxidation-reduction. Nature. 402(6757):47–52. doi:10.1038/46972.

Pandey AK, Pain J, Dancis A, Pain D. 2019. Mitochondria export iron-sulfur and sulfur intermediates to the cytoplasm for iron-sulfur cluster assembly and tRNA thiolation in yeast. J Biol Chem. 294(24):9489–9502. doi:10.1074/jbc.RA119.008600.

Pánek T, Simpson AGB, Hampl V, Čepička I. 2014. Creneis carolina gen. et sp. nov. (Heterolobosea), a Novel Marine Anaerobic Protist with Strikingly Derived Morphology and Life Cycle. Protist. 165(4):542–567. doi:10.1016/j.protis.2014.05.005.

Park JS, Kolisko M, Heiss AA, Simpson AGB. 2009. Light microscopic observations, ultrastructure, and molecular phylogeny of Hicanonectes teleskopos n. g., n. sp., a deep-branching relative of diplomonads. J Eukaryot Microbiol. 56(4):373–384. doi:10.1111/j.1550-7408.2009.00412.x.

Park JS, Kolisko M, Simpson AGB. 2010. Cell morphology and formal description of Ergobibamus cyprinoides n. g., n. sp., another Carpediemonas-like relative of diplomonads. J Eukaryot Microbiol. 57(6):520–528. doi:10.1111/j.1550-7408.2010.00506.x.

Parra G, Bradnam K, Korf I. 2007. CEGMA: a pipeline to accurately annotate core genes in eukaryotic genomes. Bioinformatics. 23(9):1061–1067. doi:10.1093/bioinformatics/btm071.

Pastore C, Adinolfi S, Huynen MA, Rybin V, Martin S, Mayer M, Bukau B, Pastore A. 2006. YfhJ, a Molecular Adaptor in Iron-Sulfur Cluster Formation or a Frataxin-like Protein? Structure. 14(5):857–867. doi:10.1016/j.str.2006.02.010.

Patraa S, Barondeaua DP. 2019. Mechanism of activation of the human cysteine desulfurase complex by frataxin. Proc Natl Acad Sci U S A. 116(39):19421–19430. doi:10.1073/pnas.1909535116.

Paul VD, Lill R. 2015. Biogenesis of cytosolic and nuclear iron-sulfur proteins and their role in genome stability. Biochim Biophys Acta - Mol Cell Res. 1853(6):1528–1539. doi:10.1016/j.bbamcr.2014.12.018.

Peters JW. 1998. X-ray Crystal Structure of the Fe-Only Hydrogenase (CpI) from Clostridium pasteurianum to 1.8 Angstrom Resolution. Science (80-). 282(5395):1853–1858. doi:10.1126/science.282.5395.1853.

Petrovic A, Davis CT, Rangachari K, Clough B, Wilson RJMI, Eccleston JF. 2008. Hydrodynamic characterization of the SufBC and SufCD complexes and their interaction with fluorescent adenosine nucleotides. Protein Sci. 17(7):1264–1274. doi:10.1110/ps.034652.108.

Pilet E, Nicolet Y, Mathevon C, Douki T, Fontecilla-Camps JC, Fontecave M. 2009. The role of the maturase HydG in [FeFe]-hydrogenase active site synthesis and assembly. FEBS Lett. 583(3):506–511. doi:10.1016/j.febslet.2009.01.004.

Plank DW, Kennedy MC, Beinert H, Howard JB. 1989. Cysteine labeling studies of beef heart aconitase containing a 4Fe, a cubane 3Fe, or a linear 3Fe cluster.

Pohl T, Walter J, Stolpe S, Soufo JHD, Grauman PL, Friedrich T. 2007. Effects of the deletion of the Escherichia coli frataxin homologue CyaY on the respiratory NADH:ubiquinone oxidoreductase. BMC Biochem. 8:13. doi:10.1186/1471-2091-8-13.

Poinar GO. 2009. Description of an early Cretaceous termite (Isoptera: Kalotermitidae) and its associated intestinal protozoa, with comments on their co-evolution. Parasites and Vectors. 2(1):12. doi:10.1186/1756-3305-2-12.

Pokharel S, Campbell JL. 2012. Cross talk between the nuclease and helicase activities of Dna2: role of an essential iron-sulfur cluster domain. Nucleic Acids Res. 40(16):7821–30. doi:10.1093/nar/gks534.

Pondarré C, Antiochos BB, Campagna DR, Clarke SL, Greer EL, Deck KM, McDonald A, Han AP, Medlock A, Kutok JL, et al. 2006. The mitochondrial ATP-binding cassette transporter Abcb7 is essential in mice and participates in cytosolic iron-sulfur cluster biogenesis. Hum Mol Genet. 15(6):953–964. doi:10.1093/hmg/ddl012.

Poor CB, Wegner S V., Li H, Dlouhy AC, Schuermann JP, Sanishvili R, Hinshaw JR, Riggs-Gelasco PJ, Outten CE, He C. 2014. Molecular mechanism and structure of the Saccharomyces cerevisiae iron regulator Aft2. Proc Natl Acad Sci U S A. 111(11):4043–4048. doi:10.1073/pnas.1318869111.

Pugh RA, Honda M, Leesley H, Thomas A, Lin Y, Nilges MJ, Cann IKO, Spies M. 2008. The iron-containing domain is essential in Rad3 helicases for coupling of ATP hydrolysis to DNA translocation and for targeting the helicase to the single-stranded DNA-double-stranded DNA junction. J Biol Chem. 283(3):1732–1743. doi:10.1074/jbc.M707064200.

Puglisi R, Yan R, Adinolfi S, Pastore A. 2016. A new tessera into the interactome of the isc Operon: A novel interaction between HscB and IscS. Front Mol Biosci. 3(SEP). doi:10.3389/fmolb.2016.00048.

Py B, Barras F. 2010. Building Fe–S proteins: bacterial strategies. Nat Rev Microbiol. 8(6):436–446. doi:10.1038/nrmicro2356. http://www.nature.com/doifinder/10.1038/nrmicro2356.

Py B, Gerez C, Angelini S, Planel R, Vinella D, Loiseau L, Talla E, Brochier-Armanet C, Garcia Serres R, Latour J-M, et al. 2012. Molecular organization, biochemical function, cellular role and evolution of NfuA, an atypical Fe-S carrier. Mol Microbiol. 86(1):155–171. doi:10.1111/j.1365-2958.2012.08181.x.

Py B, Gerez C, Huguenot A, Vidaud C, Fontecave M, Ollagnier de Choudens S, Barras F. 2018. The ErpA/NfuA complex builds an oxidation-resistant Fe-S cluster delivery pathway. J Biol Chem. 293(20):7689–7702. doi:10.1074/jbc.RA118.002160.

Pyrih J, Pyrihová E, Kolísko M, Stojanovová D, Basu S, Harant K, Haindrich AC, Doležal P, Lukeš J, Roger A, et al. 2016. Minimal cytosolic iron-sulfur cluster assembly machinery of Giardia intestinalis is partially associated with mitosomes. Mol Microbiol. 102(4):701–714. doi:10.1111/mmi.13487.

Radek R. 1999. Flagellates, bacteria and fungi associated with termites. Ecotropica. 5:183–196.

Rajagopalan S, Teter SJ, Zwart PH, Brennan RG, Phillips KJ, Kiley PJ. 2013. Studies of IscR reveal a unique mechanism for metal-dependent regulation of DNA binding specificity. Nat Struct Mol Biol. 20(6):740–747. doi:10.1038/nsmb.2568.

Rajski SR, Barton JK. 2001. How different DNA-binding proteins affect long-range oxidative damage to DNA. Biochemistry. 40(18):5556–5564. doi:10.1021/bi002684t.

Reeve JN, Beckler GS, Cram DS, Hamilton PT, Brown JW, Krzycki JA, Kolodziej AF, Alex L, Orme-Johnson WH, Walsh CT. 1989. A hydrogenase-linked gene in Methanobacterium thermoautotrophicum strain delta H encodes a polyferredoxin. Proc Natl Acad Sci U S A. 86(9):3031–3035. doi:10.1073/pnas.86.9.3031.

Riboldi GP, Verli H, Frazzon J. 2009. Structural studies of the Enterococcus faecalis SufU [Fe-S] cluster protein. BMC Biochem. 10(1):1–10. doi:10.1186/1471-2091-10-3.

Richards TA, Van Der Giezen M. 2006. Evolution of the Isd11-IscS complex reveals a single α- proteobacterial endosymbiosis for all eukaryotes. Mol Biol Evol. 23(7):1341–1344. doi:10.1093/molbev/msl001.

Rivas M, Becerra A, Peretó J, Bada JL, Lazcano A. 2011. Metalloproteins and the Pyrite-based Origin of Life: A Critical Assessment. Orig Life Evol Biosph. 41(4):347–356. doi:10.1007/s11084-011-9238-1.

Rodriguez-Quinones F, Bosch R, Imperial J. 1993. Expression of the nifBfdxNnifOQ region of Azotobacter vinelandii and its role in nitrogenase activity. J Bacteriol. 175(10):2926–2935. doi:10.1128/jb.175.10.2926-2935.1993.

Roger AJ, Muñoz-Gómez SA, Kamikawa R. 2017. The Origin and Diversification of Mitochondria. Curr Biol. 27(21):R1177–R1192. doi:10.1016/j.cub.2017.09.015.

Rohde M, Trncik C, Sippel D, Gerhardt S, Einsle O. 2018. Crystal structure of VnfH, the iron protein component of vanadium nitrogenase. J Biol Inorg Chem. 23(7):1049–1056. doi:10.1007/s00775-018-1602-4.

Roche B, Agrebi R, Huguenot A, Ollagnier de Choudens S, Barras F, Py B. 2015. Turning Escherichia coli into a Frataxin-Dependent Organism. Casadesús J, editor. PLoS Genet. 11(5):e1005134. doi:10.1371/journal.pgen.1005134.

Roche B, Huguenot A, Barras F, Py B. 2015. The iron-binding CyaY and IscX proteins assist the ISC-catalyzed Fe-S biogenesis in Escherichia coli. Mol Microbiol. 95(4):605–623. doi:10.1111/mmi.12888.

Romano CA, Sontz PA, Barton JK. 2011. Mutants of the base excision repair glycosylase, endonuclease III: DNA charge transport as a first step in lesion detection. Biochemistry. 50(27):6133–6145. doi:10.1021/bi2003179.

Rose IA, O'Connell EL. 1967. Mechanism of aconitase action. I. The hydrogen transfer reaction. J Biol Chem. 242(8):1870–1879.

Rosing MT, Frei R. 2004. U-rich Archaean sea-£oor sediments from Greenland ^ indications of s 3700 Ma oxygenic photosynthesis. Elsevier. 217(3–4):237–244. doi:10.1016/S0012-821X(03)00609-5.

Ross DS. 2008. A quantitative evaluation of the iron-sulfur world and its relevance to life's origins. In: Astrobiology. Vol. 8. p. 267–272.

Rouault TA. 2019. The indispensable role of mammalian iron sulfur proteins in function and regulation of multiple diverse metabolic pathways. BioMetals. 32(3). doi:10.1007/s10534-019-00191-7.

Rubio LM, Ludden PW. 2008. Biosynthesis of the Iron-Molybdenum Cofactor of Nitrogenase. Annu Rev Microbiol. 62(1):93–111. doi:10.1146/annurev.micro.62.081307.162737.

Rudolf J, Makrantoni V, Ingledew WJ, Stark MJRR, White MF. 2006. The DNA Repair Helicases XPD and FancJ Have Essential Iron-Sulfur Domains. Mol Cell. 23(6):801–808. doi:10.1016/j.molcel.2006.07.019.

Russell MJ, Hall AJ. 1997. The emergence of life from iron monosulphide bubbles at a submarine hydrothermal redox and pH front. J Geol Soc London. 154(3):377–402. doi:10.1144/gsjgs.154.3.0377.

Russell MJ, Hall AJ, Martin W. 2010. Serpentinization as a source of energy at the origin of life. Geobiology. 8(5):355–371. doi:10.1111/j.1472-4669.2010.00249.x.

Saini A, Mapolelo DT, Chahal HK, Johnson MK, Outten FW. 2010. SufD and SufC ATPase activity are required for iron acquisition during in vivo Fe-S cluster formation on SufB. Biochemistry. 49(43):9402–9412. doi:10.1021/bi1011546.

Santos JA, Alonso-Garciá N, Macedo-Ribeiro S, Barbosa Pereira PJ. 2014. The unique regulation of iron-sulfur cluster biogenesis in a Gram-positive bacterium. Proc Natl Acad Sci U S A. 111(22):E2251–E2260. doi:10.1073/pnas.1322728111.

Dos Santos PC, Fang Z, Mason SW, Setubal JC, Dixon R. 2012. Distribution of nitrogen fixation and nitrogenase-like sequences amongst microbial genomes. BMC Genomics. 13(1):162. doi:10.1186/1471-2164-13-162.

Dos Santos PC, Johnson DC, Ragle BE, Unciuleac MC, Dean DR. 2007. Controlled expression of nif and isc iron-sulfur protein maturation components reveals target specificity and limited functional replacement between the two systems. J Bacteriol. 189(7):2854–2862. doi:10.1128/JB.01734-06.

Dos Santos PC, Smith AD, Frazzon J, Cash VL, Johnson MK, Dean DR. 2004. Iron-sulfur cluster assembly: NifU-directed activation of the nitrogenase Fe protein. J Biol Chem. 279(19):19705–19711. doi:10.1074/jbc.M400278200.

Sato T, Kuwahara H, Fujita K, Noda S, Kihara K, Yamada A, Ohkuma M, Hongoh Y. 2014. Intranuclear verrucomicrobial symbionts and evidence of lateral gene transfer to the host protist in the termite gut. ISME J. 8(5):1008–1019. doi:10.1038/ismej.2013.222.

Seidler A, Jaschkowitz K, Wollenberg M. 2001. Incorporation of iron-Sulfur clusters in membrane-bound proteins. In: Biochemical Society Transactions. Vol. 29. Biochem Soc Trans. p. 418–421.

Selbach B, Earles E, Dos Santos PC. 2010. Kinetic analysis of the bisubstrate cysteine desulfurase sufs from bacillus subtilis. Biochemistry. 49(40):8794–8802. doi:10.1021/bi101358k.

Selbach BP, Chung AH, Scott AD, George SJ, Cramer SP, Dos Santos PC. 2014. Fe-S Cluster Biogenesis in Gram-Positive Bacteria: SufU Is a Zinc-Dependent Sulfur Transfer Protein. Biochemistry. 53(1):152–160. doi:10.1021/bi4011978. .

Selbach BP, Pradhan PK, Dos Santos PC. 2013. Protected sulfur transfer reactions by the Escherichia coli Suf system. Biochemistry. 52(23):4089–4096. doi:10.1021/bi4001479.

Selvadurai K, Wang P, Seimetz J, Huang RH. 2014. Archaeal Elp3 catalyzes tRNA wobble uridine modification at C5 via a radical mechanism. Nat Chem Biol. 10(10):810–812. doi:10.1038/nchembio.1610.

Sergiev P V., Golovina AY, Prokhorova I V., Sergeeva O V., Osterman IA, Nesterchuk M V., Burakovsky DE, Bogdanov AA, Dontsova OA. 2011. Modifications of ribosomal RNA: From enzymes to function. In: Ribosomes. Springer Vienna. p. 97–110.

Serio AW, Pechter KB, Sonenshein AL. 2006. Bacillus subtilis aconitase is required for efficient late-sporulation gene expression. J Bacteriol. 188(17):6396–6405. doi:10.1128/JB.00249-06.

Shakamuri P, Zhang B, Johnson MK. 2012. Monothiol glutaredoxins function in storing and transporting [Fe 2S2] clusters assembled on IscU scaffold proteins. J Am Chem Soc. 134(37):15213–15216. doi:10.1021/ja306061x.

Sheftel AD, Stehling O, Pierik AJ, Netz DJA, Kerscher S, Elsasser H-P, Wittig I, Balk J, Brandt U, Lill R. 2009. Human Ind1, an Iron-Sulfur Cluster Assembly Factor for Respiratory Complex I. Mol Cell Biol. 29(22):6059–6073. doi:10.1128/mcb.00817-09.

Sheftel AD, Wilbrecht C, Stehling O, Niggemeyer B, Elsässer H-PP, Mühlenhoff U, Lill R. 2012. The human mitochondrial ISCA1, ISCA2, and IBA57 proteins are required for [4Fe-4S] protein maturation. Fox TD, editor. Mol Biol Cell. 23(7):1157–1166. doi:10.1091/mbc.e11-09-0772.

Shen G, Balasubramanian R, Wang T, Wu Y, Hoffart LM, Krebs C, Bryant DA, Golbeck JH. 2007. SufR coordinates two [4Fe-4S]2+,1+ clusters and functions as a transcriptional repressor of the sufBCDS operon and an autoregulator of sufR in cyanobacteria. J Biol Chem. 282(44):31909–31919. doi:10.1074/jbc.M705554200.

Shepard EM, Byer AS, Betz JN, Peters JW, Broderick JB. 2016. A redox active [2Fe-2S] cluster on the hydrogenase maturase HydF. Biochemistry. 55(25):3514–3527. doi:10.1021/acs.biochem.6b00528.

Shi R, Proteau A, Villarroya M, Moukadiri I, Zhang L, Trempe J-F, Matte A, Armengod ME, Cygler M. 2010. Structural Basis for Fe–S Cluster Assembly and tRNA Thiolation Mediated by IscS Protein–Protein Interactions. Petsko GA, editor. PLoS Biol. 8(4):e1000354. doi:10.1371/journal.pbio.1000354.

Shigi N. 2014. Biosynthesis and functions of sulfur modifications in tRNA. Front Genet. 5(APR). doi:10.3389/fgene.2014.00067.

Shisler KA, Broderick JB. 2014. Glycyl radical activating enzymes: Structure, mechanism, and substrate interactions. Arch Biochem Biophys. 546:64–71. doi:10.1016/j.abb.2014.01.020.

Shutt TE, Gray MW. 2006. Twinkle, the mitochondrial replicative DNA helicase, is widespread in the eukaryotic radiation and may also be the mitochondrial DNA primase in most eukaryotes. J Mol Evol. 62(5):588–599. doi:10.1007/s00239-005-0162-8.

Schindelin H, Kisker C, Schlessman JL, Howard JB, Rees DC. 1997. Structure of ADP·AlF4/--stabilized nitrogenase complex and its implications for signal transduction. Nature. 387(6631):370–376. doi:10.1038/387370a0.

Schneider RE, Brown MT, Shiflett AM, Dyall SD, Hayes RD, Xie Y, Loo JA, Johnson PJ. 2011. The Trichomonas vaginalis hydrogenosome proteome is highly reduced relative to mitochondria, yet complex compared with mitosomes. Int J Parasitol. 41(13–14):1421–1434. doi:10.1016/j.ijpara.2011.10.001.

Schormann N, Ricciardi R, Chattopadhyay D. 2014. Uracil-DNA glycosylases-Structural and functional perspectives on an essential family of DNA repair enzymes. Protein Sci. 23(12):1667–1685. doi:10.1002/pro.2554.

Schwartz CJ, Giel JL, Patschkowski T, Luther C, Ruzicka FJ, Beinert H, Kiley PJ. 2001. IscR, an Fe-S cluster-containing transcription factor, represses expression of escherichia coli genes encoding Fe-S cluster assembly proteins. Proc Natl Acad Sci U S A. 98(26):14895–14900. doi:10.1073/pnas.251550898.

Simpson AGB. 2003. Cytoskeletal organization, phylogenetic affinities and systematics in the contentious taxon Excavata (Eukaryota). Int J Syst Evol Microbiol. 53(6):1759–1777. doi:10.1099/ijs.0.02578-0.

Simpson AGB, Radek R, Dacks JB, O'Kelly CJ. 2002. How oxymonads lost their groove: An ultrastructural comparison of Monocercomonoides and excavate taxa. J Eukaryot Microbiol. 49(3):239–248. doi:10.1111/j.1550-7408.2002.tb00529.x.

Sipos K, Lange H, Fekete Z, Ullmann P, Lill R, Kispal G. 2002. Maturation of cytosolic iron-sulfur proteins requires glutathione. J Biol Chem. 277(30):26944–26949. doi:10.1074/jbc.M200677200.

Slamovits CH, Keeling PJ. 2006a. A high density of ancient spliceosomal introns in oxymonad excavates. BMC Evol Biol. 6:34. doi:10.1186/1471-2148-6-34.

Slamovits CH, Keeling PJ. 2006b. Pyruvate-phosphate dikinase of oxymonads and parabasalia and the evolution of pyrophosphate-dependent glycolysis in anaerobic eukaryotes. Eukaryot Cell. 5(1):148–154. doi:10.1128/EC.5.1.148-154.2006.

Smith AC, Blackshaw JA, Robinson AJ. 2012. MitoMiner: a data warehouse for mitochondrial proteomics data. Nucleic Acids Res. 40(Database issue):D1160-7. doi:10.1093/nar/gkr1101.

Smith AD, Jameson GNL, Dos Santos PC, Agar JN, Naik S, Krebs C, Frazzon J, Dean DR, Huynh BH, Johnson MK. 2005. NifS-mediated assembly of [4Fe-4S] clusters in the N- and C-terminal domains of the NifU Scaffold protein. Biochemistry. 44(39):12955–12969. doi:10.1021/bi051257i.

Sofia HJ. 2001. Radical SAM, a novel protein superfamily linking unresolved steps in familiar biosynthetic pathways with radical mechanisms: functional characterization using new analysis and information visualization methods. Nucleic Acids Res. 29(5):1097–1106. doi:10.1093/nar/29.5.1097.

Sontz PA, Muren NB, Barton JK. 2012. DNA charge transport for sensing and signaling. Acc Chem Res. 45(10):1792–1800. doi:10.1021/ar3001298.

Srinivasan V, Netz DJA, Webert H, Mascarenhas J, Pierik AJ, Michel H, Lill R. 2007. Structure of the Yeast WD40 Domain Protein Cia1, a Component Acting Late in Iron-Sulfur Protein Biogenesis. Structure. 15(10):1246–1257. doi:10.1016/j.str.2007.08.009.

Stairs CW, Eme L, Brown MW, Mutsaers C, Susko E, Dellaire G, Soanes DM, Van Der Giezen M, Roger AJ. 2014. A SUF Fe-S cluster biogenesis system in the mitochondrion-related organelles of the anaerobic protist Pygsuia. Curr Biol. 24(11):1176–1186. doi:10.1016/j.cub.2014.04.033. http://dx.doi.org/10.1016/j.cub.2014.04.033.

Stehling O, Mascarenhas J, Vashisht AA, Sheftel AD, Niggemeyer B, Rösser R, Pierik AJ, Wohlschlegel JA, Lill R. 2013. Human CIA2A (FAM96A) and CIA2B (FAM96B) integrate maturation of different subsets of cytosolic-nuclear iron-sulfur proteins and iron homeostasis. Cell Metab. 18(2):187–198. doi:10.1016/j.cmet.2013.06.015.

Stehling O, Vashisht AA, Mascarenhas J, Jonsson ZO, Sharma T, Netz DJA, Pierik AJ, Wohlschlegel JA, Lill R. 2012. MMS19 assembles iron-sulfur proteins required for DNA metabolism and genomic integrity. Science (80-). 337(6091):195–199. doi:10.1126/science.1219723.

Stechmann A, Hamblin K, Pérez-Brocal V, Gaston D, Richmond GSS, van der Giezen M, Clark CG, Roger AJ. 2008. Organelles in Blastocystis that Blur the Distinction between Mitochondria and Hydrogenosomes. Curr Biol. 18(8):580–585. doi:10.1016/j.cub.2008.03.037.

Stejskal F, Å lapeta J, ÄtrnÃ¡ctÃ¡ V, Keithly JS. 2003. A Narf -like gene from Cryptosporidium parvum resembles homologues observed in aerobic protists and higher eukaryotes. FEMS Microbiol Lett. 229(1):91–96. doi:10.1016/S0378-1097(03)00794-8.

Stemmler TL, Lesuisse E, Pain D, Dancis A. 2010. Frataxin and mitochondrial FeS cluster biogenesis. J Biol Chem. 285(35):26737–26743. doi:10.1074/jbc.R110.118679.

Stingl U, Radek R, Yang H, Brune A. 2005. ‘Endomicrobia’: Cytoplasmic symbionts of termite gut protozoa form a separate phylum of prokaryotes. Appl Environ Microbiol. 71(3):1473–1479. doi:10.1128/AEM.71.3.1473-1479.2005.

Su X, Lin Z, Lin H. 2013. The biosynthesis and biological function of diphthamide. Crit Rev Biochem Mol Biol. 48(6):515–521. doi:10.3109/10409238.2013.831023.

Sutak R, Dolezal P, Fiumera HL, Hrdy I, Dancis A, Delgadillo-Correa M, Johnson PJ, Muller M, Tachezy J. 2004. Mitochondrial-type assembly of FeS centers in the hydrogenosomes of the amitochondriate eukaryote Trichomonas vaginalis. Proc Natl Acad Sci. 101(28):10368–10373. doi:10.1073/pnas.0401319101.

Suzuki Y, Noma A, Suzuki T, Senda M, Senda T, Ishitani R, Nureki O. 2007. Crystal Structure of the Radical SAM Enzyme Catalyzing Tricyclic Modified Base Formation in tRNA. J Mol Biol. 372(5):1204–1214. doi:10.1016/j.jmb.2007.07.024.

Šlapeta J, Keithly JS. 2004. Cryptosporidium parvum Mitochondrial-Type HSP70 Targets Homologous and Heterologous Mitochondria. Eukaryot Cell. 3(2):483–494. doi:10.1128/EC.3.2.483-494.2004.

Tagawa K, Arnon DI. 1962. Ferredoxins as electron carriers in photosynthesis and in the biological production and consumption of hydrogen gas. Nature. 195(4841):537–543. doi:10.1038/195537a0.

Tachezy J, Sánchez LB, Müller M. 2001. Mitochondrial type iron-sulfur cluster assembly in the amitochondriate eukaryotes Trichomonas vaginalis and Giardia intestinalis, as indicated by the phylogeny of IscS. Mol Biol Evol. 18(10):1919–1928. doi:10.1093/oxfordjournals.molbev.a003732.

Takahashi Y, Tokumoto U. 2002. A third bacterial system for the assembly of iron-sulfur clusters with homologs in Archaea and plastids. J Biol Chem. 277(32):28380–28383. doi:10.1074/jbc.C200365200.

Tan G, Lu J, Bitoun JP, Huang H, Ding H. 2009. IscA/SufA paralogues are required for the [4Fe-4S] cluster assembly in enzymes of multiple physiological pathways in Escherichia coli under aerobic growth conditions. Biochem J. 420(3):463–472. doi:10.1042/BJ20090206.

Tanifuji G, Takabayashi S, Kume K, Takagi M, Nakayama T, Kamikawa R, Inagaki Y, Hashimoto T. 2018. The draft genome of Kipferlia bialata reveals reductive genome evolution in fornicate parasites. PLoS One. 13(3). doi:10.1371/journal.pone.0194487.

Tapley TL, Vickery LE. 2004. Preferential substrate binding orientation by the molecular chaperone HscA. J Biol Chem. 279(27):28435–28442. doi:10.1074/jbc.M400803200.

Tirupati B, Vey JL, Drennan CL, Bollinger JM. 2004a. Kinetic and structural characterization of Slr0077/SufS, the essential cysteine desulfurase from Synechocystis sp. PCC 6803. Biochemistry. 43(38):12210–12219. doi:10.1021/bi0491447.

Tirupati B, Vey JL, Drennan CL, Bollinger JM. 2004b. Kinetic and Structural Characterization of Slr0077 / SufS , the Essential Cysteine. Biochemistry. 43(5):12210–12219. doi:10.1021/bi0491447.

Toh SM, Xiong L, Bae T, Mankin AS. 2008. The methyltransferase YfgB/RlmN is responsible for modification of adenosine 2503 in 23S rRNA. RNA. 14(1):98–106. doi:10.1261/rna.814408.

Tokumoto U, Kitamura S, Fukuyama K, Takahashi Y. 2004. Interchangeability and distinct properties of bacterial Fe-S cluster assembly systems: Functional replacement of the isc and suf operons in Escherichia coli with the nifSU-like operon from Helicobacter pylori. J Biochem. 136(2):199–209. doi:10.1093/jb/mvh104.

Tokumoto U, Takahashi Y. 2001. Genetic Analysis of the isc Operon in Escherichia coli Involved in the Biogenesis of Cellular Iron-Sulfur Proteins. J Biochem. 130(1):63–71. doi:10.1093/oxfordjournals.jbchem.a002963.

Tong WH, Jameson GNL, Huynh BH, Rouault TA. 2003. Subcellular compartmentalization of human Nfu, an iron-sulfur cluster scaffold protein, and its ability to assemble a [4Fe-4S] cluster. Proc Natl Acad Sci U S A. 100(17):9762–9767. doi:10.1073/pnas.1732541100.

Touati D. 2000. Iron and oxidative stress in bacteria. Arch Biochem Biophys. 373(1):1–6. doi:10.1006/abbi.1999.1518.

Tovar J, León-Avila G, Sánchez LB, Sutak R, Tachezy J, Van Der Giezen M, Hernández M, Müller M, Lucocq JM. 2003. Mitochondrial remnant organelles of Giardia function in iron-Sulfur protein maturation. Nature. 426(6963):172–176. doi:10.1038/nature01945.

Treitli SC, Kolisko M, Husník F, Keeling PJ, Hampl V. 2019. Revealing the metabolic capacity of Streblomastix strix and its bacterial symbionts using singlecell metagenomics. Proc Natl Acad Sci U S A. 116(39):19675–19684. doi:10.1073/pnas.1910793116.

Treitli SC, Kotyk M, Yubuki N, Jirounková E, Vlasáková J, Smejkalová P, Šípek P, Čepička I, Hampl V. 2018. Molecular and Morphological Diversity of the Oxymonad Genera Monocercomonoides and Blattamonas gen. nov. Protist. 169(5):744–783. doi:10.1016/j.protis.2018.06.005.

Trotter V, Vinella D, Loiseau L, De Choudens SO, Fontecave M, Barras F. 2009. The CsdA cysteine deSulfurase promotes Fe/S biogenesis by recruiting Suf components and participates to a new Sulfur transfer pathway by recruiting CsdL (ex-YgdL), a ubiquitin-modifying-like protein. Mol Microbiol. 74(6):1527–1542. doi:10.1111/j.1365-2958.2009.06954.x.

Tsai CL, Barondeau DP. 2010. Human frataxin is an allosteric switch that activates the Fe-S cluster biosynthetic complex. Biochemistry. 49(43):9132–9139. doi:10.1021/bi1013062.

Tsaousis AD. 2019. On the Origin of Iron/Sulfur Cluster Biosynthesis in Eukaryotes. Front Microbiol. 10(November). doi:10.3389/fmicb.2019.02478.

Tsaousis AD, Gentekaki E, Eme L, Gaston D, Roger AJ. 2014. Evolution of the cytosolic iron-sulfur cluster assembly machinery in Blastocystis species and other microbial eukaryotes. Eukaryot Cell. 13(1):143–153. doi:10.1128/EC.00158-13.

Tsaousis AD, Ollagnier de Choudens S, Gentekaki E, Long S, Gaston D, Stechmann A, Vinella D, Py B, Fontecave M, Barras F, et al. 2012. Evolution of Fe/S cluster biogenesis in the anaerobic parasite Blastocystis. Proc Natl Acad Sci. 109(26):10426–10431. doi:10.1073/pnas.1116067109.

Tse ECM, Zwang TJ, Barton JK. 2017. The Oxidation State of [4Fe4S] Clusters Modulates the DNA-Binding Affinity of DNA Repair Proteins. J Am Chem Soc. 139(36):12784–12792. doi:10.1021/jacs.7b07230.

Tuteja N, Tuteja R. 2004. Prokaryotic and eukaryotic DNA helicases: Essential molecular motor proteins for cellular machinery. Eur J Biochem. 271(10):1835–1848. doi:10.1111/j.1432-1033.2004.04093.x.

Unciuleac MC, Chandramouli K, Naik S, Mayer S, Boi HH, Johnson MK, Dean DR. 2007. In vitro activation of apo-aconitase using a [4Fe-4S] cluster-loaded form of the IscU [Fe - S] cluster scaffolding protein. Biochemistry. 46(23):6812–6821. doi:10.1021/bi6026665.

Upadhyay AS, Stehling O, Panayiotou C, Rösser R, Lill R, Överby AK. 2017. Cellular requirements for iron-sulfur cluster insertion into the antiviral radical SAM protein viperin. J Biol Chem. 292(33):13879–13889. doi:10.1074/jbc.M117.780122.

Upadhyay AS, Vonderstein K, Pichlmair A, Stehling O, Bennett KL, Dobler G, Guo JT, Superti-Furga G, Lill R, Överby AK, et al. 2014. Viperin is an iron-sulfur protein that inhibits genome synthesis of tick-borne encephalitis virus via radical SAM domain activity. Cell Microbiol. 16(6):834–848. doi:10.1111/cmi.12241.

Urbonavicius J, Qian Q, Durand JM, Hagervall TG, Björk GR. 2001. Improvement of reading frame maintenance is a common function for several tRNA modifications. EMBO J. 20(17):4863–73. doi:10.1093/emboj/20.17.4863.

Urzica E, Pierik AJ, Mühlenhoff U, Lill R. 2009. Crucial role of conserved cysteine residues in the assembly of two iron-sulfur clusters on the CIA protein Nar1. Biochemistry. 48(22):4946–4958. doi:10.1021/bi900312x.

Uzarska MA, Dutkiewicz R, Freibert SA, Lill R, Mühlenhoff U. 2013. The mitochondrial Hsp70 chaperone Ssq1 facilitates Fe/S cluster transfer from Isu1 to Grx5 by complex formation. Fox TD, editor. Mol Biol Cell. 24(12):1830–1841. doi:10.1091/mbc.E12-09-0644.

Uzarska MA, Nasta V, Weiler BD, Spantgar F, Ciofi-Baffoni S, Saviello MR, Gonnelli L, Mï¿½hlenhoff U, Banci L, Lill R, et al. 2016. Mitochondrial Bol1 and Bol3 function as assembly factors for specific iron-sulfur proteins. Elife. 5(AUGUST). doi:10.7554/eLife.16673.

Vacek V, Novák LVF, Treitli SC, Táborský P, Čepička I, Kolísko M, Keeling PJ, Hampl V. 2018. Fe–S Cluster Assembly in Oxymonads and Related Protists. Ruiz-Trillo I, editor. Mol Biol Evol. 35(11):2712–2718. doi:10.1093/molbev/msy168.

Valasatava Y, Rosato A, Banci L, Andreini C. 2016. MetalPredator: a web server to predict iron-sulfur cluster binding proteomes. Bioinformatics. 32(18):2850–2852. doi:10.1093/bioinformatics/btw238.

Vanin AF. 2009. Dinitrosyl iron complexes with thiolate ligands: Physico-chemistry, biochemistry and physiology. Nitric Oxide - Biol Chem. 21(1):1–13. doi:10.1016/j.niox.2009.03.005.

Vashisht AA, Yu CC, Sharma T, Ro K, Wohlschlegel JA. 2015. The association of the xeroderma pigmentosum group D DNA helicase (XPD) with transcription factor IIH is regulated by the cytosolic iron-sulfur cluster assembly pathway. J Biol Chem. 290(22):14218–14225. doi:10.1074/jbc.M115.650762.

Velayudhan J, Karlinsey JE, Frawley ER, Becker LA, Nartea M, Fang FC. 2014. Distinct roles of the Salmonella enterica serovar typhimurium CyaY and YggX proteins in the biosynthesis and repair of iron-sulfur clusters. Infect Immun. 82(4):1390–1401. doi:10.1128/IAI.01022-13.

Venkateswara Rao P, Holm RH. 2004. Synthetic Analogues of the Active Sites of Iron-Sulfur Proteins. Chem Rev. 104(2):527–559. doi:10.1021/cr020615+.

Vernis L, Facca C, Delagoutte E, Soler N, Chanet R, Guiard B, Faye G, Baldacci G. 2009. A newly identified essential complex, Dre2-Tah18, controls mitochondria integrity and cell death after oxidative stress in yeast. PLoS One. 4(2). doi:10.1371/journal.pone.0004376.

Vey JL, Drennan CL. 2011. Structural insights into radical generation by the radical SAM superfamily. Chem Rev. 111(4):2487–2506. doi:10.1021/cr9002616.

Vickery LE, Cupp-Vickery JR. 2007. Molecular chaperones HscA/Ssq1 and HscB/Jac1 and their roles in iron-sulfur protein maturation. Crit Rev Biochem Mol Biol. 42(2):95–111. doi:10.1080/10409230701322298.

Vignais PM, Billoud B. 2007. Occurrence, classification, and biological function of hydrogenases: An overview. Chem Rev. 107(10):4206–4272. doi:10.1021/cr050196r.

Vignais PM, Billoud B, Meyer J. 2001. Classification and phylogeny of hydrogenases. FEMS Microbiol Rev. 25(4):455–501. doi:10.1111/j.1574-6976.2001.tb00587.x.

Vinella D, Brochier-Armanet C, Loiseau L, Talla E, Barras F. 2009. Iron-sulfur (Fe/S) protein biogenesis: Phylogenomic and genetic studies of A-type carriers. PLoS Genet. 5(5). doi:10.1371/journal.pgen.1000497.

Van Vranken JG, Jeong MY, Wei P, Chen YC, Gygi SP, Winge DR, Rutter J. 2016. The mitochondrial acyl carrier protein (ACP) coordinates mitochondrial fatty acid synthesis with iron sulfur cluster biogenesis. Elife. 5(AUGUST). doi:10.7554/eLife.17828.

Waas WF, Druzina Z, Hanan M, Schimmel P. 2007. Role of a tRNA base modification and its precursors in frameshifting in eukaryotes. J Biol Chem. 282(36):26026–26034. doi:10.1074/jbc.M703391200.

Wada K, Sumi N, Nagai R, Iwasaki K, Sato T, Suzuki K, Hasegawa Y, Kitaoka S, Minami Y, Outten FW, et al. 2009. Molecular Dynamism of Fe-S Cluster Biosynthesis Implicated by the Structure of the SufC2-SufD2Complex. J Mol Biol. 387(1):245–258. doi:10.1016/j.jmb.2009.01.054.

Wachnowsky C, Fidai I, Cowan JA. 2016. Iron–sulfur cluster exchange reactions mediated by the human Nfu protein. J Biol Inorg Chem. 21(7):825–836. doi:10.1007/s00775-016-1381-8.

Wachtershauser G. 1990. Evolution of the first metabolic cycles. Proc Natl Acad Sci. 87(1):200–204. doi:10.1073/pnas.87.1.200.

Wächtershäuser G. 1988. Before enzymes and templates: theory of surface metabolism. Microbiol Rev. 52(4):452–484. doi:10.1128/mmbr.52.4.452-484.1988.

Wächtershäuser G. 1992. Groundworks for an evolutionary biochemistry: The iron-Sulfur world. Prog Biophys Mol Biol. 58(2):85–201. doi:10.1016/0079-6107(92)90022-X.

Wang T, Shen G, Balasubramanian R, McIntosh L, Bryant DA, Golbeck JH. 2004. The sufR Gene (sll0088 in Synechocystis sp. Strain PCC 6803) Functions as a Repressor of the sufBCDS Operon in Iron-Sulfur Cluster Biogenesis in Cyanobacteria. J Bacteriol. 186(4):956–967. doi:10.1128/JB.186.4.956-967.2004.

Wang W, Huang H, Tan G, Si F, Liu M, Landry AP, Lu J, Ding H. 2010. In vivo evidence for the iron-binding activity of an iron-sulfur cluster assembly protein IscA in Escherichia coli. Biochem J. 432(3):429–436. doi:10.1042/BJ20101507.

Wang Z, Wu M. 2015. An integrated phylogenomic approach toward pinpointing the origin of mitochondria. Sci Rep. 5. doi:10.1038/srep07949.

Wayne Outten F. 2015. Recent advances in the Suf Fe-S cluster biogenesis pathway: Beyond the Proteobacteria. Biochim Biophys Acta - Mol Cell Res. 1853(6):1464–1469. doi:10.1016/j.bbamcr.2014.11.001.

Webert H, Freibert SA, Gallo A, Heidenreich T, Linne U, Amlacher S, Hurt E, Mühlenhoff U, Banci L, Lill R. 2014. Functional reconstitution of mitochondrial Fe/S cluster synthesis on Isu1 reveals the involvement of ferredoxin. Nat Commun. 5(1):1–12. doi:10.1038/ncomms6013.

Weiner BE, Huang H, Dattilo BM, Nilges MJ, Fanning E, Chazin WJ. 2007. An iron-sulfur cluster in the C-terminal domain of the p58 subunit of human DNA primase. J Biol Chem. 282(46):33444–33451. doi:10.1074/jbc.M705826200.

Wilcoxen J, Arragain S, Scandurra AA, Jimenez-Vicente E, Echavarri-Erasun C, Pollmann S, Britt RD, Rubio LM. 2016. Electron Paramagnetic Resonance Characterization of Three Iron-Sulfur Clusters Present in the Nitrogenase Cofactor Maturase NifB from Methanocaldococcus infernus. J Am Chem Soc. 138(24):7468–7471. doi:10.1021/jacs.6b03329.

Willemse D, Weber B, Masino L, Warren RM, Adinolfi S, Pastore A, Williams MJ. 2018. Rv1460, a SufR homologue, is a repressor of the suf operon in Mycobacterium tuberculosis. Rouault T, editor. PLoS One. 13(7):e0200145. doi:10.1371/journal.pone.0200145.

Williams BAP, Hirt RP, Lucocq JM, Embley TM. 2002. A mitochondrial remnant in the microsporidian Trachipleistophora hominis. Nature. 418(6900):865–869. doi:10.1038/nature00949.

Wittschieben BO, Otero G, de Bizemont T, Fellows J, Erdjument-Bromage H, Ohba R, Li Y, Allis CD, Tempst P, Svejstrup JQ. 1999. A novel histone acetyltransferase is an integral subunit of elongating RNA polymerase II holoenzyme. Mol Cell. 4(1):123–8. doi:10.1016/s1097-2765(00)80194-x.

Wollenberg M, Berndt C, Bill E, Schwenn JD, Seidler A. 2003. A dimer of the FeS cluster biosynthesis protein IscA from cyanobacteria binds a [2Fe2S] cluster between two protomers and transfers it to [2Fe2S] and [4Fe4S] apo proteins. Eur J Biochem. 270(8):1662–1671. doi:10.1046/j.1432-1033.2003.03522.x.

Wollers S, Layer G, Garcia-Serres R, Signor L, Clemancey M, Latour JM, Fontecave M, De Choudens SO. 2010. Iron-sulfur (Fe-S) cluster assembly: The SufBCD complex is a new type of Fe-S scaffold with a flavin redox cofactor. J Biol Chem. 285(30):23331–23341. doi:10.1074/jbc.M110.127449.

Wolski SC, Kuper J, Hänzelmann P, Truglio JJ, Croteau DL, Van Houten B, Kisker C. 2008. Crystal structure of the FeS cluster-containing nucleotide excision repair helicase XPD. PLoS Biol. 6(6):1332–1342. doi:10.1371/journal.pbio.0060149.

Wu Y, Brosh RM. 2012. DNA helicase and helicase-nuclease enzymes with a conserved iron-sulfur cluster. Nucleic Acids Res. 40(10):4247–4260. doi:10.1093/nar/gks039.

Xu F, Jerlström-Hultqvist J, Einarsson E, Ástvaldsson Á, Svärd SG, Andersson JO. 2014. The Genome of Spironucleus salmonicida Highlights a Fish Pathogen Adapted to Fluctuating Environments. PLoS Genet. 10(2). doi:10.1371/journal.pgen.1004053.

Xu F, Jex A, Svärd SG. 2020. A chromosome-scale reference genome for Giardia intestinalis WB. Sci Data. 7(1):1–8. doi:10.1038/s41597-020-0377-y.

Yan F, Lamarre JM, Röhrich R, Wiesner J, Jomaa H, Markin AS, Fujimori DG. 2010. RImN and Cfr are Radical SAM Enzymes Involved in Methylation of Ribosomal RNA. J Am Chem Soc. 132(11):3953–3964. doi:10.1021/ja910850y.

Yan R, Adinolfi S, Pastore A. 2015. Ferredoxin, in conjunction with NADPH and ferredoxin-NADP reductase, transfers electrons to the IscS/IscU complex to promote iron-sulfur cluster assembly. Biochim Biophys Acta - Proteins Proteomics. 1854(9):1113–1117. doi:10.1016/j.bbapap.2015.02.002.

Yan Z, Maruyama A, Arakawa T, Fushinobu S, Wakagi T. 2016. Crystal structures of archaeal 2-oxoacid:ferredoxin oxidoreductases from Sulfolobus tokodaii. Sci Rep. 6. doi:10.1038/srep33061.

Yang H, Schmitt-Wagner D, Stingl U, Brune A. 2005. Niche heterogeneity determines bacterial community structure in the termite gut (Reticulitermes santonensis). Environ Microbiol. 7(7):916–932. doi:10.1111/j.1462-2920.2005.00760.x.

Yang J, Bitoun JP, Ding H. 2006. Interplay of IscA and IscU in biogenesis of iron-sulfur clusters. J Biol Chem. 281(38):27956–27963. doi:10.1074/jbc.M601356200.

Yarlett N, Hackstein JHP. 2005. Hydrogenosomes: One Organelle, Multiple Origins. Bioscience. 55(8):657–668. doi:10.1641/0006-3568(2005)055[0657:hoomo]2.0.co;2.

Ye H, Jeong SY, Ghosh MC, Kovtunovych G, Silvestri L, Ortillo D, Uchida N, Tisdale J, Camaschella C, Rouault TA. 2010. Glutaredoxin 5 deficiency causes sideroblastic anemia by specifically impairing heme biosynthesis and depleting cytosolic iron in human erythroblasts. J Clin Invest. 120(5):1749–1761. doi:10.1172/JCI40372.

Yeo W-S, Lee J-H, Lee K-C, Roe J-H. 2006. IscR acts as an activator in response to oxidative stress for the *suf* operon encoding Fe-S assembly proteins. Mol Microbiol. 61(1):206–218. doi:10.1111/j.1365-2958.2006.05220.x.

Yokoyama N, Nonaka C, Ohashi Y, Shioda M, Terahata T, Chen W, Sakamoto K, Maruyama C, Saito T, Yuda E, et al. 2018. Distinct roles for U-type proteins in iron–sulfur cluster biosynthesis revealed by genetic analysis of the Bacillus subtilis sufCDSUB operon. Mol Microbiol. 107(6):688–703. doi:10.1111/mmi.13907.

Yoon H, Golla R, Lesuisse E, Pain J, Donald JE, Lyver ER, Pain D, Dancis A. 2012. Mutation in the Fe-S scaffold protein Isu bypasses frataxin deletion. Biochem J. 441(1):473–480. doi:10.1042/BJ20111637.

Yoon H, Knight SAB, Pandey A, Pain J, Turkarslan S, Pain D, Dancis A. 2015. Turning Saccharomyces cerevisiae into a Frataxin-Independent Organism. PLoS Genet. 11(5):e1005135. doi:10.1371/journal.pgen.1005135.

Yoon T, Cowan JA. 2003. Iron-sulfur cluster biosynthesis. Characterization of frataxin as an iron donor for assembly of [2Fe-2S] clusters in ISU-type proteins. J Am Chem Soc. 125(20):6078–6084. doi:10.1021/ja027967i.

Young AP, Bandarian V. 2011. Pyruvate is the source of the two carbons that are required for formation of the imidazoline ring of 4-demethylwyosine. Biochemistry. 50(49):10573–10575. doi:10.1021/bi2015053.

Young AP, Bandarian V. 2013. Radical mediated ring formation in the biosynthesis of the hypermodified tRNA base wybutosine. Curr Opin Chem Biol. 17(4):613–618. doi:10.1016/j.cbpa.2013.05.035.

Youssef NH, Couger MB, Struchtemeyer CG, Liggenstoffer AS, Prade RA, Najar FZ, Atiyeh HK, Wilkins MR, Elshahed MS. 2013. The genome of the anaerobic fungus orpinomyces sp. strain c1a reveals the unique evolutionary history of a remarkable plant biomass degrader. Appl Environ Microbiol. 79(15):4620–4634. doi:10.1128/AEM.00821-13.

Yubuki N, Huang SSC, Leander BS. 2016. Comparative Ultrastructure of Fornicate Excavates, Including a Novel Free-living Relative of Diplomonads: Aduncisulcus paluster gen. et sp. nov. Protist. 167(6):584–596. doi:10.1016/j.protis.2016.10.001.

Yubuki N, Simpson AGB, Leander BS. 2013. Comprehensive Ultrastructure of Kipferlia bialata Provides Evidence for Character Evolution within the Fornicata (Excavata). Protist. 164(3):423–439. doi:10.1016/j.protis.2013.02.002.

Yuda E, Tanaka N, Fujishiro T, Yokoyama N, Hirabayashi K, Fukuyama K, Wada K, Takahashi Y. 2017. Mapping the key residues of SufB and SufD essential for biosynthesis of iron-sulfur clusters. Sci Rep. 7(1):9387. doi:10.1038/s41598-017-09846-2.

Yuvaniyama P, Agar JN, Cash VL, Johnson MK, Dean DR. 2000. NifS-directed assembly of a transient [2Fe-2S] cluster within the NifU protein. Proc Natl Acad Sci U S A. 97(2):599–604. doi:10.1073/pnas.97.2.599.

Zarsky V, Tachezy J, Dolezal P. 2012. Tom40 is likely common to all mitochondria. Curr Biol. 22(12):R479–R481. doi:10.1016/j.cub.2012.03.057.

Zelena M, 2020, Functional study of the SUF pathway in the cell of *Monocercomonoides exilis* and *Paratrimastix pyriformis*, Diploma thesis, Charles University, Czech Republic

Zeng J, Geng M, Jiang H, Liu Y, Liu J, Qiu G. 2007. The IscA from Acidithiobacillus ferrooxidans is an iron-sulfur protein which assemble the [Fe4S4] cluster with intracellular iron and sulfur. Arch Biochem Biophys. 463(2):237–244. doi:10.1016/j.abb.2007.03.024.

Zhang Q, Táborský P, Silberman JD, Pánek T, Čepička I, Simpson AGB. 2015. Marine Isolates of Trimastix marina Form a Plesiomorphic Deep-branching Lineage within Preaxostyla, Separate from Other Known Trimastigids (Paratrimastix n. gen.). Protist. 166(4):468–491. doi:10.1016/j.protis.2015.07.003.

Zhang Y, Lyver ER, Nakamaru-Ogiso E, Yoon H, Amutha B, Lee D-WD-W, Bi E, Ohnishi T, Daldal F, Pain D, et al. 2008. Dre2, a Conserved Eukaryotic Fe/S Cluster Protein, Functions in Cytosolic Fe/S Protein Biogenesis. Mol Cell Biol. 28(18):5569–5582. doi:10.1128/MCB.00642-08.

Zhang Y, Zhu X, Torelli AT, Lee M, Dzikovski B, Koralewski RM, Wang E, Freed J, Krebs C, Ealick SE, et al. 2010. Diphthamide biosynthesis requires an organic radical generated by an iron-Sulfur enzyme. Nature. 465(7300):891–896. doi:10.1038/nature09138.

Zhao D, Curatti L, Rubio LM. 2007. Evidence for nifU and nifS participation in the biosynthesis of the iron-molybdenum cofactor of nitrogenase. J Biol Chem. 282(51):37016–37025. doi:10.1074/jbc.M708097200.

Zheng L, Cash VL, Flint DH, Dean DR. 1998. Assembly of iron-sulfur clusters. Identification of an iscSUA-hscBA-fdx gene cluster from Azotobacter vinelandii. J Biol Chem. 273(21):13264–72. doi:10.1074/jbc.273.21.13264.

Zheng L, Dean DR. 1994. Catalytic formation of a nitrogenase iron-sulfur cluster. J Biol Chem. 269(29):18723–18726.

Zheng L, Kennedy MC, Blondin GA, Beinert H, Zalkin H. 1992. Binding of cytosolic aconitase to the iron responsive element of porcine mitochondrial aconitase mRNA. Arch Biochem Biophys. 299(2):356–360. doi:10.1016/0003-9861(92)90287-7.

Zheng L, White RH, Cash VL, Dean DR. 1994. Mechanism for the Desulfurization of L-Cysteine Catalyzed by the nifS Gene Product. Biochemistry. 33(15):4714–4720. doi:10.1021/bi00181a031.

Zheng L, White RH, Cash VL, Jack RF, Dean DR. 1993. Cysteine desulfurase activity indicates a role for NIFS in metallocluster biosynthesis. Proc Natl Acad Sci U S A. 90(7):2754–8. doi:10.1073/pnas.90.7.2754.

Zheng L, Zhou M, Guo Z, Lu H, Qian L, Dai H, Qiu J, Yakubovskaya E, Bogenhagen DF, Demple B, et al. 2008. Human DNA2 Is a Mitochondrial Nuclease/Helicase for Efficient Processing of DNA Replication and Repair Intermediates. Mol Cell. 32(3):325–336. doi:10.1016/j.molcel.2008.09.024.

Zhou S, Sitaramaiah D, Noon KR, Guymon R, Hashizume T, McCloskey JA. 2004. Structures of two new ‘minimalist’ modified nucleosides from archaeal tRNA. Bioorg Chem. 32(2):82–91. doi:10.1016/j.bioorg.2003.09.005.

Zhu X, Dzikovski B, Su X, Torelli AT, Zhang Y, Ealick SE, Freed JH, Lin H. 2011. Mechanistic understanding of Pyrococcus horikoshii Dph2, a [4Fe-4S] enzyme required for diphthamide biosynthesis. Mol Biosyst. 7(1):74–81. doi:10.1039/c0mb00076k.

Zwang TJ, Tse ECM, Barton JK. 2018. Sensing DNA through DNA Charge Transport. ACS Chem Biol. 13(7):1799–1809. doi:10.1021/acschembio.8b00347.

12 List of Publications and authors contribution

Zubáčová Z, Novák L, Bublíková J, Vojtěch Vacek, Jan Fousek, Jakub Rídl, Jan Tachezy, Pavel Doležal, Cestmír Vlček, Vladimír Hampl. The mitochondrion-like organelle of *Trimastix pyriformis* contains the complete glycine cleavage system. *PLoS One*. 2013;8(3):e55417. doi:10.1371/journal.pone.0055417

- *in silico* search for mitochondrion related genes

Karnkowska A, Vacek V, Zubáčová Z, Treitli SC, Petrželková R, Eme L, et al. A Eukaryote without a Mitochondrial Organelle. Curr Biol. Elsevier; 2016; 26:1274–84. https://doi.org/10.1016/j.cub.2016.03.053.

- preparation gDNA a mRNA for sequencing, manual annotation of Fe-S cluster assembly genes, immunofluorescence localization of SUF genes in *T. vaginalis* and *S. cerevisiae*

Vacek V, Novák LVF, Treitli SC, Táborský P, Čepička I, Kolísko M, et al. Fe-S Cluster Assembly in Oxymonads and Related Protists. Mol Biol Evol. 2018; https://doi.org/10.1093/molbev/msy168.

- *In silico* searches for Fe-S cluster assembly genes, phylogenetic analyses

Karnkowska A, Treitli SC, Brzoň O, Novák L, Vacek V, Soukal P, Barlow LD, Herman EK, Pipaliya SV, Pánek T, et al. 2019 The Oxymonad Genome Displays Canonical Eukaryotic Complexity in the Absence of a Mitochondrion. Mol Biol Evol. 36(10):2292–2312. doi:10.1093/molbev/msz147.

- Prediction and annotation of Fe-S proteins and comparison to other anaerobic protists.

Vacek V, Peňa-Diaz P, Py B, Hampl V. 2020. Functional characterisation of the SUF pathway from the amitochondriate eukaryote *Monocercomonoides exilis.* Manuscript in preparation.

- *In silico* analyses and protein modelling, complementation experiments, Bacterial adenylate cyclase two-hybrid experiments

OPEN ACCESS Freely available online

PLOS ONE

The Mitochondrion-Like Organelle of *Trimastix pyriformis* Contains the Complete Glycine Cleavage System

Zuzana Zubáčová[1], Lukáš Novák[1], Jitka Bublíková[1], Vojtěch Vacek[1], Jan Fousek[2], Jakub Rídl[2], Jan Tachezy[1], Pavel Doležal[1], Čestmír Vlček[2], Vladimír Hampl[1]*

1 Charles University in Prague, Faculty of Science, Department of Parasitology, Prague, Czech Republic, **2** Institute of Molecular Genetics of the Academy of Sciences of the Czech Republic, Prague, Czech Republic

Abstract

All eukaryotic organisms contain mitochondria or organelles that evolved from the same endosymbiotic event like classical mitochondria. Organisms inhabiting low oxygen environments often contain mitochondrial derivates known as hydrogenosomes, mitosomes or neutrally as mitochondrion-like organelles. The detailed investigation has shown unexpected evolutionary plasticity in the biochemistry and protein composition of these organelles in various protists. We investigated the mitochondrion-like organelle in *Trimastix pyriformis,* a free-living member of one of the three lineages of anaerobic group Metamonada. Using 454 sequencing we have obtained 7 037 contigs from its transcriptome and on the basis of sequence homology and presence of N-terminal extensions we have selected contigs coding for proteins that putatively function in the organelle. Together with the results of a previous transcriptome survey, the list now consists of 23 proteins – mostly enzymes involved in amino acid metabolism, transporters and maturases of proteins and transporters of metabolites. We have no evidence of the production of ATP in the mitochondrion-like organelle of *Trimastix* but we have obtained experimental evidence for the presence of enzymes of the glycine cleavage system (GCS), which is part of amino acid metabolism. Using homologous antibody we have shown that H-protein of GCS localizes into vesicles in the cell of *Trimastix*. When overexpressed in yeast, H- and P-protein of GCS and cpn60 were transported into mitochondrion. In case of H-protein we have demonstrated that the first 16 amino acids are necessary for this transport. Glycine cleavage system is at the moment the only experimentally localized pathway in the mitochondrial derivate of *Trimastix pyriformis*.

Citation: Zubáčová Z, Novák L, Bublíková J, Vacek V, Fousek J, et al. (2013) The Mitochondrion-Like Organelle of *Trimastix pyriformis* Contains the Complete Glycine Cleavage System. PLoS ONE 8(3): e55417. doi:10.1371/journal.pone.0055417

Editor: Valdur Saks, Université Joseph Fourier, France

Received September 10, 2012; **Accepted** December 22, 2012; **Published** March 13, 2013

Funding: This work was supported by the Grant Agency of the Charles University 97309 (to JB) and by Czech Science Foundation P506/12/1010 (to VH). The funders had no role in study design, data collection and analysis, decision to publish, or preparation of the manuscript.

Competing Interests: The authors have declared that no competing interests exist.

* E-mail: vlada@natur.cuni.cz

Introduction

In the last decades, systematic research has considerably improved our knowledge regarding the functions of mitochondrial homologues in many eukaryotic lineages. Particular interest has been paid to microbial parasites and protists that thrive facultatively or obligatorily under anaerobic or microaerophilic conditions (for recent reviews see e.g. [1–3]). It has been shown that their mitochondria often deviate remarkably from the text-book picture. For example, various reductions of components of membrane electron transport chain can be found. Instead of canonical four complexes plus F_oF_1 ATPase, the complexes III and IV are absent in *Blastocystis* and *Nyctotherus* derivates of mitochondrion [4–7]. The path of electrons in these truncated electron transport chains ends at fumarate or in the case of *Blastocystis* also at oxygen to which the transfer is mediated by the complex of alternative oxidase [4–7]. Many obligatory anaerobes and microaerophiles lack a respiratory chain completely [3,8,9] and the enzyme [FeFe]hydrogenase provides the sink for electrons produced by redox reactions in their organelles. This enzyme transfers these electrons to protons producing hydrogen gas, a typical feature of hydrogenosomes that represent one functional class of organelles homologous to mitochondrion. Notable variation has evolved also in the enzymatic machinery metabolizing pyruvate. In mitochondria of anaerobes and microaerophiles, the canonical pyruvate dehydrogenase complex is usually substituted by the analogous enzymes pyruvate:ferredoxin oxidoreductase, pyruvate:NADH oxidoreductase or pyruvate formate lyase [10–12]. Some organisms possess two or even all three types of these enzymes. Finally, neither the metabolism of pyruvate nor the ATP production is a function common to all mitochondrial homologues. These processes are absent in the most minimalistic versions of these organelles – mitosomes of *Giardia*, *Entamoeba*, *Cryptosporidium* and microsporidia [8,13–17]. Yet, the mitochondria even in their miniature form are apparently still essential for eukaryotic cells, as all eukaryotes studied so far possess them. The functions of these minimalistic mitochondrial homologues (mitosomes) and perhaps the most basic function of all mitochondrial homologues, has not been established yet. The synthesis of FeS clusters is often mentioned in this context [18].

Metamonada is a group composed exclusively of anaerobes and microaerophiles [19,20]. The mitochondrial organelles of two

metamonad lineages, parabasalids (i.e. *Trichomonas*) and fornicates (i.e. *Giardia*), have been extensively studied. It has been reported that the proteome of purified hydrogenosomes of *Trichomonas vaginalis* consists of more than 500 proteins, however, many of them may be only externally associated [9,21]. The metabolism of the parabasalid hydrogenosome has been reconstructed to fine details and most enzymes have been biochemically characterized [22]. 139 proteins have been found in the mitosomal fraction of *Giardia*, however, only 20 of them have been experimentally verified as *bona fide* mitosomal proteins [8]. The only biochemically verified function of the *Giardia* mitosome remains the synthesis of FeS clusters [23]. The third lineage of Metamonada – Preaxostyla – consists of oxymonads and *Trimastix* [24]. Nothing is known about the mitochondrial homologues of oxymonads and besides one observation [25] no such organelles have been observed in this group. Double membrane bounded organelles have been described in *Trimastix* [26–28]. Several transcripts typical for mitochondrial proteins have been found among 10 000 transcriptome reads of *Trimastix pyriformis* (see Table 1 in [29]). Four of these transcripts (cpn60, H-protein, T-protein and P1-protein of glycine cleavage system) contained short extension at their 5' end in comparison with bacterial homologues, i.e. putative mitochondrial targeting sequences. However, none of these presequences are recognized by prediction software trained to recognize these sequences in other organisms. Likewise, none of these proteins have been experimentally localized to a cellular compartment. In this paper, we build on this previous work and present a more thorough transcriptome analysis based on 454 sequencing and more importantly bring the first experimental evidence for localization of cpn60 and enzymes of glycine cleavage system in the mitochondrial homologue of *Trimastix*.

Results

Proteins putatively localized to *Trimastix* mitochondrion-like organelle

In order to detect proteins putatively localized in the organelle of *Trimastix*, we have generated new set of transcriptomic data. In two runs of 454 sequencing of *Trimastix* mRNA we have produced in total 643 758 reads of *Trimastix* mRNA that were assembled into 7 037 contigs and 33 204 singletons. The contigs were automatically annotated using dCAS pipeline (http://exon.niaid.nih.gov). The contigs and singletons were then screened using HMM for proteins of protein transport machinery and mitochondrial carriers. Selected candidates were manually investigated for the presence of functional domains. Furthermore, the set of contigs and singletons was searched using standalone BLAST with *Giardia intestinalis* mitosomal proteins, *Trichomonas vaginalis* hydrogenosomal proteins and TCA cycle enzymes as queries. Best hits were further screened by predictor of protein localization Euk-mPloc 2.0. [30]. Putative organellar proteins predicted by Euk-mPloc, in which the presence of N-terminal targeting presequence is expected, were investigated for the presence of N-terminal targeting signal by three predictor programs (Table S1). Besides two exceptions (HydE and ornithine transcarbamylase), the proteins were not strongly predicted as mitochondrially targeted. Nevertheless, 9 proteins (including HydE and ornithine transcarbamylase) showed N-terminal extensions relative to the bacterial homologues in their alignments (Figure S1). Even if most of these extensions were not recognized as putative targeting peptides, we still consider this possibility and below present experimental evidence that the extension present in the H-protein of glycine cleavage system is indeed required for protein targeting into mitochondrion. We used the presence of an N-terminal extension as an important criterion for inclusion in the list of proteins predicted to localize into the mitochondrion-like organelle. Proteins in which the extension was not demonstrated were included only if they were functionally linked to other proteins in the list (hydG, P2-protein of glycine cleavage system) or if they were considered as strictly or almost strictly mitochondrially localized proteins (e.g. Tom40, Sam50, hydG, mitochondrial processing peptidase). The final list of proteins predicted to localize into the mitochondrion-like organelle of *Trimastix* on the basis of current data and the basis of data of Hampl et al. [29] is given in Table 1.

These proteins are involved in amino acid metabolism (glycine cleavage system, serine hydroxymethyltransferase, ornithine transcarbamylase), co-factor metabolism (pyridine nucleotide transhydrogenase $\beta+\alpha$, lipoyltransferase), transport and maturation of proteins (Tom40, Sam50, one member of Tim17 family, Pam18, mitochondrial processing peptidase, cpn60 and [FeFe]hydrogenase maturases) and transport of other metabolites (proteins of membrane carrier family). Mitochondrial type aconitase is the only enzyme involved in energy metabolism that was included in the list. Enzymes of pyruvate:ferredoxin oxidoreductase (PFO) and [FeFe]hydrogenase were not listed because there are no strong indications that they are localized in the organelle. Neither [FeFe]hydrogenase nor PFO contained obvious N-terminal extensions. The substrate specificity of four identified membrane carriers (PFAM PF00153) was estimated according to the sequence similarity as well as to the presence of the residues known to be involved in the substrate binding [31]. Hence, the inner membrane of the mitochondrion-like organelle likely accommodates the ADP/ATP, 2-oxodicarboxylate and folate carriers. Although the fourth identified protein shares the signature motives of the protein family, the substrate specificity could not be estimated due to the high sequence divergence.

Glycine cleavage system is localized to *Trimastix* mitochondrion-like organelle

Given the fact that the complete set of glycine cleavage system (GCS) enzymes has been found in the transcriptome of *Trimastix* and that three of these proteins (H-, P1- and T-protein) contained 5' extensions, it seem likely that the complete glycine cleavage system is localized in the organelle. To corroborate this hypothesis we have performed three experiments.

Firstly, we have used the *Saccharomyces cerevisiae* heterologous expression system with the assumption that protein localized into the mitochondrion-like organelles in *Trimastix* will also be recognized as mitochondrial protein by the yeast mitochondrion. As a positive control we have over-expressed a GFP-tagged version of *Trimastix* cpn60, the classical mitochondrial marker, in yeast. The fluorescence microscopy showed that the GFP signal co-localized with the signal from MitoTracker that highlighted yeast mitochondria (Figure 1). This demonstrates that the protein transport machinery of the yeast mitochondrion is able to recognize *Trimastix* organellar proteins. Analogously to cpn60, we over-expressed GFP-tagged P1- and H-proteins. The fluorescence microscopy showed that the GFP signal co-localized with the signal from MitoTracker (Figure 1) indicating that both proteins were transported into the yeast mitochondria. As a negative control we have over-expressed a GFP tagged H-protein that was truncated at the N-terminus and started with the 17^{th} amino acid. The truncated H-protein remained in the cytosol of yeast (Figure 1). Besides serving as a negative control, the latter experiment also confirmed our expectation that the N-terminal extension observed in H-protein bears a signal necessary for targeting of the protein into the mitochondrion-like organelle.

Table 1. List of the proteins putatively localized in the mitochondrion-like organelle of *Trimastix pyriformis*.

Product	Sequence accession numbers	N-terminal extension	Experimental evidence
Aconitase TCA cycle enzyme	EU086483	Yes	No
hydE Maturation of [FeFe] hydrogenase	JX657285	Yes	No
hydF* Maturation of [FeFe] hydrogenase	JX657286	Yes	No
hydG Maturation of [FeFe] hydrogenase	JX657287	?	No
H-protein of glycine cleavage system central protein in GCS	EU086492	Yes	Yes
P1-protein of GCS Glycine dehydrogenase (decarboxylating) subunit 1	EU086490	Yes	Yes
P2-protein of GCS Glycine dehydrogenase (decarboxylating) subunit 2	EU086491	?	No
L-protein of GCS Dihydrolipoyl dehydrogenase	EU086501	No	No
T-protein of GCS Aminomethyltransferase	EU086485	Yes	No
Lipoyltransferase Lipoylisation of enzymes	EU086495	?	No
Serine hydroxymethyltransferase* Amino acid metabolism	JX657288	Yes	No
Ornithine transcarbamylase* Amino acid metabolism	JX657289	Yes	No
Tom40 Protein transport	EU086500	NA	No
Sam50* Protein transport	JX657290	NA	No
Tim17 protein family member* Protein transport	JX657291	No	No
Pam18* Protein transport	JX657292	No	No
Mitochondrial processing protease α subunit Targeting sequence cleavage	EU086496	No	No
Cpn60 Protein folding	EU086489	Yes	Yes
Pyridine nucleotide transhydrogenase beta+alpha NAD and NADP interconversion	EU086499	No	No
Membrane carrier 1 Putative ATP/ADP transporter	EU086488	No	No
Membrane carrier 2* Putative 2-oxodicarboxylate carrier	JX657293	No	No
Membrane carrier 3 Putative folate carrier	EU086487	?	No
Membrane carrier 4* Transporter with unknown specificity	JX657294	?	No

*The transcripts were identified in this study
doi:10.1371/journal.pone.0055417.t001

Secondly, we have used immunofluorescence microscopy (Figure 2A, Figure S2) with two antibodies against the H-protein of GCS – a commercial antibody against human H-protein (green signal) and our in-house prepared antibody against *Trimastix* H-protein (red signal). The green signal showed several spots that co-localized with the red signal revealing dozens of bodies (putative mitochondrion-like organelles) distributed predominantly around the nucleus and in the posterior-ventral part of the cell.

Finally, we have applied the antibody against *Trimastix* H-protein on the Western blot of cell fractions of *Trimastix* (Figure 2B). The signal of the expected size appeared in the high speed pellet (HSP) and in the total lysate of *Trimastix* but neither in the lysate of bacteria from the *Trimastix* culture (Bact) nor in the supernatant (Sup) that contains the cytoplasm of *Trimastix*.

To see whether the organelle of *Trimastix* produces observable proton potential, we have stained the cell of *Trimastix* with MitoTracker Red CMXRos dye that specifically accumulates in the mitochondria upon the presence of the membrane potential. No stained vesicles were observed in *Trimastix* cells and only diffused cytosolic signal was detected. Similar results were obtained when MitoTracker Green FM was used, which does not require membrane potential (not shown).

Discussion

In this second transcriptomic study of *Trimastix pyriformis* we have produced, using 454 technology, more than 60x more reads which formed 2,6x more contigs (not counting singletons) than in the previous study [29]. Despite the massive increase in the amount of data, we were able to predict only 8 new proteins that putatively localize to the mitochondrion-like organelle (marked by stars in the Table 1). These include HydF, serine hydroxymethyltransferase, ornithine transcarbamylase, Sam50, Tim17 protein family member and Pam18. The number of contigs assembled (7 037 in this data set) is unlikely to cover the complete transcriptome and so the discovery of new organellar proteins is expected in the future.

In addition to the *in silico* study, we gathered the first experimental evidence in support of organellar localization of cpn60 and two of the four enzymes of glycine cleavage system (H- and P1-protein). The evidence for putative functions of the mitochondrion-like organelle is discussed below.

Amino acid metabolism

As many as seven enzymes in the list are directly involved in amino acid metabolism, namely H-, P1-, P2-, T- and L-protein of GCS, serine hydroxymethyltransferase (SHMT) and ornithine

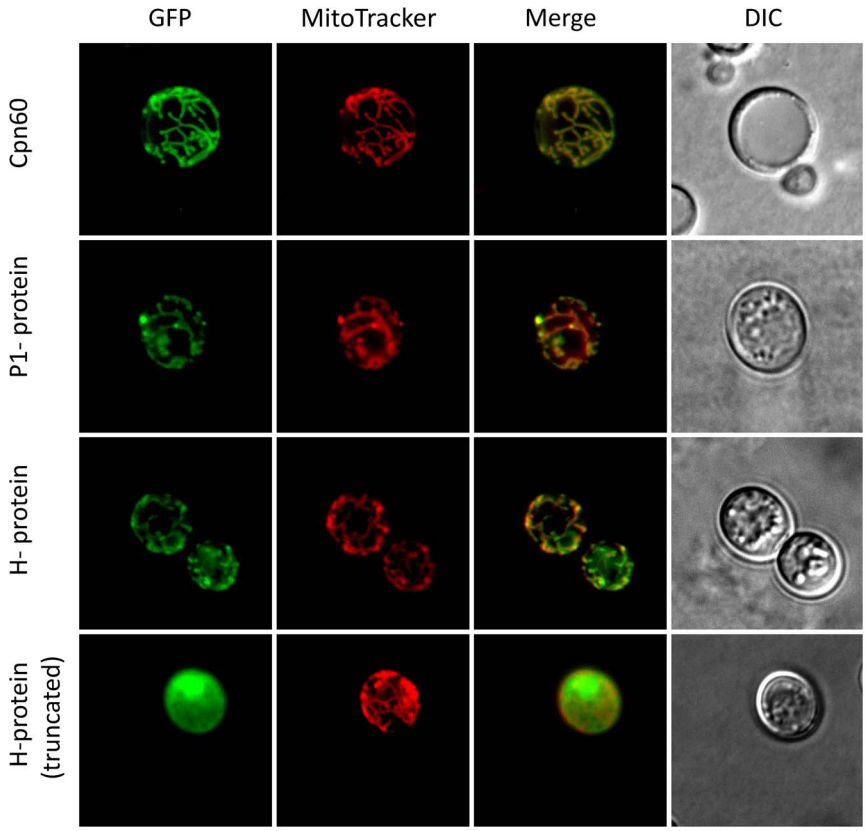

Figure 1. Over-expression of *Trimastix* proteins in yeast. The over-expression of GFP tagged proteins of *Trimastix* in *Saccharomyces cerevisiae*. The columns represent the signals from GFP tag (green), MitoTracker (red), merged GFP and MitoTracker and DIC. Rows represent individual proteins: cpn60, P1-protein of GCS, H-protein of GCS and H-protein of GCS truncated of the first 16 amino acids.
doi:10.1371/journal.pone.0055417.g001

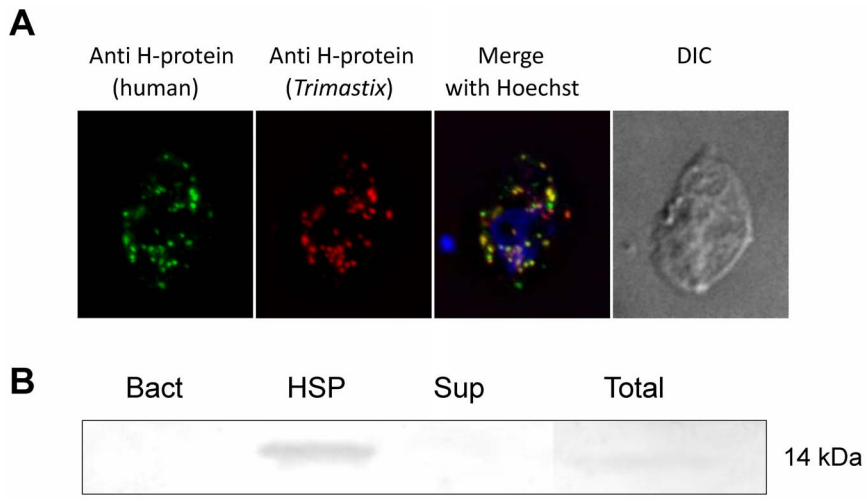

Figure 2. H-protein of GCS localizes into vesicles (putative mitochondrion-like organelles) in *Trimastix pyriformis*. A) Immunofluorescence microscopy of the *Trimastix pyriformis* cell. The green signal from antiH-protein (human) co-localizes with red signal from the antiH-protein (*Trimastix*). The DNA is stained blue with Hoechst. B) Western blot on the cellular fractions of *Trimastix pyriformis*. The lines represent pure bacteria *Citrobacter* sp. from the culture (Bact), high speed pellet of *Trimastix* (HSP), supernatant of *Trimastix* (Sup), total lysate of *Trimastix* (Total).
doi:10.1371/journal.pone.0055417.g002

transcarbamylase (OTC), the eighth enzyme, lipoyltransferase, is involved only indirectly by lipoylisation of the H-protein [32].

The GCS catalyses a cycle of glycine catabolising reactions producing methyl-tetrahydrofolate, NADH and CO_2 and it can function also in the opposite direction [33]. In eukaryotes, the cycle is typically localized in the mitochondrion. The evidence for the localization of GCS in the mitochondrion-like organelle of *Trimastix pyriformis* seems to be relatively strong. All five enzymes are present in the transcriptome (the two subunits of P-protein are coded as separate proteins). Three of them (H, P1 and T) carry an N-terminal extension and in the case of H-protein we have shown that the N-terminal extension is necessary for its targeting to the yeast mitochondrion. Two of these proteins (H and P1) have been transported into the mitochondrion when over-expressed in yeast, and finally the H-protein has been shown to be present in vesicles (putative mitochondrion-like organelles) in *Trimastix*, by co-localization of two antibodies. Although the ultimate evidence of immunoelectron microscopy of *Trimastix* with anti H-protein antibodies is still missing, considering the fact that GCS has never been observed outside mitochondria or relative organelles in other eukaryotes, the presence of the pathway in the mitochondrion-like organelle of *Trimastix* is very likely.

Serine hydroxymethyltransferase catalyses a reversible conversion of L-serine and tetrahydrofolate to glycine and 5,10-methylenetetrahydrofolate. The reaction may therefore be directly connected to GCS. Various isoforms of SHMT are present in the cytosol, mitochondria and plastids of eukaryotes [34]. The *Trimastix* enzyme contains an N-terminal extension when compared to the bacterial counterparts and so we regard it as putatively localized into the mitochondrion-like organelle (Figure S1).

Ornithine transcarbamylase catalyses the reaction between ornithine and carbamoyl phosphate with the formation of citrulline. This reaction is a part of arginine catabolism in some protists (arginine dihydrolase pathway) and of the urea cycle in mammals. The arginine dihydrolase pathway consists of three enzymes: arginine deiminase (ADI), OTC and carbamoyl kinase (CK). It is localized in the hydrogenosome of *Neocallimastix frontalis* [35] but in the cytosol of *Giardia* [36], where it represents an important source of ATP. In *Trichomonas vaginalis*, the pathway is believed to be present also in the cytosol, however one enzyme of the pathway, ADI, was found in the hydrogenosome [37]. While ADI was not found in the transcriptome, CK is likely present in *Trimastix pyriformis*. Similar to OTC, the *Trimastix* CK is related to prokaryotic CKs but unlike OTC it apparently does not carry an N-terminal extension and therefore was not included in the Table 1. The prokaryotic nature of both enzymes suggests that they may represent bacterial contamination of the transcriptome data set. On the other hand, the relatively high number of reads for these transcripts (1486 for OTC and 640 for CK), which is more than the number of reads of H-protein of GCS (233 reads) or SHMT (210 reads) indicate that they may represent *bona fide Trimastix* enzymes. The prokaryotic origin of *Trimastix* enzymes is, in fact, quite common and other examples of such enzymes are the P1-protein of GCS [29], for which organellar localization was confirmed experimentally in this paper, and 4 out of 10 glycolytic enzymes [38]. The confirmation of the presence and cellular localization of arginine dihydrolase pathway in *Trimastix pyriformis* deserves future research.

Energy metabolism

The only protein in the list directly involved in the energy metabolism is a tricarboxylic-acid-cycle-enzyme aconitase. The localization of a sole enzyme from the cycle in the compartment is, however, very suspicious, and this localization must be verified experimentally before it should be considered more seriously. Even if its localization was confirmed the actual function of the solitary enzyme would remain questionable. Nevertheless this protein fulfills the conditions to be included in the list. Being a homologue of mitochondrial type aconitase and not the cytosolic version it was predicted to localize in the mitochondrion-like organelle by Euk-mPloc 2.0. and, furthermore, it contains a short N-terminal extension.

The set of all three maturases of [FeFe]hydrogenase was found in the transcriptome. Contigs for two of them have complete N-terminus with an extension. These enzymes are essential for maturation of [FeFe]hydrogenase in bacteria [39] but they have been reported from only 5 eukaryotes so far: *Trichomonas vaginalis*, *Chlamydomonas reinhardtii*, *Mastigamoeba balamuthi*, *Acanthamoeba castelanii* and *Andalucia incarcerate* [10,40,41]. In *Trichomonas* and *Chlamydomonas* these proteins are localized in the hydrogenosomes and plastids respectively [40,41]. It is generally believed that the maturases are always localized in the organelle where they assist the maturation of the H-cluster of [FeFe]hydrogenase. The presence of the N-terminal extensions makes them serious candidates for organellar proteins in *Trimastix*. The presence of maturases would suggest that the [FeFe]hydrogenase itself is present in the organelle as well. So far we have no evidence for the localization of [FeFe]hydrogenase and none of the three homologues present among the transcripts bears N-terminal extension indicating the organellar localization. For this reason, [FeFe]hydrogenase was not included in the Table 1. The same applies to pyruvate:ferredoxin oxidoreductase, an enzyme that is often functionally connected to [FeFe]hydrogenase.

Protein transport

Six proteins involved in the transport, processing and maturation of proteins (not counting the specific [FeFe]hydrogenase maturases) have been found: Tom40, Sam50, one member of Tim17/22/23 family, Pam18, α subunit of mitochondrial processing peptidase (αMPP) and cpn60 (Figure 3). This set of proteins represents the basic functional core of protein transport machinery: Tom40 and Tim17/22/23 being the outer- and inner-membrane transport pores, respectively, Sam50 functions as assembly machinery for Tom40 and Pam18 being the part of the motor complex associated with Tim17/22/23 translocase. Upon protein import the MPP cleaves off the targeting peptides and cpn60 assists the protein folding. The *Trimastix* protein transport machinery in this composition would be slightly more complex than the machinery in the mitosome of *Giardia* where the inner membrane pore and Sam50 is missing [8]. We however expect that the *Trimastix* protein transport machinery set is not complete yet and more components will be discovered in the future. Conspicuously absent from all *Trimastix* genomic data sets are the genes encoding βMPP and mtHsp70, two proteins that have been found in most mitochondrion-related organelles examined to date.

Other membrane proteins

Pyridine nucleotide transhydrogenase (PNT) used to be regarded as a specific protein of the inner membrane of the mitochondrion [42] until Yousuf et al. [43] have shown that it localizes into vesicles different from mitosomes in *Entamoeba histolytica*. PNT transfers hydride ion between NAD(H) and NADP(H) and simultaneously transfers proton across the membrane [44]. Structurally the protein functions as a homodimer and each monomer consist of two domains α and β. These domains are expressed as separate proteins in prokaryotes but as a single

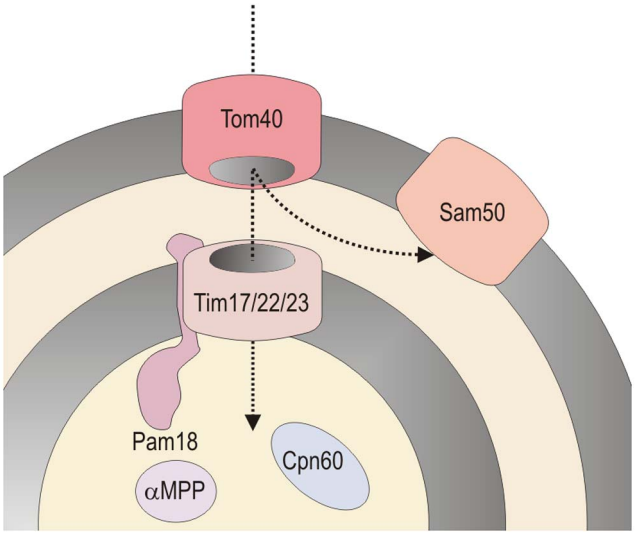

Figure 3. Schematic representation of protein import machinery in *Trimastix pyriformis* mitochondrion-like organelle.
doi:10.1371/journal.pone.0055417.g003

protein in eukaryotes. In the first study of the transcriptome of *Trimastix* [29], we found the domains in separate contigs and concluded that they were expressed independently as in prokaryotes. In the assembly of the 454 reads, however, the two subunits appeared in a single contig suggesting that the two domains are encoded by a single gene and expressed as a single protein like in other eukaryotes.

In the present and previous study we have identified altogether four members of the mitochondrial carrier family and we designated them as membrane carrier protein 1–4. As proteins from this family have also been reported from the membranes of peroxisomes and plastids [45–47], their presence in the membrane of mitochondrion-like organelle is only putative. The carriers designated now as carriers 1 and 3 have been previously reported upon [29], the carriers 2 and 4 were identified in the current data set. The carrier 3 listed in the Table 1 in [29] has been excluded from the current list, as we have serious doubts about its affiliation into mitochondrial carrier family. According to the conserved residues and phylogenetic relationships to other carriers we expect that carrier 1 transports adenine nucleotides (e.g. ATP, NAD), carrier 2 transports 2-oxodicarboxylates (e.g. 2-oxoglutarate) and carrier 3 transports folate. The substrate specificity of carrier 4 cannot be predicted from the sequence itself. The presence of glycine cleavage complex in the organelle indeed requires the transport of NAD/NADH and folate but also the transport of amino acids (glycine or serine). The latter molecules may be transported by carrier 4 or by carriers that have not been identified so far. Mitochondrial carriers typically need a proton potential across the inner mitochondrial membrane to properly function [31]. As we were not able to detect a proton potential using MitoTracker Red, it is possible that the carriers can operate under small or even without membrane potential. Similarly the carrier proteins of peroxisomes [31] and *Entamoeba* mitosomes [48] are thought to be membrane potential-independent.

Conclusions

The transcriptome sequencing using 454 technology enriched the list of proteins putatively localized into the mitochondrion-like organelle of *Trimastix* to a total number of 23 proteins. Most of these proteins are involved in the metabolism of amino acids, transport and maturation of proteins and transport of metabolites. Neither PFO nor [FeFe]hydrogenase were included in the list as there is no evidence for them to be present in the organelle neither there is evidence that the organelle produces ATP. Mitochondrial localization of most of the listed proteins remains only putative and should be confirmed experimentally in the future. The first such evidence has been presented for the enzymes of glycine cleavage complex, which is at the moment the only experimentally localized pathway in the *Trimastix* mitochondrion-like organelle.

Materials and Methods

Preparation of *T. pyriformis* cDNA

T. pyriformis (strain RCP-MX, ATCC 50935) total RNA was isolated from 16×10^7 cells using TRIzol Reagent (Invitrogen). *T. pyriformis* mRNA transcriptome was captured from total RNA with Dynabeads mRNA Purification Kit (Invitrogen). cDNA was then prepared using Smarter PCR cDNA Synthesis Kit (Clontech) according to the manufacturer̀s protocol with 19 cycles of cDNA amplification.

454 transcriptome sequencing and annotation

Sequencing library optimized for Roche/454 Titanium sequencing was prepared using GS FLX Titanium Rapid Library Preparation Kit from double-stranded cDNA. Fragment library was titrated by enrichment and prepared for sequencing by emulsion PCR on two regions of a two-region GS-FLX Titanium PicoTitreTM plate. The reads were cleaned of all adaptor/primer and polyA sequence. Newbler (v2.6; Roche/454 Sequencing) and the default parameters (40 bp overlap; 90% identity) were used for the assembly of 644 537 reads (average length 399 bp). These were assembled into 7 037 contigs and 6 255 isogroups (33 204 singletons remained). Isogroups can either represent alternatively spliced genes (with contigs indicating exons, and isotigs representing splice forms), or sets of recently duplicated genes (with contigs representing regions of divergence since duplication, and isotigs representing the divergent genes) either as gene families or multiple alleles of the same gene.

All contigs were automatically annotated using dCAS pipeline (http://exon.niaid.nih.gov). In this pipeline all the contigs were analyzed by SignalP 3.0 server [49] to predict import signals and with TMHMM2.0 server [50] to predict transmembrane α-helices. Local BLASTX search against downloaded NCBI database (non redundant protein database from 11.7.2012) was used for annotation of contigs.

Candidate proteins of membrane protein translocation complexes were determined by HMM search of all six frame translation of contigs and singletons. The selected transcripts were further analyzed by HHpred search at http://toolkit.tuebingen.mpg.de/hhpred [51].

Standalone BLAST searches against the *Trimastix* contigs and singletons were performed in BioEdit 7.1.3.0. [52] using the set of 20 mitosomal proteins of *Giardia intestinalis* [8] and 413 hydrogenosomal proteins of *Trichomonas vaginalis* (Table S1 in [9]) as queries. The best hits were further submitted to Euk-mPloc 2.0 [30] for prediction of cellular localization. Proteins that were predicted to localize into mitochondria or chloroplasts were further investigated. For each such candidate for mitochondrial matrix protein, 10–20 closest eukaryotic and prokaryotic homologues were downloaded from the GenBank. The proteins were aligned and the alignment was manually refined in BioEdit 7.1.3.0. [52]. The completeness of the *Trimastix* protein sequences, the start codons and the presence or absence of N-terminal

extension were estimated based on this alignment. *Trimastix* proteins that exhibited N-terminal extension relatively to the prokaryotic homologues were selected.

The sequences of newly determined candidate organellar proteins are stored in GenBank under accession numbers JX657285-JX657294. The Transcriptome Shotgun Assembly project has been deposited at DDBJ/EMBL/GenBank under the accession GAFH00000000. The version described in this paper is the first version, GAFH01000000.

Preparation of constructs for over-expression in yeast

T. pyriformis genes were PCR amplified from cDNA using EmeraldAmp Max PCR Mastermix (Takara) and the following primers: Glycine cleavage system H-protein (GenBank ID: EU086492) – **5̀TCTAGA**ATGCAGCGCCTTTTCTCT (XbaI site in bold) and **5̀AAGCTT**ATGCTGGGTCTTGAGGAA (HindIII site in bold); N-terminally truncated version of H-protein – **5̀TCTAGA**ATGGCTCGGTTTGCCGGCGAG (XbaI site in bold) and **5̀AAGCTT**ATGCTGGGTCTTGAGGAA (HindIII site in bold); P1 protein of glycine cleavage system (GenBank ID: EU086490) – **5̀TCTAGA**ATGCAGAACCTTTCTCGC (XbaI site in bold) and **5̀AGCTT**CAGGGAGGCGCGCAGGGC (HindIII site in bold); cpn60 (GenBank ID: EU086489) – **5̀TCTAGA**ATGCAGGCCCTGTTTTCC (XbaI site in bold) and **5̀ AAGCTT**GAATGGCTTGGGCAGGCC (HindIII site in bold). The PCR products were cloned into pUG35 vector with GFP tag at the 3̀ end.

Transformation of yeasts

The wild type *Saccharomyces cerevisiae* strain YPH499 (ATCC number: 204679) was used in this study. Yeasts were grown on plates with YPD agar medium (for 500 ml: D-glucose, Penta: 10 g; yeast extract, Oxoid: 5 g; trypticase peptone, BBL: 10 g; agar, Oxoid: 6 g) at 30°C. Transformation of the yeasts with 2 μg of plasmid DNA was performed using LiAc/SS-DNA/PEG method according to Gietz and Schiestl [53]. Transformants were selected on synthetic drop-out medium without uracil (for 500 ml: D-glucose, Penta: 10 g; yeast nitrogen base, Sigma: 3,35 g; yeast synthetic drop-out medium supplement, Sigma: 0,96 g; agar, Oxoid: 6 g) at 30°C. Only transformants containing plasmids with cloned *T. pyriformis* genes were able to grow on medium lacking uracil. Expression of GFP-tagged proteins of *T. pyriformis* in yeasts was analyzed 3 days after transformation. Mitochondria were labeled with MitoTracker Red CMXRos dye (Molecular probes, cat. # M7512).

Antibody production

Rat polyclonal antibody was raised against *T. pyriformis* GCS H-protein. A 6xHis-tagged version of this protein was expressed from plasmid pET42b in *Escherichia coli* BL21 DE3. Protein was purified by immobilized-metal affinity chromatography using Ni-NTA resin under denaturing conditions using 8 M urea according to the protocol described in the QIAExpressionist handbook (Qiagen). A rat was immunized with purified protein in acrylamide gel for a period of 12 weeks (300 μg of antigen was used per 1 subcutaneous injection every 4 weeks).

The serum specific for *T. pyriformis* GCS H-protein was tested for reactivity on Western blot using *Trimastix* cell fractions (whole cell lysate, cytoplasm, high speed pellet) as well as *Citrobacter* sp. lysate.

Trimastix fractionation of cellular extracts

T. pyriformis cell fractions (cytosol and organelle-rich fraction) were obtained by differential centrifugation as previously described [54] with slight modifications. *T. pyriformis* (2.5 liters of the cell culture) was filtered from bacteria using Cyclopore Track Etched Membrane, 3μm (Whatman). Filtered *Trimastix* was pelleted by centrifugation for 10 minutes at 3000 x g. Cells were resuspended in 1 ml of cold 3% LB medium (L3022, Sigma; for 3% LB dilute 30 ml of LB medium in 970 ml of distilled water) containing protease inhibitor cocktail (Roche, cat. # 11836170001). Cells were placed on ice and homogenized by sonication (1–2 times for 1 minute at amplitude 40). Cells were checked by light microscope after each round of sonication. Homogenate was centrifuged for 10 minutes at 500 x g at 4°C. The pellet was discarded. The supernatant was centrifuged 30 minutes at 100000 x g at 4°C to pellet the organelles. Organelles were resuspended to final volume of 50μl of 3% LB medium containing protease inhibitor cocktail. The supernatant containing the cytosol was centrifuged again for 45 minutes at 100000 x g at 4°C. The pellet was discarded.

T. pyriformis cell fractions were analyzed by SDS-PAGE and Western blotting.

Preparation on *Trimastix pyriformis* immunofluorescence slides

The slides were prepared using immunostaining protocol with coverslips according to Dawson et al. [55] with the following modifications. *Trimastix* cells in the growth medium were fixed with 2% paraformaldehyde solution for 30 minutes at room temperature. Fixed cells were dispensed on coverslips coated with 15 μl of Poly-L-lysine solution (Sigma) and left for one hour to adhere. Coverslips with adhered cells were air dried. Preparations were blocked with PEMBALG solution (PEM buffer; 1% BSA; 0,5% cold water fish skin gelatin; 100 mM lysine; 0,1% sodium azide) for 30 minutes at room temperature. Cells were incubated overnight with antibodies against human GCS H (Abnova) and against *Trimastix* GCS H (both diluted 1:200) on parafilm. Preparations were incubated on parafilm with secondary antibodies AlexaFluor 488 Goat Anti-Mouse and AlexaFluor 594 Goat Anti-Rabbit (Molecular probes) diluted 1:1000. Coverslips were washed three times with PEM buffer. The last wash was performed with addition of the Hoechst 33342 stain (Molecular probes) into PEM buffer (1:1000 of dilution). Coverslips were mounted onto slides using VECTASHIELD Mounting Medium (Vector Laboratories).

Immunofluorescence microscopy

The images were collected using a fluorescence microscope IX81 equipped with IX2-UCB camera (Olympus) with a 100x immersion oil objective and CellR software. Images were processed by ImageJ software (NIH, Bethesda, MD, USA).

Supporting Information

Figure S1 The N-terminal parts of protein alignments demonstrating the presence of extension in *Trimastix* protein relatively to the prokaryotic homologues.
(PDF)

Figure S2 Immunofluorescence microscopy of two additional *Trimastix pyriformis* cells. The green signal from antiH-protein (human) co-localizes with red signal from the antiH-protein (*Trimastix*). The DNA is stained blue with Hoechst.
(PDF)

Table S1 The probability of mitochondrial localization of selected *Trimastix* proteins as predicted by PSORT II, TargetP and Multiloc2 programs.
(DOCX)

Acknowledgments

Authors would like to thank Veronika Harsová for technical assistance and Joel B. Dacks for proofreading and helpful comments.

Author Contributions

Conceived and designed the experiments: VH JT ZZ PD CV. Performed the experiments: ZZ LN VV JR JB JF. Analyzed the data: VH PD CV. Contributed reagents/materials/analysis tools: VH CV. Wrote the paper: VH.

References

1. Hjort K, Goldberg AV, Tsaousis AD, Hirt RP, Embley TM (2010) Diversity and reductive evolution of mitochondria among microbial eukaryotes. Philos Trans R Soc Lond B Biol Sci 365:713–27.
2. Shiflett AM, Johnson PJ (2010) Mitochondrion-related organelles in eukaryotic protists. Annu Rev Microbiol 64:409–29.
3. Müller M, Mentel M, van Hellemond JJ, Henze K, Woehle C, et al. (2012) Biochemistry and evolution of anaerobic energy metabolism in eukaryotes. Microbiol Mol Biol Rev 76:444–95.
4. Boxma B, de Graaf RM, van der Staay GW, van Alen TA, Ricard G, et al. (2005) An anaerobic mitochondrion that produces hydrogen. Nature 434:74–9.
5. Stechmann A, Hamblin K, Pérez-Brocal V, Gaston D, Richmond GS, et al. (2008) Organelles in *Blastocystis* that blur the distinction between mitochondria and hydrogenosomes. Curr Biol 18:580–5.
6. Pérez-Brocal V, Clark CG (2008) Analysis of two genomes from the mitochondrion-like organelle of the intestinal parasite *Blastocystis*: complete sequences, gene content, and genome organization. Mol Biol Evol 25:2475–82.
7. Denoeud F, Roussel M, Noel B, Wawrzyniak I, Da Silva C, et al. (2011) Genome sequence of the stramenopile *Blastocystis*, a human anaerobic parasite. Genome Biol 12:R29.
8. Jedelský PL, Doležal P, Rada P, Pyrih J, Smíd O, et al. (2011) The minimal proteome in the reduced mitochondrion of the parasitic protist *Giardia intestinalis*. PLoS One 6:e17285.
9. Schneider RE, Brown MT, Shiflett AM, Dyall SD, Hayes RD, et al. (2011) The *Trichomonas vaginalis* hydrogenosome proteome is highly reduced relative to mitochondria, yet complex compared with mitosomes. Int J Parasitol 41:1421–34.
10. Hug LA, Stechmann A, Roger AJ (2010) Phylogenetic distributions and histories of proteins involved in anaerobic pyruvate metabolism in eukaryotes. Mol Biol Evol 27:311–324.
11. Stairs CW, Roger AJ, Hampl V (2011) Eukaryotic pyruvate formate lyase and its activating enzyme were acquired laterally from a Firmicute. Mol Biol Evol 28:2087–99.
12. Hampl V, Stairs CW, Roger AJ (2011) The tangled past of eukaryotic enzymes involved in anaerobic metabolism. Mob Genet Elements 1:71–74.
13. Katinka MD, Duprat S, Cornillot E, Metenier G, Thomarat F, et al. (2001) Genome sequence and gene compaction of the eukaryote parasite *Encephalitozoon cuniculi*. Nature 414: 450–453.
14. Goldberg AV, Molik S, Tsaousis AD, Neumann K, Kuhnke G, et al. (2008) Localization and functionality of microsporidian iron-sulphur cluster assembly proteins. Nature 452: 624–628.
15. Mogi T, Kita K (2012) Diversity in mitochondrial metabolic pathways in parasitic protists *Plasmodium* and *Cryptosporidium*. Parasitol Int 59:305–12.
16. Dolezal P, Dagley MJ, Kono M, Wolynec P, Likić VA, et al. (2010) The essentials of protein import in the degenerate mitochondrion of *Entamoeba histolytica*. PLoS Pathogen 6:e1000812.
17. Mi-ichi F, Makiuchi T, Furukawa A, Sato D, Nozaki T (2011) Sulfate activation in mitosomes plays an important role in the proliferation of *Entamoeba histolytica*. PLoS Negl Trop Dis 5:e1263.
18. Lill R, Kispal G (2000) Maturation of cellular Fe-S proteins: an essential fiction of mitochondria. Trends Biochem Sci 2000 25:352-6.
19. Cavalier-Smith T (2003) The excavate protozoan phyla Metamonada Grassé emend. (Anaeromonadea, Parabasalia, *Carpediemonas*, Eopharyngia) and Loukozoa emend. (Jakobea, *Malawimonas*): their evolutionary affinities and new higher taxa. Int J Syst Evol Microbiol 53:1741–58.
20. Hampl V, Hug L, Leigh JW, Dacks JB, Lang BF, et al. (2009) Phylogenomic analyses support the monophyly of Excavata and resolve relationships among eukaryotic "supergroups". Proc Natl Acad Sci U S A 106:3859–64.
21. Rada P, Doležal P, Jedelský PL, Bursac D, Perry AJ, et al. (2011) The core components of organelle biogenesis and membrane transport in the hydrogenosomes of *Trichomonas vaginalis*. PLoS One 6:e24428.
22. Hrdy I, Tachezy J, Müller M (2008) Metabolism of trichomonad hydrogenosomes. In: Tachezy J, editor. Hydrogenosomes and Mitosomes:Mitochondria of Anaerobic Euakryotes.Berlin, Heidelberg: Springer-Verlag.pp. 114–145.
23. Tovar J, León-Avila G, Sánchez LB, Sutak R, Tachezy J, et al. (2003) Mitochondrial remnant organelles of *Giardia* function in iron-sulphur protein maturation. Nature 426:172–6.
24. Simpson AG (2003) Cytoskeletal organization, phylogenetic affinities and systematic in the contentious taxon Excavata (Eukaryota). Int J Syst Evol Microbiol 53:1759–77.
25. Carpenter KJ, Waller RF, Keeling PJ (2008) Surface morphology of *Saccinobaculus* (Oxymonadida): implications for character evolution and function in oxymonads. Protist 159:209–21.
26. Brugerolle G, Patterson D (1997) Ultrastructure of *Trimastix convexa* Hollande, an amitochondriate anaerobic flagellate with a previously undescribed organization. Europ J Protistol 33: 121–130.
27. O'Kelly CJ, Farmer MA, Nerad TA (1999) Ultrastructure of *Trimastix pyriformis* (Klebs) Bernard et al.: similarities of *Trimastix* species with retortamonad and jakobid flagellates. Protist 150: 149–162.
28. Simpson AGB, Bernard C, Patterson DJ (2000) The ultrastructure of *Trimastix marina* Kent, 1880 (eukaryota), an excavate flagellate. Europ J Protistol 36: 229–251.
29. Hampl V, Silberman JD, Stechmann A, Diaz-Triviño S, Johnson PJ, et al. (2008) Genetic evidence for a mitochondriate ancestry in the 'amitochondriate' flagellate *Trimastix pyriformis*. PLoS One 3:e1383.
30. Chou KC, Shen HB (2010) A new method for predicting the subcellular localization of eukaryotic proteins with both single and multiple sites: EukmPLoc 2.0. PLoS One 5:e9931.
31. Kunji ER, Robinson AJ (2006) The conserved substrate binding site of mitochondrial carriers. Biochim Biophys Acta 1757:1237–48.
32. Fujiwara K, Okamura-Ikeda K, Packer L, Motokawa Y (1997) Synthesis and Characterization of Selenolipoylated H-protein of the Glycine Cleavage System J Biol Chem 272: 19880-19883.
33. Douce R, Bourguignon J, Neuburger M, Rebeille F (2001) The glycine decarboxylase system: a fascinating complex. Trends Plant Sci 6: 167–176.
34. Besson V, Nauburger M, Rebeille F, Douce R (1995) Evidence for three serine hydroxymethyltransferases in green leaf cells. Purification and characterization of the mitochondrial and chloroplastic isoforms". Plant Physiol Biochem 33: 665–673.
35. Gelius-Dietrich G, Ter Braak M, Henze K (2007) Mitochondrial steps of arginine biosynthesis are conserved in the hydrogenosomes of the chytridiomycete *Neocallimastix frontalis*. J Eukaryot Microbiol 54:42–4.
36. Touz MC, Rópolo AS, Rivero MR, Vranych CV, Conrad JT (2008) Arginine deiminase has multiple regulatory roles in the biology of *Giardia lamblia*. J Cell Sci 121:2930–8.
37. Morada M, Smid O, Hampl V, Sutak R, Lam B, et al. (2011) Hydrogenosome-localization of arginine deiminase in *Trichomonas vaginalis*. Mol Biochem Parasitol 176:51–4.
38. Stechmann A, Baumgartner M, Silberman JD, Roger AJ (2006) The glycolytic pathway of *Trimastix pyriformis* is an evolutionary mosaic. BMC Evol Biol 6:101.
39. Meyer J (2007) [FeFe] hydrogenases and their evolution: a genomic perspective. Cell Mol Life Sci 64: 1063–1084.
40. Posewitz MC, King PW, Smolinski SL, Zhang L, Seibert M, et al. (2004) Discovery of two novel radical S-adenosylmethionine proteins required for the assembly of an active [Fe] hydrogenase. J Biol Chem 279: 25711–25720.
41. Putz S, Doležal P, Gelius-Dietrich G, Boháčová L, Tachezy J, et al. (2006) Fe-hydrogenase maturases in the hydrogenosomes of *Trichomonas vaginalis*. Eukaryot Cell 5: 579–586.
42. Clark CG, Roger AJ (1995) Direct evidence for secondary loss of mitochondria in *Entamoeba histolytica*. Proc Natl Acad Sci U S A 92:6518–21.
43. Yousuf MA, Mi-ichi F, Nakada-Tsukui K, Nozaki T (2010) Localization and targeting of an unusual pyridine nucleotide transhydrogenase in *Entamoeba histolytica*. Eukaryot Cell 9:926-33.
44. Olausson T, Fjellstrom O, Meuller J, Rydstrom J (1995) Molecular biology of nicotinamide nucleotide transhydrogenase–a unique proton pump. Biochim Biophys Acta 1231: 1–19.
45. Palmieri L, Rottensteiner H, Girzalsky W, Scarcia P, Palmieri F, et al. (2001) Identification and functional reconstitution of the yeast peroxisomal adenine nucleotide transporter. EMBO J 20: 5049–5059.
46. Bedhomme M, Hoffmann M, McCarthy EA, Gambonnet B, Moran RG, et al. (2005) Folate metabolism in plants: an *Arabidopsis* homolog of the mammalian mitochondrial folate transporter mediates folate import into chloroplasts. J Biol Chem 280: 34823–34831.
47. Satre M, Mattei S, Aubry L, Gaudet P, Pelosi L, et al. (2007) Mitochondrial carrier family: Repertoire and peculiarities of the cellular slime mould *Dictyostelium discoideum*. Biochimie 89: 1058–1069.
48. Dolezal P, Dagley MJ, Kono M, Wolynec P, Likić VA, et al. (2010) The essentials of protein import in the degenerate mitochondrion of *Entamoeba histolytica*. PLoS Pathog 6:e1000812.

49. Emanuelsson O, Brunak S, von Heijne G, Nielsen H (2007) Locating proteins in the cell using TargetP, SignalP and related tools. Nat Protoc 2: 953–971.
50. Krogh A, Larsson B, von Heijne G, Sonnhammer EL (2001) Predicting transmembrane protein topology with a hidden Markov model: application to complete genomes. J Mol Biol 305:567–80.
51. Söding J, Biegert A, Lupas AN (2005) The HHpred interactive server for protein homology detection and structure prediction. Nucleic Acids Res. 33(Web Server issue):W244–8.
52. Hall TA (1999) BioEdit: a user-friendly biological sequence alignment editor and analysis program for Windows 95/98/NT. Nucl Acids Symp Ser 41:95–98.
53. Gietz RD, Schiestl RH, Willems AR, Woods RA (1995) Studies on the transformation of intact yeast cells by the LiAc/SS-DNA/PEG procedure. Yeast 11:355–60.
54. Drmota T, Proost P, Van Ranst M, Weyda F, Kulda J, et al. (1996) Iron-ascorbate cleavable malic enzyme from hydrogenosomes of *Trichomonas vaginalis*: purification and characterization. Mol Biochem Parasitol 83:221–34.
55. Dawson SC, Pham JK, House SA, Slawson EE, Cronembold D, et al. (2008) Stable transformation of an episomal protein-tagging shuttle vector in the piscine diplomonad *Spironucleus vortens*. BMC Microbiol 8:71.

Article

Current Biology

A Eukaryote without a Mitochondrial Organelle

Graphical Abstract

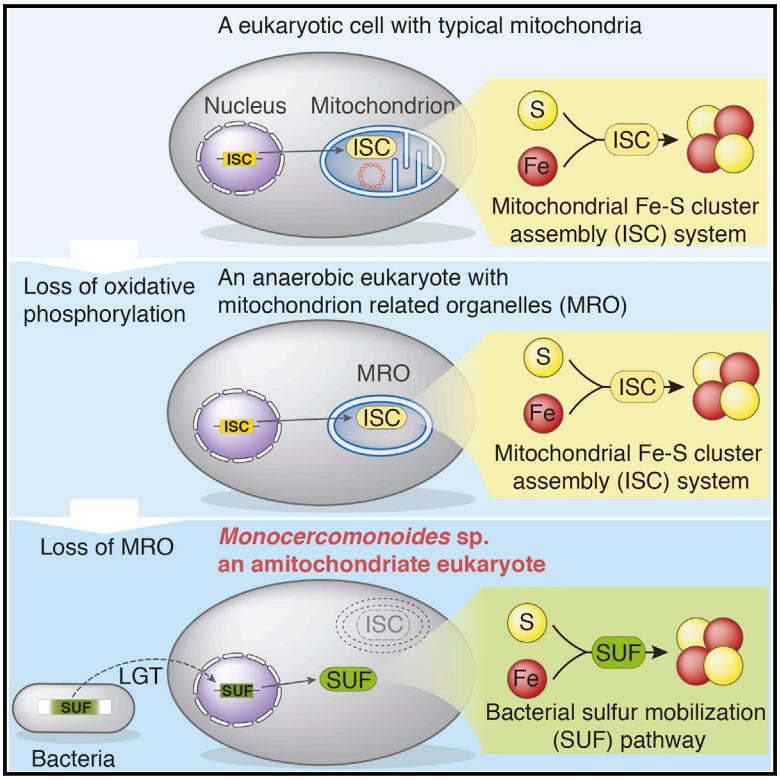

Highlights

- *Monocercomonoides* sp. is a eukaryotic microorganism with no mitochondria
- The complete absence of mitochondria is a secondary loss, not an ancestral feature
- The essential mitochondrial ISC pathway was replaced by a bacterial SUF system

Authors

Anna Karnkowska, Vojtěch Vacek, Zuzana Zubáčová, ..., Joel B. Dacks, Čestmír Vlček, Vladimír Hampl

Correspondence

ankarn@biol.uw.edu.pl (A.K.), vlada@natur.cuni.cz (V.H.)

In Brief

Karnkowska et al. overturn the paradigm that eukaryotes must have mitochondria. Their genomic investigation of the anaerobic microbial eukaryote *Monocercomonoides* sp. reveals a complete lack of mitochondrial organelle and functions including Fe-S cluster synthesis, which is carried out in the cytosol by a laterally acquired bacterial pathway.

Karnkowska et al., 2016, Current Biology *26*, 1274–1284
May 23, 2016
http://dx.doi.org/10.1016/j.cub.2016.03.053

CellPress

Current Biology
Article

A Eukaryote without a Mitochondrial Organelle

Anna Karnkowska,[1,2,7,*] Vojtěch Vacek,[1] Zuzana Zubáčová,[1] Sebastian C. Treitli,[1] Romana Petrželková,[3] Laura Eme,[4] Lukáš Novák,[1] Vojtěch Žárský,[1] Lael D. Barlow,[5] Emily K. Herman,[5] Petr Soukal,[1] Miluše Hroudová,[6] Pavel Doležal,[1] Courtney W. Stairs,[4] Andrew J. Roger,[4] Marek Eliáš,[3] Joel B. Dacks,[5] Čestmír Vlček,[6] and Vladimír Hampl[1,*]

[1]Department of Parasitology, Charles University in Prague, Prague 12843, Czech Republic
[2]Department of Molecular Phylogenetics and Evolution, University of Warsaw, Warsaw 00478, Poland
[3]Department of Biology and Ecology, University of Ostrava, Ostrava 710 00, Czech Republic
[4]Department of Biochemistry and Molecular Biology, Dalhousie University, Halifax, NS B3H 4R2, Canada
[5]Department of Cell Biology, University of Alberta, Edmonton, AB T6G 2H7, Canada
[6]Institute of Molecular Genetics, Academy of Sciences of the Czech Republic, Prague 14220, Czech Republic
[7]Present address: Department of Botany, University of British Columbia, Vancouver, BC V6T 1Z4, Canada
*Correspondence: ankarn@biol.uw.edu.pl (A.K.), vlada@natur.cuni.cz (V.H.)
http://dx.doi.org/10.1016/j.cub.2016.03.053

SUMMARY

The presence of mitochondria and related organelles in every studied eukaryote supports the view that mitochondria are essential cellular components. Here, we report the genome sequence of a microbial eukaryote, the oxymonad *Monocercomonoides* sp., which revealed that this organism lacks all hallmark mitochondrial proteins. Crucially, the mitochondrial iron-sulfur cluster assembly pathway, thought to be conserved in virtually all eukaryotic cells, has been replaced by a cytosolic sulfur mobilization system (SUF) acquired by lateral gene transfer from bacteria. In the context of eukaryotic phylogeny, our data suggest that *Monocercomonoides* is not primitively amitochondrial but has lost the mitochondrion secondarily. This is the first example of a eukaryote lacking any form of a mitochondrion, demonstrating that this organelle is not absolutely essential for the viability of a eukaryotic cell.

INTRODUCTION

Mitochondria are organelles that arose through the endosymbiotic integration of an α-proteobacterial endosymbiont into the proto-eukaryote host cell. During the course of eukaryotic evolution, the genome and proteome of the mitochondrial compartment have been significantly modified, and many functions have been gained, lost, or relocated [1]. In extreme cases, the derivatives of mitochondria in anaerobic protists had become so modified that they had been overlooked [2] or not recognized as homologous to the mitochondrion [3]. Indeed, in the 1980s, the Archezoa hypothesis [4] proposed that some microbial eukaryotes primitively lacked mitochondria, peroxisomes, stacked Golgi apparatus, spliceosomal introns, and sexual reproduction. However, over the following decade, double-membraned organelles were identified in all investigated putative Archezoa. The final nail in the coffin of the Archezoa hypothesis was the demonstration that these organelles all contain some mitochondrial marker proteins, such as those involved in the iron-sulfur cluster (ISC) Fe-S clusters biogenesis system, translocases, maturases, and/or molecular chaperones known to facilitate the import of proteins into mitochondria. It is now widely accepted that mitochondria or mitochondrion-related organelles (MROs) are essential compartments in all contemporary eukaryotes and that mitochondrial endosymbiosis took place before radiation of all extant eukaryotes [5].

Metamonada, originally part of the Archezoa, are now classified as one of the main clades of the eukaryotic "super-group" Excavata [6] and are comprised of microaerophilic or anaerobic unicellular eukaryotes that are often specialized parasites or symbionts. Detailed cell and molecular biological studies, including genome sequencing, have been undertaken only for three parasitic species from two metamonad lineages—*Giardia intestinalis* [7] and *Spironucleus salmonicida* [8] (Fornicata) and *Trichomonas vaginalis* [9] (Parabasalia), which have provided important information regarding the functions of their MROs. The third lineage of metamonads, Preaxostyla, contains the basal paraphyletic free-living trimastigids and the derived endobiotic oxymonads [10]. The presence of mitochondrial homologs has been convincingly demonstrated in *Paratrimastix* (formerly *Trimastix*) *pyriformis*, although the biochemical functions of these organelles are largely unknown [11]. Endobiotic oxymonads belong to the least-studied former Archezoa. Here, we describe the first complete genome sequence analysis of an oxymonad, *Monocercomonoides* sp. PA203. We find that although this organism is a standard eukaryotic cell in other respects, it completely lacks any traces of a mitochondrion.

RESULTS AND DISCUSSION

Genome Characteristics

Using the 454 whole-genome shotgun sequencing methodology, we generated a draft genome sequence of the oxymonad *Monocercomonoides* sp. PA203, assembled into 2,095 scaffolds at ~35× coverage (see Experimental Procedures). The estimated size of the genome (~75 Mb) and the number of predicted protein-coding genes (16,629) is intermediate between what is found in diplomonads and *T. vaginalis* (Table 1). Almost 67% of predicted protein-coding genes contain introns (~1.9 introns per gene on average; Table 1). The assembly contains genes encoding tRNAs for all 20 amino acids, and ~50 ribosomal

Table 1. Overview of Metamonada Genomes

Taxa	Size (Mbp)	Guanine-Cytosine Content (%)	Protein-Coding Loci	Repetitive Regions	No. of Introns
Monocercomonoides sp. PA 203	~75	36.8	16,629	~38%	32,328
Trichomonas vaginalis isolate G3 [9]	~160	32.7	~60,000	~65%	65
Giardia intestinalis WB-C6 [7]	~11.7	49	6,480	9%	4
Spironucleus salmonicida ATCC 50377 [8]	12.9	33.4	8,076	5.2%	3

See also Tables S1 and S3.

DNA units were identified on small contigs outside the main assembly (see Supplemental Experimental Procedures). To estimate completeness of the genome sequence, we performed transcriptome mapping, in which 96.9% of transcripts mapped to the genome (see Supplemental Experimental Procedures), and checked the representation of core eukaryotic genes. Using the Core Eukaryotic Genes Mapping Approach (CEGMA) [12], we recovered 63.3% of core eukaryotic genes, a greater fraction than in the *G. intestinalis* genome (46.6%). However, when we excluded genes encoding mitochondrial proteins from the CEGMA dataset and used manually curated *Monocercomonoides* sp. gene models, the percentage of recovered genes increased to 90% (Table S1). For another set of 163 conserved eukaryotic genes used for phylogenomic analyses, the percentage of recovered genes exceeded 95% (Table S2). As the last measure of completeness, we identified 77 out of 78 conserved families of cytosolic eukaryotic ribosomal proteins [13] (Table S3), with the single exception of L41e, which is very short, difficult to detect, and has not been identified in other Metamonada genomes. Phylogenomic analysis (Figure 1) confirmed the relationship of *Monocercomonoides* sp. to *P. pyriformis* and other Metamonada and demonstrated that the *Monocercomonoides* lineage forms a much shorter branch relative to parabasalids and diplomonads. All these measures suggest that the assembled *Monocercomonoides* sp. genome sequence is nearly complete and its encoded proteins are, on average, less divergent than those of *G. intestinalis* and *T. vaginalis*.

With the first oxymonad genome sequence in hand, we focused our attention on one of the most puzzling aspects of their biology—the elusive nature of their mitochondrion.

Absence of Mitochondrial Proteins

No genes that are typically encoded on mitochondrial genomes (mtDNA) of other eukaryotes were found among the assembled scaffolds, suggesting that, like other metamonads, *Monocercomonoides* sp. lacks mtDNA. Next, we searched for homologs of nuclear genome-encoded proteins typically associated with mitochondria or MROs in other eukaryotes. The homologous core of the protein import machinery is regarded as strong evidence for the common origin of all mitochondria [14, 15]. As such, the presence of components of the translocases of the outer membrane (TOM) and inner membrane (TIM), sorting and assembly machinery (SAM) complex, and mitochondrial molecular chaperones (Hsp70 and Cpn60) in hydrogenosomes, mitosomes, and other MROs demonstrates that these organelles are related to mitochondria [16, 17]. While we were able to identify homologs of cytosolic chaperonins in the *Monocercomonoides* sp. genomic sequence, we were unable to identify homologs of any component of the mitochondrial import machinery (Figure 2A; Experimental Procedures; Tables S3 and S4).

All MROs, with the exception of the *G. intestinalis* mitosome [18], are known to export or import ATP and other metabolites typically using transporters from the mitochondrial carrier family (MCF) or, in mitosomes of the microsporidian *Encephalitozoon cuniculi* [19], by the bacterial-type (NTT-like) nucleotide transporters. We did not identify in the *Monocercomonoides* sp. genome any homologs of genes encoding known mitochondrial metabolite transport proteins (Figure 2A; Table S4).

Fe-S clusters are essential biological cofactors associated with many different proteins and are therefore synthesized de novo in every organism across the tree of life [20]. In eukaryotes, this is done mostly by the mitochondrial ISC assembly system and the cytosolic iron-sulfur assembly (CIA) system [21]. Analyses of the *Monocercomonoides* sp. genome revealed the presence of a CIA system but a complete lack of components of the ISC system (Figure 2A; Table S3; Experimental Procedures).

We could not identify either of two possible enzymes involved in the synthesis of cardiolipin, a phospholipid specific for energy-transducing membranes [22]. The majority of eukaryotes synthesize cardiolipins, and the process is localized to mitochondria, but a complete lack of cardiolipin has been experimentally shown for *G. intestinalis*, *T. vaginalis*, and *E. cuniculi* [22]. Furthermore, we could not identify any component of the endoplasmic reticulum (ER)-mitochondria encounter structure (ERMES; Figure 2A) [23].

We identified only two orthologs of the set of proteins predicted to localize to the mitochondrion-related compartment of the closely related *P. pyriformis* [11]: aspartate/ornithine carbamoyltransferase family protein and pyridine nucleotide transhydrogenase. Neither protein has an exclusively mitochondrial localization in eukaryotes [24, 25], and the *Monocercomonoides* sp. orthologs do not contain predicted mitochondrial targeting sequences.

To complement the targeted homology-based searches, we also performed an extensive search for putative homologs of known mitochondrial proteins using a pipeline based on the Mitominer database [26], which was enriched with identified mitochondrial proteins of diverse anaerobic eukaryotes with MROs (Experimental Procedures). The search recovered 76 *Monocercomonoides* sp. proteins as candidates for functions in a putative mitochondrion (Figure 2B; Table S5). Similarly to *G. intestinalis*, *T. vaginalis*, and *E. histolytica*, used as controls, the selected candidates were mainly proteins that are obviously not mitochondrial (e.g., histones) or for which the annotation is too general (e.g. "kinase domain-containing protein"), indicating that the specificity of the pipeline in organisms with

Figure 1. Unrooted Phylogeny of Eukaryotes Inferred from a 163-Protein Supermatrix

The tree displayed was inferred using PhyloBayes (CAT + Poisson substitution model). A maximum-likelihood (ML) tree inferred from the same supermatrix using RAxML (not shown) was very similar to the PhyloBayes tree, with the topological differences in the poorly resolved area comprising Chloroplastida, Cryptophyta, Glaucophyta, and Haptophyta, and in the position of Metamonada, in the ML tree placed sister (with strong bootstrap support) to Discoba. The branch support values shown are posterior probabilities (>0.95) from the PhyloBayes analysis and bootstrap values (>50%) from the ML analysis. Three branches are shown shortened to the indicated percentage of their actual length to fit them on the page. See also Table S2.

divergent mitochondrion is low. However, unlike all other control organisms, in which the search always recovered at least a few mitochondrial hallmark proteins, the set of 76 *Monocercomonoides* sp. candidates did not contain any such proteins. Only 11 of the *Monocercomonoides* candidates fall in the GO category "metabolism," but they do not assemble any obvious metabolic pathway. In summary, this approach (Table S5) failed to reveal any credible set of mitochondrial protein in *Monocercomonoides* sp.

As an alternative to homology searches, we have also attempted to identify mitochondrial proteins by searching for several types of signature sequences. The matrix proteins of mitochondria and MROs are expected to contain conserved N-terminal targeting signals needed for the targeted import into MROs [14]. We performed in silico prediction of mitochondrial targeting signals in the predicted *Monocercomonoides* sp. proteome and identified 107 candidate proteins (Figure 2A; Experimental Procedures; Table S6A). The presence of a predicted targeting signal by itself does not prove the targeting, as such amino acid sequences can also appear at random [27]. Functional annotation revealed that a majority of proteins recovered by this search fall into the Kyoto Encyclopedia of Genes and Genomes (KEGG) category "genetic information processing." Given the absence of a mitochondrial genome, or organellar translation machinery, it is unlikely that these proteins function in an MRO. Only eight candidates were assigned to the KEGG category "metabolism," and they are part of several different metabolic pathways. Finally, only three proteins were predicted to have a mitochondrial

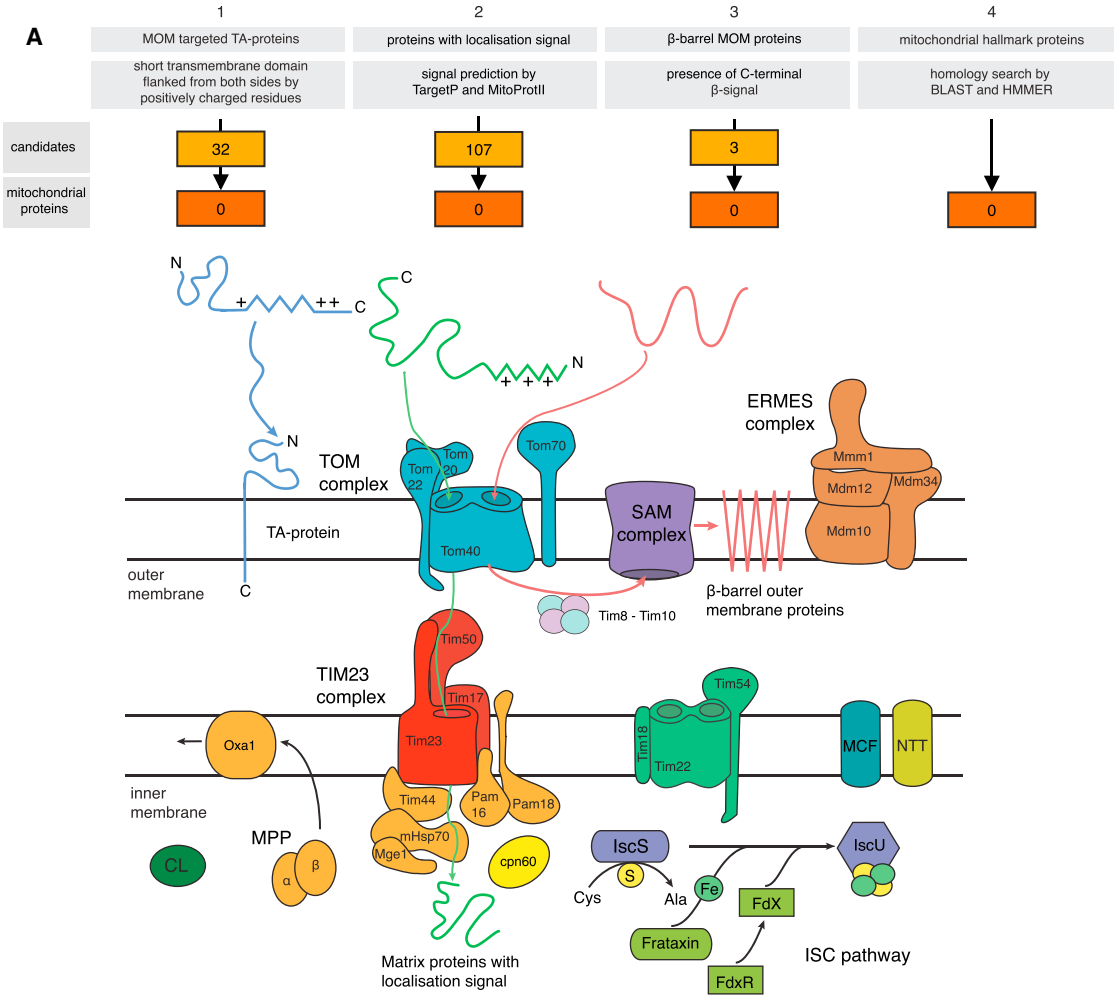

Figure 2. Search Strategies for Proteins Functionally Related to the Mitochondrion in *Monocercomonoides*

(A) Search strategies for mitochondrial proteins and for protein-localization signatures in a canonical eukaryotic cell (details are given in Supplemental Experimental Procedures): (1) mitochondrial outer membrane (MOM)-targeted tail-anchored (TA) proteins (Table S6B), (2) proteins with a mitochondrial targeting signal (Table S6A), (3) β-barrel MOM proteins, (4) 41 mitochondrial hallmarks proteins (Table S4), components of TOM and TIM translocases, cpn60, ERMES complex, ISC pathway components, cardiolipin synthase (CL).

(B) Semiautomatic pipeline for retrieving homologs of mitochondrial proteins from proteomes. We used a custom database for homology searching of mitochondrial proteins in the predicted proteomes of *Monocercomonoides* sp., *Giardia intestinalis*, *Entamoeba histolytica*, *Trichomonas vaginalis*, *Blastocystis* sp. subtype 7, and *Saccharomyces cerevisiae* (Table S5).

See also Tables S4, S5, and S6.

targeting signal and homology to a Mitominer protein (hydrolase-like family protein MONOS_10795, cytosolic TCP-1/cpn60 chaperonin family protein MONOS_13132, and ribonuclease Z MONOS_6181). This also suggests that both pipelines failed to recover specific sets of mitochondrial proteins but instead detected only low-specificity "noise."

The outer mitochondrial membranes accommodate two special classes of proteins, β-barrel and tail-anchored (TA) proteins, which are devoid of the N-terminal targeting signals and instead use specific C-terminal signals [28, 29]. We have identified 32 candidates for TA proteins in the predicted proteome, several of which appeared to be ER-targeted proteins. None of these had the hallmark characteristics of proteins targeted to the mitochondrial outer membrane (Figure 2A; Experimental Procedures; Table S6B). We also failed to identify any credible candidates for β-barrel outer membrane proteins (BOMPs) (Figure 2A; Experimental Procedures).

In summary, our comprehensive examination of the *Monocercomonoides* sp. genome based on homology searches and searches for specific N-terminal and C-terminal signals failed to recover proteins typically associated with MROs, including mitochondrial translocases, metabolite transporters and the ISC system for Fe-S cluster synthesis, ERMES, and enzymes responsible for cardiolipin synthesis.

In order to verify that our inability to find any reliable mitochondrial proteins is not caused by possible unprecedented divergence of *Monocercomonoides* sp. proteins or a failure of our methods, we searched for hallmark proteins of another cellular system, so far not observed in *Monocercomonoides* sp.—the Golgi complex. In this case, using homology-based searches, we detected numerous Golgi-associated proteins, including components of the COPI, AP-1, AP-3, AP-4, COG, GARP, TRAPPI, and Retromer complexes and Rab GTPases regulating transport to and from the Golgi (Table S3). This suggests the presence of Golgi-like compartments in oxymonads [30], despite the absence of a cytologically discernible Golgi apparatus.

The specific absence of mitochondria-associated proteins in *Monocercomonoides* sp. implies the legitimate absence of a mitochondrial compartment. If so, then how does the *Monocercomonoides* cell function without this organelle?

Energy Metabolism without a Mitochondrion

In order to compare the metabolism of *Monocercomonoides* sp. with anaerobic protists retaining mitochondrial compartments, we performed manual annotation of proteins of core pathways of energy metabolism normally associated with the presence and function of a MRO. As with many other organisms with secondarily reduced mitochondria, the *Monocercomonoides* sp. genome does not encode any enzymes for aerobic energy generation (e.g., TCA cycle or electron transport chain proteins). We did identify a complete set of glycolytic enzymes, including the alternative enzymes for anaerobic glycolysis [31], as well as the anaerobic fermentation enzymes pyruvate:ferredoxin oxidoreductase (PFOR) and [FeFe]-hydrogenases (Table S3). [FeFe]-hydrogenase maturases were absent, which is not unprecedented as they are also missing from *G. intestinalis* and *E. histolytica*, anaerobic parasites that are both capable of cytosolic H_2 production [32, 33]. Neither PFOR nor [FeFe]-hydrogenase has a predicted mitochondrial targeting sequence, and heterologous expression in *T. vaginalis* suggests a cytosolic localization of PFOR (Figure S1). In summary, *Monocercomonoides* sp. glucose metabolism appears to produce ATP via substrate-level phosphorylation steps in an extended glycolysis pathway, and the reduced co-factors are re-oxidized by fermentation, ultimately producing acetate and ethanol, or by [FeFe]-hydrogenase producing hydrogen gas. The situation in *Monocercomonoides* sp. is virtually identical to *G. intestinalis* and *E. histolytica*, which independently reduced their mitochondria to mitosomes and all the ATP production occurs in the cytosol [34–36].

In addition to extended glycolysis, *Monocercomonoides* sp. contains a complete set of three genes for enzymes involved in arginine deiminase pathway—arginine deiminase, ornithine carbamoyltransferase, and carbamate kinase. This pathway may also be used for ATP production by arginine degradation as in *T. vaginalis* and *G. intestinalis* [37, 38]. In *G. intestinalis*, this pathway produces eight times more ATP than sugar metabolism.

Fe-S Cluster Assembly without a Mitochondrion

Every eukaryotic cell contains a CIA machinery, which assists the final stages of the assembly of Fe-S clusters in proteins functioning in the eukaryotic cytosol and nucleus. Eight proteins were shown to be involved in the CIA pathway in yeast and humans: Cfd1, NUBP1 (Nbp35), NARFL (Nar1), CIAO1 (Cia1), Dre2, Tah18, Cia2, and MMS19. Four of them (i.e., Nbp35, Nar1, Cia1, and Cia2) [21] are conserved among eukaryotes and also present in the *Monocercomonoides* sp. genome (Table S3). We did not identify Cfd1 and MMS19, which are missing from many other eukaryotes, and Dre2 and Tah18, which are missing from the anaerobic protists containing MROs (including *E. histolytica*, *Mastigamoeba balamuthi*, *T. vaginalis*, *G. intestinalis*, and *Blastocystis* sp.) [21].

Despite the presence of the CIA pathway, it is commonly suggested that mitochondria and related organelles are essential to eukaryotic cells because the mitochondrial ISC system plays a critical role in the initial phase of the formation of cytosolic Fe-S clusters [20]. Although the ISC system is a near-universally conserved pathway in eukaryotes and seems to be the unifying feature of mitochondria and related organelles, genes encoding proteins of the mitochondrial ISC pathway have not been detected in the *Monocercomonoides* sp. genome. The functional replacement of the ISC system has been reported for only two lineages, *Pygsuia biforma* (Breviatea) and Archamoebae. A methanoarcheal sulfur mobilization (SUF) system [39] or a bacterial nitrogen fixation (NIF) [40] has apparently replaced the ISC system in the *P. biforma* and the Archamoebae lineages, respectively. Conflicting data exist on the localization of the NIF system in *E. histolytica* [41, 42]; however, in *M. balamuthi*, the NIF system localizes in the cytosol and the MRO [43].

The major issue remains: how does *Monocercomonoides* sp. form Fe-S clusters? Unexpectedly, we identified genes encoding four subunits of the SUF system: SufB, SufC, and fused SufS and SufU (Table S3). SufS is a "two-component" cysteine desulfurase, and its activity might be enhanced by SufE or SufU [44, 45]. In *Monocercomonoides* sp., SufS is fused with SufU, which is a unique feature. SufB and SufC can form a scaffold complex in prokaryotes, and SufB2C2 complex is capable of binding and transferring 4Fe-4S clusters to a recipient apoprotein [46]. All identified SUF system proteins apparently retain all important catalytic sites (Figure S2) and may perform de novo Fe-S clusters biogenesis by themselves or in concert with the CIA machinery. The SUF system for Fe-S cluster synthesis is found in plastids, bacteria, and archaea and has also been found in two microbial eukaryotes *P. biforma* [39] and *Blastocystis* sp. [47]. The

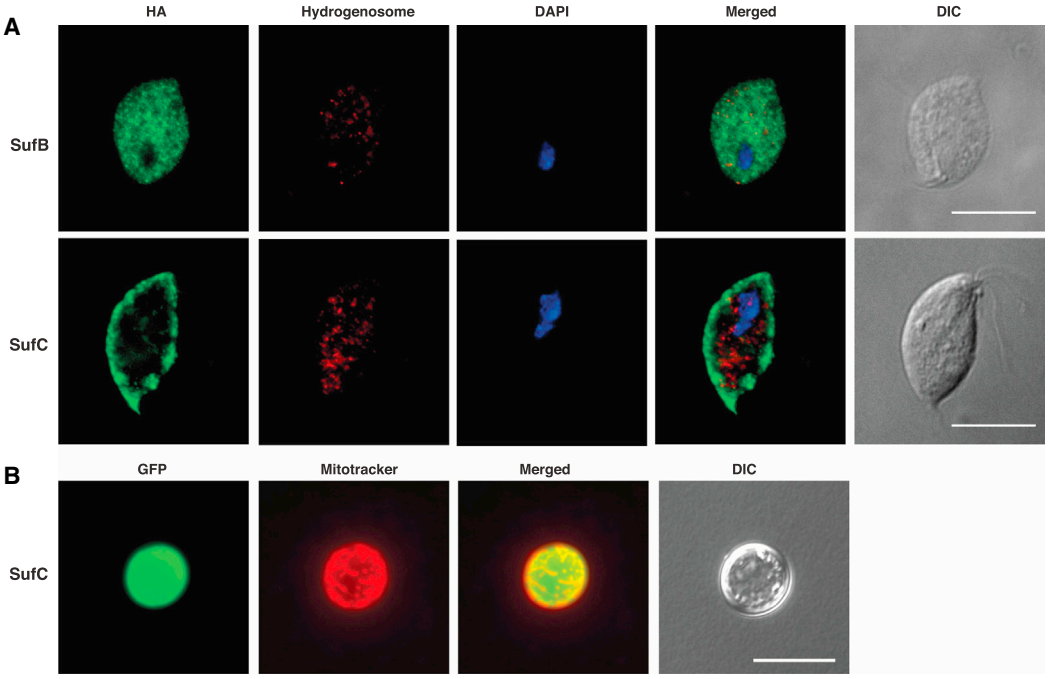

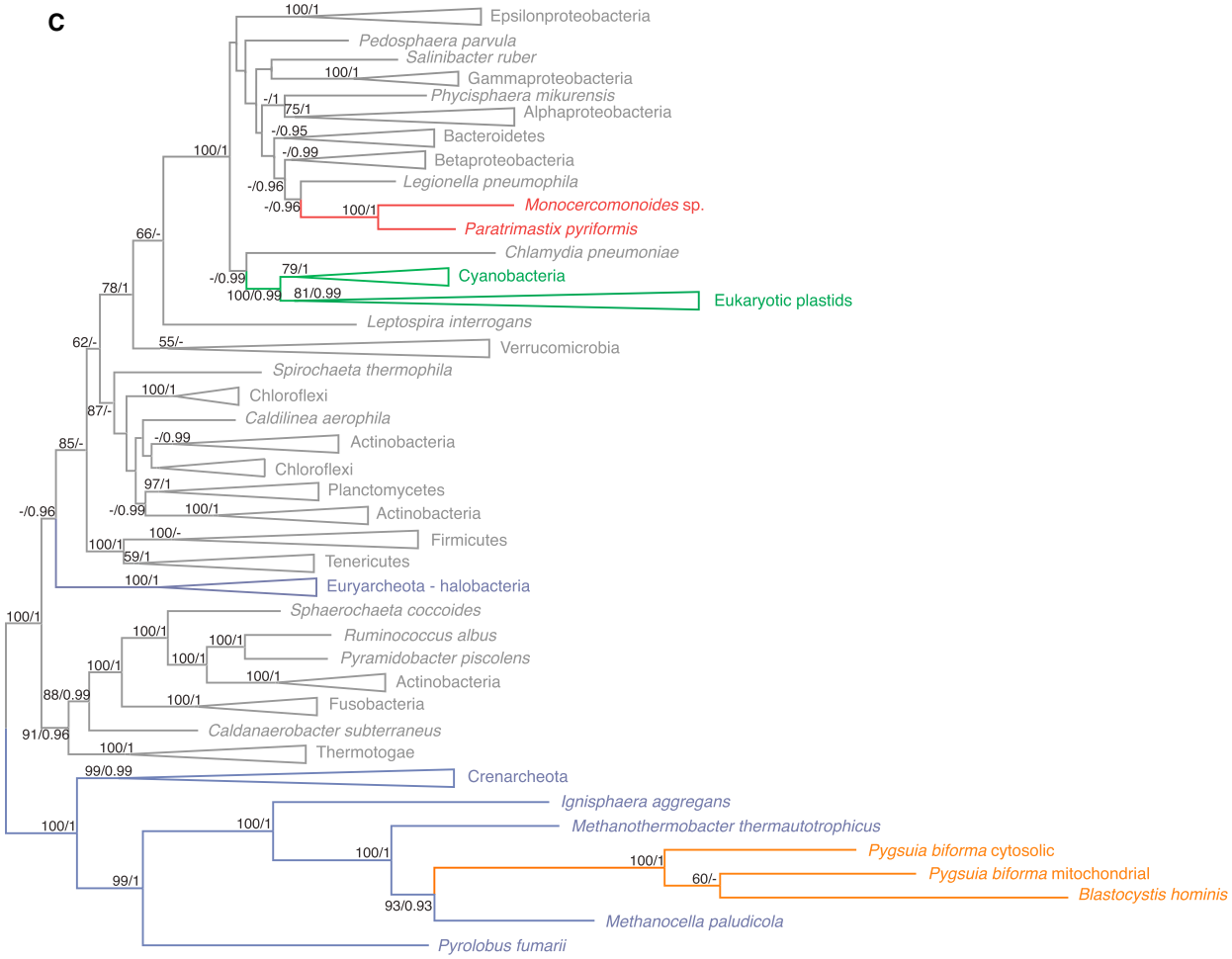

(legend on next page)

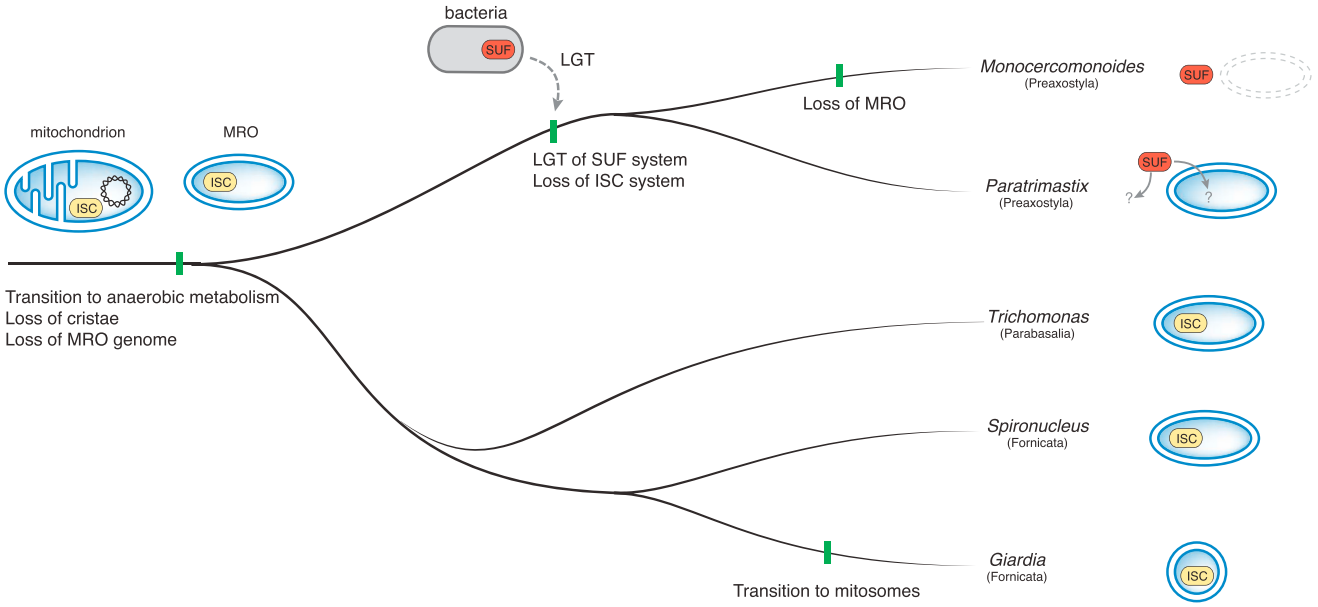

Figure 4. Reductive Evolution of Mitochondria in Metamonads

Transition to an anaerobic lifestyle occurred in a common ancestor of metamonads and was followed by reduction of mitochondria to MROs, accompanied by the loss of cristae and genome, and the transition to anaerobic metabolism. The ISC pathway for Fe-S cluster synthesis was present in a metamonad common ancestor. Further reduction to a mitosome took place in the *Giardia intestinalis* lineage. We propose that in the common ancestor of *Paratrimastix pyriformis* and *Monocercomonoides*, a SUF system acquired through LGT from bacteria substituted the MRO-localized ISC system. Subsequently, the MRO was lost completely in the lineage leading to *Monocercomonoides* sp. Localization of the SUF pathway in *P. pyriformis* is unknown.

presence of spliceosomal introns in the putative SufC and SufSU of *Monocercomonoides* confirms that these proteins are not prokaryotic contamination. Furthermore, fluorescence in situ hybridization (FISH) with *sufB* and *sufC* gene probes demonstrated their presence in the *Monocercomonoides* sp. nucleus (Figure S3). Importantly, homologs of these proteins were detected in the *P. pyriformis* genome, the closest sequenced relative to *Monocercomonoides*. The SUF system components of both *Monocercomonoides* sp. and *P. pyriformis* do not contain recognizable mitochondrial targeting signals, and our experiments with heterologous expression of *Monocercomonoides* sp. SufB and SufC proteins in *T. vaginalis* (Figure 3A) and SufC protein in yeast (Figure 3B) support a cytosolic localization. Phylogenetic analyses indicate that this SUF system was acquired by an ancestor of *Monocercomonoides* and *Paratrimastix* by lateral gene transfer (LGT) from bacteria independently of all other SUF-containing eukaryotes (Figure 3C). We propose that the acquisition of a cytosolic SUF system made the ancestral ISC system in the mitochondrion dispensable, which led to its loss and, in the *Monocercomonoides* lineage, to the complete loss of MROs (Figure 4).

Conclusions

Mitochondria and related organelles are currently considered to be indispensable components of eukaryotic cells. The genome sequence of *Monocercomonoides* sp. reported here suggests that this is not the case. Despite extensive searches, no mitochondrial marker proteins such as membrane protein translocases and metabolite transporters were identified. Crucially, the mitochondrion-specific ISC pathway for Fe-S cluster biogenesis is absent and apparently was replaced by a bacterial SUF system that functions in the cytosol. On the other hand, genes encoding other features once thought to be absent from these divergent eukaryotic cells, i.e., the Golgi body, were readily identifiable. The genome also contains genes for essential cytosolic pathways of energy metabolism, although we did observe examples of metabolic streamlining characteristic of other anaerobic or microaerophilic eukaryotes.

Figure 3. Heterologous Expression of *Monocercomonoides* sp. SUF System Proteins and Phylogeny of Concatenated SufB, SufC, and SufS Homologs

(A) Heterologous expression of *Monocercomonoides* sp. SufB and SufC proteins in *Trichomonas vaginalis*. *Monocercomonoides* sp. proteins with a C-terminal HA tag were expressed in *T. vaginalis* and visualized by an anti-HA antibody (green). The signal of the anti-HA antibody does not co-localize with hydrogenosomes stained using an anti-malic enzyme antibody (red). The nucleus was stained using DAPI (blue). Scale bar, 10 μm.

(B) Heterologous expression of *Monocercomonoides* sp. SufC protein in *Saccharomyces cerevisiae*. *Monocercomonoides* sp. proteins tagged with GFP were expressed in *S. cerevisiae* (green). The GFP signal does not co-localize with the yeast mitochondria stained by Mitotracker (red). Scale bar, 10 μm.

(C) Unrooted ML tree of concatenated SufB, SufC, and SufS sequences. Bootstrap support values above 50 and posterior probabilities greater than 0.75 are shown. *Monocercomonoides* sp. and *Paratrimastix pyriformis* are shown in red, eukaryotic plastids and cyanobacteria in green, *Blastocystis* sp. and *Pygsuia biforma* in orange, bacteria in gray, and archaea in blue.

See also Figures S1–S3.

Reduction of mitochondria is known from various eukaryotic lineages adapted to anaerobic lifestyle [48]. Mitosomes in *Giardia*, *Entamoeba*, and Microsporidia represent the most extreme cases of mitochondrial reduction known to date, and yet they still contain recognizable mitochondrial protein translocases and usually an ISC system. The specific absence of all these mitochondrial proteins in the genome of *Monocercomonoides* sp. indicates that this eukaryote has dispensed with the mitochondrial compartment completely. In principle, we cannot exclude the possibility that a mitochondrion exists in *Monocercomonoides* sp. whose protein composition has been altered entirely. However, such a hypothetical organelle could not be recognized as a mitochondrion homolog by any available means. Without any positive evidence for the latter scenario, we suggest that the complete absence of mitochondrial markers and pathways points to the bona fide absence of the organelle. Because all known oxymonads are obligate animal symbionts, and mitochondrial homologs are present in the close free-living sister lineage *Paratrimastix*, the absence of mitochondrion in *Monocercomonoides* sp. must be secondary. We hypothesize that the acquisition of the SUF system predated the loss of the mitochondrial ISC system in the common ancestor of Preaxostyla and allowed for the complete loss of the organelle in *Monocercomonoides* sp. lineage, the first known truly secondarily amitochondriate eukaryote.

EXPERIMENTAL PROCEDURES

Genome and Transcriptome Sequencing

All experiments were performed on the *Monocercomonoides* sp. PA203 strain. The culture (2 L with a cell density of approximately 4 × 10^5 cells/mL) was filtered to remove most of the bacteria before isolation of DNA (culturing and filtration details in Supplemental Experimental Procedures). DNA was isolated using DNeasy Blood and Tissue Kit (QIAGEN). Total genomic DNA was sequenced using a Genome Sequencer 454 GS FLX+ with XL+ reagents. A total of seven sequencing runs were performed, including four shotgun runs on libraries with the average fragment length of 500 to 800 and three runs on a 3-kb paired-end library. Two RNA sequencing (RNA-seq) experiments were performed using 454 and Illumina sequencing platforms. Details of sequencing are given in Supplemental Experimental Procedures.

Roche's assembler Newbler v.2.6 was used to generate a genome sequence assembly from 454 single and pair end reads. The final assembly consisted of 2,095 scaffolds spanning almost 75 Mb of the genome. The N50 scaffold size is 71.4 kb. Transcriptome assembly of the 454 data was performed by Newbler v.2.8 with default parameters, and Illumina-generated transcriptomic data were assembled using Trinity [49] (details in Supplemental Experimental Procedures). The CEGMA [12] was used to estimate the number of conserved eukaryotic genes in the *Monocercomonoides* sp. genome assembly (Table S1) and presence of cytosolic ribosomal eukaryotic proteins as an additional measure of completeness (Table S3).

Genome Annotation and Gene Searching

For the structural annotation, Augustus v.2.7 [50, 51], PASA2 [52], and EVM [53] were used. Gene models of particular interest were manually evaluated with the help of RNA-seq data or considering conservation with homologs (details in Supplemental Experimental Procedures).

Functional annotation was assigned to genes by similarity searches of predicted proteins using BLASTP [54] against the NCBI non-redundant protein database [55] and HMMER3 [56] searches of domain hits in the Pfam protein families database [57]. Additional annotation was performed using the KEGG automatic annotation server [58]. Annotation files are available at the web page http://www.protistologie.cz/hampllab/data.html.

tRNA genes were predicted with tRNAscan-SE [59]; rDNA sequences were not present in the original main assembly, but they were identified in contigs not assembled into scaffolds and added to the main assembly.

The *Monocercomonoides* sp. genome database was searched using the TBLASTN [54] algorithm, and *Monocercomonoides* proteome database and six-frame translation of the genomic sequence were searched using the BLASTP [54] algorithm or the profile hidden Markov model (HMM) searching method *phmmer* from the HMMER3 [56] package. We used a wide range of queries described in Supplemental Experimental Procedures.

Phylogenetic Analyses

We performed a number of maximum-likelihood and Bayesian phylogenetic analyses: (1) phylogenomic analyses of eukaryotes based on 163 genes and 70 taxa; (2) phylogenetic analyses of genes for SUF pathway enzymes; and (3) individual gene trees to support functional annotation of genes (details in Supplemental Experimental Procedures).

Subcellular Localization Prediction

Subcellular localization prediction for the *Monocercomonoides* sp. proteome was performed using TargetP v.1.1 [60] and MitoProt II v.1.101 [61]. TA proteins were identified and analyzed based on presence of a transmembrane domain (TMD) of moderate hydrophobicity flanked by positively charged residues [29, 62] (details in Supplemental Experimental Procedures). BOMPs were identified based on the presence of a conserved C-terminal β-signal, using a previously described pipeline [63].

Mitochondrial Protein Searching Using a Mitominer-Based Database

We prepared a custom database of mitochondrial proteins to search for genes encoding proteins with putative mitochondrial localization. The custom database was based on the MitoMiner database [26] reference set containing 12,925 proteins from 11 eukaryotic mitochondrial proteomes, which was enriched by known or predicted MRO-localized proteins of *E. histolytica*, *G. intestinalis*, *P. biforma*, *S. salmonicida*, *T. vaginalis*, and *P. pyriformis*. Homologs of proteins from this database were searched in the predicted proteome of *Monocercomonoides* sp. and in the predicted proteomes of *Blastocystis* sp., *E. histolytica*, *G. intestinalis*, *S. cerevisiae*, and *T. vaginalis*, which were used as control datasets. While searching the control datasets, the proteins of the searched organism were removed from the custom database. In the last step, only those candidates were kept whose first hit in the NCBI database [55] contained a predictable mitochondrial targeting signal (score > 0.5 in TargetP v.1.1 [60] and MitoProt II v.1.101 [61]). Further details are given in Supplemental Experimental Procedures.

FISH

We performed FISH experiments with labeled probes to determine whether the genes for SUF system proteins physically reside in the *Monocercomonoides* sp. genome or represent bacterial contamination. Details on preparation of labeled probes are given in Supplemental Experimental Procedures.

One liter of *Monocercomonoides* sp. culture was filtered to remove bacteria, and the cells were pelleted by centrifugation for 10 min at 2,000 × *g* at 4°C. FISH with digoxigenin-labeled probes was performed according to a previously described procedure [64] omitting the colchicine procedure. Cell nuclei and the probes were denatured under a coverslip in a single step in 50 μL of 50% formamide in 2 × SSC at 70°C for 5 min. Preparations were observed using an IX81 microscope (Olympus) equipped with an IX2-UCB camera. Images were processed using Cell software (Olympus) and ImageJ 1.42q.

Heterologous Protein Expression and Microscopy in *Trichomonas vaginalis*

The *T. vaginalis* transfection system was used to assess subcellular localization of SufB, SufC, and PFOR proteins. *Monocercomonoides* sp. cDNA preparation was performed as described for transcriptome sequencing (Supplemental Experimental Procedure). Constructs with the hemagglutinin (HA) tag fused to the 3′ end of the coding sequences of the studied genes were prepared and expressed in *T. vaginalis*, an anaerobic protist related to *Monocercomonoides* sp. and bearing a hydrogenosome (details are given in Supplemental Experimental Procedures). *Monocercomonoides* sp. proteins

expressed in *T. vaginalis* cells were visualized using standard techniques [14] (details are given in Supplemental Experimental Procedures).

Saccharomyces cerevisiae Heterologous Expression System

This expression system was used to confirm the results from the *T. vaginalis* expression system for SufC protein. The procedure was analogous to the one described in [11]. Details are given in Supplemental Experimental Procedures.

ACCESSION NUMBERS

Sequence data for the genome reads (experiment number SRX1470187), the 454 transcriptome reads sequenced using the 454 platform (experiment number SRX1453820), and the Illumina transcriptome reads sequenced using the Illumina platform (experiment number SRX1453675) have been deposited to the NCBI Sequence Read Archive under accession number SRA: SRP066769. The accession number for the *Monocercomonoides* sp. PA203 genome reported in this paper is GenBank: LSRY00000000. The accession number for the 454 transcriptome project reported in this paper is GenBank: GEEG00000000. The accession number for the Illumina transcriptome project reported in this paper is GenBank: GEEL00000000. The versions described in this paper are versions LSRY01000000, GEEG01000000, and GEEL01000000. Further additional information on the genome analysis can be found at http://www.protistologie.cz/hampllab/data.html.

SUPPLEMENTAL INFORMATION

Supplemental Information includes Supplemental Experimental Procedures, three figures, and six tables and can be found with this article online at http://dx.doi.org/10.1016/j.cub.2016.03.053.

AUTHOR CONTRIBUTIONS

The project was conceived in the laboratory of V.H. with the contribution of J.B.D. Genome and 454 transcriptome sequencing was performed by the Laboratory of Genomics and Bioinformatics. A.K. and V.H. coordinated the project. Z.Z. isolated genomic DNA. V.V. and V.H. isolated RNA. M.H. prepared sequencing libraries. Č.V. and A.K. assembled data. A.K. curated data, analyzed genomic and transcriptomic data, and conducted gene prediction and automatic functional annotation. A.K., V.V., S.C.T., R.P., L.N., V.Ž., L.D.B., E.K.H., M.E., and V.H. performed manual annotation. A.K., V.V., P.D., C.W.S., and V.H. performed mitochondrial gene searching. Z.Z. performed FISH experiments. V.V., Z.Z., and S.C.T. performed immunolocalization experiments. A.K., V.V., R.P., L.D.B., E.K.H., P.S., and L.E. performed phylogenetic analyses. A.K., V.V., Z.Z., S.C.T., and R.P. prepared figures. A.K. and V.H. wrote the manuscript in collaboration with A.J.R., M.E., and J.B.D., and all authors edited and approved the manuscript.

ACKNOWLEDGMENTS

A.K. and V.H. were supported by the Ministry of Education, Youth and Sports of CR within the National Sustainability Program II (Project BIOCEV-FAR) LQ1604 and by the project "BIOCEV" (CZ.1.05/1.1.00/02.0109). V.H. and sequencing were supported by Czech Science foundation project P506-12-1010. Z.Z. and localization experiments were funded by Czech Science foundation project 510 13-22333P. E.K.H. was supported by a Vanier Canada Graduate Scholarship and an Alberta Innovates – Health Solutions Graduate Studentship. The work of L.E., C.W.S., and A.J.R. was supported by a regional partnerships program grant (62809) from the Canadian Institute of Health Research and the Nova Scotia Health Research Foundation. The work of L.D.B., E.K.H., and J.B.D. was supported by an NSERC Discovery grant and an Alberta Innovates Technology Futures New Faculty Award to J.B.D. R.P. and M.E. were supported by Czech Science foundation project 15-16406S.

Received: December 23, 2015
Revised: March 5, 2016
Accepted: March 23, 2016
Published: May 12, 2016

REFERENCES

1. Huynen, M.A., Duarte, I., and Szklarczyk, R. (2013). Loss, replacement and gain of proteins at the origin of the mitochondria. Biochim. Biophys. Acta *1827*, 224–231.
2. Tovar, J., León-Avila, G., Sánchez, L.B., Sutak, R., Tachezy, J., van der Giezen, M., Hernández, M., Müller, M., and Lucocq, J.M. (2003). Mitochondrial remnant organelles of Giardia function in iron-sulphur protein maturation. Nature *426*, 172–176.
3. Lindmark, D.G., and Müller, M. (1973). Hydrogenosome, a cytoplasmic organelle of the anaerobic flagellate Tritrichomonas foetus, and its role in pyruvate metabolism. J. Biol. Chem. *248*, 7724–7728.
4. Cavalier-Smith, T. (1987). Eukaryotes with no mitochondria. Nature *326*, 332–333.
5. Gray, M.W. (2012). Mitochondrial evolution. Cold Spring Harb. Perspect. Biol. *4*, a011403.
6. Adl, S.M., Simpson, A.G.B., Lane, C.E., Lukeš, J., Bass, D., Bowser, S.S., Brown, M.W., Burki, F., Dunthorn, M., Hampl, V., et al. (2012). The revised classification of eukaryotes. J. Eukaryot. Microbiol. *59*, 429–493.
7. Morrison, H.G., McArthur, A.G., Gillin, F.D., Aley, S.B., Adam, R.D., Olsen, G.J., Best, A.A., Cande, W.Z., Chen, F., Cipriano, M.J., et al. (2007). Genomic minimalism in the early diverging intestinal parasite Giardia lamblia. Science *317*, 1921–1926.
8. Xu, F., Jerlström-Hultqvist, J., Einarsson, E., Astvaldsson, A., Svärd, S.G., and Andersson, J.O. (2014). The genome of Spironucleus salmonicida highlights a fish pathogen adapted to fluctuating environments. PLoS Genet. *10*, e1004053.
9. Carlton, J.M., Hirt, R.P., Silva, J.C., Delcher, A.L., Schatz, M., Zhao, Q., Wortman, J.R., Bidwell, S.L., Alsmark, U.C.M., Besteiro, S., et al. (2007). Draft genome sequence of the sexually transmitted pathogen Trichomonas vaginalis. Science *315*, 207–212.
10. Zhang, Q., Táborský, P., Silberman, J.D., Pánek, T., Čepička, I., and Simpson, A.G.B. (2015). Marine isolates of Trimastix marina form a plesiomorphic deep-branching lineage within Preaxostyla, separate from other known Trimastigids (Paratrimastix n. gen.). Protist *166*, 468–491.
11. Zubáčová, Z., Novák, L., Bublíková, J., Vacek, V., Fousek, J., Rídl, J., Tachezy, J., Doležal, P., Vlček, C., and Hampl, V. (2013). The mitochondrion-like organelle of Trimastix pyriformis contains the complete glycine cleavage system. PLoS ONE *8*, e55417.
12. Parra, G., Bradnam, K., and Korf, I. (2007). CEGMA: a pipeline to accurately annotate core genes in eukaryotic genomes. Bioinformatics *23*, 1061–1067.
13. Lecompte, O., Ripp, R., Thierry, J.C., Moras, D., and Poch, O. (2002). Comparative analysis of ribosomal proteins in complete genomes: an example of reductive evolution at the domain scale. Nucleic Acids Res. *30*, 5382–5390.
14. Dolezal, P., Likic, V., Tachezy, J., and Lithgow, T. (2006). Evolution of the molecular machines for protein import into mitochondria. Science *313*, 314–318.
15. Zarsky, V., Tachezy, J., and Dolezal, P. (2012). Tom40 is likely common to all mitochondria. Curr. Biol. *22*, R479–R481, author reply R481–R482.
16. Dolezal, P., Smíd, O., Rada, P., Zubácová, Z., Bursać, D., Suták, R., Nebesárová, J., Lithgow, T., and Tachezy, J. (2005). Giardia mitosomes and trichomonad hydrogenosomes share a common mode of protein targeting. Proc. Natl. Acad. Sci. USA *102*, 10924–10929.
17. Burri, L., Williams, B.A.P., Bursac, D., Lithgow, T., and Keeling, P.J. (2006). Microsporidian mitosomes retain elements of the general mitochondrial targeting system. Proc. Natl. Acad. Sci. USA *103*, 15916–15920.
18. Jedelský, P.L., Doležal, P., Rada, P., Pyrih, J., Smíd, O., Hrdý, I., Sedinová, M., Marcinčiková, M., Voleman, L., Perry, A.J., et al. (2011). The minimal proteome in the reduced mitochondrion of the parasitic protist Giardia intestinalis. PLoS ONE *6*, e17285.

19. Tsaousis, A.D., Kunji, E.R.S., Goldberg, A.V., Lucocq, J.M., Hirt, R.P., and Embley, T.M. (2008). A novel route for ATP acquisition by the remnant mitochondria of Encephalitozoon cuniculi. Nature *453*, 553–556.
20. Lill, R. (2009). Function and biogenesis of iron-sulphur proteins. Nature *460*, 831–838.
21. Tsaousis, A.D., Gentekaki, E., Eme, L., Gaston, D., and Roger, A.J. (2014). Evolution of the cytosolic iron-sulfur cluster assembly machinery in Blastocystis species and other microbial eukaryotes. Eukaryot. Cell *13*, 143–153.
22. Tian, H.-F., Feng, J.-M., and Wen, J.-F. (2012). The evolution of cardiolipin biosynthesis and maturation pathways and its implications for the evolution of eukaryotes. BMC Evol. Biol. *12*, 32.
23. Wideman, J.G., Gawryluk, R.M.R., Gray, M.W., and Dacks, J.B. (2013). The ancient and widespread nature of the ER-mitochondria encounter structure. Mol. Biol. Evol. *30*, 2044–2049.
24. Yarlett, N., Lindmark, D.G., Goldberg, B., Moharrami, M.A., and Bacchi, C.J. (1994). Subcellular localization of the enzymes of the arginine dihydrolase pathway in Trichomonas vaginalis and Tritrichomonas foetus. J. Eukaryot. Microbiol. *41*, 554–559.
25. Yousuf, M.A., Mi-ichi, F., Nakada-Tsukui, K., and Nozaki, T. (2010). Localization and targeting of an unusual pyridine nucleotide transhydrogenase in Entamoeba histolytica. Eukaryot. Cell *9*, 926–933.
26. Smith, A.C., Blackshaw, J.A., and Robinson, A.J. (2012). MitoMiner: a data warehouse for mitochondrial proteomics data. Nucleic Acids Res. *40*, D1160–D1167.
27. Lucattini, R., Likic, V.A., and Lithgow, T. (2004). Bacterial proteins predisposed for targeting to mitochondria. Mol. Biol. Evol. *21*, 652–658.
28. Denic, V. (2012). A portrait of the GET pathway as a surprisingly complicated young man. Trends Biochem. Sci. *37*, 411–417.
29. Borgese, N., Brambillasca, S., and Colombo, S. (2007). How tails guide tail-anchored proteins to their destinations. Curr. Opin. Cell Biol. *19*, 368–375.
30. Mowbrey, K., and Dacks, J.B. (2009). Evolution and diversity of the Golgi body. FEBS Lett. *583*, 3738–3745.
31. Liapounova, N.A., Hampl, V., Gordon, P.M.K., Sensen, C.W., Gedamu, L., and Dacks, J.B. (2006). Reconstructing the mosaic glycolytic pathway of the anaerobic eukaryote Monocercomonoides. Eukaryot. Cell *5*, 2138–2146.
32. Lloyd, D., Ralphs, J.R., and Harris, J.C. (2002). Giardia intestinalis, a eukaryote without hydrogenosomes, produces hydrogen. Microbiology *148*, 727–733.
33. Nixon, J.E.J., Field, J., McArthur, A.G., Sogin, M.L., Yarlett, N., Loftus, B.J., and Samuelson, J. (2003). Iron-dependent hydrogenases of Entamoeba histolytica and Giardia lamblia: activity of the recombinant entamoebic enzyme and evidence for lateral gene transfer. Biol. Bull. *204*, 1–9.
34. van der Giezen, M., and Tovar, J. (2005). Degenerate mitochondria. EMBO Rep. *6*, 525–530.
35. Müller, M., Mentel, M., van Hellemond, J.J., Henze, K., Woehle, C., Gould, S.B., Yu, R.-Y., van der Giezen, M., Tielens, A.G.M., and Martin, W.F. (2012). Biochemistry and evolution of anaerobic energy metabolism in eukaryotes. Microbiol. Mol. Biol. Rev. *76*, 444–495.
36. Makiuchi, T., and Nozaki, T. (2014). Highly divergent mitochondrion-related organelles in anaerobic parasitic protozoa. Biochimie *100*, 3–17.
37. Schofield, P.J., Edwards, M.R., Matthews, J., and Wilson, J.R. (1992). The pathway of arginine catabolism in Giardia intestinalis. Mol. Biochem. Parasitol. *51*, 29–36.
38. Yarlett, N., Martinez, M.P., Moharrami, M.A., and Tachezy, J. (1996). The contribution of the arginine dihydrolase pathway to energy metabolism by Trichomonas vaginalis. Mol. Biochem. Parasitol. *78*, 117–125.
39. Stairs, C.W., Eme, L., Brown, M.W., Mutsaers, C., Susko, E., Dellaire, G., Soanes, D.M., van der Giezen, M., and Roger, A.J. (2014). A SUF Fe-S cluster biogenesis system in the mitochondrion-related organelles of the anaerobic protist Pygsuia. Curr. Biol. *24*, 1176–1186.
40. van der Giezen, M., Cox, S., and Tovar, J. (2004). The iron-sulfur cluster assembly genes iscS and iscU of Entamoeba histolytica were acquired by horizontal gene transfer. BMC Evol. Biol. *4*, 7.
41. Maralikova, B., Ali, V., Nakada-Tsukui, K., Nozaki, T., van der Giezen, M., Henze, K., and Tovar, J. (2010). Bacterial-type oxygen detoxification and iron-sulfur cluster assembly in amoebal relict mitochondria. Cell. Microbiol. *12*, 331–342.
42. Mi-ichi, F., Abu Yousuf, M., Nakada-Tsukui, K., and Nozaki, T. (2009). Mitosomes in Entamoeba histolytica contain a sulfate activation pathway. Proc. Natl. Acad. Sci. USA *106*, 21731–21736.
43. Nývltová, E., Šuták, R., Harant, K., Šedinová, M., Hrdy, I., Paces, J., Vlček, Č., and Tachezy, J. (2013). NIF-type iron-sulfur cluster assembly system is duplicated and distributed in the mitochondria and cytosol of Mastigamoeba balamuthi. Proc. Natl. Acad. Sci. USA *110*, 7371–7376.
44. Loiseau, L., Ollagnier-de-Choudens, S., Nachin, L., Fontecave, M., and Barras, F. (2003). Biogenesis of Fe-S cluster by the bacterial Suf system: SufS and SufE form a new type of cysteine desulfurase. J. Biol. Chem. *278*, 38352–38359.
45. Riboldi, G.P., de Oliveira, J.S., and Frazzon, J. (2011). Enterococcus faecalis SufU scaffold protein enhances SufS desulfurase activity by acquiring sulfur from its cysteine-153. Biochim. Biophys. Acta *1814*, 1910–1918.
46. Chahal, H.K., and Outten, F.W. (2012). Separate FeS scaffold and carrier functions for $SufB_2C_2$ and SufA during in vitro maturation of [2Fe2S] Fdx. J. Inorg. Biochem. *116*, 126–134.
47. Tsaousis, A.D., Ollagnier de Choudens, S., Gentekaki, E., Long, S., Gaston, D., Stechmann, A., Vinella, D., Py, B., Fontecave, M., Barras, F., et al. (2012). Evolution of Fe/S cluster biogenesis in the anaerobic parasite Blastocystis. Proc. Natl. Acad. Sci. USA *109*, 10426–10431.
48. Maguire, F., and Richards, T.A. (2014). Organelle evolution: a mosaic of 'mitochondrial' functions. Curr. Biol. *24*, R518–R520.
49. Grabherr, M.G., Haas, B.J., Yassour, M., Levin, J.Z., Thompson, D.A., Amit, I., Adiconis, X., Fan, L., Raychowdhury, R., Zeng, Q., et al. (2011). Full-length transcriptome assembly from RNA-Seq data without a reference genome. Nat. Biotechnol. *29*, 644–652.
50. Stanke, M., and Waack, S. (2003). Gene prediction with a hidden Markov model and a new intron submodel. Bioinformatics *19* (*Suppl 2*), ii215–ii225.
51. Stanke, M., Schöffmann, O., Morgenstern, B., and Waack, S. (2006). Gene prediction in eukaryotes with a generalized hidden Markov model that uses hints from external sources. BMC Bioinformatics *7*, 62.
52. Haas, B.J., Delcher, A.L., Mount, S.M., Wortman, J.R., Smith, R.K., Jr., Hannick, L.I., Maiti, R., Ronning, C.M., Rusch, D.B., Town, C.D., et al. (2003). Improving the Arabidopsis genome annotation using maximal transcript alignment assemblies. Nucleic Acids Res. *31*, 5654–5666.
53. Haas, B.J., Salzberg, S.L., Zhu, W., Pertea, M., Allen, J.E., Orvis, J., White, O., Buell, C.R., and Wortman, J.R. (2008). Automated eukaryotic gene structure annotation using EVidenceModeler and the Program to Assemble Spliced Alignments. Genome Biol. *9*, R7.
54. Altschul, S.F., Madden, T.L., Schäffer, A.A., Zhang, J., Zhang, Z., Miller, W., and Lipman, D.J. (1997). Gapped BLAST and PSI-BLAST: a new generation of protein database search programs. Nucleic Acids Res. *25*, 3389–3402.
55. Pruitt, K.D., Tatusova, T., and Maglott, D.R. (2005). NCBI Reference Sequence (RefSeq): a curated non-redundant sequence database of genomes, transcripts and proteins. Nucleic Acids Res. *33*, D501–D504.
56. Finn, R.D., Clements, J., and Eddy, S.R. (2011). HMMER web server: interactive sequence similarity searching. Nucleic Acids Res. *39*, W29-37.
57. Punta, M., Coggill, P.C., Eberhardt, R.Y., Mistry, J., Tate, J., Boursnell, C., Pang, N., Forslund, K., Ceric, G., Clements, J., et al. (2012). The Pfam protein families database. Nucleic Acids Res. *40*, D290–D301.
58. Moriya, Y., Itoh, M., Okuda, S., Yoshizawa, A.C., and Kanehisa, M. (2007). KAAS: an automatic genome annotation and pathway reconstruction server. Nucleic Acids Res. *35*, W182-5.

59. Lowe, T.M., and Eddy, S.R. (1997). tRNAscan-SE: a program for improved detection of transfer RNA genes in genomic sequence. Nucleic Acids Res. *25*, 955–964.

60. Emanuelsson, O., Brunak, S., von Heijne, G., and Nielsen, H. (2007). Locating proteins in the cell using TargetP, SignalP and related tools. Nat. Protoc. *2*, 953–971.

61. Claros, M.G., and Vincens, P. (1996). Computational method to predict mitochondrially imported proteins and their targeting sequences. Eur. J. Biochem. *241*, 779–786.

62. Borgese, N., Colombo, S., and Pedrazzini, E. (2003). The tale of tail-anchored proteins: coming from the cytosol and looking for a membrane. J. Cell Biol. *161*, 1013–1019.

63. Imai, K., Fujita, N., Gromiha, M.M., and Horton, P. (2011). Eukaryote-wide sequence analysis of mitochondrial β-barrel outer membrane proteins. BMC Genomics *12*, 79.

64. Zubáčová, Z., Krylov, V., and Tachezy, J. (2011). Fluorescence in situ hybridization (FISH) mapping of single copy genes on Trichomonas vaginalis chromosomes. Mol. Biochem. Parasitol. *176*, 135–137.

Fe–S Cluster Assembly in Oxymonads and Related Protists

Vojtěch Vacek,[1] Lukáš V.F. Novák,[1] Sebastian C. Treitli,[1] Petr Táborský,[2] Ivan Čepička,[2] Martin Kolísko,[3,4] Patrick J. Keeling,[4] and Vladimír Hampl*,[1]

[1]Department of Parasitology, Faculty of Science, Charles University, BIOCEV, Vestec, Czech Republic

[2]Department of Zoology, Faculty of Science, Charles University, Prague, Czech Republic

[3]Institute of Parasitology, Biology Centre, Czech Academy of Science, České Budějovice, Czech Republic

[4]Department of Botany, University of British Columbia, Vancouver, British Columbia, Canada

***Corresponding author:** E-mail: vlada@natur.cuni.cz.

Associate editor: Iñaki Ruiz-Trillo

Abstract

The oxymonad *Monocercomonoides exilis* was recently reported to be the first eukaryote that has completely lost the mitochondrial compartment. It was proposed that an important prerequisite for such a radical evolutionary step was the acquisition of the SUF Fe–S cluster assembly pathway from prokaryotes, making the mitochondrial ISC pathway dispensable. We have investigated genomic and transcriptomic data from six oxymonad species and their relatives, composing the group Preaxostyla (Metamonada, Excavata), for the presence and absence of enzymes involved in Fe–S cluster biosynthesis. None possesses enzymes of mitochondrial ISC pathway and all apparently possess the SUF pathway, composed of SufB, C, D, S, and U proteins, altogether suggesting that the transition from ISC to SUF preceded their last common ancestor. Interestingly, we observed that SufDSU were fused in all three oxymonad genomes, and in the genome of *Paratrimastix pyriformis*. The donor of the SUF genes is not clear from phylogenetic analyses, but the enzyme composition of the pathway and the presence of SufDSU fusion suggests Firmicutes, Thermotogae, Spirochaetes, Proteobacteria, or Chloroflexi as donors. The inventory of the downstream CIA pathway enzymes is consistent with that of closely related species that retain ISC, indicating that the switch from ISC to SUF did not markedly affect the downstream process of maturation of cytosolic and nuclear Fe–S proteins.

Key words: **Preaxostyla, SUF, amitochondriate, CIA, oxymonads.**

Letter

Iron–sulfur clusters are small inorganic prosthetic groups, which are among the most ancient and versatile cofactors. Their main function is mediating electron transport, which makes them a key part of many important processes such as photosynthesis, respiration, DNA replication and repair, and regulation of gene expression (Rudolf et al. 2006; Fuss et al. 2015; Paul and Lill 2015).

There are three pathways for the Fe–S clusters synthesis known in prokaryotes—NIF (nitrogen fixation), ISC (iron sulfur cluster), and SUF (sulfur utilization factor). The basic process of the Fe–S cluster biogenesis is similar in all three (Roche et al. 2013·). Sulfur (S^{2-}) is provided by cysteine desulfurase (NifS, IscS, SufS). The source of iron (Fe^{2+}) is unclear, however, for the mitochondrial ISC pathway frataxin is expected to be the provider (Pastore and Puccio 2013; Yoon et al. 2015). The sulfur and iron ions are first combined into a cluster on a scaffold protein (NifU, IscU, SufB–SufD complex), from which the cluster is transferred onto an apoprotein.

In eukaryotic cells, three compartments have distinct pathways for Fe–S cluster synthesis. Mitochondria typically use the ISC pathway, which was inherited from the alphaproteobacterial endosymbiont (Tachezy et al. 2001; Braymer and Lill 2017). This holds also for most mitochondrion-related organelles including the mitosomes of *Giardia intestinalis* (Tovar et al. 2003) and microsporidia (Katinka et al. 2001; Goldberg et al 2008), and hydrogenosomes of *Trichomonas vaginalis* (Sutak et al. 2004). Exceptions to this rule are found in mitochondrion-related organelles of *Pygsuia biforma*, *Mastigamoeba balamuthi*, and *Entamoeba histolytica* (Ali et al. 2004; van der Giezen et al. 2004; Mi-ichi et al. 2009; Nyvltova et al. 2013; Stairs et al. 2014), which contain SUF, NIF, or possibly none of these pathways, respectively. Eukaryotic plastids contain the SUF pathway, which was inherited from the cyanobacterial ancestor (Balk and Pilon 2011).

In the eukaryotic cytosol, the Fe–S cluster-containing proteins are formed by a cytosolic iron–sulfur cluster assembly (CIA), which is also responsible for maturation of nuclear Fe–S proteins. In yeast and human, the pathway contains at least eleven essential proteins (Sharma et al. 2010; Netz et al. 2014; Lill et al. 2015). CIA is unique to eukaryotes and most of its components do not have prokaryotic homologs, apart from Nbp35 (Boyd et al. 2009) and Cia2 (Tsaousis et al. 2014). It has been experimentally shown that the mitochondrial ISC pathway is necessary for the function of the CIA, probably because it synthesizes and transports an uncharacterized sulfur containing precursor to the cytosol (Kispal et al. 1999; Gerber et al. 2004; Biederbick et al. 2006; Pondarré et al. 2006). Dependency on ISC is interpreted as a major reason for the retention of mitochondrion-related organelles in anaerobic eukaryotes (Williams et al. 2002). Maturation of the cytosolic

Fe–S proteins by the CIA pathway starts with the formation of [4Fe–4S] cluster on the Cfd1-Nbp35 scaffold (Hausmann et al. 2005; Netz et al. 2012), transfer of electrons from NADPH is mediated by Dre2 and diflavin reductase Tah18 is required for this process (Zhang et al. 2008; Netz et al. 2010). The [4Fe–4S] cluster from Cfd1-Nbp35 is transferred to a target apoprotein by Nar1 and the late-acting CIA components Cia1, Cia2, and Met18, which form the so-called CIA-targeting complex (Lill et al. 2015).

A unique combination of the Fe–S cluster assembly enzymes has been found in a flagellate *Monocercomonoides exilis* (strains PA203; Treitli et al. 2018) from the group of Oxymonadida (Karnkowska et al. 2016). *Monocercomonoides exilis* contains the CIA pathway, however, the ISC pathway is absent together along with all other mitochondrial proteins. As there is no microscopic evidence for the existence of a mitochondrion, this is interpreted as showing the mitochondrion has been lost altogether (Karnkowska et al. 2016), which makes this oxymonad unique among eukaryotes. Instead of ISC, *M. exilis* contains SUF pathway, which is slightly reduced compared with bacterial pathways, containing only three proteins—SufB, SufC, and SufSU. SufSU represents a fusion of SufS (cysteine desulfurase) and SufU (an enhancer of SufS in prokaryotes; Albrecht et al. 2010, 2011; Riboldi et al. 2011; Karnkowska et al. 2016).

The *M. exilis* SUF proteins are not specifically related to plastid homologues, or homologues from any other microbial eukaryotes, but rather to enzymes found in eubacteria, and to homologues in the transcriptome of *Paratrimastix pyriformis*, a sister taxon of oxymonads (Zhang et al. 2015; Karnkowska et al. 2016). It has been proposed that the pathway was acquired by horizontal gene transfer (HGT) from a eubacterium in the common ancestor of *Monocercomonoides* and *Paratrimastix*. This apparently preceded the loss of mitochondria in *M. exilis*, because *P. pyriformis* retains a mitochondrion-related organelle (Hampl et al. 2008; Zubáčová et al. 2013). Localization of the SUF pathway in *P. pyriformis* is unknown and in *M. exilis* heterologous localizations in *Saccharomyces cerevisiae* and *T. vaginalis* suggest cytosolic localization (Karnkowska et al. 2016).

Oxymonads and *P. pyriformis* are classified into the group Preaxostyla within phylum Metamonada (supergroup Excavata; Hampl et al. 2009; Adl et al. 2012). All representatives of two other Metamonada lineages (Parabasalia and Fornicata) contain the ancestral ISC pathway and no genes for enzymes in the SUF pathway have been observed in these lineages, indicating that this modification of Fe–S cluster assembly is specific to Preaxostyla. This may have served as a precondition for the mitochondrial loss in oxymonads. To further reveal the evolutionary history of this unique evolutionary switch, we investigated genomes and transcriptomes of 16 members of Preaxostyla for presence of genes and/or transcripts involved in Fe–S cluster synthesis.

Results and Discussion

The following Preaxostyla data sets were investigated in this study: genomic assemblies of *M. exilis* strain PA203 (Karnkowska et al. 2016), *Blattamonas nauphoetae* strain NAU3, and *P. pyriformis* strain ATCC 50935, single cell genome assembly of *Streblomastix strix*, three single cell transcriptome assemblies of *Saccinobaculus doroaxostylus* (SD1, SD2, SDN), three single cell transcriptome assemblies of *Saccinobaculus ambloaxostylus* (Amblo-1, Amblo-5, Amblo-5), one single cell transcriptome assembly of *Oxymonas* sp., two single cell transcriptome assemblies of *Streblomastix* sp. (Streblo-1, Streblo-4), one single cell transcriptome assembly of *Pyrsonympha* sp., transcriptome assembly of *Trimastix marina* strain PCT (Leger et al. 2017), and transcriptome assembly of trimastigid "MORAITIKA". Quality and coverage varied extremely between data sets, which was probably the main reason for the lack of some genes/transcripts especially in the single cell genomes and transcriptomes.

The data were searched for all known components of ISC, SUF, CIA, and NIF pathways. In all examined data sets, we were unable to identify any gene involved in the ISC and NIF pathways, but we identified genes or gene fragments for proteins involved in the SUF and CIA pathways in all examined organisms with exception of "Streblo-4" (figs. 1 and 2). Mitochondrial targeting peptides were not predicted in any complete SUF proteins (supplementary table S1, Supplementary Material online), indicating cytosolic localization of these proteins.

Contaminants among the CIA proteins were not expected, because they have no close prokaryotic homologues. To filter prokaryotic contamination of SUF genes/transcripts and to exclude those that were severely truncated, sequences with >70% nucleotide similarity to prokaryotic sequences in NCBI and also sequences shorter than 65 aa were not included in further analyses. Phylogenetic trees were then constructed for individual SUF components (supplementary figs. S1–S4, Supplementary Material online). Every protein tree resolved a major Preaxostyla clade (shown in green in supplementary figs. S1–S4, Supplementary Material online). Sequences derived from the genomic assemblies were present only in this major clade, suggesting that this clade represents *bona fide* Preaxostyla genes. Species composition of this clade in every protein tree suggests that it was acquired prior to the last common ancestor of Preaxostyla.

Some sequences branched robustly (ML bootstrap >90%) outside this major clade (shown in red in supplementary figs. S1–S4, Supplementary Material online). Origin of these sequences is unclear, they may result from prokaryotic contaminations or more recent lineage specific HGT. For this reason, these sequences were not included in the concatenation analysis. Such outlying SUF proteins were especially common in the data set of *Oxymonas* sp. (supplementary figs. S1–S4, Supplementary Material online). These were all unique to *Oxymonas* and no closely related orthologues were found in any other oxymonad, suggesting that this data set contains high level of prokaryotic contamination. In contrast, we identified six closely related SufS genes from *S. doroaxostylus* isolate SDN, *Streblomastix* sp. (Streblo-1), *S. ambloaxostylus* (Amblo-5), and trimastigid "MORAITIKA." They formed a well-supported clade (ML bootstrap 100) that was deeply nested in a clade containing mixture of Archaea and Eubacteria (supplementary fig. S4, Supplementary Material online). These

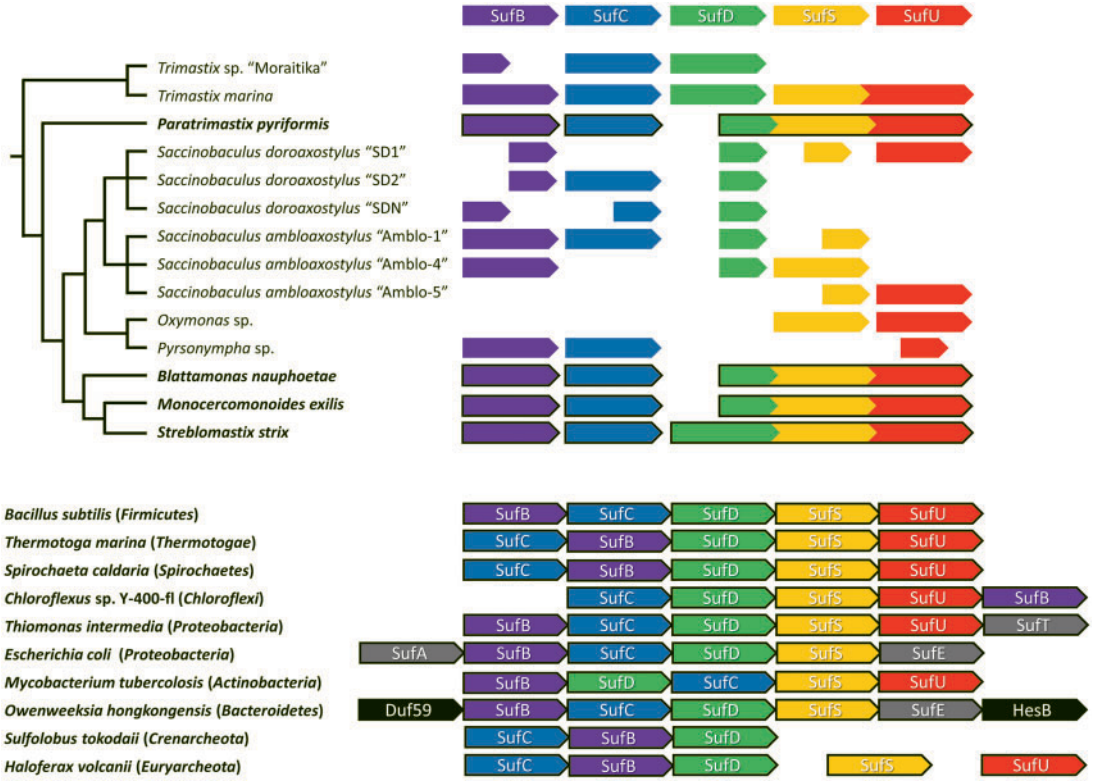

Fig. 1. Inventory of SUF proteins in Preaxostyla. The scheme shows SUF genes/transcripts identified in the members of Preaxostyla. The relationship within this groups is indicated by the tree. For organisms in bold, genomic data were investigated, in others transcriptomic or single cell transcriptomic data sets were used. Completeness of a gene/transcript is indicated by the length of the arrow. The order of Preaxostyla genes does not reflect their order in the genome. Gene fusions are marked by fused arrows. At the bottom are given schemes of typical SUF gene operons in representatives of prokaryotic groups, see supplementary figure S5, Supplementary Material online for broader prokaryotic representation.

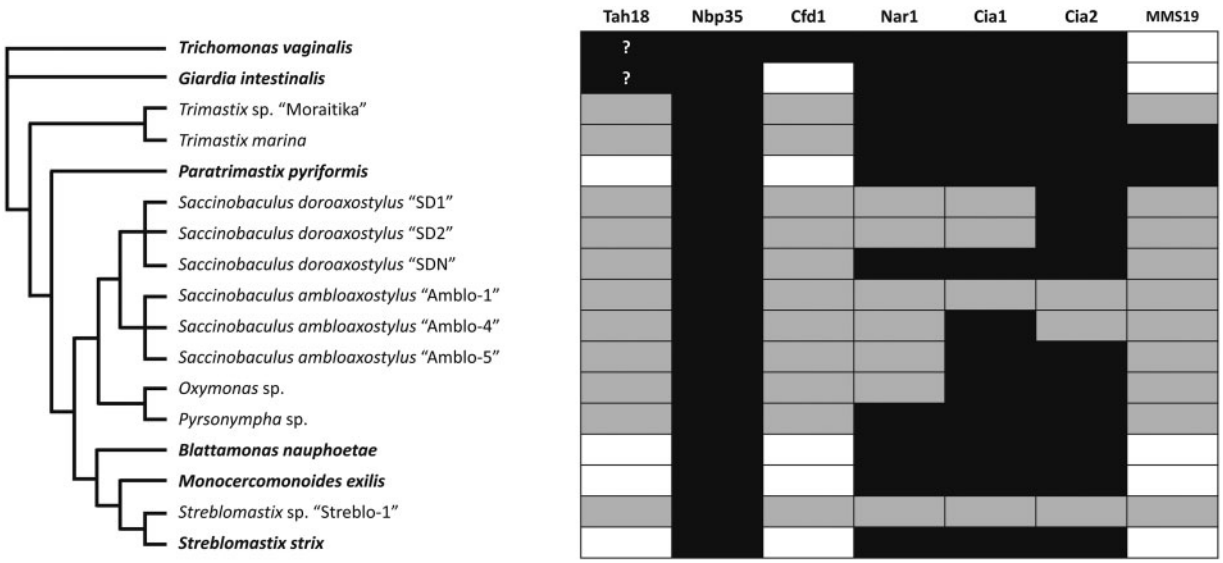

Fig. 2. Inventory of CIA proteins in Preaxostyla. Scheme shows the presence (black) or absence (white/gray) of CIA genes/transcripts in Preaxostyla with reference to Metamonada represented by *G. intestinalis* and *T. vaginalis*. White/grey shading indicates that the gene was not identified in available genome/transcriptome, respectively. The gene inventory of *T. vaginalis* and *G. intestinalis* was taken from Pyrih et al. 2016. Question marks indicate uncertain orthology to Tah18.

sequences may represent contaminants from closely related prokaryotes, but it is also possible given the fact that these genes do not share a high level of identity and were found in a larger number of species, that they represent a second and independent acquisition of SufS by a subset of Preaxostyla. It should be noted, however, that these homologues were identified only in transcriptomes with overall low quality and high level of contamination, and most critically that

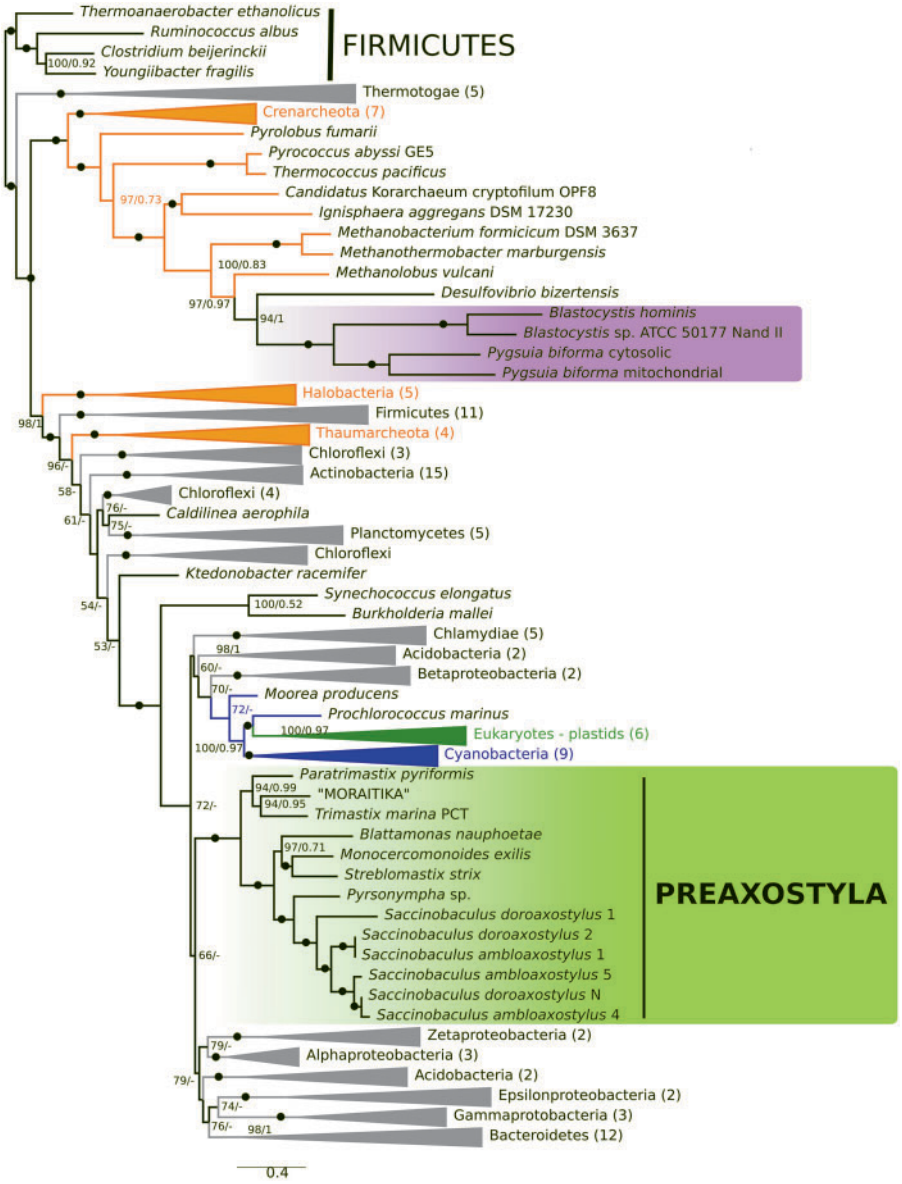

Fig. 3. Phylogenetic analysis of concatenated SufB, C, D, and S proteins. The topology of the tree was calculated by ML in IQ-TREE using partition-specific models. Numbers at nodes represent statistical support in regular ML bootstraps/Bayesian posterior probabilities. The support 99/0.99 and higher is indicated by filled circles, values <50 and 0.5 are not shown.

the sequences putatively ascribed to *Streblomastix* do not contain evidence of the alternative genetic code typical for this oxymonad (Keeling and Leander 2003).

A concatenated tree of SufB, SufC, SufD, and SufS was constructed including sequences from "green clades" with reliable Preaxostyla origin (fig. 3). In this tree, all Preaxostyla formed a single and well-supported clade (RaxML/MrBayes support 100/1) with an internal topology consistent with the relationships among Preaxostyla (Treitli et al. 2018). This result strongly suggests that the whole pathway originated in their common ancestor and was inherited vertically since then.

Three proteins of the pathway (SufD, S, and U) are fused (SufDSU) in *M. exilis*, *B. nauphoetae*, *S. strix*, and *P. pyriformis*. The homology of the N-terminal part of this protein with SufD has not been recognized previously (Karnkowska et al. 2016). Similar fusion is also present in the transcriptome of *T. marina*, where we identified a fusion of SufSU but SufD is on an independent contig. No fusions were evident in other data sets, but this may be a result of the fragmented nature of the data, making fusions hard to detect. A scheme of the detected SUF genes/transcripts and their fusions is shown in figure 1 (see supplementary fig. S5, Supplementary Material online for broader representation of prokaryotes). The phylogeny of SUFs (fig. 3) was unable to resolve the position of Preaxostyla sequences within prokaryotes. However, the arrangement of SUF operons in sequenced prokaryotic genomes suggests Firmicutes, Thermotogae, Spirochaetes, Proteobacteria, or Chloroflexi as probable donors. Operons in these groups are consistent with the SUF pathway composition as well as the SufDSU gene order found in Preaxostyla fusion genes.

The inventory of the CIA genes in Preaxostyla is in general very similar to that of other metamonads, including Nbp35,

Cia1, Nar1, and Cia2 (Pyrih et al. 2016; fig. 2). Preaxostyla lack proteins associated with the mitochondrion (Erv1 and Atm1), and proteins Dre2 and Tah18. Their absence is not surprising as the Dre2 is often missing in anaerobes (Basu et al. 2014; Tsaousis et al. 2014) and neither Erv1 nor Atm1 was found in other metamonads (Pyrih et al. 2016). The primary function of Tah18 is to provide electrons for Dre2 (Netz et al. 2010), so in the absence of Dre2 it is reasonable that Tah18 was probably lost as well. We were not able to identify MMS19 in any of the studied oxymonads, but protein containing N-terminal MMS19 domain was present in *P. pyriformis* (fig. 2). The conserved inventory of CIA proteins in Preaxostyla contrasts with the major switch of the upstream Fe–S cluster assembly pathway in this group and indicates functional robustness of the CIA pathway.

Materials and Methods

For single cell transcriptomes (*S. doroaxostylus*, *S. ambloaxostylus*, *Oxymonas* sp., *Streblomastix* spp., and *Pyrsonympha*), cells were manually picked by micropipette, washed 1–2 times, and then deposited directly into single cell lysis buffer and frozen in −80 °C freezer. Single cell cDNA was then amplified following Picelli et al. (2014) and Kolisko et al. (2014) protocols. Illumina Nextera XT protocol was used for sequencing library construction. Transcriptomes were assembled by Trinity 2.0.6 (Grabherr et al. 2011) and for quality trimming trimmomatic0.32 (Bolger et al. 2014) with default settings was used.

The trimastigid "MORAITIKA" was maintained as a monoeukaryotic polyxenic culture in the ATCC medium 1525 at room temperature. Total RNA was isolated from 300 ml of culture using TRI Reagent (Sigma). Isolated RNA was purified by Qiagen RNeasy Mini Kit (Qiagen) and RNase-Free DNase Set (Qiagen) according to the manufacturer's protocol. Total RNA was sent to EMBL where the libraries were prepared. Contigs were assembled by Trinity 2014-04-13p1 (Grabherr et al. 2011), quality trimming was done by fastx version 0.0.13 (fastq_quality_filter -Q33 -q 20 -p 70), contigs shorter than 200 nt were discarded.

The single cell of *S. strix* was manually picked by micropipette from gut content of the termite *Zootermopsis angusticolis*, three times washed in Trager U media, then DNA was isolated and the whole genome was amplified using illustra Single Cell GenomiPhi DNA Amplification Kit (GE Healthcare) according to the manufacturer's protocol. The amplified DNA was purified using Agencourt AMPure XP (Beckman Coulter), and sequencing libraries were prepared using Illumina TruSeq DNA PCR-Free (Illumina) for HiSeq 2500 or with Ligation Sequencing Kit 1D (Oxford Nanopore Technologies) for Oxford Nanopore sequencing. Draft genome was assembled as a hybrid assembly using SPAdes 3.10.0 (Bankevich et al. 2012; Antipov et al. 2016). Binning of the assembled data and separation of the eukaryotic genome from bacterial sequences was done using tetranucleotide frequencies using tetraESOM method (Dick et al. 2009), together with blast analysis of the assembled data.

Blattamonas nauphoetae strain NAU3 was grown as a monoeukaryotic polyxenic culture in modified TYSGM media (Diamond 1982) without gastric mucin. The genomic DNA was sequenced using Illumina MiSeq (coverage 62x) and Oxford Nanopore MinIon (coverage 2x) technology and assembled using the SPAdes 3.7.1 (Bankevich et al. 2012; Antipov et al. 2016) followed by scaffolding with SSPACE basic V2 (Boetzer et al. 2011) using the Illumina mate-pair reads.

Paratrimastix pyriformis was grown in a monoeukaryotic polyxenic culture on rye grass cerophyll infusion (Sonneborn's Paramecium medium, ATCC #802) at room temperature. The genomic DNA was isolated using DNeasy Blood & Tissue Kit (Qiagen). The *P. pyriformis* draft genome sequence was sequenced and assembled from raw genomic reads produced by 454, Illumina HiSeq (coverage 894x), and PacBio (coverage 11x) sequencing technologies using SPAdes 3.11.1 (Bankevich et al. 2012; Antipov et al. 2016) assembly toolkit. Automatic gene prediction for the *S. strix*, *B. nauphoetae* and *P. pyriformis* draft genomes was done using Augustus 3.2.3 (Stanke and Waack 2003).

Nucleotide data sets predicted proteins were searched by TBLASTN algorithms; six-frame translations of the transcriptomes and predicted proteomes were searched by BLASTP. Proteins not identified by BLAST were searched for by HMMER. In the BLAST searches, we have used full gene inventories of *M. exilis*, *Escherichia coli*, and *Bacillus subtilis* for the SUF pathway, *S. cerevisiae*, *T. vaginalis*, *G. intestinalis*, and *E. coli* for the ISC pathway, *Azotobacter vinelandii*, *E. histolytica*, and *M. balamuthii* for the NIF pathway and *S. cerevisiae* and human for the CIA pathway. HMMER searches were performed by HMMER 3.1b2 (Eddy 2011) using curated Pfam and custom created models for the aforementioned genes. Sequences of SUF and CIA pathway genes/proteins retrieved from unpublished data sets were deposited in GenBank under accession numbers MH608120–MH608208.

Sequences were aligned by MAFFT v. 7.222 (Katoh et al. 2002) and trimmed with BMGE 1.12 software (Criscuolo and Gribaldo 2010) using blosum30 matrix. Gene fragments originating from different assemblies of the same species (namely SufC—SDN_lcl|TR24651|c0_g1_i1 and SDN_lcl|TR10532|c0_g1_i1, SufS—SD1_lcl|TR11348|c0_g2_i1 and SD1_lcl|TR17340|c0_g1_i1) were concatenated to increase phylogenetic resolution. Alignments are available upon request. Phylogenetic trees were constructed by IQ-TREE v 1.6.1 (Nguyen et al. 2015) using the best fitting models according to Bayesian information criterion predicted by ModelFinder (Kalyaanamoorthy et al. 2017)—LG4M for SufS and SufD, C20 for SufC, and EX_EHO for SufD. For analysis of the concatenated alignment, gene-partition-specific models given above were used. Bayesian analysis was performed for concatenated data set using MrBayes 3.2 (Ronquist et al. 2012) with two runs, each of four chains of 10 mil. generations, sampling frequency 500 generations and uniform WAG+gamma+covarion model for the whole concatenate. The value of the average standard deviation of split frequencies did not drop below the 0.01; however, both chains have shown stable plateau of likelihood values after 1×10^6

generations. Tree from first 1×10^6 generations were discarded as burn-in before consensus tree calculation.

Supplementary Material

Supplementary data are available at *Molecular Biology and Evolution* online.

Acknowledgments

This work was supported by the Czech Science Foundation (project 15-16406S to V.H.), by the European Research Council (ERC) under the European Union's Horizon 2020 research and innovation programme (grant agreement No 771592 to VH) the Grant Agency of Charles University (Project 1584314 to V.V.), the Ministry of Education, Youth and Sports of CR within the National Sustainability Program II (Project BIOCEV-FAR) LQ1604, by the project "BIOCEV" (CZ.1.05/1.1.00/02.0109), by the Centre for research of pathogenicity and virulence of parasites reg. nr.: CZ.02.1.01/0.0/0.0/16_019/0000759, by the Natural Sciences and Engineering Council of Canada (project RGPIN-2014-03994 to P.J.K.), by a grant from the Tula Foundation to the UBC Centre for Microbial Diversity and Evolution, by Purkyne Fellowship to M.K. (Czech Academy of Sciences). Computational resources were provided by the CESNET LM2015042 and the CERIT Scientific Cloud LM2015085, provided under the programme "Projects of Large Research, Development, and Innovations Infrastructures."

References

Adl SM, Simpson AGB, Lane CE, Lukeš J, Bass D, Bowser SS, Brown MW, Burki F, Dunthorn M, Hampl V, et al. 2012. The revised classification of eukaryotes. *J Eukaryot Microbiol*. 59(5):429–493.

Albrecht AG, Netz DJA, Miethke M, Pierik AJ, Burghaus O, Peuckert F, Lill R, Marahiel MA. 2010. SufU is an essential iron–sulfur cluster scaffold protein in *Bacillus subtilis*. *J Bacteriol*. 192(6):1643–1651.

Albrecht AG, Peuckert F, Landmann H, Miethke M, Seubert A, Marahiel MA. 2011. Mechanistic characterization of sulfur transfer from cysteine desulfurase SufS to the iron–sulfur scaffold SufU in *Bacillus subtilis*. *FEBS Lett*. 585(3):465–470.

Ali V, Shigeta Y, Tokumoto U, Takahashi Y, Nozaki T. 2004. An intestinal parasitic protist, *Entamoeba histolytica*, possesses a non-redundant nitrogen fixation-like system for iron–sulfur cluster assembly under anaerobic conditions. *J Biol Chem*. 279(16):16863–16874.

Antipov D, Korobeynikov A, McLean JS, Pevzner PA. 2016. HybridSPAdes: an algorithm for hybrid assembly of short and long reads. *Bioinformatics* 32(7):1009–1015.

Balk J, Pilon M. 2011. Ancient and essential: the assembly of iron–sulfur clusters in plants. *Trends Plant Sci*. 16(4):218–226.

Bankevich A, Nurk S, Antipov D, Gurevich AA, Dvorkin M, Kulikov AS, Lesin VM, Nikolenko SI, Pham S, Prjibelski AD, et al. 2012. SPAdes: a new genome assembly algorithm and its applications to single-cell sequencing. *J Comput Biol*. 19(5):455–477.

Basu S, Netz DJ, Haindrich AC, Herlerth N, Lagny TJ, Pierik AJ, Lill R, Lukeš J. 2014. Cytosolic iron–sulphur protein assembly is functionally conserved and essential in procyclic and bloodstream Trypanosoma brucei. *Mol Microbiol*. 93(5):897–910.

Biederbick A, Stehling O, Rosser R, Niggemeyer B, Nakai Y, Elsasser H-P, Lill R. 2006. Role of human mitochondrial Nfs1 in cytosolic iron–sulfur protein biogenesis and iron regulation. *Mol Cell Biol*. 26(15):5675–5687.

Boetzer M, Henkel CV, Jansen HJ, Butler D, Pirovano W. 2011. Scaffolding pre-assembled contigs using SSPACE. *Bioinformatics* 27(4):578–579.

Bolger AM, Lohse M, Usadel B. 2014. Trimmomatic: a flexible trimmer for Illumina sequence data. *Bioinformatics* 30(15):2114–2120.

Boyd JM, Drevland RM, Downs DM, Graham DE. 2009. Archaeal ApbC/Nbp35 homologs function as iron–sulfur cluster carrier proteins. *J Bacteriol*. 191(5):1490–1497.

Braymer JJ, Lill R. 2017. Iron–sulfur cluster biogenesis and trafficking in mitochondria. *J Biol Chem*. 292(31):12754–12763.

Criscuolo A, Gribaldo S. 2010. BMGE (Block Mapping and Gathering with Entropy): a new software for selection of phylogenetic informative regions from multiple sequence alignments. *BMC Evol Biol*. 10(1):210.

Diamond LS. 1982. A new liquid medium for xenic cultivation of *Entamoeba histolytica* and other lumen-dwelling protozoa. *J Parasitol*. 68(5):958–959.

Dick GJ, Andersson AF, Baker BJ, Simmons SL, Thomas BC, Yelton AP, Banfield JF. 2009. Community-wide analysis of microbial genome sequence signatures. *Genome Biol*. 10(8):R85.

Eddy SR. 2011. Accelerated profile HMM searches. Pearson WR, editor. *PLoS Comput Biol*. 7(10):e1002195.

Fuss JO, Tsai CL, Ishida JP, Tainer JA. 2015. Emerging critical roles of Fe–S clusters in DNA replication and repair. *Biochim Biophys Acta-Mol Cell Res*. 1853(6):1253–1271.

Gerber J, Neumann K, Prohl C, Muhlenhoff U, Lill R. 2004. The yeast scaffold proteins Isu1p and Isu2p are required inside mitochondria for maturation of cytosolic Fe/S proteins. *Mol Cell Biol*. 24(11):4848–4857.

van der Giezen M, Cox S, Tovar J. 2004. The iron–sulfur cluster assembly genes iscS and iscU of *Entamoeba histolytica* were acquired by horizontal gene transfer. *BMC Evol Biol*. 4:7.

Goldberg AV, Molik S, Tsaousis AD, Neumann K, Kuhnke G, Delbac F, Vivares CP, Hirt RP, Lill R, Embley TM. 2008. Localization and functionality of microsporidian iron–sulphur cluster assembly proteins. *Nature* 452(7187):624–628.

Grabherr MG, Haas BJ, Yassour M, Levin JZ, Thompson DA, Amit I, Adiconis X, Fan L, Raychowdhury R, Zeng Q, et al. 2011. Full-length transcriptome assembly from RNA-Seq data without a reference genome. *Nat Biotechnol*. 29(7):644–652.

Hampl V, Hug L, Leigh JW, Dacks JB, Lang BF, Simpson AGB, Roger AJ. 2009. Phylogenomic analyses support the monophyly of Excavata and resolve relationships among eukaryotic "supergroups". *Proc Natl Acad Sci USA*. 106(10):3859–3864.

Hampl V, Silberman JD, Stechmann A, Diaz-Triviño S, Johnson PJ, Roger AJ. 2008. Genetic evidence for a mitochondriate ancestry in the "amitochondriate" flagellate *Trimastix pyriformis*. *PLoS One* 3(1):e1383.

Hausmann A, Netz DJA, Balk J, Pierik AJ, Muhlenhoff U, Lill R. 2005. The eukaryotic P loop NTPase Nbp35: an essential component of the cytosolic and nuclear iron–sulfur protein assembly machinery. *Proc Natl Acad Sci USA*. 102(9):3266–3271.

Kalyaanamoorthy S, Minh BQ, Wong TKF, von Haeseler A, Jermiin LS. 2017. ModelFinder: fast model selection for accurate phylogenetic estimates. *Nat Methods*. 14(6):587–589.

Karnkowska A, Vacek V, Zubáčová Z, Treitli SC, Petrželková R, Eme L, Novák L, Žárský V, Barlow LD, Herman EK, et al. 2016. A eukaryote without a mitochondrial organelle. *Curr Biol*. 26(10):1274–1284.

Katinka MD, Duprat S, Cornillot E, Méténier G, Thomarat F, Prensier G, Barbe V, Peyretaillade E, Brottier P, Wincker P, et al. 2001. Genome sequence and gene compaction of the eukaryote parasite Encephalitozoon cuniculi. *Nature* 414(6862):450–453.

Katoh K, Misawa K, Kuma K, Miyata T. 2002. MAFFT: a novel method for rapid multiple sequence alignment based on fast Fourier transform. *Nucleic Acids Res*. 30(14):3059–3066.

Keeling PJ, Leander BS. 2003. Characterisation of a Non-canonical genetic code in the oxymonad *Streblomastix strix*. *J Mol Biol*. 326(5):1337–1349.

Kispal G, Csere P, Prohl C, Lill R. 1999. The mitochondrial proteins Atm1p and Nfs1p are essential for biogenesis of cytosolic Fe/S proteins. *EMBO J*. 18(14):3981–3989.

Kolisko M, Boscaro V, Burki F, Lynn DH, Keeling PJ. 2014. Single-cell transcriptomics for microbial eukaryotes. *Curr Biol*. 24(22): R1081–R1082.

Leger MM, Kolisko M, Kamikawa R, Stairs CW, Kume K, Čepička I, Silberman JD, Andersson JO, Xu F, Yabuki A, et al. 2017. Organelles that illuminate the origins of Trichomonas hydrogenosomes and Giardia mitosomes. *Nat Ecol Evol*. 1(4):0092.

Lill R, Dutkiewicz R, Freibert SA, Heidenreich T, Mascarenhas J, Netz DJ, Paul VD, Pierik AJ, Richter N, Stümpfig M, et al. 2015. The role of mitochondria and the CIA machinery in the maturation of cytosolic and nuclear iron–sulfur proteins. *Eur J Cell Biol*. 94(7–9):280–291.

Mi-ichi F, Yousuf MA, Nakada-Tsukui K, Nozaki T. 2009. Mitosomes in *Entamoeba histolytica* contain a sulfate activation pathway. *Proc Natl Acad Sci USA*. 106(51):21731–21736.

Netz DJA, Mascarenhas J, Stehling O, Pierik AJ, Lill R. 2014. Maturation of cytosolic and nuclear iron–sulfur proteins. *Trends Cell Biol*. 24(5):303–312.

Netz DJA, Pierik AJ, Stümpfig M, Bill E, Sharma AK, Pallesen LJ, Walden WE, Lill R. 2012. A bridging [4Fe–4S] cluster and nucleotide binding are essential for function of the Cfd1-Nbp35 complex as a scaffold in iron–sulfur protein maturation. *J Biol Chem*. 287(15):12365–12378.

Netz DJA, Stümpfig M, Doré C, Mühlenhoff U, Pierik AJ, Lill R. 2010. Tah18 transfers electrons to Dre2 in cytosolic iron–sulfur protein biogenesis. *Nat Chem Biol*. 6(10):758–765.

Nguyen LT, Schmidt HA, Von Haeseler A, Minh BQ. 2015. IQ-TREE: a fast and effective stochastic algorithm for estimating maximum-likelihood phylogenies. *Mol Biol Evol*. 32(1):268–274.

Nyvltova E, Sutak R, Harant K, Sedinova M, Hrdy I, Paces J, Vlcek C, Tachezy J. 2013. NIF-type iron–sulfur cluster assembly system is duplicated and distributed in the mitochondria and cytosol of *Mastigamoeba balamuthi*. *Proc Natl Acad Sci USA*. 110(18): 7371–7376.

Pastore A, Puccio H. 2013. Frataxin: a protein in search for a function. *J Neurochem*. 126:43–52.

Paul VD, Lill R. 2015. Biogenesis of cytosolic and nuclear iron–sulfur proteins and their role in genome stability. *Biochim Biophys Acta-Mol Cell Res*. 1853(6):1528–1539.

Picelli S, Faridani OR, Björklund ÅK, Winberg G, Sagasser S, Sandberg R. 2014. Full-length RNA-seq from single cells using Smart-seq2. *Nat Protoc*. 9(1):171–181.

Pondarré C, Antiochos BB, Campagna DR, Clarke SL, Greer EL, Deck KM, McDonald A, Han AP, Medlock A, Kutok JL, et al. 2006. The mitochondrial ATP-binding cassette transporter Abcb7 is essential in mice and participates in cytosolic iron–sulfur cluster biogenesis. *Hum Mol Genet*. 15(6):953–964.

Pyrih J, Pyrihová E, Kolísko M, Stojanovová D, Basu S, Harant K, Haindrich AC, Doležal P, Lukeš J, Roger A, et al. 2016. Minimal cytosolic iron–sulfur cluster assembly machinery of *Giardia intestinalis* is partially associated with mitosomes. *Mol Microbiol*. 102(4):701–714.

Riboldi GP, Larson TJ, Frazzon J. 2011. Enterococcus faecalis sufCDSUB complements *Escherichia coli* sufABCDSE. *FEMS Microbiol Lett*. 320(1):15–24.

Roche B, Aussel L, Ezraty B, Mandin P, Py B, Barras F. 2013. Reprint of: iron/sulfur proteins biogenesis in prokaryotes: formation, regulation and diversity. *Biochim Biophys Acta-Bioenergy*. 1827(8–9):923–937.

Ronquist F, Teslenko M, Van Der Mark P, Ayres DL, Darling A, Höhna S, Larget B, Liu L, Suchard MA, Huelsenbeck JP. 2012. Mrbayes 3.2: efficient bayesian phylogenetic inference and model choice across a large model space. *Syst Biol*. 61(3):539–542.

Rudolf J, Makrantoni V, Ingledew WJ, Stark MJR, White MF. 2006. The DNA repair helicases XPD and FancJ have essential iron–sulfur domains. *Mol Cell*. 23(6):801–808.

Sharma AK, Pallesen LJ, Spang RJ, Walden WE. 2010. Cytosolic iron–sulfur cluster assembly (CIA) system: factors, mechanism, and relevance to cellular iron regulation. *J Biol Chem*. 285(35):26745–26751.

Stairs CW, Eme L, Brown MW, Mutsaers C, Susko E, Dellaire G, Soanes DM, Van Der Giezen M, Roger AJ. 2014. A SUF Fe–S cluster biogenesis system in the mitochondrion-related organelles of the anaerobic protist Pygsuia. *Curr Biol*. 24(11):1176–1186.

Stanke M, Waack S. 2003. Gene prediction with a hidden Markov model and a new intron submodel. *Bioinformatics* 19(Suppl. 2):ii215–ii225.

Sutak R, Dolezal P, Fiumera HL, Hrdy I, Dancis A, Delgadillo-Correa M, Johnson PJ, Muller M, Tachezy J. 2004. Mitochondrial-type assembly of FeS centers in the hydrogenosomes of the amitochondriate eukaryote *Trichomonas vaginalis*. *Proc Natl Acad Sci USA*. 101(28):10368–10373.

Tachezy J, Sánchez LB, Müller M. 2001. Mitochondrial type iron–sulfur cluster assembly in the amitochondriate eukaryotes *Trichomonas vaginalis* and *Giardia intestinalis*, as indicated by the phylogeny of IscS. *Mol Biol Evol*. 18(10):1919–1928.

Tovar J, León-Avila G, Sánchez LB, Sutak R, Tachezy J, Van Der Giezen M, Hernández M, Müller M, Lucocq JM. 2003. Mitochondrial remnant organelles of Giardia function in iron–sulphur protein maturation. *Nature* 426(6963):172–176.

Treitli SC, Kotyk M, Yubuki N, Jirounková E, Vlasáková J, Smejkalová P, Šípek P, Čepička I, Hampl V. 2018. Molecular and morphological diversity of the Oxymonad Genera Monocercomonoides and Blattamonas gen. nov. *Protist* 169(5):744–783.

Tsaousis AD, Gentekaki E, Eme L, Gaston D, Roger AJ. 2014. Evolution of the cytosolic iron–sulfur cluster assembly machinery in Blastocystis species and other microbial eukaryotes. *Eukaryot Cell*. 13(1):143–153.

Williams BAP, Hirt RP, Lucocq JM, Embley TM. 2002. A mitochondrial remnant in the microsporidian *Trachipleistophora hominis*. *Nature* 418(6900):865–869.

Yoon H, Knight SAB, Pandey A, Pain J, Turkarslan S, Pain D, Dancis A. 2015. Turning *Saccharomyces cerevisiae* into a frataxin-independent organism. *PLoS Genet*. 11(5):e1005135.

Zhang Q, Táborský P, Silberman JD, Pánek T, Čepička I, Simpson AGB. 2015. Marine isolates of *Trimastix marina* form a plesiomorphic deep-branching lineage within preaxostyla, separate from other known trimastigids (*Paratrimastix* n. gen.). *Protist* 166(4):468–491.

Zhang Y, Lyver ER, Nakamaru-Ogiso E, Yoon H, Amutha B, Lee D-W, Bi E, Ohnishi T, Daldal F, Pain D, et al. 2008. Dre2, a conserved eukaryotic Fe/S cluster protein, functions in cytosolic Fe/S protein biogenesis. *Mol Cell Biol*. 28(18):5569–5582.

Zubáčová Z, Novák L, Bublíková J, Vacek V, Fousek J, Rídl J, Tachezy J, Doležal P, Vlček Č, Hampl V. 2013. The mitochondrion-like organelle of *Trimastix pyriformis* contains the complete glycine cleavage system. *PLoS One* 8(3):e55417.

The Oxymonad Genome Displays Canonical Eukaryotic Complexity in the Absence of a Mitochondrion

Anna Karnkowska,*[,1,2] Sebastian C. Treitli,[1] Ondřej Brzoň,[1] Lukáš Novák,[1] Vojtěch Vacek,[1] Petr Soukal,[1] Lael D. Barlow,[3] Emily K. Herman,[3] Shweta V. Pipaliya,[3] Tomáš Pánek,[4] David Žihala,[4] Romana Petrželková,[4] Anzhelika Butenko,[4] Laura Eme,[5,6] Courtney W. Stairs,[5,6] Andrew J. Roger,[5] Marek Eliáš,[4,7] Joel B. Dacks,[3] and Vladimír Hampl*[,1]

[1]Department of Parasitology, BIOCEV, Faculty of Science, Charles University, Vestec, Czech Republic

[2]Department of Molecular Phylogenetics and Evolution, Faculty of Biology, Biological and Chemical Research Centre, University of Warsaw, Warsaw, Poland

[3]Division of Infectious Disease, Department of Medicine, University of Alberta, Edmonton, Canada

[4]Department of Biology and Ecology, Faculty of Science, University of Ostrava, Ostrava, Czech Republic

[5]Department of Biochemistry and Molecular Biology, Dalhousie University, Halifax, Canada

[6]Department of Cell and Molecular Biology, Uppsala University, Uppsala, Sweden

[7]Institute of Environmental Technologies, Faculty of Science, University of Ostrava, Ostrava, Czech Republic

***Corresponding authors:** E-mails: ankarn@biol.uw.edu.pl; vlada@natur.cuni.cz.

Associate editor: Fabia Ursula Battistuzzi

Abstract

The discovery that the protist *Monocercomonoides exilis* completely lacks mitochondria demonstrates that these organelles are not absolutely essential to eukaryotic cells. However, the degree to which the metabolism and cellular systems of this organism have adapted to the loss of mitochondria is unknown. Here, we report an extensive analysis of the *M. exilis* genome to address this question. Unexpectedly, we find that *M. exilis* genome structure and content is similar in complexity to other eukaryotes and less "reduced" than genomes of some other protists from the Metamonada group to which it belongs. Furthermore, the predicted cytoskeletal systems, the organization of endomembrane systems, and biosynthetic pathways also display canonical eukaryotic complexity. The only apparent preadaptation that permitted the loss of mitochondria was the acquisition of the SUF system for Fe–S cluster assembly and the loss of glycine cleavage system. Changes in other systems, including in amino acid metabolism and oxidative stress response, were coincident with the loss of mitochondria but are likely adaptations to the microaerophilic and endobiotic niche rather than the mitochondrial loss per se. Apart from the lack of mitochondria and peroxisomes, we show that *M. exilis* is a fully elaborated eukaryotic cell that is a promising model system in which eukaryotic cell biology can be investigated in the absence of mitochondria.

Key words: **amitochondrial eukaryote, cell biology, Monocercomonoides, oxymonads, protist genomics.**

Article

Introduction

Mitochondria are core features of the eukaryotic cell. In addition to their signature role in ATP generation, they are integrated in diverse cellular processes including the biosynthesis and catabolism of amino acids, lipids, and carbohydrates, environmental stress tolerance, and the regulation of cell death. Despite the many independent transformations of the mitochondria into metabolically reduced and modified versions present in anaerobic organisms (Roger et al. 2017), mitochondria or mitochondrion-related organelles (MROs) were considered indispensable due to their essential core function(s) such as the biosynthesis of Fe–S clusters (Williams et al. 2002; Gray 2012; Lill et al. 2012).

However, the discovery of the first truly amitochondriate eukaryote, *Monocercomonoides* sp. PA203 (Karnkowska et al. 2016) showed that the outright loss of mitochondria is possible. This organism, now classified as *Monocercomonoides exilis* (Treitli et al. 2018), remains the only deeply inspected amitochondriate eukaryote, although the same status may hold true for its relatives, based on the limited cytological data from other oxymonads (Hampl 2017). Importantly, the ancestor of this lineage must have possessed a mitochondrial organelle, given the well-documented presence of MROs in relatives of oxymonads (Zubáčová et al. 2013; Leger et al. 2017). By studying *M. exilis*, we can determine how mitochondrial loss affects the rest of the cell and affords a unique opportunity to examine cellular systems that are normally integrated with mitochondria in a context where the organelle is absent.

Monocercomonoides exilis is a bacterivorous tetraflagellate living as a putative commensal in the intestine of caviomorph rodents (fig. 1*a* and *b*) (Treitli et al. 2018). Like all oxymonads,

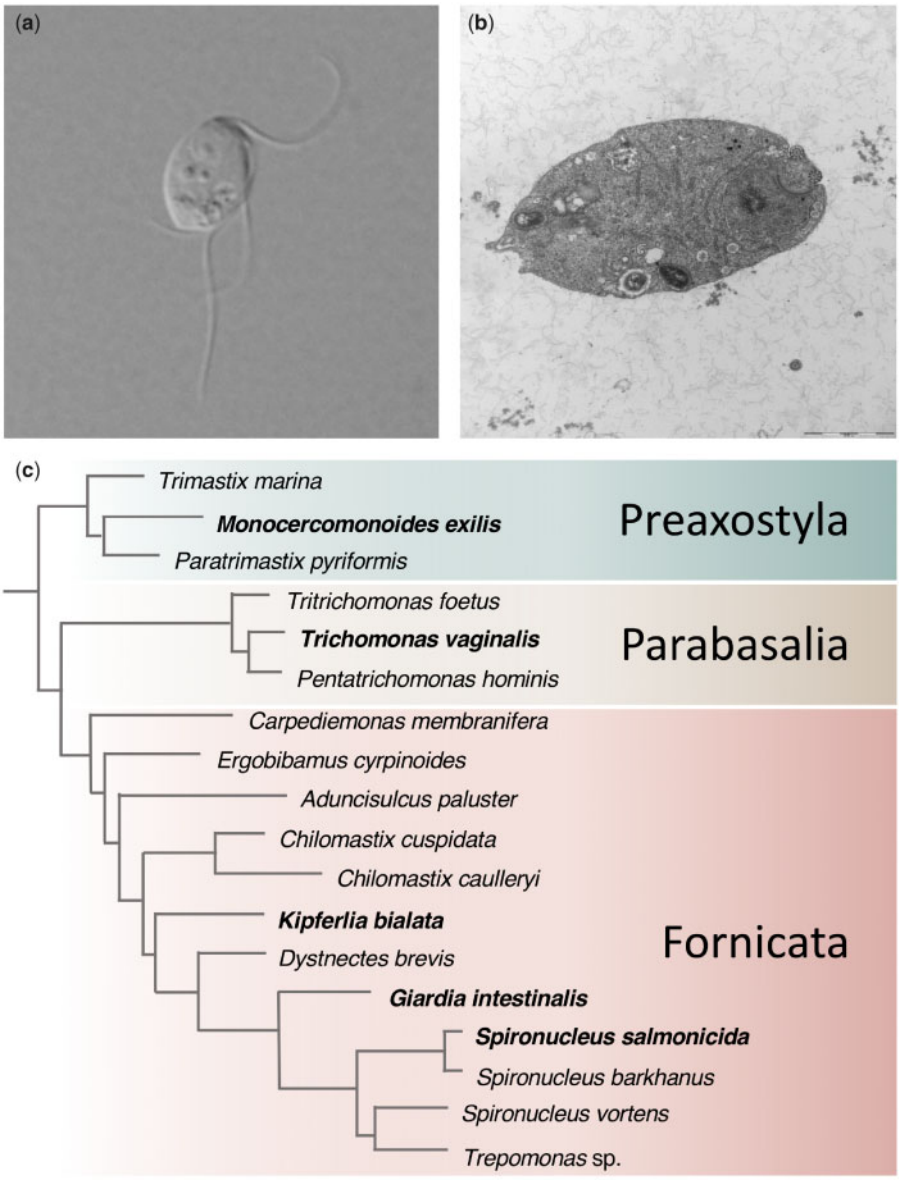

FIG. 1. The overall morphology of *Monocercomonoides exilis* and phylogeny of Metamonada. (*a*) A living cell of *M. exilis* PA203 under differential interference contrast (DIC). (*b*) TEM micrograph of *M. exilis* PA203 (credit Naoji Yubuki). (*c*) Relationships within Metamonada inferred from a phylogenomic data set (Leger et al. 2017); organisms with sequenced genomes are in bold.

M. exilis has a single long microtubular rodlike axostyle that originates from the nuclear region and is connected to the basal bodies by a characteristic fiber (i.e., the preaxostyle) consisting of a sheet of microtubules and a nonmicrotubular layer. Electron microscopic imaging of *M. exilis* showed that it lacks any conspicuous Golgi apparatus and mitochondria (Treitli et al. 2018).

Monocercomonoides exilis is a representative of a broader group of endobiotic protists called the oxymonads, which together with the free-living trimastigids, constitute the clade Preaxostyla, one of the three principal lineages of Metamonada (Leger et al. 2017; Adl et al. 2019) (fig. 1*c*). Metamonada comprise solely anaerobic/microaerophilic unicellular organisms with a diverse array of MRO types (Leger et al. 2017). Many metamonads are also parasites of agricultural or medical importance, three of which have become subject of in-depth genomic investigations: the parabasalid *Trichomonas vaginalis* (Carlton et al. 2007), the diplomonads *Giardia intestinalis* (Morrison et al. 2007), and *Spironucleus salmonicida* (Xu et al. 2014). A draft genome sequence has been reported for a free-living representative of the Fornicata, *Kipferlia bialata* (Tanifuji et al. 2018). Our *M. exilis* genome project has complemented this sampling by targeting a nonparasitic endobiont and the first representative of Preaxostyla. However, the initial genomic analysis of *M. exilis* was tightly focused on demonstrating mitochondrial absence (Karnkowska et al. 2016). Here, we present an in-depth analysis of the *M. exilis* draft genome sequence that addresses the genomic and cellular impact of mitochondrial loss in the context of metamonad evolution.

Results and Discussion

Focused Ion Beam Scanning Electron Microscope (FIB-SEM) Tomography of the Cell

To supplement the genomic analyses, corroborate the absence of mitochondria and Golgi stacks, and address several other predictions from the genomic information, we probed the *M. exilis* cell architecture by FIB-SEM tomography. We sectioned major parts of two cells fixed by two different protocols (supplementary videos S1 and S2, Supplementary Material online). The data obtained are consistent with previous transmission electron microscopy (TEM) investigation (Treitli et al. 2018). Importantly, although we acknowledge that the resolution of the microscopy could still allow for undetected highly reduced mitosomes, we did not observe any conspicuous mitochondria or MROs in this systematic examination of the *M. exilis* cells.

Genome and Predicted Proteome Features

The draft genome of *M. exilis* (Karnkowska et al. 2016, BioProject: PRJNA304271) is assembled into 2,095 scaffolds with an estimated genome size of ~75 Mb and an average GC content 36.8% (with coding regions and intergenic regions represented by 41.3% and 29% GC, respectively; table 1). By mapping sequencing reads onto the consensus genome assembly, we observed 5,150 of potential single nucleotide polymorphisms (SNPs), with the average SNP density of ~0.04 per kb. The vast majority of alternative bases have a frequency <20% (supplementary fig. S1, Supplementary Material online) suggesting that *M. exilis* cells are monoploid and most polymorphisms represent sequencing errors. This is consistent with previous fluorescence in situ hybridization (FISH) results that revealed a single signal for SUF genes in most nuclei (Karnkowska et al. 2016).

Extensive sequence diversity in terminal telomeric repeats has been found across eukaryotes where the most common, and likely ancestral, repeat type is TTAGGG (Fulnecková et al. 2013). In *M. exilis*, we identified this TTAGGG repeat element in 13 telomeric regions with at least 5 telomeric repeats at the beginning/end of the scaffold. FISH analyses with probes against telomeric repeats support the sequencing results demonstrating an average of 13 telomeric puncta in *M. exilis* nuclei (supplementary fig. S2, Supplementary Material online), suggesting the presence of 6 or 7 chromosomes. The length of telomeric regions estimated by the terminal restriction fragment method (Kimura et al. 2010) varied from 300 bases to 9 kb with a mean telomeric length of ~2.1 kb (supplementary fig. S2, Supplementary Material online).

Manual curation of the previously reported *M. exilis* genome annotation (Karnkowska et al. 2016) led to many changes including corrections of gene models and addition of new models for genes missed by the automated method originally employed. In total, 831 genes were manually curated in this study, which, together with previously curated genes (Karnkowska et al. 2016), yields a total of 1,172 manually curated genes in the current annotation release (supplementary table S1, Supplementary Material online). Three scaffolds—01876, 01882, and 01991—were recognized as probable contaminants and removed from the new version of assembly. The revised number of protein-coding genes in the *M. exilis* genome is 16,768. Homology-based approaches assigned putative functions to 6,476 (39%) *M. exilis* protein-coding genes, including 2,753 genes with domain annotations. This percentage is comparable with other metamonads, ranging from 15% of functionally annotated genes for *T. vaginalis* G3 (TrichDB Release 35) to 45% for *G. intestinalis* assemblage BGS (GiardiaDB Release 35). The annotated genome assembly and predicted genes for *M. exilis* will be available in the next release of GiardiaDB (https://giardiadb.org; last accessed 30 June, 2019).

Table 1. Summary of the *Monocercomonoides exilis* Genome Sequence Data.

Feature	Value
Genome	
Size of assembly (bp)	74,712,536
G + C content (%)	36.8
No. of scaffolds	2,092
N50 scaffold size (bp)	71,440
Protein-coding genes	
No. of predicted genes	16,768
No. of genes with introns	11,124
Mean gene length (bp)	2,703.8
Gene G + C content (%)	41.3
Mean length of intergenic regions (bp)	870.5
Intergenic G + C content (%)	29
Introns	
No. of predicted introns	31,693
Average no. of introns per gene	1.9
Intron G + C content (%)	25.2
Mean intron length (bp)	124.3
Noncoding RNA genes	
No. of predicted tRNA genes	153
No. of predicted 18S-5.8S-28S rDNA units	~50

The predicted proteins encoded by *M. exilis*, other metamonads and the heterolobosean *Naegleria gruberi* were clustered to define putative groups of orthologs (orthogroups) (fig. 2). Of the 2,031 orthogroups represented in *M. exilis*, the highest number (1,688, i.e., 83%) is shared with *N. gruberi*, which was previously suggested to be overrepresented, relative to other eukaryotes, in ancestral eukaryotic proteins (i.e., proteins that were present in the last eukaryotic common ancestor [LECA]) (Fritz-Laylin et al. 2010). The degree of orthogroup overlap was lower with *T. vaginalis* (1,564, i.e., 77%) and even more limited with diplomonads (1,057 for *G. intestinalis* and 1,065 for *S. salmonicida*, i.e., 52%). This pattern suggests that *M. exilis* has lost fewer ancestral eukaryotic proteins than other metamonads. Therefore, despite the absence of mitochondria, the proteome of *M. exilis* is likely more representative of the proteome of ancestral metamonads than that of either diplomonads or parabasalids.

The largest gene family in the *M. exilis* genome encodes protein tyrosine kinases (supplementary table S2, Supplementary Material online). The vast majority (320 out of 332 predicted tyrosine kinases) belong to the diverse tyrosine kinase-like group (supplementary table S3, Supplementary Material online). Although this group is also

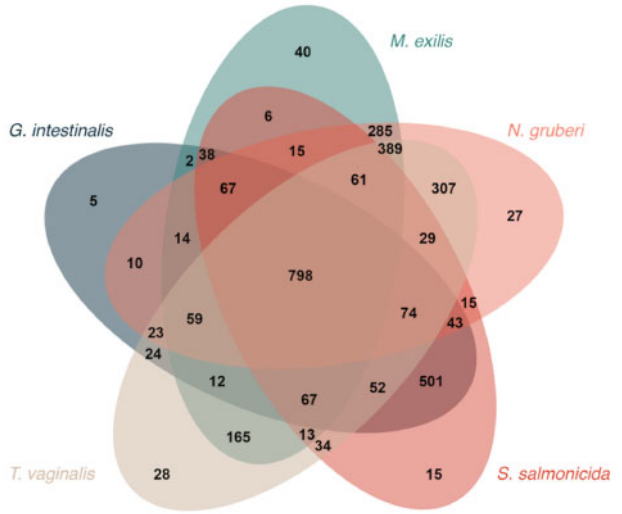

FIG. 2. Venn diagram of orthologous clusters shared and unique to *Monocercomonoides exilis*, other metamonads, and *Naegleria gruberi*.

expanded in *T. vaginalis* (Carlton et al. 2007), neither classical tyrosine kinases (TK group) nor members of the related tyrosine kinase-like group were identified in *G. intestinalis* (Manning et al. 2011), and only one occurs in *S. salmonicida* (Xu et al. 2014). Other abundant families in *M. exilis* include the Ras superfamily GTPases, cysteine proteases, and thioredoxins (see below) (supplementary table S2, Supplementary Material online).

Intron Gain and Loss in the *M. exilis* Lineage

Parasitic metamonad genomes sequenced so far are characterized by a scarcity of introns. Only 6 *cis*-spliced introns and 5 unusual split *trans*-spliced introns were found in *G. intestinalis* (Kamikawa et al. 2011; Franzén et al. 2013), 4 *cis*-spliced introns in *S. salmonicida* (Xu et al. 2014; Roy 2017), and 65 in *T. vaginalis* (Carlton et al. 2007). In contrast, we previously reported over 32,000 introns in the genome of *M. exilis* (Karnkowska et al. 2016). Sequencing of the free-living metamonad *K. bialata* revealed >120,000 introns, the highest number noted in metamonads so far (Tanifuji et al. 2018). We were unable to compare the *M. exilis* and *K. bialata* genomes because we completed our analyses prior to the release of the *Kipferlia* data.

With additional manual curation of gene models, the current estimate of the number of spliceosomal introns in *M. exilis* genome is 31,693, with an average number of 1.9 and 0.8 introns per gene and per kb of coding sequence, respectively. The high intron density is consistent with the previous report of introns in the oxymonad *Streblomastix strix* (Slamovits and Keeling 2006) and comparable with other free-living protists (e.g., *Dictyostelium discoideum*) (Eichinger et al. 2005) and well within the range exhibited by conventional eukaryotic genomes (Rogozin et al. 2012; Irimia and Roy 2014). The ubiquity of canonical GT-AG and lack of AT-AC boundaries indicates that only the major (U2-dependent) introns are present, which is consistent with the absence of minor (U12-dependent) spliceosome components (supplementary table S1, Supplementary Material online). The large number of introns in this organism increases the energetic cost of gene expression (Lynch and Marinov 2015). Clearly, sufficient ATP is produced in *M. exilis* by substrate-level phosphorylation to meet these costs in the absence of aerobically respiring mitochondria (Hampl et al. 2019).

To understand the origin and evolution of introns in *M. exilis*, we performed an analysis of the relative contribution of retention of ancestral introns and insertion of lineage-specific introns in the *M. exilis* genome. We analyzed introns in a set of 100 conserved eukaryotic genes with well-established orthologs in 34 reference species across representative lineages of eukaryotes (fig. 3). In total, these genes and species comprised 3,546 intron positions, 201 of them represented in *M. exilis* homologs. We used Dollo parsimony to reconstruct intron gains and losses along the eukaryote phylogeny using three alternative root positions. With one of the root positions, the LECA is inferred to have harbored 432 introns in this gene set, 65 of which have been retained in *M. exilis* (fig. 3*a*). This accounts for more than 30% of the *M. exilis* introns analyzed, a proportion similar to other eukaryotes (fig. 3*b*). The other two root positions give similar estimates (supplementary fig. S3*a* and *b*, Supplementary Material online). The absence of the remaining ancestral introns from the *M. exilis* genome could be explained by massive intron loss along the stem lineage of Metamonada, that is, before the split of the lineages leading to *M. exilis* on one side and the diplomonads plus *T. vaginalis* clade on the other (fig. 3*a*). However, it is to be noted that the recently sequenced genome of the diplomonad relative *K. bialata* is reported to include >120,000 introns (Tanifuji et al. 2018), so it is possible that many of these losses are in fact specific for Preaxostyla or oxymonads. Likewise, although our analysis suggests substantial acquisition of new introns in the *M. exilis* lineage (fig. 3*a* and supplementary fig. S3*a* and *b*, Supplementary Material online), the new data from *K. bialata* make it likely that many of these gains are more ancient (having occurred already in the metamonad stem lineage).

Genome Maintenance and Expression in *M. exilis*

Given the extraordinary absence of mitochondrial organelles from *M. exilis*, we examined genes encoding components of other cellular systems to assess whether they were similarly reduced or unusual.

We first investigated the systems responsible for maintenance and expression of the *M. exilis* nuclear genome. We identified all expected universally conserved genes encoding nucleus-functioning proteins (Iyer et al. 2008). For example, *M. exilis* encodes all four core histones (H2A, seven variants; H2B, three variants; H3; two variants; and H4, one variant) as well as the linker histone H1 (supplementary table S1, Supplementary Material online).

All essential components involved in DNA unwinding, primer synthesis, and DNA replication were also present in the *M. exilis* genome (supplementary table S1, Supplementary Material online). The origin recognition complex of *G. intestinalis* and *T. vaginalis* each contain ORC1 and ORC4, whereas *S. salmonicida* relies on a CDC6 complex. In *M. exilis*, we were only able to identify ORC1. In terms of replication machinery, most metamonads do not encode replication protein A

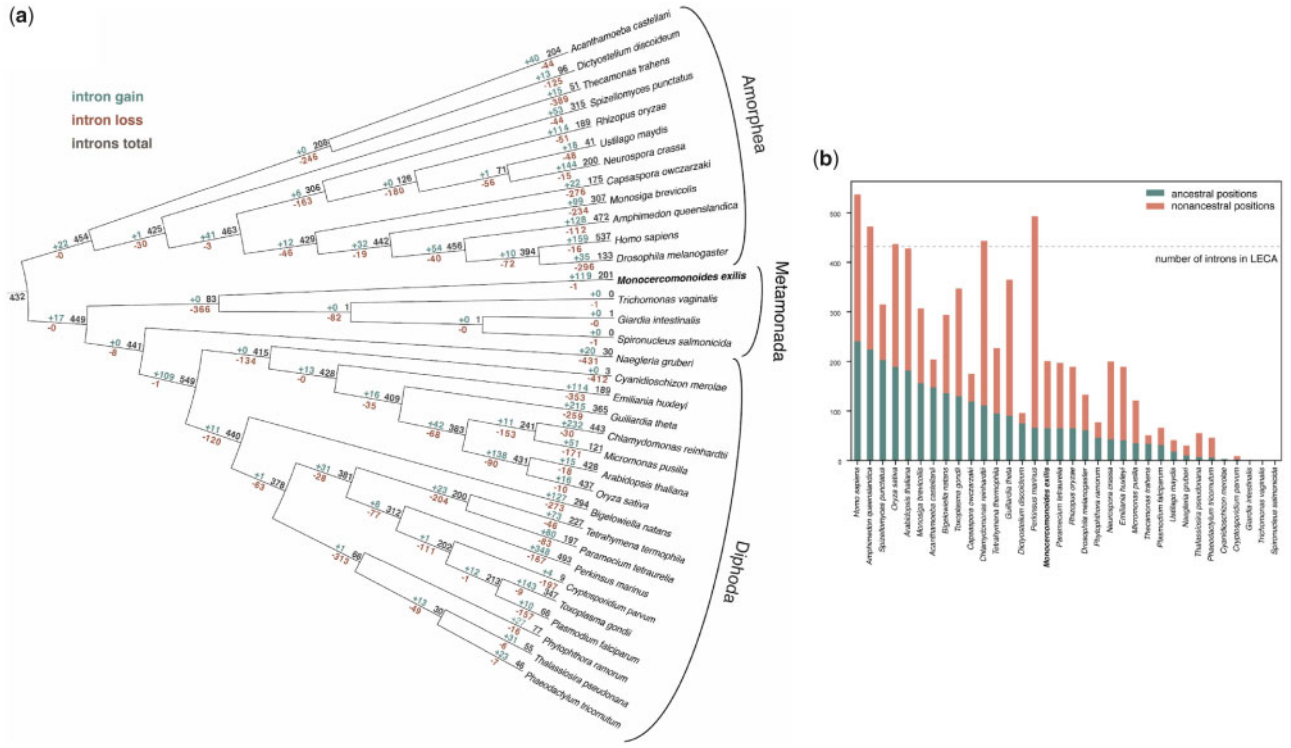

FIG. 3. Intron gains and losses along the eukaryote phylogeny. (*a*) Intron gains and losses along the eukaryote phylogeny as reconstructed by Dollo parsimony. The numbers are derived from an analysis of 3,546 intron positions in a reference set of 100 groups of orthologous genes of 34 phylogenetically diverse species. Root of the eukaryote phylogeny was considered between Amorphea and the remaining eukaryotes included in the analysis. (*b*) Numbers of ancestral (i.e., inherited from the LECA) and nonancestral (i.e., lineage-specific) introns in different eukaryotes. Derived from the analysis described in (a).

heterotrimeric complex or have a drastically reduced complex consisting of only one protein in the case of diplomonads (Morrison et al. 2007; Xu et al. 2014). Surprisingly, we identified all subunits of the replication protein A heterotrimeric complex in *M. exilis* (supplementary table S4, Supplementary Material online). In addition, similar to eukaryotes in general (Forterre et al. 2007), *M. exilis* employs two different types of topoisomerase I, Topo IB and Topo III, whereas parabasalids and fornicates have retained only the latter type (supplementary table S4, Supplementary Material online).

We similarly identified most of the components of various DNA repair pathways including base excision repair, nucleotide excision repair, and mismatch repair pathways (Costa et al. 2003; Kunkel and Erie 2005; Almeida and Sobol 2007; Fukui 2010) (supplementary tables S1 and S4, Supplementary Material online). The mismatch repair pathway appears to be complete in all other sequenced metamonads, whereas the base excision repair and nucleotide excision repair pathways are most complete in *M. exilis*, especially when compared with *G. intestinalis* or *S. salmonicida* (Marchat et al. 2011) (supplementary table S4, Supplementary Material online). The nonhomologous end joining pathway involved in repairing double-strand breaks is missing in *M. exilis*, similarly to other metamonads (Carlton et al. 2007; Morrison et al. 2007). However, the homologous recombination repair pathway for double-strand breaks repair is encoded in the *M. exilis* genome (supplementary table S4, Supplementary Material online) and looks more complete in *M. exilis* than in other metamonads.

We also investigated the complement of general transcription factors in *M. exilis* and identified subunits of all general transcription factors known to be highly conserved among eukaryotes (Orphanides et al. 1996; Latchman 1997; de Mendoza et al. 2013) (supplementary table S1, Supplementary Material online). Notably, *M. exilis* possesses both subunits of TFIIA, the primary function of which is stabilization of the preinitiation complex and assistance in the binding of TBP to the TATA box in promoters (Tang et al. 1996). The presence of TFIIA is in agreement with the presence of TATA-like motifs in ~52% of *M. exilis* promoter regions (3,374/6,509 genes with predicted UTR) (supplementary fig. S4, Supplementary Material online). In contrast, *T. vaginalis* lacks TFIIA, and an M3 motif has replaced the TATA box in this lineage (Smith et al. 2011).

Regarding the translation machinery, we identified 30 proteins in the *M. exilis* genome annotated as eukaryotic initiation factors or their associated factors (supplementary table S1, Supplementary Material online). This set is nearly complete compared with the mammalian translation machinery and it is almost identical to the sets of eukaryotic initiation factors present in the genomes of *T. vaginalis* and *G. intestinalis* (Kanehisa et al. 2014) (supplementary table S1, Supplementary Material online). Of note is the presence in *M. exilis* of enzymes responsible for the formation of

diphthamide (supplementary table S1, Supplementary Material online), a modified histidine residue present in archaeal and eukaryotic elongation factor 2 and important for its proper function (Su et al. 2013). The retention of this modification in *M. exilis* contrasts with the situation in parabasalids recently shown to have lost diphthamide biosynthesis genes (Narrowe et al. 2018).

Actin and Tubulin Cytoskeleton

The extensive cytoskeletal apparatus, including the hallmark oxymonad axostyle, is one of the better-described fascinating aspects of the cellular architecture of *Monocercomonoides* (Radek 1994; Treitli et al. 2018). Like many other cellular systems of *Monocercomonoides*, the actin and tubulin cytoskeletons of diplomonads and parabasalids depart in various ways from the general picture seen in other eukaryotes. The metamonad actin cytoskeleton is reduced and modified (supplementary tables S1 and S5, Supplementary Material online), with the highest reduction in *G. intestinalis* (Morrison et al. 2007; Paredez et al. 2014). *Monocercomonoides exilis* shares some of the unusual modifications with other metamonads, as it, for example, lacks proteins containing the myosin head domain, a trait that has so far only been reported from some rhodophytes, *T. vaginalis*, and diplomonads (Sebé-Pedrós et al. 2014; Brawley et al. 2017). On the other hand, it stands out by possessing a more complete set of actin family proteins (including actin-related proteins; ARPs) than other metamonads. Specifically, it has retained ARP4 and ARP6, important nuclear ARPs serving in several chromatin-remodeling complexes (Oma and Harata 2011), and also a gene for the actin-binding protein villin. However, its actual repertoire of proteins associated with the actin cytoskeleton is less complex than that of *T. vaginalis* (Kollmar et al. 2012) (supplementary tables S1 and S5, Supplementary Material online).

Monocercomonoides exilis encodes a conventional set of tubulins that is similar to those found in other metamonad organisms. All metamonads analyzed contain at least one complete gene for alpha-, beta-, gamma-, delta-, and epsilon-tubulin. The sixth ancestral eukaryotic paralog, zeta-tubulin, has frequently been lost during eukaryote evolution (Findeisen et al. 2014) and is also missing from metamonads including *M. exilis* (supplementary tables S1 and S5, Supplementary Material online). All metamonads also contain multiple members of both groups of motor proteins associated with microtubules, that is, kinesins (primarily mediating plus end-directed transport) and dyneins (mediating minus end-directed transport and flagellar motility). Our comprehensive phylogenetic analysis (supplementary fig. S5, Supplementary Material online) showed that the family of kinesins is well represented in metamonads. Of the 17 previously defined kinesin families with wide taxonomic distribution (Wickstead et al. 2010), only 3 are missing from metamonads as a whole, albeit others may be only patchily distributed in the group (supplementary table S5, Supplementary Material online).

Dyneins are large multi-subunit complexes consisting of one or more dynein heavy chains (DHC) and a variable number of intermediate chains, light intermediate chains, and light chains. Interestingly, eukaryotes use just a single dynein complex (called cytoplasmic dynein 1) for nearly all cytoplasmic minus end-directed transport (Roberts et al. 2013). In accordance with the previous reports for *G. intestinalis* and *T. vaginalis* (Wickstead and Gull 2012), *M. exilis* lacks two important components of the cytoplasmic dynein 1 complex, namely the specific intermediate (DYNC1I1) and light intermediate (DYNC1LI) chains, while keeping the heavy chain (DHC1) that constitutes the center of the complex. In eukaryotes, the presence of the cytoplasmic dynein 1 is coupled to the presence of the dynactin complex, a large multisubunit protein complex that enhances the motor processivity and acts as an adapter between the motor complex and the cargo. *Trichomonas vaginalis* and *G. intestinalis* have been reported as rare examples of eukaryotes lacking the dynactin complex in the presence of cytoplasmic dynein 1 (Hammesfahr and Kollmar 2012). Here, we show that all subunits specific to the dynactin complex are also missing from *M. exilis*, suggesting the absence of the complex from metamonads in general. The set of the axonemal dyneins is nearly complete in metamonads including *M. exilis* (supplementary fig. S6, Supplementary Material online). We are the first to report the dynein intermediate chain WDR34, a specific component of the intraflagellar transport dynein in metamonads.

The conservation of microtubule-dependent chromosome separation across extant eukaryotes strongly suggests that this feature was present in LECA. Microtubules and chromatids are connected by the kinetochore, a multiprotein structure that is assembled on centromeric chromatin. Based on comparative studies, orthologs of 70 kinetochore proteins have been identified in various eukaryotes suggesting that LECA had a complex kinetochore structure (van Hooff et al. 2017). However, the metamonads that have been studied to date have closed or semiopen mitosis (Ribeiro et al. 2002; Sagolla et al. 2006) and their kinetochores are divergent and degenerated in comparison to kinetochores of model organisms such as human or yeast (van Hooff et al. 2017). Of the 70 kinetochore orthologs, we have identified 15 in *M. exilis*, a comparable number to those identified in *G. intestinalis* (16), and slightly fewer than in *T. vaginalis* (27) (supplementary table S6, Supplementary Material online). Although the kinetochore is reduced, all investigated metamonads possess the most conserved components including Skp1, Plk, Aurora, or CenA suggesting the presence of a functional kinetochore in these species.

Overall, our analyses suggest that except for dispensing with myosin-based motility and the dynactin complex—traits shared by all metamonads for which genome data is available to date—*M. exilis* has a relatively canonical complement of cytoskeletal proteins.

Standard and Unconventional Aspects of the Endomembrane System

The endomembrane system is a critical interface between an organism and its extracellular environment, and it underpins host-parasite interactions in many microbial eukaryotes. The *M. exilis* endomembrane system noticeably lacks any reported morphologically recognizable Golgi bodies (Radek 1994;

Treitli et al. 2018) prompting suggestions of organelle absence similar to mitochondria. From our FIB-SEM data (supplementary videos S1 and S2, supplementary fig. S7, Supplementary Material online), we note that the cells contain a well-developed endoplasmic reticulum (ER), which sometimes forms stacks superficially resembling Golgi. However, these ER structures can clearly be distinguished by the ribosomes attached to their surfaces. Golgi stacks were not observed. On the other hand, our previous genomic analyses identified 84 genes that serve as indicators of Golgi presence, starkly contrasting with the absence of mitochondrial hallmark proteins (Karnkowska et al. 2016). To better characterize the endomembrane system of *M. exilis*, we have expanded our genomic analysis of membrane-trafficking machinery.

Monocercomonoides exilis has a relatively canonical complement of endomembrane system proteins (fig. 4) encoding most of the basic eukaryotic set (Koumandou et al. 2007). It shows neither extensive reduction nor expansion of this set as observed in the *G. intestinalis* (Morrison et al. 2007) and *T. vaginalis* (Carlton et al. 2007) genomes, respectively. For several protein membrane-trafficking complexes, we observed multiple versions of some components, but the lack of others. The retromer complex transports internalized plasma membrane receptors from endosomes to the trans-Golgi network (Seaman 2004). Although the cargo-recognition subcomplex was identified in *M. exilis*, neither membrane-deforming sorting nexin proteins nor the conventional cargo protein, Vps10, could be found. This is unusual, but not unprecedented, in eukaryotes (Koumandou et al. 2011). We found an expanded set of components for ESCRT II, III and IIIa subcomplexes, but a lack of all but Vps23 of the ESCRT I subunits. ESCRT complexes are best known for their role in protein degradation at the multivesicular body (MVB) and functional MVBs have been identified in *Tetrahymena* which also possesses only Vps23 as its ESCRT I (Leung et al. 2008; Cole et al. 2015). The genomic data predict that MVBs should exist in *M. exilis*, and indeed candidate MVBs—that is, single-membrane bound small compartments with internal vesicles—were frequently observed in the FIB-SEM images (supplementary fig. S7). The presence of this organelle could be significant as these compartments are the source of exosomes which are implicated in host-endobiotic interactions (Schorey et al. 2015). Finally, we observed at least two sets of all components of the HOPS complex that acts at the late endosome, but we were unable to identify any of the subunits that are specific to the CORVET complex that acts upstream at the early endosomes. Intriguingly, the Vps39, a HOPS-specific component has been recently shown to function in vacuole-mitochondria contact sites (vCLAMP), with Tom40 as the direct binding partner on mitochondria (González Montoro et al. 2018). This highlights the potential to use *M. exilis* to disentangle nonmitochondrial functions of this protein without the indirect effect on mitochondria. Similarly, Vps13, has been proposed to be present in several membrane contact sites, including endosome–mitochondrion contacts (Park et al. 2016) and proven to influence mitochondrial morphology in human cells (Yeshaw et al. 2019). Four Vps13 paralogs are encoded in the *M. exilis* genome.

We observed multiple paralogs of subunits in some endosomal-associated complexes potentially indicating diversified endolysosomal pathways. Some of the paralog expansions were small, such as the adaptor protein complexes, Rab11, and endosomal Qa-SNAREs together with their interacting SM proteins. Other complexes were more extensively expanded, including four paralogs of Syn6, EpsinR, Vps34, and TBC-F, five SMAP paralogs, and eight VAMP7 R-SNAREs. It is particularly striking that, despite encoding a single copy of the Rab7-specific GEFs Mon1 and CCZ1 (supplementary fig. S8 and supplementary table S1, Supplementary Material online) like other eukaryotes, *M. exilis* has an expanded set of Rab7 paralogs, including nine "conventional" Rab7 paralogs and a clade of nine additional very divergent Rab7-like (Rab7L) paralogs not found in other eukaryotes so far (supplementary fig. S9, Supplementary Material online). Some Rab7L loci are apparently nonfunctional (with coding sequences disrupted by mutations), indicating birth-and-death evolution of this gene group. Hence, we speculate that the Rab7L clade is involved in a novel, rapidly evolving endocytic process in *M. exilis*. Consistent with the observed diversified complement of endolysosomal membrane-trafficking machinery, we also noted that the cytoplasm contains numerous vesicles with electron lucent matrix some of them containing food particles (putative phagosomes), and others resembling endosomes of various shapes and sizes (supplementary fig. S7, Supplementary Material online). The conspicuous dark round globules observed in supplementary video S1, Supplementary Material online, are very likely glycogen granules observed also under classical TEM (Treitli et al. 2018).

Expanded Set of Proteolytic Enzymes

Proteases are important virulence factors for parasites and are known to degrade the host's extracellular matrix during the invasion (Sajid and McKerrow 2002). We identified 122 protease homologs, divided into 4 catalytic classes (cysteine, metallo, serine, and threonine) and 14 families according to Merops protease classification (Rawlings et al. 2008) (supplementary table S7, Supplementary Material online). The expansion of cysteine proteases is consistent with the expanded complement of Cathepsin B cysteine proteases previously observed in *M. exilis* (Dacks et al. 2008). We confirmed that the *M. exilis* genome encodes 44 Cathepsin B paralogs but no Cathepsin L genes (supplementary fig. S10). The high number of cysteine proteases is surprising because *M. exilis* is considered a commensal rather than a parasite. The large number of cysteine proteases previously reported for parasitic metamonads are often thought to be involved in tissue destruction or host defense (Carlton et al. 2007; Xu et al. 2014).

Salvage of Nucleotides from the Gut Environment

Gut symbionts often lose the ability to biosynthesize cellular building blocks like nucleotides, and *M. exilis* appears to be no exception. *Monocercomonoides exilis* lacks enzymes for de novo synthesis and catabolism of purines or pyrimidines

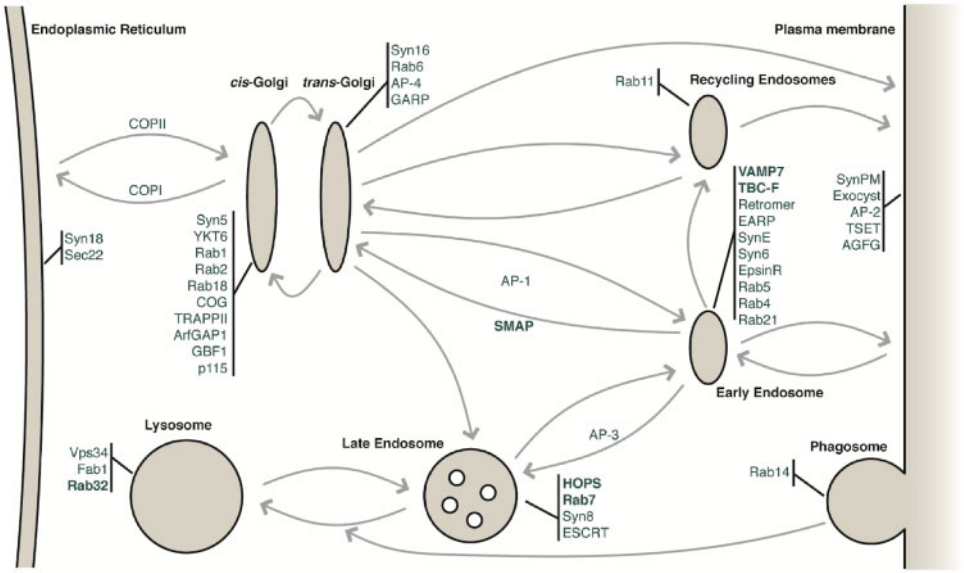

FIG. 4. Results of bioinformatic analysis of membrane-trafficking machinery in *Monocercomonoides exilis*. The presence of membrane-trafficking compartments and pathways is hypothesized as shown, based on the complement of trafficking machinery identified, and the function of their homologs in model systems. Selected membrane-trafficking proteins and protein complexes identified in the genome of *Monocercomonoides exilis* are shown. Several genes for membrane-trafficking proteins appear to have undergone lineage-specific duplications, and these are shown in bold font.

(supplementary table S1 and supplementary fig. S11, Supplementary Material online). This implies that the cell depends on external sources of these compounds that are incorporated into the nucleotide pool by salvage pathways in a manner similar to *T. vaginalis*, *G. intestinalis*, and several trypanosomatids (de Koning et al. 2005) (supplementary table S8, Supplementary Material online). However, there are some notable differences to other metamonads in the set of enzymes that may be used for salvaging of nucleotides (Aldritt et al. 1985; Munagala and Wang 2002; Munagala and Wang 2003). Probably the most crucial difference is that *M. exilis*, unlike *T. vaginalis* and *G. intestinalis*, does not rely on the salvage of deoxyribonucleotides (Wang and Cheng 1984; Baum et al. 1989), as it can convert ribonucleotides to deoxyribonucleotides by the action of ribonucleoside-triphosphate reductase.

Is the Absence of Mitochondrion Reflected in Modifications of Any Cellular System?

Mitochondria are tightly integrated into various systems/pathways in typical eukaryotic cells (Roger et al. 2017). It is therefore of interest to investigate how these systems are affected by the loss of mitochondria in *M. exilis*. Changes related to mitochondrial loss can be divided into three categories: 1) preadaptations, which subsequently made mitochondria dispensable, 2) functions lost concomitantly with mitochondria, and 3) postadaptations that evolved to compensate for the absence of mitochondria. Only specific changes in *M. exilis* not present in other Metamonada should be considered, but one should always keep in mind that even *M. exilis*-specific features may reflect adaptation to anaerobiosis or endobiotic lifestyle with no direct link to mitochondrial loss.

Like many anaerobic protists, *M. exilis* cannot synthesize ATP by oxidative phosphorylation; instead, the ATP is synthesized via glycolysis in the cytosol (Karnkowska et al. 2016). Coupled with the loss of oxidative phosphorylation, *M. exilis* does not encode genes for any of the tricarboxylic acid cycle enzymes (Karnkowska et al. 2016).

In some anaerobic organisms, glycolysis-derived pyruvate is oxidized to acetyl-CoA by pyruvate:ferredoxin oxidoreductase with the concomitant reduction of ferredoxin, which, in turn, serves as an electron donor for hydrogen evolution via an [FeFe]-hydrogenase (HYD). In *G. intestinalis* and *Entamoeba histolytica*, the resulting acetyl-CoA can be fermented to ethanol, catalyzed by the bifunctional aldehyde/alcohol dehydrogenase E (ADHE), or is converted to acetate by acetyl-CoA synthetase (ADP-forming) (Ginger et al. 2010). The latter reaction produces one molecule of ATP. We identified homologs of PFO, HYD, ADHE, and acetyl-CoA synthetase in the *M. exilis* genome (fig. 5 and supplementary table S1, Supplementary Material online). Acetate may be further fermented to aldehyde and ethanol by aldehyde dehydrogenase and ADHE suggesting that ethanol may be the final fermentation product in *M. exilis*.

As we reported previously, *M. exilis* possesses a complete arginine deiminase pathway that enables it to produce ATP by conversion of arginine to ornithine, NH_3, and CO_2 (Novák et al. 2016). Further analyses of its genome suggest that *M. exilis* can generate ATP by metabolizing other amino acids, including tryptophan, cysteine, serine, threonine, and methionine (fig. 6*a* and *b*, Supplementary Material online), as was previously reported in other protists (Anderson and Loftus 2005). One notable aspect of the amino acid catabolism in *M. exilis* is the presence of tryptophanase, an enzyme which occurs rarely in eukaryotes and has been found so far only

FIG. 5. Carbon and energy metabolism in *Monocercomonoides exilis*. Glucose metabolism (brown), pyruvate metabolism (red), and pentose-phosphate metabolism (green). Abbreviations and Enzyme Commission numbers are given in supplementary table S1, Supplementary Material online.

in anaerobic protists *T. vaginalis*, *Tritrichomonas foetus*, *Mastigamoeba balamuthi*, *Blastocystis* spp., *Pygsuia biforma*, and *E. histolytica* (Eme et al. 2017). Among the products of tryptophan degradation by tryptophanase is indole, a signaling molecule important, for example, for interactions between mammalian host and enteric bacteria, and indeed, *Ma. balamuthi* was shown to produce significant amounts of indole (Nývltová et al. 2017). The pentose-phosphate pathway (PPP) is integrated with the main metabolic energy generating pathways. PPP is involved in the generation of NADPH and pentose sugars and has an oxidative and a nonoxidative phase. We were unable to find homologs of the enzymes for

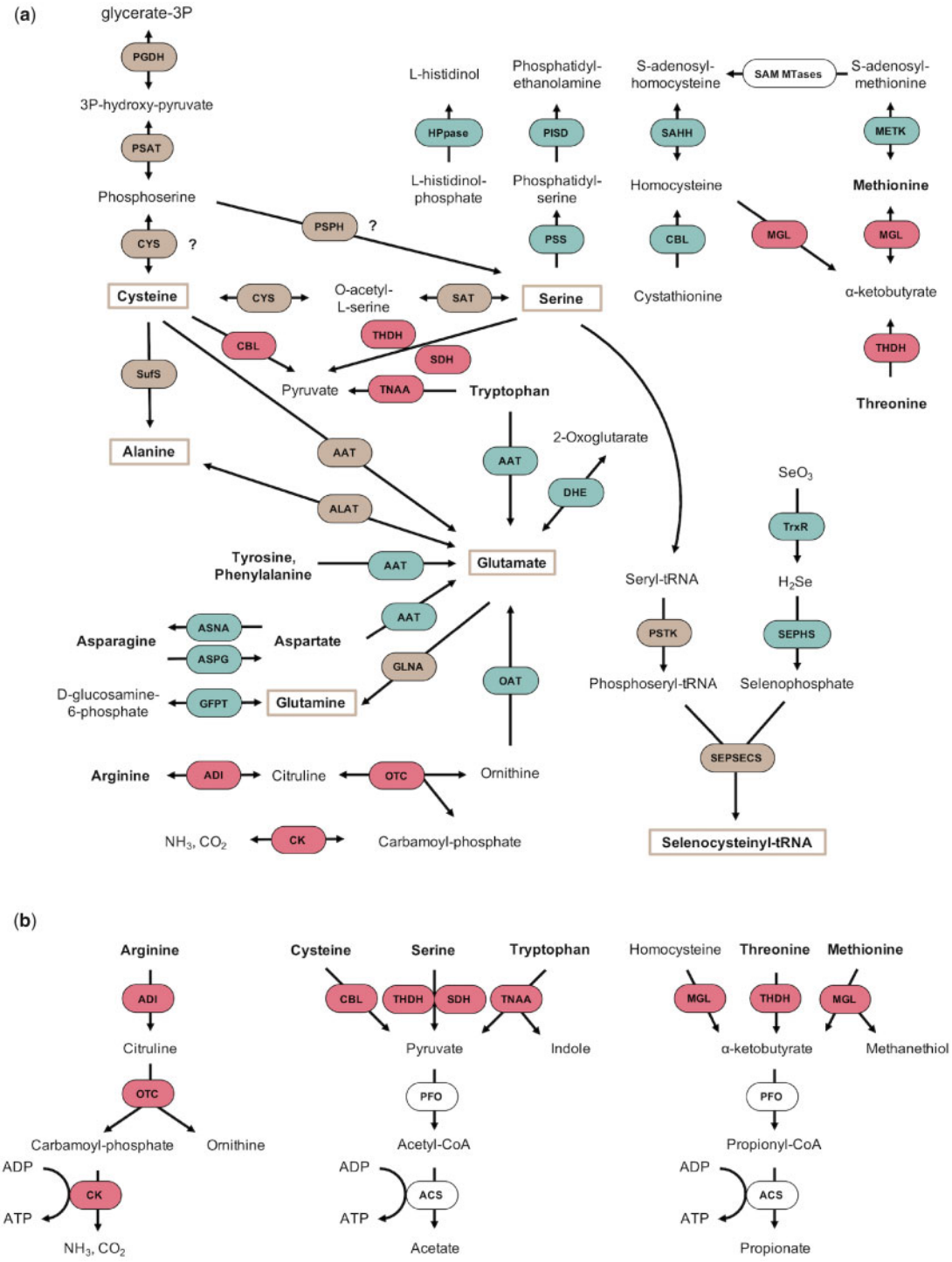

FIG. 6. Putative amino acid related biochemical pathways in *Monocercomonoides exilis*. (*a*) Amino acid metabolism. (*b*) Reactions putatively involved in ATP production by amino acids catabolism. Abbreviations and Enzyme Commission numbers are given in supplementary table S1, Supplementary Material online. Brown color indicates enzymes and products of putative amino acid biosynthesis pathways. Red color indicates enzymes putatively involved in ATP production by amino acids catabolism. Question marks indicate alternative pathways for cysteine and serine biosynthesis. "SAM MTases" stands for various S-adenosyl-methionine-dependent methyltransferases.

the oxidative phase but identified those for the nonoxidative one (fig. 5 and supplementary table S1, Supplementary Material online). We propose that the oxidative phase is likely absent in *M. exilis*, which is not unusual, as a truncated PPP has also been observed in *E. histolytica* (Loftus et al. 2005). The dehydrogenase reactions of the oxidative PPP are considered as one of the primary cellular sources of NADPH; therefore, NADPH must be synthesized via an alternative route in *M. exilis*. One such NADPH-generating enzyme might be the putative NAD(P)-dependent glyceraldehyde-3-phosphate dehydrogenase (GAPN) identified in the *M. exilis* genome (supplementary table S1, Supplementary Material online). It was

proposed that GAPN plays an important role in NADPH generation in bacteria and archaea (Spaans et al. 2015). Interestingly, the *M. exilis* GAPN was identified as a lateral gene transfer (LGT) candidate (supplementary table S9, Supplementary Material online). In summary, the NAD(P)H and ATP generation pathways in *M. exilis* resemble those reported for mitosome-bearing anaerobes, and so there is no indication that they were affected by the complete loss of mitochondria.

An essential function of mitochondria and MROs in eukaryotes is the synthesis of Fe–S proteins. The ISC pathway, otherwise considered to be an essential house-keeping pathway in eukaryotes, was functionally replaced in all examined Preaxostyla by the SUF pathway (Vacek et al. 2018). We have argued previously that this replacement was a preadaptation for the subsequent loss of mitochondria in this lineage (Karnkowska et al. 2016). This unprecedented event apparently did not influence the number of Fe–S proteins in the cell, as we identified 70 candidates for such proteins in *M. exilis*, with no essential Fe–S protein missing (supplementary table S10, Supplementary Material online). With the exception of xanthine dehydrogenase containing a 2Fe–2S cluster, all other proteins, for which the type of cluster can be estimated, appear to have 4Fe–4S clusters. Similarly, 4Fe–4S clusters are more abundant than 2Fe–2S clusters in other anaerobes (Andreini et al. 2017). The presence of the full array of essential Fe–S proteins in *M. exilis* suggests that its cytosolic SUF and CIA systems are fully capable of satisfying cellular Fe–S cluster needs.

In most eukaryotes, fatty acid metabolism is integrated between the mitochondria, ER and peroxisomes. *Monocercomonoides exilis* possesses all the proteins necessary for the synthesis of diacylglycerol and for the interconversion of phosphatidylcholine, phosphotidylethanolamine, and phosphatidylserine from phosphatidate. It also possesses a suite of putatively ER-localized fatty acid biosynthesis proteins for very long fatty acid elongation by using malonyl-CoA (supplementary table S1, Supplementary Material online). However, we were unable to identify components for shorter chain fatty acid biosynthesis or fatty acid degradation pathways. Reduction of the fatty acid synthesis complex is also known from other microaerophilic protists such as *G. intestinalis* (Morrison et al. 2007) and *E. histolytica* (Loftus et al. 2005), both mitosome-possessing gut parasites. Given the lack of some lipid biosynthetic and degradation pathways, and the lack of any MRO in *M. exilis*, we searched for evidence of peroxisomes, an organelle that has long been predicted as also absent due based on microscopic evidence. Loss of peroxisomes (and peroxins) has been confirmed in several groups across the tree of eukaryotes and is often associated with the reduction of mitochondria (Žárský and Tachezy 2015; Gabaldón et al. 2016). We searched the *M. exilis* genome for peroxin homologs, but only Pex19, a cytosolic receptor for proteins targeted to the peroxisomal membrane, was found. This suggests that *M. exilis* lacks peroxisomes and that retention of Pex19 reflects a peroxisome-independent function of the protein, possibly associated with the ER (Yamamoto and Sakisaka 2018). This result is also consistent with our failure to identify any of the ER-localized Dsl1 complex subunits, as losses of peroxisomes and Dsl1 subunits are correlated (Klinger et al. 2013). As the peroxisomes are lost in many anaerobes, their absence cannot be attributed to the loss of mitochondria.

A second key role of both mitochondria and peroxisomes is the oxidative stress response. Lack of oxygen-dependent mitochondria and their reduction to MROs reduce the impact of the organelle on the production of reactive species in anaerobic and microaerophilic protists. However, many of them are transiently exposed to oxygen and have evolved a variety of strategies to cope with oxygen stress. Intracellular proteins and low-molecular-weight thiols are the main cellular antioxidants present in anaerobic protists (Müller et al. 2003). In the *M. exilis* genome, we identified superoxide dismutase responsible for the radical anion ($O^{2-\cdot}$) detoxification to O_2 and H_2O_2. We also found candidates for catalase and peroxiredoxins, which are involved in reduction of H_2O_2 to O_2 and H_2O, and hybrid cluster protein and rubrerythrin, which decompose H_2O_2 to H_2O (supplementary fig. S12 and supplementary table S1, Supplementary Material online). Peroxiredoxins must be recharged by reduction in reaction with thioredoxin, which also have been identified in the *M. exilis* genome (supplementary fig. S12 and supplementary table S1, Supplementary Material online). In other metamonads such as *G. intestinalis* or *S. salmonicida*, the main nonprotein thiol is cysteine (Brown et al. 1993; Stairs et al. 2019); the putative ability of *M. exilis* to synthesize cysteine suggests that cysteine might be also the main nonprotein thiol in this organism.

Our analysis of the *M. exilis* genome revealed an expanded repertoire of genes involved in oxygen stress response, mainly acquired by LGT from bacteria (supplementary table S9, Supplementary Material online). *Monocercomonoides exilis* genome encodes homologs of not only ruberythrin, nitroreductase, and flavodiiron protein but also rare among eukaryotic microaerophiles, of catalase, and hemerythrin, an enzyme involved in the protection of Fe–S cluster-containing proteins from oxidative damage in microaerophilic bacteria (Kendall et al. 2014) (supplementary table S9, Supplementary Material online). This enlarged set of proteins involved in oxygen stress response might be related to the complete loss of mitochondria. However, as many microaerophilic/anaerobic protists are also known to possess an expanded set of oxygen stress response proteins, this feature of *M. exilis* may instead just be reflective of its ecological niche.

Amino acid biosynthesis is another canonical mitochondrial function. *Monocercomonoides exilis* seems to be able to synthesize at least alanine, serine, cysteine, and selenocysteine, and, assuming availability of 2-oxoglutarate, also glutamate and glutamine (relevant biosynthetic pathways are highlighted in brown in fig. 6*a*). The crucial first step seems to be the synthesis of serine from a glycolysis intermediate 3-phosphoglycerate by a pathway consisting of three reactions. A gene encoding the enzyme catalyzing the third reaction, phosphoserine phosphatase, was not conclusively identified in *M. exilis* genome, but a possible candidate is the protein MONOS_5832 which is similar to the phosphoserine

phosphatase recently characterized in *E. histolytica* (Kumari et al. 2019). Alternatively, it has been shown that the conversion of phosphoserine to cysteine can be catalyzed by cysteine synthase in *T. vaginalis* (Westrop et al. 2006); this might also be the case for *M. exilis*. The reconstructed amino acid metabolic network (fig. 6*a*, supplementary table S1, Supplementary Material online) of *M. exilis* is more complex than those reported for *G. intestinalis* (Morrison et al. 2007), *E. histolytica* (Loftus et al. 2005), and *Cryptosporidium parvum* (Abrahamsen et al. 2004), but less complex than the amino acid metabolism of *T. vaginalis* (Carlton et al. 2007). *Monocercomonoides exilis* also lacks the glycine cleavage system (GCS) and serine hydroxymethyltransferase (SHMT), which are both present in its close relative *Paratrimastix pyriformis*, where they localize into the MRO (Hampl et al. 2008; Zubáčová et al. 2013). Related to amino acid metabolism and translation is the finding that the *M. exilis* genome encodes components of selenium utilization machinery, including enzymes responsible for the synthesis of selenocysteinyl-tRNA and the translation factor SelB required for selenocysteine incorporation into proteins during translation (supplementary table S1, Supplementary Material online). *Trichomonas vaginalis* and *G. intestinalis* do not utilize selenium, but certain *Spironucleus* species possess selenoproteins and selenocysteine biosynthesis machinery, with predicted roles in oxygen defense (Stairs et al. 2019). The latter proteins are related to the proteins we identified in *M. exilis* (Roxström-Lindquist et al. 2010). Out of the 49 genes encoding the 34 enzymes putatively involved in amino acid metabolism discussed above, 17 are of prokaryotic origin (supplementary table S9, Supplementary Material online) and were likely acquired via LGT. For comparison, the reconstructed amino acid metabolism of *T. vaginalis* contains 36 enzymes, 9 of which were identified as LGT candidates (Carlton et al. 2007). In summary, only the absences of GCS (a strictly mitochondrial complex) and SHMT are directly related to the absence of mitochondria. The loss of these enzymes, which might have accompanied the transition to an endobiotic lifestyle, removed another essential function from the MRO of the *M. exilis* ancestor, preadapting it for loss of the organelle.

In model systems, the mitochondrion is involved in the regulation of calcium homeostasis in the cell. The calcium flux is regulated by opening of Ca^{2+} channels on the cytoplasmic membrane and by pumping of Ca^{2+} into extracellular space and into the internal Ca^{2+} stores. The ER, mitochondria, and other endomembrane vesicles function as these stores (Contreras et al. 2010; García-Sancho 2014). In *M. exilis*, we identified five paralogs of the plasma membrane calcium-cation exchangers which are responsible for the regulation of the intracellular Ca^{2+} concentration (Yu and Choi 1997). Additionally, we identified seven paralogs of P-type Ca^{2+}-ATPases which also transport Ca^{2+} ions across the plasma membrane (Schatzmann 1966) and the ER membrane (Vandecaetsbeek et al. 2011). For comparison, *T. vaginalis* possesses four and six of these respective paralogs (not shown). This suggests that there were no obvious changes in the inventory of Ca^{2+} transporters associated with the loss of mitochondria.

The final systems we specifically examined were related to autophagy and cell death. While analyzing the membrane-trafficking system, we noted the presence of seven homologs of Rab32, including representatives of both main ancestral paralogs in this family (Rab32A and Rab32B; Elias et al. 2012). In mammalian cells, Rab32 proteins are associated with specialized lysosome-derived compartments, ER, mitochondria, and autophagosomes. We hypothesized that some aspects of the extended endolysosomal machinery described above, especially the multiple paralogs of Rab32, in the absence of mitochondria, could be related to the autophagosomal machinery. We therefore further examined the autophagosomal machinery encoded in the *M. exilis* genome (fig. 7 and discussed below).

Autophagy, the process by which large cellular compartments and cytosolic complexes are degraded, involves the mitochondria, as well as the ER, via the regulation of calcium, reactive oxygen-species, and physical association (Gomez-Suaga et al. 2017). Approximately 30 proteins, found broadly conserved across eukaryotes, are involved in the initiation, formation, and function of the autophagosomes (Gomez-Suaga et al. 2017). Interestingly, the AuTophaGy related 1 complex (Atg1; mammalian ULKs 1, 2, and 3) is almost entirely missing in *M. exilis*, *T. vaginalis*, and *N. gruberi*. The exceptions are a single divergent Atg11 homolog in *M. exilis* and Atg1 homologs in the other two protists. As this complex plays a role in the early steps of autophagosome formation, its absence suggests an alternative mechanism for membrane nucleation, as many other core autophagy proteins are present in these organisms. Phagosomal membrane nucleation and elongation downstream of Atg1 occurs by activation of the class III phosphatidylinositol 3-kinase (PtdIns3K) complex, which appears to be present in *M. exilis*. Membrane expansion is mediated by the Atg8 and Atg12 ubiquitinlike conjugation systems. Although the Atg8 complex is present, we did not identify components of the Atg12 Ubl conjugation system in *M. exilis*. As Atg12 is found in both *T. vaginalis* and *N. gruberi*, this pathway may be in the process of being lost in *M. exilis*, suggesting that the Atg8 complex is capable of membrane elongation alone. Indeed, several proteins known to support the function of Atg8, but not considered core autophagy machinery, are present in *M. exilis*, including sequestosome-1 (p62), which binds to Atg8 to facilitate degradation of ubiquitinated proteins, and HOG1, which enhances the stability of Atg8. Retrieval of proteins involved in autophagosome formation is mediated by the Atg9-Atg18 complex, both of which are present in *M. exilis*. However, the Atg18-interacting protein Atg2, which modulates lipid droplet size, is not found in *M. exilis* or *T. vaginalis*. The genomic complement identified suggests that *M. exilis* should be capable of generating autophagosomes, despite some canonical components not being identified. Consistent with this, we observed membranes that resembled the beginning structures of autophagosomes, the Omegasome (supplementary fig. S7 and supplementary videos S1 and S2, Supplementary Material online). However, confirming the identity of this structure,

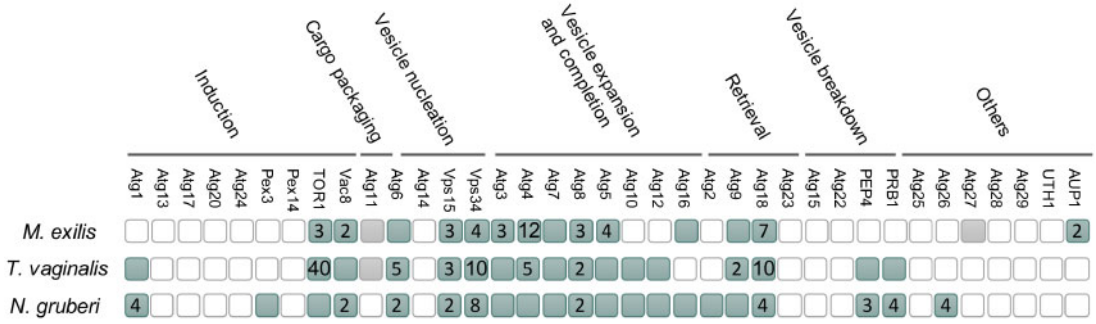

FIG. 7. Autophagy proteins in *Monocercomonoides exilis*, *Trichomonas vaginalis*, and *Naegleria gruberi*. Homologs of autophagy machinery identified by BlastP and pHMMER. Filled squares indicate presence of the component, whereas numbers indicate multiple paralogs. Missing squares indicate that the component could not be identified using these methods. Gray squares indicate a putative homolog whose identity could not be confirmed by reverse BLAST. Categories defined as in Duszenko et al. (2011).

and of the putative MVBs mentioned above, must await development of a transfection system in *M. exilis* for tagging and localization of the relevant molecular components. As might be expected, we could not find any orthologs of the proteins specifically involved in mitophagy (i.e., SLT2, UTH1, PTC6, FUNDC1, BNIP3, and BNIP3L) or pexophagy (i.e., PINK1, PARK2, PEX3, and PEX14) encoded in the *M. exilis* genome. Although a comprehensive analysis of the mitophagy-specific machinery, with deep sampling of eukaryotic genomes, has not been performed, analyses have shown that at least some of the machinery is conserved across the breadth of eukaryotes (Wu et al. 2017). Therefore, the loss of mitophagy proteins represents an example of a system likely lost together with mitochondria.

As the final step in the search for proteins involved in specific adaptations to the loss of mitochondria, we carefully inspected the list of genes that are unique to *M. exilis*, as recovered by Orthofinder (fig. 2). We could ascribe a function to 1,126 of these genes; another 196 genes probably function in trans- or retro-position or are derived from integrated viruses (supplementary table S11, Supplementary Material online). We have not found any example of gene(s) clearly related to the loss of mitochondrial function.

In summary, we have previously suggested that the significant reorganization of Fe–S cluster assembly machinery in *M. exilis* represented the key preadaptation for the loss of mitochondria (Karnkowska et al. 2016) and here we add that another such preadaptation could have been the loss of GCS and SHMT, which took place after the split from the *P. pyriformis* lineage. We have not found any clear case of function lost concomitantly with mitochondrion besides mitophagy. All other cellular systems remained relatively canonical or appear unusual probably due to involvement of host–endobiont interactions and no clear postadaptations to the amitochondriate cell organization were revealed.

Proteins Mediating Mitochondrial Dynamics Are Present in *M. exilis*

Mitochondria are organelles that constantly undergo repeated fission and fusion in order to maintain their number and quality. These dynamics are coordinated with the fundamental functions of mitochondria (Santos et al. 2018). Even reduced mitochondria, such as MROs, undergo dynamics, and many aspects of this process are shared with conventional mitochondria. Given the absence of the mitochondrial organelle in *M. exilis*, proteins involved in mitochondrial fission and fusion are expected to be absent, too. However, many of them are involved in other cellular processes than mitochondria dynamics. We searched *M. exilis* proteome for homologs of proteins annotated into Gene Ontology (GO) categories: mitochondrion localization (GO:0051646; any process in which a mitochondrion or mitochondria are transported to, and/or maintained in, a specific location within the cell) and mitochondrial organization (GO:0007005). Out of 24 identified candidates, only three appeared to be related to mitochondrial dynamics (supplementary table S12, Supplementary Material online). Two of these are dynamin-related protein (DRP) Dnm1 paralogs in *M. exilis* that are closely related to each other and fall phylogenetically to a broader subgroup of DRPs (class A; fig. 8) that includes proteins involved in mitochondrial (and peroxisomal) fission and proteins that seem to have been independently recruited to serve in various parts of the endomembrane system (Praefcke and McMahon 2004; Purkanti and Thattai 2015). In the absence of a mitochondrion, the two *M. exilis* DRPs are predicted to have a role in the dynamics of the endomembrane system, perhaps in endocytosis (in analogy to "true" dynamins and other endocytic DRPs that evolved independently in multiple eukaryotic lineages [Purkanti and Thattai 2015]). Indeed, the single DRP of *G. intestinalis* (also a member of the class A dynamins) seems to be involved in endocytosis (Zumthor et al. 2016), whereas its role in the mitosome dynamics remains unsettled (Rout et al. 2016; Voleman et al. 2017). On the other hand, at least one of the eight DRPs present in *T. vaginalis* contributes to the fission of the hydrogenosomes (Wexler-Cohen et al. 2014), indicating that MRO division in metamonads ancestrally depends on the dynamin family. It is interesting to note that MRO-possessing relatives of *M. exilis*—the trimastigids *Trimastix marina* and *P. pyriformis*—possess two different forms of class A DRPs, one apparently orthologous to the *M. exilis* DRPs and the other without an *M. exilis* counterpart (fig. 8). Since the last common ancestor of trimastigids was probably also the ancestor of oxymonads (Zhang et al. 2015; Leger et al. 2017), the

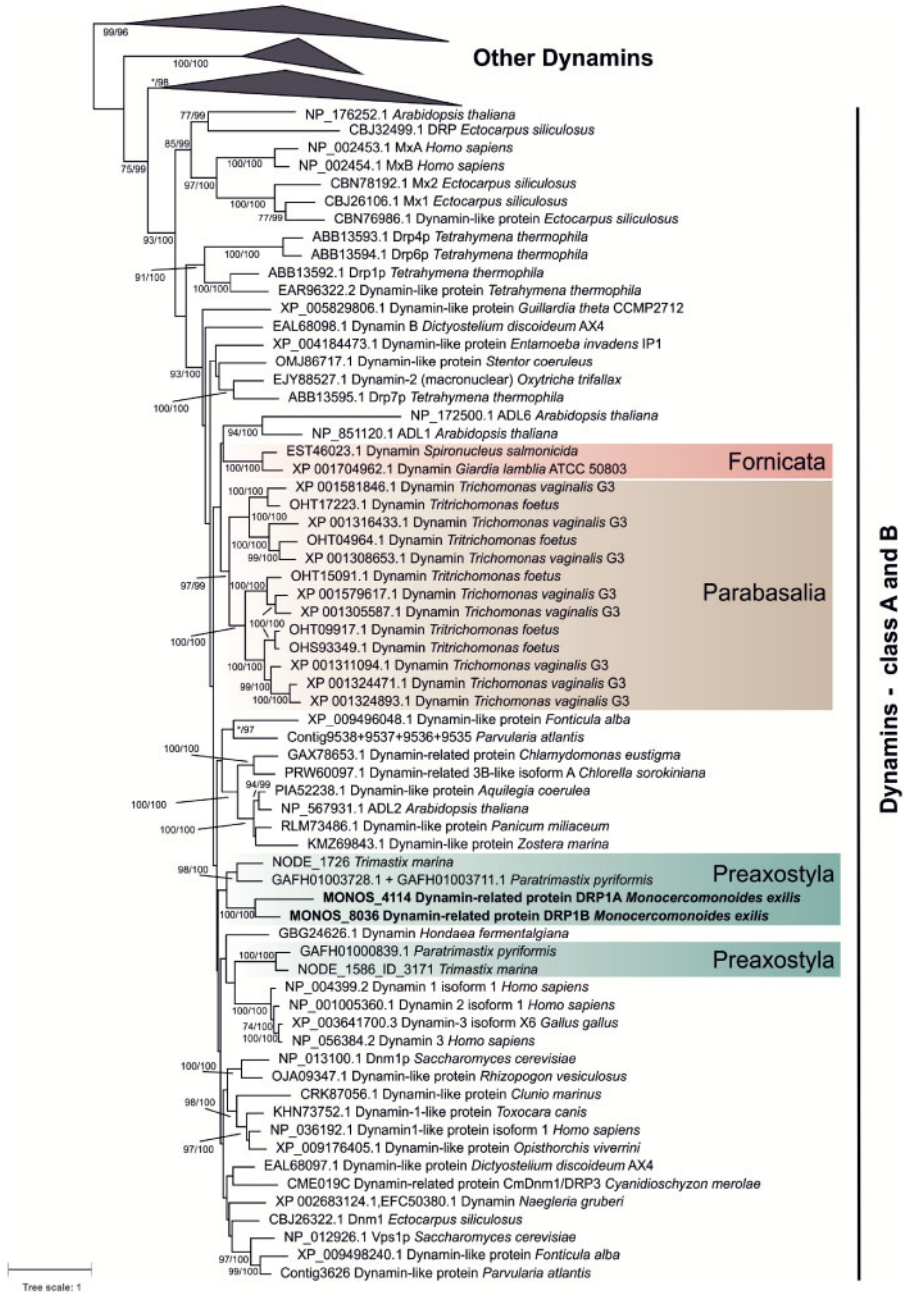

Fig. 8. Phylogenetic analysis of dynamin family showing the position of metamonad dynamins. Clades of Opa1, Mgm1, and Dynamin class C (labeled Other Dynamins) are collapsed since they do not include any metamonad dynamins. Topology is based on phylogenetic tree computed by ML method in RAxML version 8.2.11 (500 rapid bootstraps, PROTGAMMALG4X model). Branch supports were assessed by RAxML rapid bootstraps (500 replicates, only values >70 are shown) and IQ-Tree ultrafast bootstraps (5,000, only values >95 are shown). IQ-Tree 1.5.5 was run under LG+R8 model (based on model test). The final alignment contains 176 sequences and 548 amino acid positions.

absence of this second DRP form in *M. exilis* must be due to secondary loss. It is tempting to speculate that this second DRP form is involved in MRO fission in trimastigids and its absence in *M. exilis* reflects the loss of MROs.

Surprisingly, and in contrast to parabasalids and diplomonads, *M. exilis* also encodes an ortholog of MSTO1 (*misato*) protein. The MSTO1 function has been studied in humans; the protein was shown to be involved in the regulation of mitochondrial distribution and morphology and was proposed to be required for mitochondrial fusion and mitochondrial network formation (Gal et al. 2017). However, in *Drosophila melanogaster* the protein has a non-mitochondrial role, controlling the generation of mitotic microtubules by stabilizing the TCP-1 tubulin chaperone complex (Palumbo et al. 2015). The MSTO1 of *M. exilis* may have a similar nonmitochondrial function.

Conclusions

In this article, we have performed a far more extensive study of the genome of *M. exilis* in comparison to Karnkowska et

al. (2016) and have characterized many additional cellular systems and functions, including 831 new manually curated genes. Our goal was to determine how the loss of mitochondria impacts eukaryotic cell complexity. To our surprise, none of the newly examined cellular systems, including the cytoskeleton, kinetochore, membrane trafficking, autophagy, oxidative stress response, calcium flux, energy, amino acid, lipid, sugar, and nucleotide metabolism, are significantly altered relative to eukaryotes with mitochondria. The large number of introns, elaborate cytoskeleton, endomembrane system, and biosynthetic pathways, all requiring ATP, suggest that *M. exilis* is capable of providing enough ATP without a specialized ATP generating organelle. As such, *M. exilis* serves as living evidence that complex amitochondriate eukaryotic cell is a viable cell type and that such complex cells could have evolved during the evolutionary process of eukaryogenesis before the acquisition of the mitochondrion (Hampl et al. 2019).

From a cell biological perspective, *M. exilis* constitutes a unique experimental model in which to study mitochondrion-integrated systems. With the complete absence of the organelle, such systems can now be interrogated by knock-down or deletion experiments, without the confounding effects of mitochondrion-related functions. Autophagy is one example of such a system, but the same can be said for the functions of dynamins, membrane contact site proteins Vps13 and Vps39, *misato* protein, calcium flux regulatory proteins, Fe–S cluster assembly and more. The comprehensive and high-quality curated predicted proteome provided here, along with the biological insights into various cellular functions of *M. exilis*, should facilitate such future investigations.

Materials and Methods

FIB-SEM Tomography

Soft pellets of cell cultures were fixed in 2.5% glutaraldehyde and 1% formaldehyde in 0.1 M cacodylate buffer for one hour at room temperature (RT), postfixed by reduced 2% (for cell 1) or 1% (for cell 2) osmium tetroxide and 1.5% $K_3(FeCN)_6$ in 0.1 M cacodylate buffer for 1 h on ice (cell 1) or 30 min at RT (cell 2). The cell 1 was further incubated in thiocarbohydrazide for 20 min at RT and in 2% nonreduced osmium tetroxide (in ddH_2O) for 30 min at RT, the cell 2 was incubated in 1% nonreduced osmium tetroxide (in 0.1 M cacodylate buffer) for 30 min at RT. The cells were contrasted by incubating 1 h (cell 1) or 30 min (cell 2) in 1% uranyl acetate at RT, dehydrated in ethanol (cell 2) or ethanol/acetone series (cell 1) and embedded in EPON hard. Serial pictures were taken with FEI Helios NanoLab G3 UC–FIB-SEM microscope with Through lens, In Column and Mirror detectors (TLD, ICD, MD). Raw data were processed in Amira 6 software. First view through the cell in the video is made up of pictures taken with the microscope, whereas the others are calculated subsequently in Amira software.

Ploidy Estimation from *M. exilis* Sequencing Data

The genomic DNA (gDNA) of a clonal culture of *M. exilis* previously sequenced using a Genome Sequencer 454 GS FLX+ at ~35× coverage (Karnkowska et al. 2016) was used to the ploidy estimation. Genomic sequencing reads subjected to linker and quality trimming were mapped onto the previously assembled genome using CLC Genomics Workbench v. 9.5.2 with the following parameters: mismatch cost, 2; insertion cost, 3; deletion cost, 3; length fraction, 0.96; and similarity fraction, 0.96. Duplicate read removal and local realignment were performed using the same software. The resulting read mapping was used as an input for SNP calling with Platypus v. 0.8.1 with a minimum read coverage cut-off of 3 (Rimmer et al. 2014). For ploidy inference, allele frequency distribution at biallelic SNP loci in *M. exilis* was compared with the theoretical distributions in organisms with different ploidy levels (Yoshida et al. 2013).

Protein-Coding Gene Annotation

The previously reported set of gene models predicted by a combination of automated algorithms and manual curation (Karnkowska et al. 2016) was subjected to additional refinement concerning gene categories specifically targeted in the present study. This included incorporation of newly created models for previously missed genes and modification of existing models by changing exon–intron boundaries (sometimes resulting in gene model splitting/fusion) as suggested by transcriptomic evidence and/or sequence conservation within respective gene families. In addition, nine models were removed, since it turned out that the respective scaffolds (scaffold01876, scaffold01882, and scaffold01991) are most likely bacterial contaminants (based on high sequence similarity at the nucleotide level to bacterial genomes).

The automatic functional annotation was performed by similarity searches using BLAST (*e*-value $=< 1e^{-20}$) against the NCBI nr protein database and HMMER (http://hmmer.org/; last accessed 30 June, 2019) searches of domain hits from the PFAM protein family database (Finn et al. 2014). Additional annotation was performed using the KEGG Automatic Annotation Server (Moriya et al. 2007) which compares predicted genes to the manually curated KEGG Genes database (Kanehisa et al. 2014). Gene product names were assigned based on significant BlastP and domain matches. For cases, where there was no significant BLAST or domain hit, the gene was automatically assigned as a "hypothetical protein." GFF3 format was used for storing the annotation information. A set of 1,137 genes of interest was manually curated (supplementary table S1, Supplementary Material online). A locus tag identifier in the format MONOS_XXXXX was assigned to each predicted gene. Approximately 60% of the gene models remained as hypothetical proteins.

Ortholog clustering of translated proteins from annotated draft genome of *M. exilis* was performed with Orthofinder (Emms and Kelly 2015) using predicted proteomes from *T. vaginalis*, *G. intestinalis*, *S. salmonicida*, and *N. gruberi*.

Tyrosine kinases annotation was performed based on homology searches with kinase database (http://kinase.com; last accessed 30 June, 2019). For analysis of proteases the MEROPS database (Rawlings et al. 2016) was used to carry out a BlastP search of all *M. exilis* predicted proteins. Four hundred and

forty-three proteins with an *e*-value $=< 1e^{-10}$ were further analyzed and 122 were checked against MEROPS and confirmed with PFAM. For prediction of Fe–S-cluster-containing proteins the MetalPredator (Valasatava et al. 2016) was used. MetalPredator predicted that proteome of *M. exilis* contains about 54 [Fe–S] proteins. Another [Fe–S] proteins were predicted using BlastP (Altschul et al. 1997) against custom database of experimentally confirmed [Fe–S] proteins from *Escherichia coli* and *Saccharomyces cerevisiae* followed by the reciprocal BLAST against the NCBI nr database. Results were searched against InterPro database (Finn et al. 2017) to confirm presence of [Fe–S] cluster binding motif. TATA-like motif (A/G)TATTT(T/C/G) was searched in the genome assembly of *M. exilis* with the DREME algorithm (Bailey 2011). TATA-like motif was searched among annotated genes with predicted 5′ UTR in the region located 45 nucleotides upstream of the transcription start site.

Gene Searching and Identification

As queries for gene searching, published proteins from various organisms were used, most often from *Arabidopsis thaliana* from www.phytozome.net, *Dictyostelium discoideum* AX4 from NCBI, *G. intestinalis* WB from GiardiaDB.org, *Homo sapiens* from NCBI, *N. gruberi* v1.0 from genome.jgi-psf.org, *P. pyriformis* from NCBI, *T. vaginalis* G3 from TrichDB.org, *Trypanosoma brucei* TREU927 from eupathdb.org, and *Saccharomyces cerevisiae* RM11-1a from www.broad.mit.edu and S288C from NCBI. *Monocercomonoides exilis* hits were BLASTed back against the genome of the query protein and against NCBI nr database.

For identification of rapidly evolving proteins that may be difficult to detect with BLAST, more sensitive searches of the predicted *M. exilis* proteome were carried out using HMMER3.1 package (http://hmmer.org/; last accessed 30 June, 2019). Query HMMs were prepared using the hmmbuild program and input alignments of reference sequences, usually adopted from the Pfam database (seed alignments defined for the families of interest). Positive hits were evaluated as possible orthologs of the query proteins by blasting them against the NCBI protein sequence database.

We performed phylogenetic analyses and generated individual gene trees to support annotation process. Sequences were aligned using MAFFT (Katoh and Standley 2013) or MUSCLE (Edgar 2004), visually inspected and manually edited whenever necessary, and eventually trimmed with BMGE (Criscuolo and Gribaldo 2010) or manually. Maximum likelihood (ML) phylogenetic analyses were performed using one or more methods: RAxML 8.0.23 (Stamatakis 2014), IQ-TREE 1.3.11.1 (Nguyen et al. 2015), Phylobayes v4.1 (Lartillot et al. 2009), or MrBAYES v3.2.2 (Ronquist et al. 2012).

Intron Analyses

The history of intron gains and losses was studied for 100 groups of orthologous genes conserved in *M. exilis* and 33 additional representatives of different phylogenetic lineages of eukaryotes. The genes analyzed were a subset of 163 groups of orthologous genes used in a previously published phylogenomic analysis (Karnkowska et al. 2016). For the intron analyses, we excluded all species with only transcriptomic data available and two more species (*Reticulomyxa filosa* and *Chondrus crispus*) with poor representation of genes in the original data set. For *Acanthamoeba castellanii* and *S. salmonicida* 8 and 21 orthologs, respectively, missing in the original data set were identified by reciprocal blast searches of databases at NCBI and added to the alignments. Finally, groups of orthologs that lacked genes from more than one of the 34 species retained in the analysis were excluded. Information on the exon–intron structure of the genes for most species was obtained from the respective gene records in the GenBank or RefSeq databases at NCBI. For *Bigelowiella natans* and *Phytophthora ramorum*, the information was extracted from GFF files downloaded from the respective genome databases at the Joint Genome Institute (http://jgi.doe.gov/; last accessed 30 June, 2019). For five genes from *A. castellanii*, the respective models were not available in any database, so their exon–intron structure was reconstructed manually. MAFFT v7.271 with auto option (Katoh and Standley 2014) was used to align sets of orthologous protein sequences for subsequent intron mapping and definition of homologous intron positions. These analyses were performed using the Malin software (Csuros 2008). To restrict the analysis to confidently homologized introns, we filtered a total of 5,711 intron positions by keeping only those that were flanked in the protein sequence alignment by four nongap amino acid positions on both sides and that exhibit conservation of a particular amino acid in at least a half of the protein sequences aligned (i.e., "Minimum unambiguous characters at a site" was set to 17). This setting left 3,546 positions for further analyses. We then used the intron table created by Malin and a custom Python script to define ancestral introns, that is, those presumably occurring in the LECA. These were defined by intron positions represented in at least one species of Amorphea and at least one species from the remaining eukaryotic groups included in the analysis (i.e., assuming the position of the root of the eukaryote phylogeny as depicted in fig. 3*a*). The proportion of ancestral introns to the total number of introns was then plotted for each species (fig. 3*b*). Reconstruction of intron gain and loss was done in Malin using Dollo parsimony and three different species trees, using the unrooted topology as defined by our phylogenetic analysis reported previously and assuming three alternative placements of the root of the eukaryote phylogeny: between Amorphea and the remaining eukaryotes included in the analysis (fig. 3*a*); between Amorphea + Metamonada and the remaining eukaryotes included in the analysis (supplementary fig. S4*a*, Supplementary Material online); and between Metamonada and the remaining eukaryotes included in the analysis (supplementary fig. S4*b*, Supplementary Material online).

LGT Pipeline

In order to retrieve putative homologs of *M. exilis* proteins, the 16,629 predicted protein sequences (i.e., the version of the *M. exilis* proteome reported in Karnkowska et al. [2016]) were used as BlastP queries against the *nr* database at the NCBI (*e*-value cut-off: 10^{-10} and a maximum of 1,000 hits). Only data

sets containing at least four sequences were kept (4,733). Probable *M. exilis* in-paralogs (and their homologs retrieved by BlastP) were assembled in a single data set using an in-house Perl script that gathered data sets containing at least 50% of identical sequences. After this step, only 2,146 data sets remained. Since we were interested in LGT specifically from prokaryotes, we discarded data sets containing no prokaryotic homologs. This resulted in set of 824 protein data sets that were further considered for phylogenetic analyses.

A round of preliminary phylogenetic analyses was carried out in order to reduce unnecessary sequence redundancy in a reproducible fashion, and decrease computational time, thus allowing more rigorous downstream analyses. For this, each protein data set was aligned using the "MAFFT" algorithm (default parameters) from the MAFFT package v6.903 (Katoh et al. 2002). Regions of doubtful homology between sites were removed from the alignments using BMGE with default parameters, except for the substitution matrix, which was set to BLOSUM40 ("-m BLOSUM40"), and the gap threshold to 40% ("-g 0.4") (Criscuolo and Gribaldo 2010). At this step, we discarded alignments for which <80 sites were kept after trimming (154 alignments).

Preliminary phylogenetic trees were reconstructed for the remaining 670 protein alignments using FastTree 2.1.4 (with default parameters) (Price et al. 2010). An in-house Perl/Bioperl script was then used to parse these trees and automatically remove unnecessary sequence redundancy in order to reduce the size of each tree. Our method identifies sequences from closely related organisms (i.e., belonging to the same genus) that form a monophyletic clade and keeps only one representative per clade, except for *M. exilis*, for which all (in-) paralogs were kept.

A second round of phylogenetic analyses was performed using more thorough methods. Reduced protein data sets were realigned using the MAFFT-L-INS-i method of the MAFFT package, and then trimmed with BMGE (settings as previously described). ML trees were computed using RAxML 8.0.23 (Stamatakis 2014) with the LG4X model (Le et al. 2012) and statistical support was obtained from 100 rapid bootstrapping (rBS) replicates. Alignments and trees are available upon request.

An automated pipeline was developed, in-house, using Perl/Bioperl to parse phylogenetic trees and screen for LGT candidates using the following criteria: 1) *M. exilis* must branch within a clade containing no other eukaryotes with a few defined exceptions (fornicates, parabasalids, oxymonads, *P. pyriformis*, *N. gruberi*, *E. histolytica*, *Ma. balamuthi*, and *Blastocystis* sp.). These exceptions were allowed because we were interested not only in LGTs specific to *M. exilis* but also in cases of more ancient LGTs (e.g., at the various internal branches of excavate phylogeny). Similarly, we were interested in identifying genes of prokaryotic origin that are shared by *M. exilis* and other anaerobic protists. This clade containing prokaryotes and *M. exilis* (and possibly some of the allowed lineages) must have been supported by a bipartition with the rBS > 70%.

The resulting 174 candidate cases of LGTs were examined by eye taking into account all information contained in each BLAST result, alignment, sequence domain composition (see below), and phylogeny to exclude as many false positives as possible. Seventy-one genes were eventually removed from the list, leaving 103 *M. exilis* genes likely acquired by LGT (supplementary table S9, Supplementary Material online). Protein functional domains for each homolog in a given data set were identified using the HMMER 3 package (http://hmmer.org/; last accessed 30 June, 2019) against the PFAM 26.0 database (Punta et al. 2012) and were mapped onto phylogenetic trees with the ETE2 Python toolkit (Huerta-Cepas et al. 2010).

Fluorescence In Situ Hybridization

Unlabeled telomeric probes were generated using the primer dimer extension method described in Ijdo et al. (1991), but we used PrimeSTAR Max DNA polymerase (Clontech, R045A) instead of Taq polymerase for the PCR step. The purified PCR products were labeled with digoxigenin-11-dUTP, alkali stabile (Roche, 11093088910) using the DecaLabel DNA Labeling Kit (Thermo Scientific, K0621). The labeled probes were purified using columns from the QIAquick Gel Extraction Kit (Qiagen, 28704) and eluted into the final volume of 50 µl.

One liter of *M. exilis* culture was filtered to remove bacteria and the cells were pelleted by centrifugation for 10 min at 1,200 × g at 4 °C. FISH with digoxigenin-labeled probes was performed according to the previously described procedure (Zubáčová et al. 2011) except that the culture was not treated with colchicine and the stringency washes were performed at 45 °C. For probe detection, we used DyLight 594 Labeled Anti-Digoxigenin antibody (Vector Laboratories, DI-7594). Preparations were observed using an IX81 microscope (Olympus) equipped with an IX2-UCB camera. Images were processed using Cell-R software (Olympus) and Image J 1.42q. The number of signals from each nucleus was manually counted and the average number of signals was estimated from at least 50 nuclei.

Southern Blot Analysis of Telomeres

A Southern blot was performed with *M. exilis* gDNA isolated from 3,000 ml of filtered cell culture using DNeasy Blood & Tissue Kit (Qiagen, 69504). Estimation of the average telomere length was based on the method described in Kimura et al. (2010), with slight modifications. Briefly, 5 µg of gDNA was digested overnight in total volume 200 µl containing five units of the *Hin*fI (NEB, R0155S) and five units of *Rsa*I (NEB, R0167S) restriction enzymes. DNA was purified by ethanol precipitation and resuspended in 15 µl of nuclease-free water. After restriction enzyme treatment, the gDNA samples were run on a 0.8% agarose gel at 80 V for 5 h. The DNA was transferred onto a Hybond-N membrane (GE Healthcare) using vacuum blotting. The Southern blot hybridization was performed using the same probe which was used in the FISH procedure. Probe detection was done using the DIG-High Prime DNA Labelling and Detection Starter Kit II (Roche, 11585614910) according to the manufacturer's instructions. Digital images of hybridization signals were obtained using the ImageQuant LAS 4000 (GE Healthcare Life Sciences).

Supplementary Material

Supplementary data are available at *Molecular Biology and Evolution* online.

Acknowledgments

The work in the V.H. lab was supported by the Czech Science Foundation project 15-16406S. A.K. was supported by the Polish Ministry of Science and Higher Education scholarship for outstanding young researchers. Work in the J.B.D. lab was supported by a Discovery Grant from the Natural Sciences and Engineering Research Council of Canada (RES0021028). J.B.D. is the Canada Research Chair (Tier II) in Evolutionary Cell Biology. Work in the lab of M.E. was supported by the Czech Science Foundation project 18-18699S. Work in the lab of A.J.R. was supported by a transitional operating grant, MOP-142349, from the Canadian Institutes of Health Research. This project has received funding from the European Research Council (ERC) under the European Union's Horizon 2020 research and innovation programme (grant agreement No 771592). We acknowledge MEYS CR for funding within the National Sustainability Program II (project BIOCEV-FAR) LQ1604, project "BIOCEV" (CZ.1.05/1.1.00/02.0109), and the Centre for research of pathogenicity and virulence of parasites reg. nr.: CZ.02.1.01/0.0/0.0/16019/0000759. Finally, we acknowledge Markéta Dalecká and Adam Schröfel from the Imaging Methods Core Facility at BIOCEV, institution supported by the Czech-BioImaging large RI projects (LM2015062 and CZ.02.1.01/0.0/0.0/16_013/0001775, funded by MEYS CR) for their support with obtaining FIB-SEM data presented in this article.

References

Abrahamsen MS, Templeton TJ, Enomoto S, Abrahante JE, Zhu G, Lancto CA, Deng M, Liu C, Widmer G, Tzipori S. 2004. Complete genome sequence of the apicomplexan, *Cryptosporidium parvum*. *Science* 304(5669):441–445.

Adl SM, Bass D, Lane CE, Lukeš J, Schoch CL, Smirnov A, Agatha S, Berney C, Brown MW, Burki F. et al. 2019. Revisions to the classification, nomenclature, and diversity of eukaryotes. *J Eukaryot Microbiol*. 66(1):4–119.

Aldritt SM, Tien P, Wang CC. 1985. Pyrimidine salvage in *Giardia lamblia*. *J Exp Med*. 161(3):437–445.

Almeida KH, Sobol RW. 2007. A unified view of base excision repair: lesion-dependent protein complexes regulated by post-translational modification. *DNA Repair (Amst)*. 6(6):695–711.

Altschul SF, Madden TL, Schäffer AA, Zhang J, Zhang Z, Miller W, Lipman DJ. 1997. Gapped BLAST and PSI-BLAST: a new generation of protein database search programs. *Nucleic Acids Res*. 25(17):3389–3402.

Anderson IJ, Loftus BJ. 2005. *Entamoeba histolytica*: observations on metabolism based on the genome sequence. *Exp Parasitol*. 110(3):173–177.

Andreini C, Rosato A, Banci L. 2017. The relationship between environmental dioxygen and iron-sulfur proteins explored at the genome level. *PLoS One* 12(1):e0171279.

Bailey TL. 2011. DREME: motif discovery in transcription factor ChIP-seq data. *Bioinformatics* 27(12):1653–1659.

Baum KF, Berens RL, Marr JJ, Harrington JA, Spector T. 1989. Purine deoxynucleoside salvage in Giardia lamblia. *J Biol Chem*. 264(35):21087–21090.

Brawley SH, Blouin NA, Ficko-Blean E, Wheeler GL, Lohr M, Goodson HV, Jenkins JW, Blaby-Haas CE, Helliwell KE, Chan CX, et al. 2017. Insights into the red algae and eukaryotic evolution from the genome of *Porphyra umbilicalis* (Bangiophyceae, Rhodophyta). *Proc Natl Acad Sci U S A*. 114(31):E6361–E6370.

Brown DM, Upcroft JA, Upcroft P. 1993. Cysteine is the major low-molecular weight thiol in *Giardia duodenalis*. *Mol Biochem Parasitol*. 61(1):155–158.

Carlton JM, Hirt RP, Silva JC, Delcher AL, Schatz M, Zhao Q, Wortman JR, Bidwell SL, Alsmark UCM, Besteiro S, et al. 2007. Draft genome sequence of the sexually transmitted pathogen *Trichomonas vaginalis*. *Science* 315(5809):207–212.

Cole ES, Giddings TH, Ozzello C, Winey M, O'Toole E, Orias J, Hamilton E, Guerrier S, Ballard A, Aronstein T. 2015. Membrane dynamics at the nuclear exchange junction during early mating (one to four hours) in the ciliate *Tetrahymena thermophila*. *Eukaryotic Cell* 14(2):116–127.

Contreras L, Drago I, Zampese E, Pozzan T. 2010. Mitochondria: the calcium connection. *Biochim Biophys Acta* 1797(6-7):607–618.

Costa RMA, Chiganças V, Galhardo RDS, Carvalho H, Menck CFM. 2003. The eukaryotic nucleotide excision repair pathway. *Biochimie* 85(11):1083–1099.

Criscuolo A, Gribaldo S. 2010. BMGE (Block Mapping and Gathering with Entropy): a new software for selection of phylogenetic informative regions from multiple sequence alignments. *BMC Evol Biol*. 10:210.

Csuros M. 2008. Malin: maximum likelihood analysis of intron evolution in eukaryotes. *Bioinformatics* 24(13):1538–1539.

Dacks JB, Kuru T, Liapounova N, Gedamu L. 2008. Phylogenetic and primary sequence characterization of cathepsin B cysteine proteases from the oxymonad flagellate *Monocercomonoides*. *J Eukaryot Microbiol*. 55(1):9–17.

de Koning HP, Bridges DJ, Burchmore R. 2005. Purine and pyrimidine transport in pathogenic protozoa: from biology to therapy. *FEMS Microbiol Rev*. 29(5):987–1020.

de Mendoza A, Sebe-Pedros A, Sestak MS, Matejcic M, Torruella G, Domazet-Loso T, Ruiz-Trillo I. 2013. Transcription factor evolution in eukaryotes and the assembly of the regulatory toolkit in multicellular lineages. *Proc Natl Acad Sci U S A*. 110(50):E4858–E4866.

Duszenko M, Ginger ML, Brennand A, Gualdrón-López M, Colombo MI, Coombs GH, Coppens I, Jayabalasingham B, Langsley G, de Castro SL, et al. 2011. Autophagy in protists. *Autophagy* 7(2):127–158.

Edgar RC. 2004. MUSCLE: multiple sequence alignment with high accuracy and high throughput. *Nucleic Acids Res*. 32(5):1792–1797.

Eichinger L, Pachebat JA, Glöckner G, Rajandream M-A, Sucgang R, Berriman M, Song J, Olsen R, Szafranski K, Xu Q, et al. 2005. The genome of the social amoeba *Dictyostelium discoideum*. *Nature* 435(7038):43–57.

Elias M, Brighouse A, Gabernet-Castello C, Field MC, Dacks JB. 2012. Sculpting the endomembrane system in deep time: high resolution phylogenetics of Rab GTPases. *J Cell Sci*. 125(Pt 10):2500–2508.

Eme L, Gentekaki E, Curtis B, Archibald JM, Roger AJ. 2017. Lateral gene transfer in the adaptation of the anaerobic parasite *Blastocystis* to the gut. *Curr Biol*. 27(6):807–820.

Emms DM, Kelly S. 2015. OrthoFinder: solving fundamental biases in whole genome comparisons dramatically improves orthogroup inference accuracy. *Genome Biol*. 16:157.

Findeisen P, Mühlhausen S, Dempewolf S, Hertzog J, Zietlow A, Carlomagno T, Kollmar M. 2014. Six subgroups and extensive recent duplications characterize the evolution of the eukaryotic tubulin protein family. *Genome Biol Evol*. 6(9):2274–2288.

Finn RD, Attwood TK, Babbitt PC, Bateman A, Bork P, Bridge AJ, Chang H-Y, Dosztányi Z, El-Gebali S, Fraser M, et al. 2017. InterPro in 2017—beyond protein family and domain annotations. *Nucleic Acids Res*. 45(D1):D190–199.

Finn RD, Bateman A, Clements J, Coggill P, Eberhardt RY, Eddy SR, Heger A, Hetherington K, Holm L, Mistry J, et al. 2014. Pfam: the protein families database. *Nucleic Acids Res*. 42(Database issue):D222–D230.

Forterre P, Gribaldo S, Gadelle D, Serre MC. 2007. Origin and evolution of DNA topoisomerases. *Biochimie* 89(4):427–446.

Franzén O, Jerlström-Hultqvist J, Einarsson E, Ankarklev J, Ferella M, Andersson B, Svärd SG. 2013. Transcriptome profiling of *Giardia intestinalis* using strand-specific RNA-Seq. *PLoS Comput Biol*. 9(3):e1003000.

Fritz-Laylin LK, Prochnik SE, Ginger ML, Dacks JB, Carpenter ML, Field MC, Kuo A, Paredez A, Chapman J, Pham J, et al. 2010. The genome of *Naegleria gruberi* illuminates early eukaryotic versatility. *Cell* 140(5):631–642.

Fukui K. 2010. DNA mismatch repair in eukaryotes and bacteria. *J Nucleic Acids*. 2010:1–6.

Fulnecková J, Sevcíková T, Fajkus J, Lukesová A, Lukes M, Vlcek C, Lang BF, Kim E, Eliás M, Sykorová E. 2013. A broad phylogenetic survey unveils the diversity and evolution of telomeres in eukaryotes. *Genome Biol Evol*. 5(3):468–483.

Gabaldón T, Ginger ML, Michels P. 2016. Peroxisomes in parasitic protists. *Mol Biochem Parasitol*. 209(1-2):35–45.

Gal A, Balicza P, Weaver D, Naghdi S, Joseph SK, Várnai P, Gyuris T, Horváth A, Nagy L, Seifert EL, et al. 2017. MSTO1 is a cytoplasmic pro-mitochondrial fusion protein, whose mutation induces myopathy and ataxia in humans. *EMBO Mol Med*. 9(7):967–984.

García-Sancho J. 2014. The coupling of plasma membrane calcium entry to calcium uptake by endoplasmic reticulum and mitochondria. *J. Physiol*. 2:261–268.

Ginger ML, Fritz-Laylin LK, Fulton C, Cande WZ, Dawson SC. 2010. Intermediary metabolism in protists: a sequence-based view of facultative anaerobic metabolism in evolutionarily diverse eukaryotes. *Protist* 161(5):642–671.

Gomez-Suaga P, Paillusson S, Miller C. 2017. ER-mitochondria signaling regulates autophagy. *Autophagy* 13(7):1250–1251.

González Montoro A, Auffarth K, Hönscher C, Bohnert M, Becker T, Warscheid B, Reggiori F, van der Laan M, Fröhlich F, Ungermann C. 2018. Vps39 interacts with Tom40 to establish one of two functionally distinct vacuole-mitochondria contact sites. *Dev Cell* 45(5):621–636.e7.

Gray MW. 2012. Mitochondrial evolution. *Cold Spring Harb Perspect Biol*. 4(9):a011403.

Hammesfahr B, Kollmar M. 2012. Evolution of the eukaryotic dynactin complex, the activator of cytoplasmic dynein. *BMC Evol Biol*. 12:95.

Hampl V. 2017. Preaxostyla. In: Archibald J, Simpson A, Slamovits C, editors. Handbook of the Protists. Cham (Switzerland): Springer International Publishing. p. 1139–1174.

Hampl V, Čepička I, Eliáš M. 2019. Was the mitochondrion necessary to start eukaryogenesis? *Trends Microbiol*. 27(2):96–104.

Hampl V, Silberman JD, Stechmann A, Diaz-Triviño S, Johnson PJ, Roger AJ. 2008. Genetic evidence for a mitochondriate ancestry in the "amitochondriate" flagellate *Trimastix pyriformis*. *PLoS One* 3(1):e1383.

Huerta-Cepas J, Dopazo J, Gabaldón T. 2010. ETE: a python Environment for Tree Exploration. *BMC Bioinformatics* 11:24.

Ijdo JW, Wells RA, Baldini A, Reeders ST. 1991. Improved telomere detection using a telomere repeat probe (TTAGGG)n generated by PCR. *Nucleic Acids Res*. 19(17):4780.

Irimia M, Roy SW. 2014. Origin of spliceosomal introns and alternative splicing. *Cold Spring Harb Perspect Biol*. 6(6):a016071.

Iyer LM, Anantharaman V, Wolf MY, Aravind L. 2008. Comparative genomics of transcription factors and chromatin proteins in parasitic protists and other eukaryotes. *Int J Parasitol*. 38(1):1–31.

Kamikawa R, Inagaki Y, Roger AJ, Hashimoto T. 2011. Splintrons in *Giardia intestinalis*: spliceosomal introns in a split form. *Commun Integr Biol*. 4(4):454–456.

Kanehisa M, Goto S, Sato Y, Kawashima M, Furumichi M, Tanabe M. 2014. Data, information, knowledge and principle: back to metabolism in KEGG. *Nucleic Acids Res*. 42(Database issue):D199–D205.

Karnkowska A, Vacek V, Zubáčová Z, Treitli SC, Petrželková R, Eme L, Novák L, Žárský V, Barlow LD, Herman EK, et al. 2016. A eukaryote without a mitochondrial organelle. *Curr Biol*. 26(10):1274–1284.

Katoh K, Misawa K, Kuma K, Miyata T. 2002. MAFFT: a novel method for rapid multiple sequence alignment based on fast Fourier transform. *Nucleic Acids Res*. 30(14):3059–3066.

Katoh K, Standley DM. 2013. MAFFT multiple sequence alignment software version 7: improvements in performance and usability. *Mol Biol Evol*. 30(4):772–780.

Katoh K, Standley DM. 2014. MAFFT: iterative refinement and additional methods. *Methods Mol Biol*. 1079:131–146.

Kendall JJ, Barrero-Tobon AM, Hendrixson DR, Kelly DJ. 2014. Hemerythrins in the microaerophilic bacterium *Campylobacter jejuni* help protect key iron-sulphur cluster enzymes from oxidative damage. *Environ Microbiol*. 16(4):1105–1121.

Kimura M, Stone RC, Hunt SC, Skurnick J, Lu X, Cao X, Harley CB, Aviv A. 2010. Measurement of telomere length by the Southern blot analysis of terminal restriction fragment lengths. *Nat Protoc*. 5(9):1596–1607.

Klinger CM, Klute MJ, Dacks JB. 2013. Comparative genomic analysis of multi-subunit tethering complexes demonstrates an ancient pan-eukaryotic complement and sculpting in *Apicomplexa*. *PLoS One* 8(9):e76278.

Kollmar M, Lbik D, Enge S. 2012. Evolution of the eukaryotic ARP2/3 activators of the WASP family: WASP, WAVE, WASH, and WHAMM, and the proposed new family members WAWH and WAML. *BMC Res Notes* 5:88.

Koumandou VL, Dacks JB, Coulson RMR, Field MC. 2007. Control systems for membrane fusion in the ancestral eukaryote; evolution of tethering complexes and SM proteins. *BMC Evol Biol*. 7:1–17.

Koumandou VL, Klute MJ, Herman EK, Nunez-Miguel R, Dacks JB, Field MC. 2011. Evolutionary reconstruction of the retromer complex and its function in *Trypanosoma brucei*. *J Cell Sci*. 124(Pt 9):1496–1509.

Kumari P, Babuta M, Bhattacharya A, Gourinath S. 2019. Structural and functional characterisation of phosphoserine phosphatase, that plays critical role in the oxidative stress response in the parasite *Entamoeba histolytica*. *J Struct Biol*. 206(2):254-266.

Kunkel TA, Erie DA. 2005. DNA mismatch repair. *Annu Rev Biochem*. 74:681–710.

Lartillot N, Lepage T, Blanquart S. 2009. PhyloBayes 3: a Bayesian software package for phylogenetic reconstruction and molecular dating. *Bioinformatics* 25(17):2286–2288.

Latchman DS. 1997. Transcription factors: an overview. *Int J Biochem Cell Biol*. 29(12):1305–1312.

Le SQ, Dang CC, Gascuel O. 2012. Modeling protein evolution with several amino acid replacement matrices depending on site rates. *Mol Biol Evol*. 29(10):2921–2936.

Leger MM, Kolisko M, Kamikawa R, Stairs CW, Kume K, Čepička I, Silberman JD, Andersson JO, Xu F, Yabuki A, et al. 2017. Organelles that illuminate the origins of *Trichomonas* hydrogenosomes and *Giardia* mitosomes. *Nat Ecol Evol*. 1(4):0092.

Leung KF, Dacks JB, Field MC. 2008. Evolution of the multivesicular body ESCRT machinery; retention across the eukaryotic lineage. *Traffic* 9(10):1698–1716.

Lill R, Hoffmann B, Molik S, Pierik AJ, Rietzschel N, Stehling O, Uzarska MA, Webert H, Wilbrecht C, Mühlenhoff U. 2012. The role of mitochondria in cellular iron-sulfur protein biogenesis and iron metabolism. *Biochim Biophys Acta* 1823(9):1491–1508.

Loftus B, Anderson I, Davies R, Alsmark UCM, Samuelson J, Amedeo P, Roncaglia P, Berriman M, Hirt RP, Mann BJ, et al. 2005. The genome of the protist parasite *Entamoeba histolytica*. *Nature* 433(7028):865–868.

Lynch M, Marinov GK. 2015. The bioenergetic costs of a gene. *Proc Natl Acad Sci U S A*. 112(51):15690–15695.

Manning G, Reiner DS, Lauwaet T, Dacre M, Smith A, Zhai Y, Svard S, Gillin FD. 2011. The minimal kinome of *Giardia lamblia* illuminates early kinase evolution and unique parasite biology. *Genome Biol*. 12(7):R66.

Marchat LA, López-Camarillo C, Orozco E, López-Casamichana M. 2011. DNA repair in pathogenic eukaryotic cells: insights from comparative genomics of parasitic protozoan. In: Chen C, editor. Selected

topics in DNA repair. London, United Kingdom: INTECH Open Access Publisher.
Moriya Y, Itoh M, Okuda S, Yoshizawa AC, Kanehisa M. 2007. KAAS: an automatic genome annotation and pathway reconstruction server. *Nucleic Acids Res.* 35(Web Server issue):W182–W185.
Morrison HG, McArthur AG, Gillin FD, Aley SB, Adam RD, Olsen GJ, Best AA, Cande WZ, Chen F, Cipriano MJ, et al. 2007. Genomic minimalism in the early diverging intestinal parasite *Giardia lamblia*. *Science* 317(5846):1921–1926.
Müller S, Liebau E, Walter RD, Krauth-Siegel RL. 2003. Thiol-based redox metabolism of protozoan parasites. *Trends Parasitol.* 19(7):320–328.
Munagala N, Wang CC. 2002. The pivotal role of guanine phosphoribosyltransferase in purine salvage by *Giardia lamblia*. *Mol Microbiol.* 44(4):1073–1079.
Munagala NR, Wang CC. 2003. Adenosine is the primary precursor of all purine nucleotides in *Trichomonas vaginalis*. *Mol Biochem Parasitol.* 127(2):143–149.
Narrowe AB, Spang A, Stairs CW, Caceres EF, Baker BJ, Miller CS, Ettema T. 2018. Complex evolutionary history of translation elongation factor 2 and diphthamide biosynthesis in Archaea and parabasalids. *Genome Biol Evol.* 10(9):2380–2393.
Nguyen L-T, Schmidt HA, von Haeseler A, Minh BQ. 2015. IQ-TREE: a fast and effective stochastic algorithm for estimating maximum-likelihood phylogenies. *Mol Biol Evol.* 32(1):268–274.
Novák L, Zubáčová Z, Karnkowska A, Kolisko M, Hroudová M, Stairs CW, Simpson AGB, Keeling PJ, Roger AJ, Čepička I, et al. 2016. Arginine deiminase pathway enzymes: evolutionary history in metamonads and other eukaryotes. *BMC Evol Biol.* 16:197.
Nývltová E, Šuťák R, Žárský V, Harant K, Hrdý I, Tachezy J. 2017. Lateral gene transfer of *p*-cresol- and indole-producing enzymes from environmental bacteria to *Mastigamoeba balamuthi*. *Environ Microbiol.* 19(3):1091–1102.
Oma Y, Harata M. 2011. Actin-related proteins localized in the nucleus: from discovery to novel roles in nuclear organization. *Nucleus* 2(1):38–46.
Orphanides G, Lagrange T, Reinberg D. 1996. The general transcription factors of RNA polymerase II. *Genes Dev.* 10(21):2657–2683.
Palumbo V, Pellacani C, Heesom KJ, Rogala KB, Deane CM, Mottier-Pavie V, Gatti M, Bonaccorsi S, Wakefield JG. 2015. Misato controls mitotic microtubule generation by stabilizing the TCP-1 tubulin chaperone complex. *Curr Biol.* 25(13):1777–1783.
Paredez AR, Nayeri A, Xu JW, Krtkova J, Cande WZ. 2014. Identification of obscure yet conserved actin-associated proteins in *Giardia lamblia*. *Eukaryotic Cell* 13(6):776–784.
Park J-S, Thorsness MK, Policastro R, McGoldrick LL, Hollingsworth NM, Thorsness PE, Neiman AM. 2016. Yeast Vps13 promotes mitochondrial function and is localized at membrane contact sites. *Mol Biol Cell* 27(15):2435–2449.
Praefcke GJK, McMahon HT. 2004. The dynamin superfamily: universal membrane tubulation and fission molecules? *Nat Rev Mol Cell Biol.* 5(2):133–147.
Price MN, Dehal PS, Arkin AP. 2010. FastTree 2—approximately maximum-likelihood trees for large alignments. *PLoS One* 5(3):e9490.
Punta M, Coggill PC, Eberhardt RY, Mistry J, Tate J, Boursnell C, Pang N, Forslund K, Ceric G, Clements J, et al. 2012. The Pfam protein families database. *Nucleic Acids Res.* 40(Database issue):D290–D301.
Purkanti R, Thattai M. 2015. Ancient dynamin segments capture early stages of host–mitochondrial integration. *Proc Natl Acad Sci U S A.* 112(9):2800–2805.
Radek R. 1994. *Monocercomonoides termitis* n. sp., an oxymonad from the lower termite *Kalotermes sinaicus*. *Arch Protistenkd.* 144(4):373–382.
Rawlings ND, Barrett AJ, Finn R. 2016. Twenty years of the MEROPS database of proteolytic enzymes, their substrates and inhibitors. *Nucleic Acids Res.* 44(D1):D343–D350.
Rawlings ND, Morton FR, Kok CY, Kong J, Barrett AJ. 2008. MEROPS: the peptidase database. *Nucleic Acids Res.* 36(Database issue):D320–D325.
Ribeiro KC, Mariante RM, Coutinho LL, Benchimol M. 2002. Nucleus behavior during the closed mitosis of *Tritrichomonas foetus*. *Biol Cell* 94(4-5):289–301.
Rimmer A, Phan H, Mathieson I, Iqbal Z, Twigg SRF, Wilkie AOM, McVean G, Lunter G. 2014. Integrating mapping-, assembly- and haplotype-based approaches for calling variants in clinical sequencing applications. *Nat Genet.* 46(8):912–918.
Roberts AJ, Kon T, Knight PJ, Sutoh K, Burgess SA. 2013. Functions and mechanics of dynein motor proteins. *Nat Rev Mol Cell Biol.* 14(11):713–726.
Roger A, Muñoz-Gómez SA, Kamikawa R. 2017. The origin and diversification of mitochondria. *Curr Biol.* 27(21):R1177–R1192.
Rogozin IB, Carmel L, Csuros M, Koonin EV. 2012. Origin and evolution of spliceosomal introns. *Biol Direct.* 7:11.
Ronquist F, Teslenko M, van der Mark P, Ayres DL, Darling A, Höhna S, Larget B, Liu L, Suchard MA, Huelsenbeck JP. 2012. MrBayes 3.2: efficient Bayesian phylogenetic inference and model choice across a large model space. *Syst Biol.* 61(3):539–542.
Rout S, Zumthor JP, Schraner EM, Faso C, Hehl AB. 2016. An interactome-centered protein discovery approach reveals novel components involved in mitosome function and homeostasis in *Giardia lamblia*. *PLoS Pathog.* 12(12):e1006036.
Roxström-Lindquist K, Jerlström-Hultqvist J, Jørgensen A, Troell K, Svärd SG, Andersson JO. 2010. Large genomic differences between the morphologically indistinguishable diplomonads *Spironucleus barkhanus* and *Spironucleus salmonicida*. *BMC Genomics.* 11:258.
Roy SW. 2017. Transcriptomic analysis of diplomonad parasites reveals a trans-spliced intron in a helicase gene in *Giardia*. *PeerJ* 5:e2861.
Sagolla MS, Dawson SC, Mancuso JJ, Cande WZ. 2006. Three-dimensional analysis of mitosis and cytokinesis in the binucleate parasite *Giardia intestinalis*. *J Cell Sci.* 119(Pt 23):4889–4900.
Sajid M, McKerrow JH. 2002. Cysteine proteases of parasitic organisms. *Mol Biochem Parasitol.* 120(1):1–21.
Santos HJ, Makiuchi T, Nozaki T. 2018. Reinventing an organelle: the reduced mitochondrion in parasitic protists. *Trends Parasitol.* 34(12):1038–1055.
Schatzmann HJ. 1966. ATP-dependent Ca^{++}-extrusion from human red cells. *Experientia* 22(6):364–365.
Schorey JS, Cheng Y, Singh PP, Smith VL. 2015. Exosomes and other extracellular vesicles in host-pathogen interactions. *EMBO Rep.* 16(1):24–43.
Seaman MNJ. 2004. Cargo-selective endosomal sorting for retrieval to the Golgi requires retromer. *J Cell Biol.* 165(1):111–122.
Sebé-Pedrós A, Grau-Bové X, Richards TA, Ruiz-Trillo I. 2014. Evolution and classification of myosins, a paneukaryotic whole-genome approach. *Genome Biol Evol.* 6(2):290–305.
Slamovits CH, Keeling PJ. 2006. A high density of ancient spliceosomal introns in oxymonad excavates. *BMC Evol Biol.* 6:34.
Smith AJ, Chudnovsky L, Simoes-Barbosa A, Delgadillo-Correa MG, Jonsson ZO, Wohlschlegel JA, Johnson PJ. 2011. Novel core promoter elements and a cognate transcription factor in the divergent unicellular eukaryote *Trichomonas vaginalis*. *Mol Cell Biol.* 31(7):1444–1458.
Spaans SK, Weusthuis RA, van der Oost J, Kengen SWM. 2015. NADPH-generating systems in bacteria and archaea. *Front Microbiol.* 6:742.
Stairs CW, Kokla A, Ástvaldsson Á, Jerlström-Hultqvist J, Svärd S, Ettema T. 2019. Oxygen induces the expression of invasion and stress response genes in the anaerobic salmon parasite *Spironucleus salmonicida*. *BMC Biol.* 17(1):19.
Stamatakis A. 2014. RAxML version 8: a tool for phylogenetic analysis and post-analysis of large phylogenies. *Bioinformatics* 30(9):1312–1313.
Su X, Lin Z, Lin H. 2013. The biosynthesis and biological function of diphthamide. *Crit Rev Biochem Mol Biol.* 48(6):515–521.
Tang H, Sun X, Reinberg D, Ebright RH. 1996. Protein–protein interactions in eukaryotic transcription initiation: structure of the preinitiation complex. *Proc Natl Acad Sci U S A.* 93(3):1119–1124.
Tanifuji G, Takabayashi S, Kume K, Takagi M, Nakayama T, Kamikawa R, Inagaki Y, Hashimoto T. 2018. The draft genome of *Kipferlia bialata*

reveals reductive genome evolution in fornicate parasites. *PLoS One* 13(3):e0194487.
Treitli SC, Kotyk M, Yubuki N, Jirounková E, Vlasáková J, Smejkalová P, Šípek P, Čepička I, Hampl V. 2018. Molecular and morphological diversity of the oxymonad genera *Monocercomonoides* and *Blattamonas* gen. nov. *Protist* 169(5):744–783.
Vacek V, Novák LVF, Treitli SC, Táborský P, Čepička I, Kolísko M, Keeling PJ, Hampl V. 2018. Fe–S cluster assembly in oxymonads and related protists. *Mol Biol Evol*. 35(11):2712–2718.
Valasatava Y, Rosato A, Banci L, Andreini C. 2016. MetalPredator: a web server to predict iron–sulfur cluster binding proteomes. *Bioinformatics* 32(18):2850–2852.
van Hooff JJ, Tromer E, van Wijk LM, Snel B, Kops GJ. 2017. Evolutionary dynamics of the kinetochore network in eukaryotes as revealed by comparative genomics. *EMBO Rep*. 18(9):1559–1571.
Vandecaetsbeek I, Vangheluwe P, Raeymaekers L, Wuytack F, Vanoevelen J. 2011. The Ca^{2+} pumps of the endoplasmic reticulum and Golgi apparatus. *Cold Spring Harb Perspect Biol*. 3(5):pii: a004184.
Voleman L, Najdrová V, Ástvaldsson Á, Tůmová P, Einarsson E, Švindrych Z, Hagen GM, Tachezy J, Svärd SG, Doležal P. 2017. *Giardia intestinalis* mitosomes undergo synchronized fission but not fusion and are constitutively associated with the endoplasmic reticulum. *BMC Biol*. 15(1):27.
Wang CC, Cheng HW. 1984. Salvage of pyrimidine nucleosides by *Trichomonas vaginalis*. *Mol Biochem Parasitol*. 10(2):171–184.
Westrop GD, Goodall G, Mottram JC, Coombs GH. 2006. Cysteine biosynthesis in *Trichomonas vaginalis* involves cysteine synthase utilizing O-phosphoserine. *J Biol Chem*. 281(35):25062–25075.
Wexler-Cohen Y, Stevens GC, Barnoy E, van der Bliek AM, Johnson PJ. 2014. A dynamin-related protein contributes to *Trichomonas vaginalis* hydrogenosomal fission. *FASEB J*. 28(3):1113–1121.
Wickstead B, Gull K. 2012. Evolutionary biology of dyneins. In: Dyneins. Cambridge, Massachusetts US: Elsevier. p. 88–121.
Wickstead B, Gull K, Richards TA. 2010. Patterns of kinesin evolution reveal a complex ancestral eukaryote with a multifunctional cytoskeleton. *BMC Evol Biol*. 10:110.
Williams BAP, Hirt RP, Lucocq JM, Embley TM. 2002. A mitochondrial remnant in the microsporidian *Trachipleistophora hominis*. *Nature* 418(6900):865–869.
Wu X, Wu F-H, Wu Q, Zhang S, Chen S, Sima M. 2017. Phylogenetic and molecular evolutionary analysis of mitophagy receptors under hypoxic conditions. *Front Physiol*. 8:539.
Xu F, Jerlström-Hultqvist J, Einarsson E, Astvaldsson A, Svärd SG, Andersson JO. 2014. The genome of *Spironucleus salmonicida* highlights a fish pathogen adapted to fluctuating environments. *PLoS Genet*. 10(2):e1004053.
Yamamoto Y, Sakisaka T. 2018. The peroxisome biogenesis factors post-translationally target reticulon homology domain-containing proteins to the endoplasmic reticulum membrane. *Sci Rep*. 8(1):2322.
Yeshaw WM, van der Zwaag M, Pinto F, Lahaye LL, Faber AI, Gómez-Sánchez R, Dolga AM, Poland C, Monaco AP, van IJzendoorn SC, et al. 2019. Human VPS13A is associated with multiple organelles and influences mitochondrial morphology and lipid droplet motility. *Elife* 8:pii: e43561.
Yoshida K, Schuenemann VJ, Cano LM, Pais M, Mishra B, Sharma R, Lanz C, Martin FN, Kamoun S, Krause J, et al. 2013. The rise and fall of the *Phytophthora infestans* lineage that triggered the Irish potato famine. *Elife* 28(2):e00731.
Yu SP, Choi DW. 1997. Na^{+}-Ca^{2+} exchange currents in cortical neurons: concomitant forward and reverse operation and effect of glutamate. *Eur J Neurosci*. 9(6):1273–1281.
Žárský V, Tachezy J. 2015. Evolutionary loss of peroxisomes—not limited to parasites. *Biol Direct* 10:74.
Zhang Q, Táborský P, Silberman JD, Pánek T, Čepička I, Simpson A. 2015. Marine isolates of *Trimastix marina* form a plesiomorphic deep-branching lineage within Preaxostyla, separate from other known trimastigids (*Paratrimastix* n. gen.). *Protist* 166(4):468–491.
Zubáčová Z, Krylov V, Tachezy J. 2011. Fluorescence in situ hybridization (FISH) mapping of single copy genes on *Trichomonas vaginalis* chromosomes. *Mol Biochem Parasitol*. 176(2):135–137.
Zubáčová Z, Novák L, Bublíková J, Vacek V, Fousek J, Rídl J, Tachezy J, Doležal P, Vlček C, Hampl V. 2013. The mitochondrion-like organelle of *Trimastix pyriformis* contains the complete glycine cleavage system. *PLoS One* 8(3):e55417.
Zumthor JP, Cernikova L, Rout S, Kaech A, Faso C, Hehl AB. 2016. Static clathrin assemblies at the peripheral vacuole—plasma membrane interface of the parasitic protozoan *Giardia lamblia*. *PLoS Pathog*. 12(7):e1005756.

Functional characterisation of the SUF pathway from the amitochondriate eukaryote *Monocercomonoides exilis*

Manuscript in preparation

Authors: Vojtěch Vacek[1], Priscilla Peña-Diaz[1], Beatrice Py[2], Vladimír Hampl[1]

Affiliations:

[1)] Department of Parasitology, BIOCEV, Faculty of Science, Charles University, Vestec, Czech Republic.

[2)] Laboratoire de Chimie Bactérienne, Aix-Marseille Université-CNRS, Institut de Microbiologie de la Méditerranée, Marseille, France

Keywords: Fe-S cluster, Oxymonads, SUF, BACTH, complementation, Preaxostyla

Abstract:

Oxymonad *Monocercomonoides exilis* is an amitochondriate protist which contains SUF pathway —with some unique features — instead of canonical ISC pathway. In this work, we demonstrate that SUF proteins of *M. exilis* show a high level of conservation in the secondary and tertiary structure and that they contain all previously reported catalytically important residues. Although the sequence of the fusion protein SufDSU contains some unique insertions they do not disturb overall structure. Complementation experiments in *Escherichia coli* proved, that these proteins are capable of partial reconstitution of Fe-S cluster assembly in this organism. Furthermore, bacterial adenylate cyclase two-hybrid system (BACTH) showed, that SufB and SufC interact with each other and are therefore probably capable of forming a complex. Altogether our results bring first although indirect evidence that SUF system of *M. exilis* is capable of Fe-S cluster synthesis.

Introduction:

Iron-Sulfur (Fe-S) clusters are ubiquitous and ancient inorganic cofactors present in virtually all organisms and important for many cellular processes including DNA metabolism, respiration and photosynthesis (Beinert et al. 1997; Rees 2003; Pain and Dancis 2016). Fe-S clusters can exist in various conformations with the most common being the rhombic [2Fe-2S] and cubane [4Fe-4S] forms (Johnson et al. 2005). In living organisms, Fe-S clusters synthesis requires specialized machinery, which generally functions

in a three-module action: 1) sulfur is mobilised from cysteine by the activity of a cysteine desulfurase, 2) the Fe-S cluster is formed *de novo* on a scaffold protein, 3) the newly formed Fe-S cluster is transferred to the target apoprotein (Johnson et al. 2005). In living organisms, three distinct pathways for the synthesis of Fe-S clusters have evolved – the ISC pathway (**I**ron-**S**ulfhur **C**luster assembly) (Zheng et al. 1998), the NIF pathway (**NI**trogen **F**ixation) (Dean et al. 1993; Zheng et al. 1993); and the SUF pathway (**S**ulfur **U**tilisation **F**actor) (Takahashi and Tokumoto 2002).

The NIF system was described in *Azotobacter vinelandii* as the first system known to perform Fe-S cluster assembly. This system is usually specific for the maturation of nitrogenase in nitrogen-fixating bacteria where it is dedicated specifically to the maturation of the iron-molybdenum cofactor (Zheng et al. 1993; Johnson et al. 2005; Dos Santos et al. 2007; Zhao et al. 2007). The NIF system was also reported amongst some eukaryotes such as *Entamoeba histolytica* (Ali et al. 2004; Mi-ichi et al. 2009) and *Mastigamoeba balamuthi* (Nyvltova et al. 2013), but in these cells, it is probably responsible for the initial phase of the synthesis of all Fe-S clusters.

The ISC pathway was discovered as the second system for the Fe-S cluster assembly and it is considered to serve as a house-keeping pathway. It is distributed amongst bacteria and in mitochondria, which inherited it from the α-proteobacterial ancestor (Tachezy et al. 2001; Braymer and Lill 2017). In *E. coli*, it is encoded by the *iscRSUA-hscBA-fdx-iscX operon.* This system is more sensitive to oxidative stress than SUF, and its expression is inhibited by reactive oxygen species (Jang and Imlay 2010). IscS is a type I cysteine desulfurase and IscU was shown to be the scaffold protein on which the Fe-S cluster is assembled. IscS and IscU share high primary sequence similarity with NifS and NifU, respectively. HscA and HscB have been shown to facilitate the transfer of the nascent Fe-S cluster from IscU onto apoprotein in an ATP dependent mode. Fdx probably provides a source of an electron (Yan et al. 2015) and IscX was recently suggested to be the Fe donor for the pathway (Kim et al. 2014; Cai et al. 2018).

The SUF system was described as the last of the three systems but it is considered to be the evolutionary oldest and it is also the most widespread and present in all three domains of life – Archea, Bacteria and Eukaryotes (Takahashi and Tokumoto 2002). The simplest form of the SUF pathway as described from *Archaebacteria* (mainly *Euryarchaeota* and *Crenarchaeota*) consists of only two proteins SufB and SufC (Ollagnier-de-Choudens et al. 2003; Outten et al. 2003; Layer et al. 2007). As it lacks cysteine desulfurase it probably uptakes sulfur from H_2S in the environment. The more sophisticated version of the SUF system in the model bacterium *Escherichia coli* is encoded by the *suf*ABCDSE operon. Sulfur is released from cysteine by the cysteine desulfurase activity of SufS and in the form of persulfide is then transferred from SufS to the cysteine C51 of the accessory protein SufE. From SufE it is then passed to the C254 of SufB, one of the components of the scaffold complex, formed by $SufBC_2D$ (Ollagnier-de Choudens et al. 2003; Layer et al. 2007; Yuda et al. 2017). The crystal structure of the $SufBC_2D$ complex revealed the presence of a hydrophobic tunnel in *E. coli* SufB which would in theory allow S^0 transfer within SufB from C254 to C405 (Yuda et al. 2017). SufD was also proposed to play a role in Fe acquisition (Saini et al. 2010). The Fe-S cluster is then formed by the coordinated activity of the $SufBC_2D$ complex, which binds $FADH_2$ (Wollers et

al., 2010). C405 and H360 from SufB and SufD respectively, form an interface on which the nascent Fe-S cluster is formed (Yuda et al. 2017). SufD was also proposed to play a role in Fe acquisition (Saini et al. 2010). Although several stoichiometries of scaffold complexes (SufBC, SufCD and SufBCD) have been detected *in vitro*, the $SufBC_2D$ complex has been shown to be most common (Petrovic et al. 2008; Wada et al. 2009; Saini et al. 2010).

SufC is a member of the ABC ATPase superfamily and exhibits ATPase activity as well as other features and motifs typical for this family of proteins (Nachin et al. 2003; Kitaoka et al. 2006). SufC forms a head-to-tail dimer inducing structural changes to the $SufBC_2D$ complex after ATP binding, exposing C405 of SufB and H360 of SufD, which are normally buried inside of the complex (Hirabayashi et al. 2015). It was also shown that a mutation in the Walker A motif of SufC (L40R) reduced eightfold the iron content on the isolated $SufBC_2D$ complex when compared to the wild type, strongly suggesting that ATPase activity of SufC is necessary for Fe acquisition by complex (Saini et al. 2010).

In gram-positive bacteria such as *Bacilus subtillis*, the Fe-S cluster assembly SUF pathway is coded by the operon sufCDSUB, where all components are similar to the corresponding SUF homologues in *E. coli* with the exception of SufU, which shares a high sequence similarity with IscU. Pathways with similar composition were also found in Bacilli, Actinobacteria, Spirochaetes and Thermotogae (Tokumoto et al. 2004; Huet et al. 2005; Boyd et al. 2014; Wayne Outten 2015). SufU was shown to enhance the cysteine desulfurase activity of SufS (Albrecht et al. 2010; Albrecht et al. 2011; Selbach et al. 2014). Recently it was shown that SufS and SufU from *B. subtilis* can functionally replace SufS and SufE in *E. coli* and vice versa, but SufU or SufE alone were not able to replace each other on their own (Yokoyama et al. 2018a). In eukaryotes, the SUF pathway is usually localized in plastids or plastid-related organelles and is of cyanobacterial origin (Balk and Lobréaux 2005; Balk and Pilon 2011).

Synthesis of Fe-S clusters by the ISC pathway is considered to be the core function of mitochondria, including the reduced forms of these organelles called mitochondrion-related organelles (MRO) (Williams et al. 2002). MROs share some common features with mitochondria and originated from the same α-proteobacterial endosymbiosis, yet they bear different metabolic properties – such as the ATP-producing hydrogenosomes (Lindmark and Müller 1973) named after their production of H_2, and mitosomes (Tachezy and Šmíd 2019), which produce neither ATP nor H_2, and their only function in some species seems to be limited to Fe-S cluster assembly (Tovar et al. 2003). The classification of MROs has been broadened to a wide spectrum of organelles of various metabolic properties and many transitional forms (Müller et al. 2012; Leger et al. 2017). Interestingly, some protists exhibiting an MROs have also been found displaying proteins from other Fe-S cluster assembly pathways. Such is the case of *E. histolytica*, which harbours the NIF pathway most probably localised in its cytosol and the only essential function of its mitosome is sulfate activation (Ali et al. 2004; Mi-ichi et al. 2009; Maralikova et al. 2010; Mi-ichi et al. 2011).

Until the definition of MROs, organisms bearing these forms of mitochondria had been defined as “amitochondriates”. However, the first “true” amitochondriate, i.e. lacking both mitochondria and MRO, was only recently described. This organism known as *Monocercomonoides exilis* (formerly *Monocercomonoides*

Pa303) (Karnkowska et al. 2016; Treitli et al. 2018) is the most studied representative of the group Oxymonadida. Oxymonads together with trimastigids and paratrimastigids are the three sole members of Preaxostyla, a group of heterotrophic, anaerobic and/or microaerophilic flagellated protists. The former group is primarily formed by endobiotic protists found in the hindgut of lower termites and wood-eating cockroaches, meanwhile the second and third group are comprised of free-living flagellates (Hampl 2017). Phylogenetically, Preaxostyla represent one of the three lineages of Metamonada (Leger et al. 2017; Adl et al. 2019), part of the former "supergroup" Excavata (Zhang et al. 2015; Adl et al. 2019). Unlike oxymonads, the members of the paratrimastigids and trimastigid (*Paratrimastix pyriformis* and *Trimastix marina*) contains an MROs similar to hydrogenosomes (Brugerolle and Patterson 1997; O'Kelly et al. 1999; Simpson et al. 2000) one of which have been partially characterised (Hampl et al. 2008; Zubáčová et al. 2013).

The existence of MRO bearing relatives suggests that *Monocercomonoides exilis* has undergone secondary loss of its mitochondrion (Karnkowska et al. 2016). Together with its MRO, it lost all other mitochondrial pathways including the ISC, but instead, a genes for the SUF pathway enzymes were found in its genome. As Fe-S cluster assembly is considered to be the hardest core function of MROs, it has been proposed that this major rearrangement of Fe-S cluster synthesis might have been the prerequisite for the loss of the MRO in oxymonads (Karnkowska et al. 2016). Further intensive study of the *M. exilis* genome and comparison with other eukaryotes did not show any other obvious pre-adaptation for the loss of the MRO rather than the acquisition of a SUF pathway (Karnkowska et al. 2019).

The SUF pathway of *M. exilis* consists of SufB, SufC, and the fusion protein SufDSU, this later one consisting of parts with homology to SufD, SufS and SufU. This fusion was found supported by transcriptomic data. Furthermore, we were able to confirm that the same set of SUF genes, including the unique fusion protein SufDSU, is present across the diversity of Preaxostyla (Vacek et al. 2018). Heterologous localisation of *M. exilis* SufB and SufC in *Saccharomyces cerevisiae* and *Trichomonas vaginalis* suggested cytosolic localization of these proteins, neither of which contain a recognizable N-terminal targeting sequence (Karnkowska et al. 2016). The substitution of the ISC pathway by SUF does not seem to affect the CIA pathway, which exhibits a similar composition to the CIA pathways of related protists from the group Metamonada (Vacek et al. 2018), as well as the predicted set of Fe-S cluster-containing proteins is comparable with those of other anaerobically living protists (Karnkowska et al. 2019).

SufB and SufC genes have also been found in protists such as *Pygsuia biforma* (Stairs et al. 2014), *Blastocystis hominis* (Tsaousis et al. 2012), *Proteromonas lacertae*, and *Stygiella incarcerata* (Leger et al. 2016). But only in *P. biforma* they have replaced the mitochondrial ISC pathway (Stairs et al. 2014). Phylogenetic analyses suggest that SufB and SufC genes of these protists share a common origin with Methanomicrobiales (Tsaousis et al. 2012; Leger et al. 2016; Tsaousis 2019) and are unrelated to those of Preaxostyla.

In this paper we aim to bring the evidence for the functionality of the SUF pathway in *M. exilis*. Although this pathway is key for the secondary loss of the MRO in this organism and it likely provided this protist with a unique way of FeS cluster assembly, all information published until present is based solely on

in silico predictions from the genomic and transcriptomic data. Because the biochemical and genetic tools are not available for *M. exilis* at the moment, we study the functionality of *M. exilis* enzymes by complementation of their functional homologues or analogues in *E. coli* mutant strains.

Results

In silico analysis and modelling of *M. exilis* SUF proteins.

To verify potential functionality of *M. exilis* SUF pathway, we have modelled the 3D structures of *M. exilis* SUF proteins using homology based modelling by SWISS-MODEL (Waterhouse et al. 2018). . Our aim was to observe the overall structure conservation and the presence and position of functionally important residues.

The cysteine desulfurase SufS belongs to the type II cysteine desulfurases which are characteristic for the transport of cysteine-originated persulfide intermediate to a specific acceptor (SufE, SufU), often required for the activation of the enzyme (Ollagnier-de-Choudens et al. 2003; Outten et al. 2003; Riboldi et al. 2011). An additional feature of type II cysteine desulfurases is the presence of the β-hairpin motif (corresponding to residues 253-265 in *B. subtilis*) (Blauenburg et al. 2016). In the *M. exilis* SufS (**Fig. 1**), all the important residues such as the active site cysteine (C361 in *B. subtilis*), C548 in *M. exilis* and adjacent residues are well-conserved, showing a high level of similarity (42.25% sequence identity) to the sequences of SufS from *B. subtilis*, but also *E. coli* and other organisms (Blauenburg et al. 2016). The lysine residue responsible for binding of PLP (K224 in *B. subtilis*), K226 in *M. exilis* is also conserved (Selbach et al. 2010; Selbach et al. 2014). However, in comparison to other SufS sequences, the homologue of *M. exilis* exhibits three unique insertions, which divide the PLP-binding site. In the protein model, these sequences form loops on the surface of the protein yet they do not disturb the PLP-binding pocket (**Fig. 1**). The PLP-binding site was also predicted using COACH (protein-ligand binding site prediction meta-server) (Yang et al. 2013) with high probability (C-score 0.79). The H342 of *B. subtilis* SufS is referred to as the residue responsible for binding of Zn of SufU, this dissociates bond between C41 of SufU and Zn. C41 is then free to accept S^0 released from cysteine (C361 *B. subtilis*) of SufS (Fujishiro et al. 2017). Also this histidine is well-conserved in sequences of Gram-positive bacteria as well as in the sequence of *M. exilis* (position 222).

M. exilis SufU is structurally similar (sequence identity 37.50%) to its homologues from *B. subtilis*, *Enterococcus faecalis* and other Gram positive bacteria and like them it lacks the LPVVK motif typical for IscU (Riboldi et al. 2009). An amino acid insert conserved in Gram positive bacteria (also referred as GPR) of approximately 19 AA long is elongated to 27 amino acids in *M. exilis,* alongside the zinc binding residues – C98, C136, C206 and D100 (*M. exilis* numbering)

which are also present and conserved in the protein in *M. exilis* (Selbach et al. 2014; Fujishiro et al. 2017) (**Fig. 2**).

Examination of *M. exilis* SufB protein sequence and its comparison to the model of SufB from *E. coli* revealed that all previously identified residues responsible for the Fe-S cluster formation (R226, D228 C254, Q285, W287, K303, numbering from *E. coli*) are also present in the *M. exilis* homologue (**Fig. 3**). SufB residues C405 and E434, as well as H360 in SufD, reported to be responsible for creating the interface between SufB and SufD in *E. coli* are present in their counterpart in *M. exilis* (Hirabayashi et al. 2015; Yuda et al. 2017). The position of cysteine C254 (*E. coli* numbering) which probably serves as an acceptor of persulfide transferred from SufE (Yuda et al. 2017), is well conserved in the sequence of its homologue in *M. exilis* (282) and its position in the model of SufB overlaps with the position in *E. coli* (**Fig. 3**). Of the four of $FADH_2$ binding motifs predicted in *E. coli* SufB, - $P(x)_6GxN$, $R(x)_6ExxY(x)_5G(x)_8Y$, GxxL and R451, only $R(x)_6ExxY(x)_5G(x)_8Y$ and R451 are conserved in SufB of *M. exilis* (Wollers et al. 2010).

The hydrophobic tunnel which goes through the β-helix core of SufB and connects C254 with C405 was predicted by CAVER3.0 (Chovancova et al. 2012) in *E. coli* (Yuda et al. 2017). In *M . exilis* a similar tunnel can be also predicted and ranges from C293 to C434, which correspond to their counterparts in *E. coli* (data not shown).

The sequence of SufD is the least conserved of all the SUF proteins of *M. exilis* (21.45% sequence identity to SufD of *E. coli*). Of all the previously reported essential residues, it only displays H360 (*E. coli* numbering) which is involved in the formation of the interface with SufB (Yuda et al. 2017). Another residue reported to be involved in the formation of this interface is C358. In *M. exilis* an A is present instead of C in this position. This substitution, however, seems to be present in many of gram-positive bacteria. Also *M. exilis* sequence displays several relatively long insertions which have no homology with *E. coli* sequence and probably form loops (shown in red in **Fig. 4**) which are hard to model.

SufC was proposed to be responsible for the dynamic ATP-driven conformational change of $SufBC_2D$ complex, which exposes the Fe-S cluster binding site on SufB and SufD interface (Hirabayashi et al. 2015). SufC of *M. exilis* contains all the characteristic motifs of ABC ATPases such as the Walker A and Walker B motifs, the ABC signature motif, the Q-loop and the H-motif. The amino acids identified as potentially important for ATPase activity are also conserved (K40, K152, E171, D173 and H203 - *E. coli* numbering) in the sequence of *M. exilis* SufC (Kitaoka et al. 2006; Hirabayashi et al. 2015). Model comparison shows high resemblance (53.66% sequence identity) to the structure of *E. coli* SufC (**Fig. 5**).

Bacterial complementation

To verify the functionality of the *M. exilis* SUF pathway proteins, the genes SufB, SufC and SufDSU were codon optimised for expression in *E. coli* and *S. cerevisiae* and cloned into pTrc99a vector (Amann et al. 1988). The fusion protein SufDSU was cloned complete as well as in two separated modules corresponding to SufS and SufU.

Complementation experiments were carried out in *E. coli* strains deficient in the corresponding gene (for genotypes see Table 1). In the case of SufU, which is not present in *E. coli*, the strain deficient in the functional analogue SufE was used for complementation. *E. coli* transformed with the *M. exilis* genes were tested in a serial-dilutions spots growth assay on LB plates with 250, 275, 300 and 350 μM concentrations of DIP (2,2′-Bipyridyl) and 30, 40, 50 and 70μM concentrations of PMS (phenazine methosulfate) to induce iron starvation and/or oxidative stress respectively. A weak rescue effect was observed for SufB (**Fig. 6**), This rescue effect was observable only in the concentration of DIP 275μM and 30μM PMS. However, no rescue effect was observed for other genes. Overexpression of SufC had a toxic effect on *E. coli* cells when overexpressed under conditions of Fe starvation, corresponding to the same phenotype observed when overexpressing the native *E. coli* SufC (**Fig. 7**). Partial genes derived from SufDSU - SufS, SufSU and SufU of *M. exilis* failed to show any rescue effect in single-gene mutants of *E. coli* when compared to the negative control. Overexpression of these genes had a lethal effect on *E. coli* under stress conditions (data not shown).

Because the growth phenotypes of complemented *E. coli* strains were weak, we decided to verify specifically the rescue of Fe-S cluster synthesis in mevalonate dependent strains of *E. coli* (Campos et al. 2000). The LacZ gene cloned under IscR-regulated promoter allowed the measurement of Fe-S cluster production in strains of *E. coli* deficient in the respective relevant gene in SUF and ISC pathway. The strain DV1184 deficient in SufB, IscU and IscA was used for SufB and DV1249 deficient in SufS and IscS was used for SufDSU or its parts respectively (for genotypes see **Table 1**). Neither SufB nor SufDSU genes were able to fully complement their counterparts in the bacterial strains, and cells were not viable without mevalonate. To further evaluate the level of Fe-S clusters production, a β-galactosidase assay was performed, which allows detection of Fe-S cluster synthesis more sensitively than the standard growth phenotype assay. Measurements of β-galactosidase activity in DV1184 strain transfected with *M. exilis* SufB showed that the production of Fe-S clusters was partially restored when compared to controls (**Fig. 8**), suggesting that SufB is capable of partial restoration of Fe-S cluster production in *E. coli*. Parts of SufDSU gene – SufS and SufSU were capable of restoring Fe-S cluster assembly in the double

mutant strain of *E. coli* (DV1249), as measured β-galactosidase activity was significantly lower than the activity of negative control (**Fig. 8**).

M. exilis SufB and SufC forms complex with each other

Another evidence for the functionality of the SUF pathway in *M. exilis* was obtained using the BACTH assay (Bacterial Adenylate Cyclase Two Hybrid system) (Battesti and Bouveret 2012). This assay allows to test protein-protein interaction in *E. coli in vivo,* and *and takes advantage of* two catalytic domains of *Bordetella pertussis* adenylate cyclase (CyaA) toxin. These domains can be fused separately to proteins of interest, and if the proteins of interest interact, then the adenylate cyclase domains will be brought together, which will reconstitute production of cyclic AMP (cAMP). Production of cAMP can be detected by measuring the activity of β-galactosidase expressed under cAMP-dependent promotor.
Genes for SufB and SufC of *M. exilis* were cloned in to pUT18 and pKT25 vectors and expressed together in DHT1 competent cells of *E. coli* strains and the activity of β-galactosidase was measured. The activity measured in DHT 1 cells expressing SufB-pKT25 + SufC-pUT18 and expressing SufC-pKT25 + SufB-pUT18 was comparable to the activity of positive control. Therefore, restoration of the adenylate cyclase activity in *E. coli* DHT1 (**Fig. 9**) provided evidence that SufB and SufC of *M. exilis* interact in vivo in *E. coli*

Discussion:

As the genetic and biochemical tool are not available for *M. exilis*, we applied *in silico* protein modelling as well as heterologous complementation experiments to assess the functionality of SUF pathway from this organism. *In silico* analysis of *M. exilis* SufB sequence showed that all residues responsible for Fe-S cluster formation (R226, D228 C254, Q285, W287, K303, numbering from *E. coli*) are present in the aforementioned protein, as well as the residues reported to form the interface with SufD (C405 and E434 in *E. coli*). From the four described $FADH_2$ binding sites, only two are present in *M. exilis* SufB. These $FADH_2$ binding motifs are conserved only in some organisms and in some bacteria (*Yersinia* and *Salmonella*) are completely missing furthermore not just SufB is probably involved in $FADH_2$ binding because *E. coli* SufB alone is able to bind just small amounts of flavin, only the whole $SufBC_2D$ complex binds 1 eq of flavin (Wollers et al. 2010). Also exact role of $FADH_2$ is unknown as it was experimentally shown that $FADH_2$ is not necessary for the transfer of 4Fe-4S cluster to the recipient apo-protein (Wollers et al. 2010). Another difference is that sequence of *M. exilis* SufD contains an alanine instead of a cysteine on the position equivalent to C358 of *E. coli*. However this substitution did not cause any noticeable

growth defects when it was experimentally mutated in *E. coli* (Yuda et al., 2017). SufB of *M. exilis* showed a weak rescue effect on the *E. coli* strain deficient in SufB under conditions of oxidative stress and iron starvation, and its ability to substitute SufB of *E. coli* was also confirmed by the β-galactosidase assay in the aforementioned strain of *E. coli* where SufB of *M. exilis* showed significantly higher production of Fe-S clusters when compared to negative control. However, this effect was not sufficient to fully restore viability of *E. coli* without mevalonate. This may be interpreted as an impossibility of the protist scaffold protein to interact with the downstream components of the pathway, namely the transfer proteins, which ultimately deliver the freshly formed clusters into their apoproteins.

Regardless of the presence of three insertion sequences in the SufS of *M. exilis* which seemingly disrupt the PLP binding site, the *in silico* protein model of *M. exilis* SufS shows the PLP binding site of *M. exilis* SufS intact and most probably loops do not interfere with PLP binding. However, no part of the fusion protein SufDSU – SufS, SufSU or SufU – by themselves was able to restore the viability of *E. coli* strains under conditions of oxidative stress or iron starvation. Also SufS and SufSU were not able to fully restore viability of ΔISC ΔSUF strains of *E. coli*, although they were able to partially restore Fe-S cluster assembly in those strains. Possible explanation is that SufS of *M. exilis* may be unable to interact (or interact in limited way) with SufE of *E. coli* and *vice versa.* This is further supported by inability of SufU of *M. exilis* to functionally replace SufE of *E. coli*. These results would correspond with previously published experimental substitution of SufU between *B. subtilis* and SufE of *E. coli* (Yokoyama et al. 2018).

The BACTH assay showed that SufB and SufC of *M. exilis* are interacting with one another and thus capable of forming a complex.

Taken together, we bring the first but indirect evidence that the SUF system of *M. exilis* is active in Fe-S cluster assembly and despite being diverged from well-described systems such as *E. coli* and *B. subtilis* (especially in case of fusion protein SufDSU, unique for Preaxostyla) it can at least partially recover Fe-S cluster assembly in *E. coli*. Also, comparison of predicted protein models of SUF proteins of *M. exilis* with known crystal structures shows overall conservation of important catalytic and structural residues in models.

Methods:

Serial dilution spotting assay

Bacterial strains were cultivated overnight at 37°C, in 5ml of LB media with antibiotics at 225rpm. Grown cultures were reinoculated into 5 ml of fresh LB with antibiotics and cultivated in shaking at

37°C, 225 rpm until cultures reached OD_{600} = 0.6 approximately. Cultures were adjusted (diluted) with LB to equal ODs. Serial dilution from 10^{-1} to 10^{-8} were prepared in 96-well plates, and spots (5µl) were applied to plate with 8-channel pipette.

Vector preparation

For complementation experiments codon optimised genes were PCR amplified with specific primers and cloned into pTrc99A vector (Amann et al. 1988) by restriction cloning. For BACTH analysis codon optimised genes for SufB and SufC were cloned into pKT25 and pUT18 vectors by restriction cloning.

Measurements of β-galactosidase activity in MEV-dependent strains

Double mutant strains of *E. coli* strains (for genotypes of individual strains see Table 1) were transfected with prepared constructs by electroporation (2mm cuvettes, 25µFD, 2,5V, 200 Ω). Transfected cells were plated on mevalolactone (MEV)-containing plates (Campos et al. 2000) plus ampicillin (100µg/ml) and incubated in 37°C. Grown colonies were transferred in LB MEV media and grown for 24H 37 225rpm. After 24H IPTG was added to final concentration of 1mM and cells were grown for another 24H and β-galactosidase activity was measured using standard colorimetric assay of β-galactosidase activity as described by Miller [J. H. Miller (1972) Experiments in Molecular Genetics, Cold Spring Harbor Laboratory Press, Cold Spring Harbor, NY]

BACTH

Codon optimised genes were PCR amplified were cloned into vectors pUT18 and pKT25 respectively. The constructs were then transfected by heat-shock into DHT101 competent cells and plated on LB plates with selective antibiotics o final concentrations Kanamycin - 50µg/ml, Ampicilin- 100µg/ml. Selected colonies were transferred into LB with ATB were grown for 16 hours at 30˚C, at 225 rpm and β-galactosidase activity was measured using standard colorimetric assay of β-galactosidase activity as described by Miller [J. H. Miller (1972) Experiments in Molecular Genetics, Cold Spring Harbor Laboratory Press, Cold Spring Harbor, NY]

Protein modelling

Protein models were generated by SWISS-MODEL (Waterhouse et al. 2018) using best fitting crystal structure as template. Refinements of Models were graphically edited using PyMOL™ molecular graphics system version 1.8.4.0.

Table 1: list of used strains

Strain	Genotype
DV1222	MG ΔsufB ::kan
DV1225	MG ΔsufS ::kan
BP224	MG ΔsufC ::kan
DV1226	MG ΔsufE ::kan
DV1249	ΔlacZ PiscR(trans)::lacZ MEV+ ΔiscS::cat ΔsufS::kan Tn10
DV1184	ΔlacZ PiscR(trans)::lacZ MEV+ ΔiscAU ΔsufB::kan Tn10
DV1186	ΔlacZ PiscR(trans)::lacZ MEV+ ΔiscAUΔsufS::kan Tn10

All used strains are based on *E. coli* K-12 genotype

References:

Adl SM, Bass D, Lane CE, Lukeš J, Schoch CL, Smirnov A, Agatha S, Berney C, Brown MW, Burki F, et al. 2019. Revisions to the Classification, Nomenclature, and Diversity of Eukaryotes. J Eukaryot Microbiol. 66(1):4–119. doi:10.1111/jeu.12691.

Albrecht AG, Netz DJA, Miethke M, Pierik AJ, Burghaus O, Peuckert F, Lill R, Marahiel MA. 2010. SufU is an essential iron-sulfur cluster scaffold protein in Bacillus subtilis. J Bacteriol. 192(6):1643–1651. doi:10.1128/JB.01536-09.

Albrecht AG, Peuckert F, Landmann H, Miethke M, Seubert A, Marahiel MA. 2011. Mechanistic characterization of sulfur transfer from cysteine desulfurase SufS to the iron-sulfur scaffold SufU in Bacillus subtilis. FEBS Lett. 585(3):465–470. doi:10.1016/j.febslet.2011.01.005. http://dx.doi.org/10.1016/j.febslet.2011.01.005.

Ali V, Shigeta Y, Tokumoto U, Takahashi Y, Nozaki T. 2004. An Intestinal Parasitic Protist, Entamoeba histolytica, Possesses a Non-redundant Nitrogen Fixation-like System for Iron-Sulfur Cluster Assembly under Anaerobic Conditions. J Biol Chem. 279(16):16863–16874. doi:10.1074/jbc.M313314200.

Amann E, Ochs B, Abel KJ. 1988. Tightly regulated tac promoter vectors useful for the expression of unfused and fused proteins in Escherichia coli. Gene. 69(2):301–315. doi:10.1016/0378-1119(88)90440-4.

Balk J, Lobréaux S. 2005. Biogenesis of iron-sulfur proteins in plants. Trends Plant Sci. 10(7):324–331. doi:10.1016/j.tplants.2005.05.002.

Balk J, Pilon M. 2011. Ancient and essential: The assembly of iron-sulfur clusters in plants. Trends Plant Sci. 16(4):218–226. doi:10.1016/j.tplants.2010.12.006. http://dx.doi.org/10.1016/j.tplants.2010.12.006.

Battesti A, Bouveret E. 2012. The bacterial two-hybrid system based on adenylate cyclase reconstitution in Escherichia coli. Methods. 58(4):325–334. doi:10.1016/j.ymeth.2012.07.018.

Beinert H. 1997. Iron-Sulfur Clusters: Nature’s Modular, Multipurpose Structures. Science (80-). 277(5326):653–659. doi:10.1126/science.277.5326.653.

Blauenburg B, Mielcarek A, Altegoer F, Fage CD, Linne U, Bange G, Marahiel MA. 2016. Crystal Structure of Bacillus subtilis Cysteine Desulfurase SufS and Its Dynamic Interaction with Frataxin and Scaffold Protein SufU. Rouault T, editor. PLoS One. 11(7):e0158749. doi:10.1371/journal.pone.0158749.

Boyd ES, Thomas KM, Dai Y, Boyd JM, Outten FW. 2014. Interplay between Oxygen and Fe-S Cluster Biogenesis: Insights from the Suf Pathway. Biochemistry. 53(37):5834–5847. doi:10.1021/bi500488r.

Braymer JJ, Lill R. 2017. Iron–sulfur cluster biogenesis and trafficking in mitochondria. J Biol Chem. 292(31):12754–12763. doi:10.1074/jbc.R117.787101.

Brugerolle G, Patterson D. 1997. Ultrastructure of Trimastix convexa hollande, an amitochondriate anaerobic flagellate with a previously undescribed organization. Eur J Protistol. 33(2):121–130. doi:10.1016/S0932-4739(97)80029-6.

Cai K, Frederick RO, Tonelli M, Markley JL. 2018. Interactions of iron-bound frataxin with ISCU and ferredoxin on the cysteine desulfurase complex leading to Fe-S cluster assembly. J Inorg Biochem. 183:107–116. doi:10.1016/j.jinorgbio.2018.03.007.

Campos N, Rodríguez-Concepción M, Sauret-Güeto S, Gallego F, LOIS L-MM, Boronat A. 2000. Escherichia coli engineered to synthesize isopentenyl diphosphate and dimethylallyl diphosphate from mevalonate: a novel system for the genetic analysis of the 2-C-methyl-d-erythritol 4-phosphate pathway for isoprenoid biosynthesis. Biochem J. 353(1):59. doi:10.1042/0264-6021:3530059.

Dean DR, Bolin JT, Zheng L. 1993. Nitrogenase metalloclusters: structures, organization, and synthesis. J Bacteriol. 175(21):6737–6744. doi:10.1128/JB.175.21.6737-6744.1993.

Fujishiro T, Terahata T, Kunichika K, Yokoyama N, Maruyama C, Asai K, Takahashi Y. 2017. Zinc-Ligand Swapping Mediated Complex Formation and Sulfur Transfer between SufS and SufU for Iron-Sulfur Cluster Biogenesis in Bacillus subtilis. J Am Chem Soc. 139(51):18464–18467. doi:10.1021/jacs.7b11307.

Hampl V. 2017. Preaxostyla. In: Handbook of the Protists. Cham: Springer International Publishing. p. 1139–1174.

Hampl V, Silberman JD, Stechmann A, Diaz-Triviño S, Johnson PJ, Roger AJ. 2008. Genetic evidence for a mitochondriate ancestry in the ‘amitochondriate’ flagellate Trimastix pyriformis. PLoS One. 3(1):e1383. doi:10.1371/journal.pone.0001383.

Hirabayashi K, Yuda E, Tanaka N, Katayama S, Iwasaki K, Matsumoto T, Kurisu G, Outten FW, Fukuyama K, Takahashi Y, et al. 2015. Functional dynamics revealed by the structure of the SufBCD Complex, a novel ATP-binding cassette (ABC) protein that serves as a scaffold for iron-sulfur cluster biogenesis. J Biol Chem. 290(50):29717–29731. doi:10.1074/jbc.M115.680934.

Huet G, Daffé M, Saves I. 2005. Identification of the Mycobacterium tuberculosis SUF machinery as the exclusive mycobacterial system of [Fe-S] cluster assembly: Evidence for its implication in the pathogen’s survival. J Bacteriol. 187(17):6137–6146. doi:10.1128/JB.187.17.6137-6146.2005.

Chovancova E, Pavelka A, Benes P, Strnad O, Brezovsky J, Kozlikova B, Gora A, Sustr V, Klvana M, Medek P, et al. 2012. CAVER 3.0: A Tool for the Analysis of Transport Pathways in Dynamic Protein Structures. PLoS Comput Biol. 8(10). doi:10.1371/journal.pcbi.1002708.

Jang S, Imlay JA. 2010. Hydrogen peroxide inactivates the Escherichia coli Isc iron-sulphur assembly system, and OxyR induces the Suf system to compensate. Mol Microbiol. 78(6):1448–1467. doi:10.1111/j.1365-2958.2010.07418.x.

Johnson DC, Dean DR, Smith AD, Johnson MK. 2005. Structure, Function, and Formation of Biological Iron-Sulfur Clusters. Annu Rev Biochem. 74(1):247–281. doi:10.1146/annurev.biochem.74.082803.133518.

Johnson DCC, Dos Santos PCC, Dean DRR. 2005. NifU and NifS are required for the maturation of nitrogenase and cannot replace the function of isc -gene products in Azotobacter vinelandii. Biochem Soc Trans. 33(1):90–93. doi:10.1042/BST0330090.

Karnkowska A, Treitli SCSC, Brzoň O, Novák L, Vacek V, Soukal P, Barlow LDLD, Herman EKEK, Pipaliya SVSV, Pánek T, et al. 2019. The Oxymonad Genome Displays Canonical Eukaryotic Complexity in the Absence of a Mitochondrion. Mol Biol Evol. 36(10):2292–2312. doi:10.1093/molbev/msz147.

Karnkowska A, Vacek V, Zubáčová Z, Treitli SCSC, Petrželková R, Eme L, Novák L, Žárský V, Barlow LDLD, Herman EKEK, et al. 2016. A eukaryote without a mitochondrial organelle. Curr Biol. 26(10):1274–1284. doi:10.1016/j.cub.2016.03.053.

Kim JH, Bothe JR, Frederick RO, Holder JC, Markley JL. 2014. Role of IscX in iron-sulfur cluster biogenesis in Escherichia coli. J Am Chem Soc. 136(22):7933–7942. doi:10.1021/ja501260h.

Kitaoka S, Wada K, Hasegawa Y, Minami Y, Fukuyama K, Takahashi Y. 2006. Crystal structure of Escherichia coli SufC, an ABC-type ATPase component of the SUF iron-sulfur cluster assembly machinery. FEBS Lett. 580(1):137–143. doi:10.1016/j.febslet.2005.11.058.

Layer G, Aparna Gaddam S, Ayala-Castro CN, Choudens SO De, Lascoux D, Fontecave M, Outten FW. 2007. SufE transfers sulfur from SufS to SufB for iron-sulfur cluster assembly. J Biol Chem. 282(18):13342–13350. doi:10.1074/jbc.M608555200.

Leger MM, Kolisko M, Kamikawa R, Stairs CW, Kume K, Čepička I, Silberman JD, Andersson JO, Xu F, Yabuki A, et al. 2017. Organelles that illuminate the origins of Trichomonas hydrogenosomes and Giardia mitosomes. Nat Ecol Evol. 1(4):0092. doi:10.1038/s41559-017-0092.

Leger MMM, Eme L, Hug LAA, Roger AJJ. 2016. Novel Hydrogenosomes in the Microaerophilic Jakobid Stygiella incarcerata. Mol Biol Evol. 33(9):2318–2336. doi:10.1093/molbev/msw103.

Lindmark DG, Müller M. 1973. Hydrogenosome, a cytoplasmic organelle of the anaerobic flagellate Tritrichomonas foetus, and its role in pyruvate metabolism. J Biol Chem. 248(22):7724–7728.

Maralikova B, Ali V, Nakada-Tsukui K, Nozaki T, van der Giezen M, Henze K, Tovar J. 2010. Bacterial-type oxygen detoxification and iron-sulfur cluster assembly in amoebal relict mitochondria. Cell Microbiol. 12(3):331–342. doi:10.1111/j.1462-5822.2009.01397.x.

Mi-ichi F, Makiuchi T, Furukawa A, Sato D, Nozaki T. 2011. Sulfate activation in mitosomes plays an important role in the proliferation of entamoeba histolytica. Eichinger D, editor. PLoS Negl Trop Dis. 5(8):e1263. doi:10.1371/journal.pntd.0001263.

Mi-ichi F, Yousuf MA, Nakada-Tsukui K, Nozaki T. 2009. Mitosomes in Entamoeba histolytica contain a sulfate activation pathway. Proc Natl Acad Sci. 106(51):21731–21736. doi:10.1073/pnas.0907106106.

Muller M, Mentel M, van Hellemond JJ, Henze K, Woehle C, Gould SB, Yu R-Y, van der Giezen M, Tielens AGM, Martin WF. 2012. Biochemistry and Evolution of Anaerobic Energy Metabolism in Eukaryotes. Microbiol Mol Biol Rev. 76(2):444–495. doi:10.1128/mmbr.05024-11.

Nachin L, Loiseau L, Expert D, Barras F. 2003. SufC: an unorthodox cytoplasmic ABC/ATPase required for [Fe-S] biogenesis under oxidative stress. EMBO J. 22(3):427–37. doi:10.1093/emboj/cdg061.

Nyvltova E, Sutak R, Harant K, Sedinova M, Hrdy I, Paces J, Vlcek C, Tachezy J, Nývltová E, Šuták R, et al. 2013. NIF-type iron-sulfur cluster assembly system is duplicated and distributed in the mitochondria and cytosol of Mastigamoeba balamuthi. Proc Natl Acad Sci. 110(18):7371–7376. doi:10.1073/pnas.1219590110.

O’Kelly CJ, Farmer MA, Nerad TA. 1999. Ultrastructure of Trimastix pyriformis (Klebs) Bernard et al.: Similarities of Trimastix Species with Retortamonad and Jakobid Flagellates. Protist. 150(2):149–162. doi:10.1016/S1434-4610(99)70018-0.

Ollagnier-de-Choudens S, Lascoux D, Loiseau L, Barras F, Forest E, Fontecave M. 2003. Mechanistic studies of the SufS-SufE cysteine desulfurase: evidence for sulfur transfer from SufS to SufE. FEBS Lett. 555(2):263–7.

Ollagnier-de Choudens S, Nachin L, Sanakis Y, Loiseau L, Barras F, Fontecave M. 2003. SufA from Erwinia chrysanthemi. Characterization of a scaffold protein required for iron-sulfur cluster assembly. J Biol Chem. 278(20):17993–18001. doi:10.1074/jbc.M300285200.

Outten FW, Wood MJ, Muñoz FM, Storz G, Munoz FM, Storz G. 2003. The SufE protein and the SufBCD complex enhance SufS cysteine desulfurase activity as part of a sulfur transfer pathway for Fe-S cluster assembly in Escherichia coli. J Biol Chem. 278(46):45713–9. doi:10.1074/jbc.M308004200.

Pain D, Dancis A. 2016. Roles of Fe–S proteins: from cofactor synthesis to iron homeostasis to protein synthesis. Curr Opin Genet Dev. 38:45–51. doi:10.1016/j.gde.2016.03.006.

Petrovic A, Davis CT, Rangachari K, Clough B, Wilson RJMI, Eccleston JF. 2008. Hydrodynamic characterization of the SufBC and SufCD complexes and their interaction with fluorescent adenosine nucleotides. Protein Sci. 17(7):1264–1274. doi:10.1110/ps.034652.108.

Rees DC. 2003. The Interface Between the Biological and Inorganic Worlds: Iron-Sulfur Metalloclusters. Science (80-). 300(5621):929–931. doi:10.1126/science.1083075.

Riboldi GP, De Oliveira JS, Frazzon J. 2011. Enterococcus faecalis SufU scaffold protein enhances SufS desulfurase activity by acquiring sulfur from its cysteine-153. Biochim Biophys Acta - Proteins Proteomics. 1814(12):1910–1918. doi:10.1016/j.bbapap.2011.06.016.

Riboldi GP, Verli H, Frazzon J. 2009. Structural studies of the Enterococcus faecalis SufU [Fe-S] cluster protein. BMC Biochem. 10(1):1–10. doi:10.1186/1471-2091-10-3.

Saini A, Mapolelo DT, Chahal HK, Johnson MK, Outten FW. 2010. SufD and SufC ATPase activity are required for iron acquisition during in vivo Fe-S cluster formation on SufB. Biochemistry. 49(43):9402–9412. doi:10.1021/bi1011546.

Dos Santos PC, Johnson DC, Ragle BE, Unciuleac MC, Dean DR. 2007. Controlled expression of nif and isc iron-sulfur protein maturation components reveals target specificity and limited functional replacement between the two systems. J Bacteriol. 189(7):2854–2862. doi:10.1128/JB.01734-06.

Selbach B, Earles E, Dos Santos PC. 2010. Kinetic analysis of the bisubstrate cysteine desulfurase sufs from bacillus subtilis. Biochemistry. 49(40):8794–8802. doi:10.1021/bi101358k.

Selbach BP, Chung AH, Scott AD, George SJ, Cramer SP, Dos Santos PC. 2014. Fe-S Cluster Biogenesis in Gram-Positive Bacteria: SufU Is a Zinc-Dependent Sulfur Transfer Protein. Biochemistry. 53(1):152–160. doi:10.1021/bi4011978.

Simpson AGB, Bernard C, Patterson DJ. 2000. The ultrastructure of Trimastix marina kent, 1880 (Eukaryota), an excavate flagellate. Eur J Protistol. 36(3):229–251. doi:10.1016/S0932-4739(00)80001-2.

Stairs CW, Eme L, Brown MW, Mutsaers C, Susko E, Dellaire G, Soanes DM, Van Der Giezen M, Roger AJ. 2014. A SUF Fe-S cluster biogenesis system in the mitochondrion-related organelles of the anaerobic protist Pygsuia. Curr Biol. 24(11):1176–1186. doi:10.1016/j.cub.2014.04.033. http://dx.doi.org/10.1016/j.cub.2014.04.033.

Tachezy J, Sánchez LB, Müller M. 2001. Mitochondrial type iron-sulfur cluster assembly in the amitochondriate eukaryotes Trichomonas vaginalis and Giardia intestinalis, as indicated by the phylogeny of IscS. Mol Biol Evol. 18(10):1919–1928. doi:10.1093/oxfordjournals.molbev.a003732.

Tachezy J, Šmíd O. 2019. Mitosomes in Parasitic Protists. Springer, Cham. p. 205–242.

Takahashi Y, Tokumoto U. 2002. A third bacterial system for the assembly of iron-sulfur clusters with homologs in Archaea and plastids. J Biol Chem. 277(32):28380–28383. doi:10.1074/jbc.C200365200.

Tokumoto U, Kitamura S, Fukuyama K, Takahashi Y. 2004. Interchangeability and distinct properties of bacterial Fe-S cluster assembly systems: Functional replacement of the isc and suf operons in Escherichia coli with the nifSU-like operon from Helicobacter pylori. J Biochem. 136(2):199–209. doi:10.1093/jb/mvh104.

Tovar J, León-Avila G, Sánchez LB, Sutak R, Tachezy J, Van Der Giezen M, Hernández M, Müller M, Lucocq JM. 2003. Mitochondrial remnant organelles of Giardia function in iron-sulphur protein maturation. Nature. 426(6963):172–176. doi:10.1038/nature01945.

Treitli SC, Kotyk M, Yubuki N, Jirounková E, Vlasáková J, Smejkalová P, Šípek P, Čepička I, Hampl V. 2018. Molecular and Morphological Diversity of the Oxymonad Genera Monocercomonoides and Blattamonas gen. nov. Protist. 169(5):744–783. doi:10.1016/j.protis.2018.06.005.

Tsaousis AD. 2019. On the Origin of Iron/Sulfur Cluster Biosynthesis in Eukaryotes. Front Microbiol. 10(November). doi:10.3389/fmicb.2019.02478.

Tsaousis AD, Ollagnier de Choudens S, Gentekaki E, Long S, Gaston D, Stechmann A, Vinella D, Py B, Fontecave M, Barras F, et al. 2012. Evolution of Fe/S cluster biogenesis in the anaerobic parasite Blastocystis. Proc Natl Acad Sci. 109(26):10426–10431. doi:10.1073/pnas.1116067109.

Vacek V, Novák LVF, Treitli SC, Táborský P, Čepička I, Kolísko M, Keeling PJ, Hampl V. 2018. Fe–S Cluster Assembly in Oxymonads and Related Protists. Ruiz-Trillo I, editor. Mol Biol Evol. 35(11):2712–2718. doi:10.1093/molbev/msy168.

Wada K, Sumi N, Nagai R, Iwasaki K, Sato T, Suzuki K, Hasegawa Y, Kitaoka S, Minami Y, Outten FW, et al. 2009. Molecular Dynamism of Fe-S Cluster Biosynthesis Implicated by the Structure of the SufC2-SufD2Complex. J Mol Biol. 387(1):245–258. doi:10.1016/j.jmb.2009.01.054.

Waterhouse A, Bertoni M, Bienert S, Studer G, Tauriello G, Gumienny R, Heer FT, De Beer TAP, Rempfer C, Bordoli L, et al. 2018. SWISS-MODEL: Homology modelling of protein structures and complexes. Nucleic Acids Res. 46(W1):W296–W303. doi:10.1093/nar/gky427.

Wayne Outten F. 2015. Recent advances in the Suf Fe-S cluster biogenesis pathway: Beyond the Proteobacteria. Biochim Biophys Acta - Mol Cell Res. 1853(6):1464–1469. doi:10.1016/j.bbamcr.2014.11.001.

Williams BAP, Hirt RP, Lucocq JM, Embley TM. 2002. A mitochondrial remnant in the microsporidian Trachipleistophora hominis. Nature. 418(6900):865–869. doi:10.1038/nature00949.

Wollers S, Layer G, Garcia-Serres R, Signor L, Clemancey M, Latour JM, Fontecave M, De Choudens SO. 2010. Iron-sulfur (Fe-S) cluster assembly: The SufBCD complex is a new type of Fe-S scaffold with a flavin redox cofactor. J Biol Chem. 285(30):23331–23341. doi:10.1074/jbc.M110.127449.

Yan R, Adinolfi S, Pastore A. 2015. Ferredoxin, in conjunction with NADPH and ferredoxin-NADP reductase, transfers electrons to the IscS/IscU complex to promote iron-sulfur cluster assembly. Biochim Biophys Acta - Proteins Proteomics. 1854(9):1113–1117. doi:10.1016/j.bbapap.2015.02.002.

Yang J, Roy A, Zhang Y. 2013. Protein-ligand binding site recognition using complementary binding-specific substructure comparison and sequence profile alignment. Bioinformatics. 29(20):2588–2595. doi:10.1093/bioinformatics/btt447.

Yokoyama N, Nonaka C, Ohashi Y, Shioda M, Terahata T, Chen W, Sakamoto K, Maruyama C, Saito T, Yuda E, et al. 2018a. Distinct roles for U-type proteins in iron-sulfur cluster biosynthesis revealed by genetic analysis of the *Bacillus subtilis sufCDSUB* operon. Mol Microbiol. 107(6):688–703. doi:10.1111/mmi.13907.

Yokoyama N, Nonaka C, Ohashi Y, Shioda M, Terahata T, Chen W, Sakamoto K, Maruyama C, Saito T, Yuda E, et al. 2018b. Distinct roles for U-type proteins in iron–sulfur cluster biosynthesis revealed by genetic analysis of the Bacillus subtilis sufCDSUB operon. Mol Microbiol. 107(6):688–703. doi:10.1111/mmi.13907.

Yuda E, Tanaka N, Fujishiro T, Yokoyama N, Hirabayashi K, Fukuyama K, Wada K, Takahashi Y. 2017. Mapping the key residues of SufB and SufD essential for biosynthesis of iron-sulfur clusters. Sci Rep. 7(1):9387. doi:10.1038/s41598-017-09846-2.

Zhang Q, Táborský P, Silberman JD, Pánek T, Čepička I, Simpson AGB. 2015. Marine Isolates of Trimastix marina Form a Plesiomorphic Deep-branching Lineage within Preaxostyla, Separate from Other Known Trimastigids (Paratrimastix n. gen.). Protist. 166(4):468–491. doi:10.1016/j.protis.2015.07.003.

Zhao D, Curatti L, Rubio LM. 2007. Evidence for nifU and nifS participation in the biosynthesis of the iron-molybdenum cofactor of nitrogenase. J Biol Chem. 282(51):37016–37025. doi:10.1074/jbc.M708097200.

Zheng L, Cash VL, Flint DH, Dean DR. 1998. Assembly of iron-sulfur clusters. Identification of an iscSUA-hscBA-fdx gene cluster from Azotobacter vinelandii. J Biol Chem. 273(21):13264–72. doi:10.1074/jbc.273.21.13264.

Zheng L, White RH, Cash VL, Jack RF, Dean DR. 1993. Cysteine desulfurase activity indicates a role for NIFS in metallocluster biosynthesis. Proc Natl Acad Sci U S A. 90(7):2754–8. doi:10.1073/pnas.90.7.2754.

Zubáčová Z, Novák L, Bublíková J, Vacek V, Fousek J, Rídl J, Tachezy J, Doležal P, Vlček Č, Hampl V. 2013. The Mitochondrion-Like Organelle of Trimastix pyriformis Contains the Complete Glycine Cleavage System. Saks V, editor. PLoS One. 8(3):e55417. doi:10.1371/journal.pone.0055417.

Figures text

Fig. 1 – Predicted model of SufS
Predicted protein model of *M. exilis* (**A**) SufS with insertions which have no homology to marked in red and its comparison with SufS of *B. subtilis* (pdb) (**C**). Detailed view of *M. exilis* active site (**B**) containing with PLP. (**D**) - structural alignment of *M. exilis* and *B. subtilis* structures showing overall conservation of structural motifs.

Fig. 2 – Predicted model of SufU
Predicted protein model of *M. exilis* (**A**) SufU based on *B. subtilis* (6jzv) (**C**) and their structural alignment (**D**). Detail of zinc binding site of *M. exilis* SufU (**B**) consisting of residues C98, C136, C206 and D100. Gram positive bacteria specific region (Riboldi et al. 2009) is highlighted in blue. (**E**) Alignment of SufUs and IscUs – LPVVK motif of IscU is in red, GPR region is in blue and Zn binding residues are in orange.

Fig. 3 – Predicted model of SufB
Figure showing predicted protein structure of *M. exilis* SufB (**A**) compared with crystal structure of *E. coli* SufB (1awf) (**C**) and structural alignment of both structures (**B**). Residues reported to be involved in Fe-S cluster assembly (orange) in *E. coli* R226, N228, C254, Q285, W287, K303 and residues responsible for interaction with SufD (yellow) (C405 and E434 in *E. coli*) and their *M. exilis* counterparts are highlighted in models. Residues 116 – 185 of *M. exilis* are not shown as they correspond to residues (80-156) of *E. coli* omitted from crystal structure 1awf due to low electron density of this region (Hirabayashi et al. 2015).

Fig. 4 – Predicted model of SufD
Predicted protein model of SufD of *M. exilis* (**A**) structure based on crystal structure of *E. coli* (**C**) SufD (1vh4) and overlap of both structures (**B**). Model *M. exilis* SufD shows divergent loops (red) which have no sequential or structural homology to crystal structure of *E. coli* SufD and their structure is unreliable. Residues reported to form interface with SufB in *E. coli* (H360 and C358) and *M. exilis* (H472 and A470) are highlighted in orange.

Fig. 5 – Predicted model of SufC
Predicted protein model of *M. exilis* (**A**) SufC based on *E. coli* (**C**) SufC (5awf.1.c) and their structural alignment (**B**). SufC of *M. exilis* has high similarity to SufC of *E. coli* and contains all important structural motifs - Walker A and Walker B motifs, ABC signature, Q-loop, D-loop and the H-loop

Fig. 6 – Complementation of SufB in *E. coli*
Plates showing growth phenotype of transfected *E. coli* strains deficient in SufB (DV1222) under iron-starvation conditions (DIP) and oxidative stress (PMS). When under natural expression (right) upper plates and under overexpression (left) plates. Slight rescue effect can be seen for SufB of *M. exilis* when compared to negative control. (-) = DV1225/pTrc99A(empty), (+) = DV1225/pTrc99A($SufBCD_{ecoli}$), wt = *E. coli* MG1655/pTrc99A(empty), $SufB_{MONO}$ = DV1225/pTrc99A($SufB_{MONO}$), $SufSU_{MONO}$ = DV1226/pTrc99A($SufSU_{MONO}$)

Fig. 7 – Complementation of SufC in *E. coli*
Plate showing toxic effect of overexpression of SufC in *E. coli* (strain BP224) under conditions of Fe starvation. (-) = BP224/pTrc99A(empty), (+) = BP224/pTrc99A ($SufC_{ecoli}$), wt = *E. coli* MG1655/pTrc99A(empty), $SufC_{MONO}$ = BP224/pTrc99A($SufS_{MONO}$).

Fig. 8 – Measurement of Fe-S cluster assembly in double mutant strains of *E. coli*
Charts showing measurements of β-galactosidase activity in mevalonate dependent strains of *E. coli* deficient both in ISC and SUF pathway. Charts show readings of β-galactosidase cloned under IscR promoter which is inhibited by holo-IscR. Lesser the activity of β-galactosidase means higher Fe-S cluster assembly rates. Columns with asterisk are significantly different from negative control (P-test < 0.05). As negative control empty pTrc99A vector was used. Positive control SufS of *E. coli* and SufBCD of *E. coli* were used respectively. For genotypes of used strains see Table 1.

Fig. 9 – BACTH assay showing an interaction between SufB and SufC
Chart showing activity of BACTH assay of SufB and SufC cloned into pUT18 and pKT25 vectors. Results clearly show interaction between SufB and SufC as the activity of β-galactosidase is comparable with positive control. Column with asterisk are significantly different from negative control (T-test p-value < 0.05)

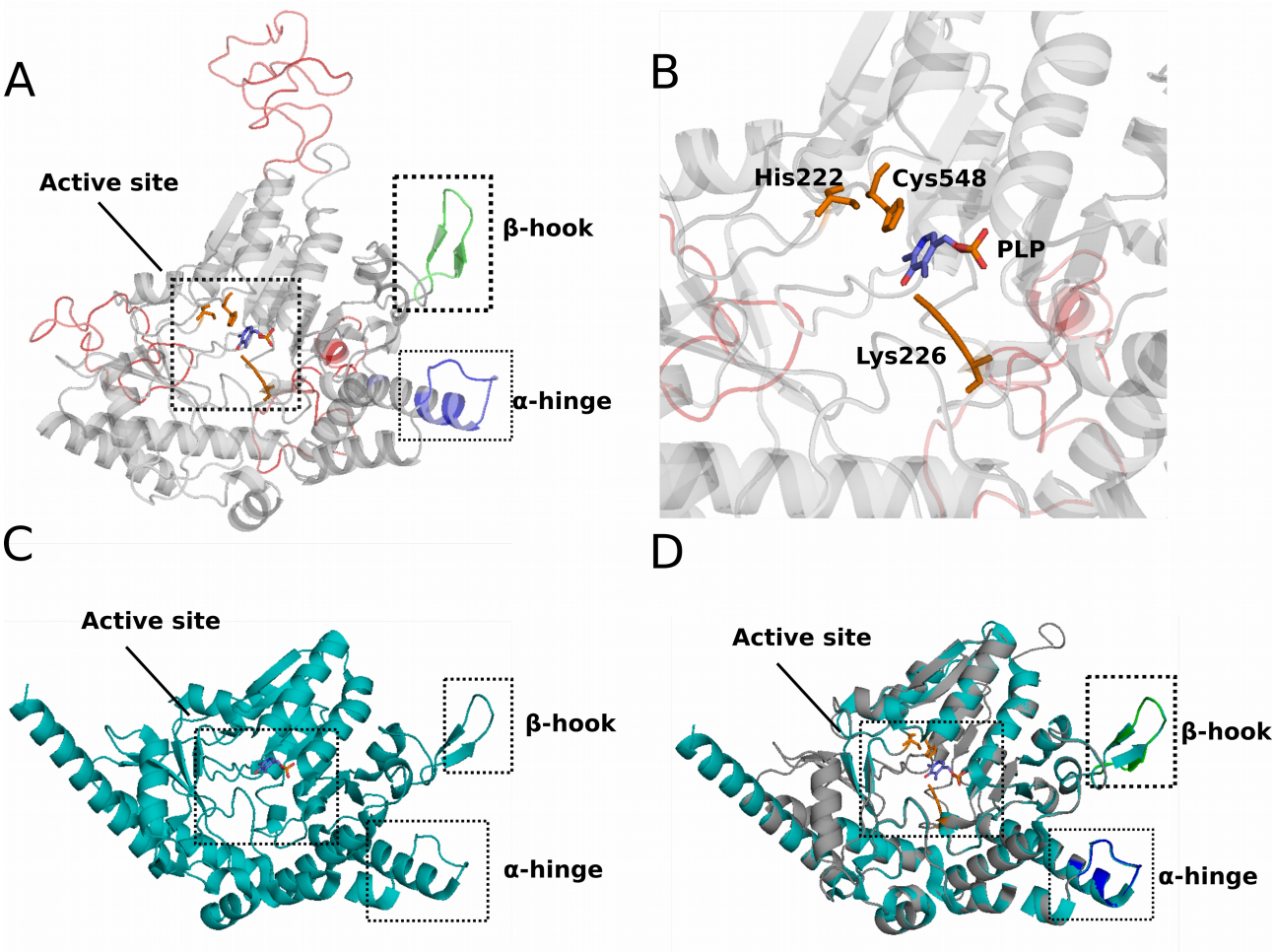

Fig. 1 – Predicted model of SufS

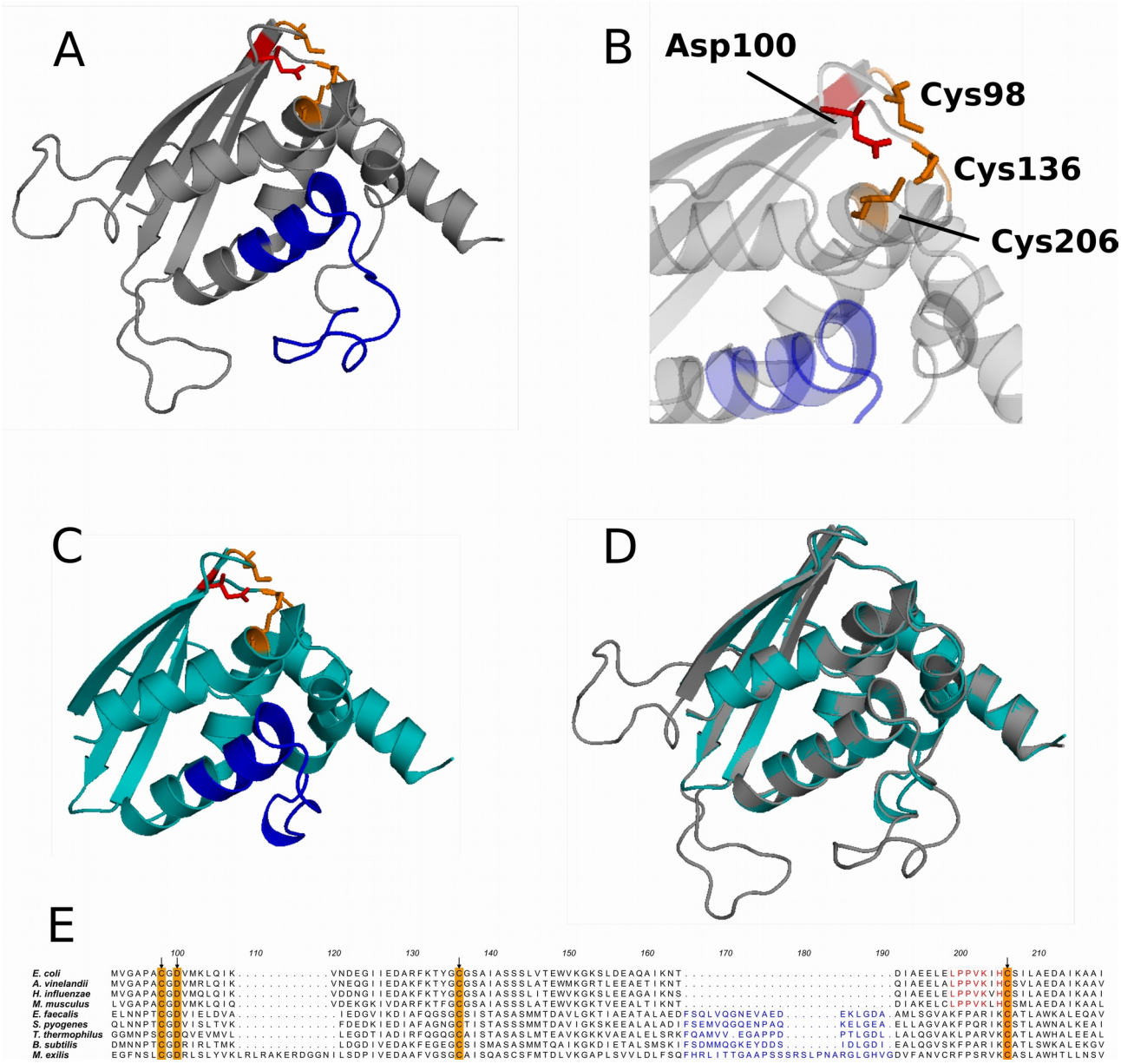

Fig. 2 – Predicted model of SufU

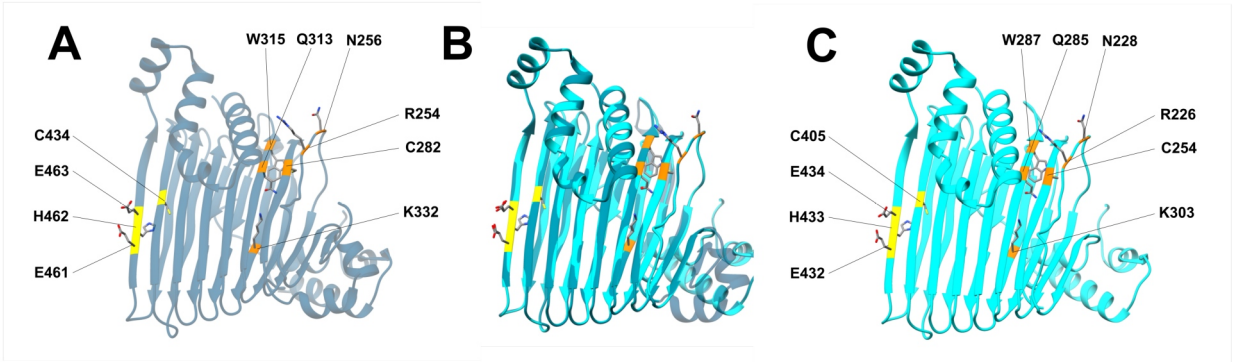

Fig. 3 – Predicted model of SufB

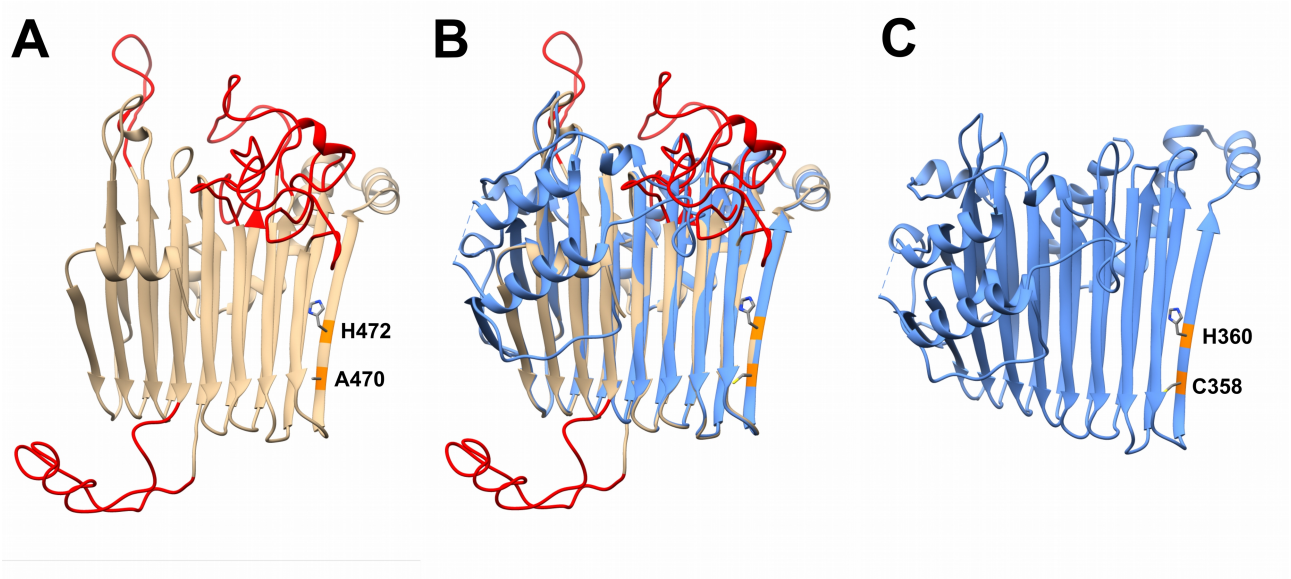

Fig. 4 – Predicted model of SufD

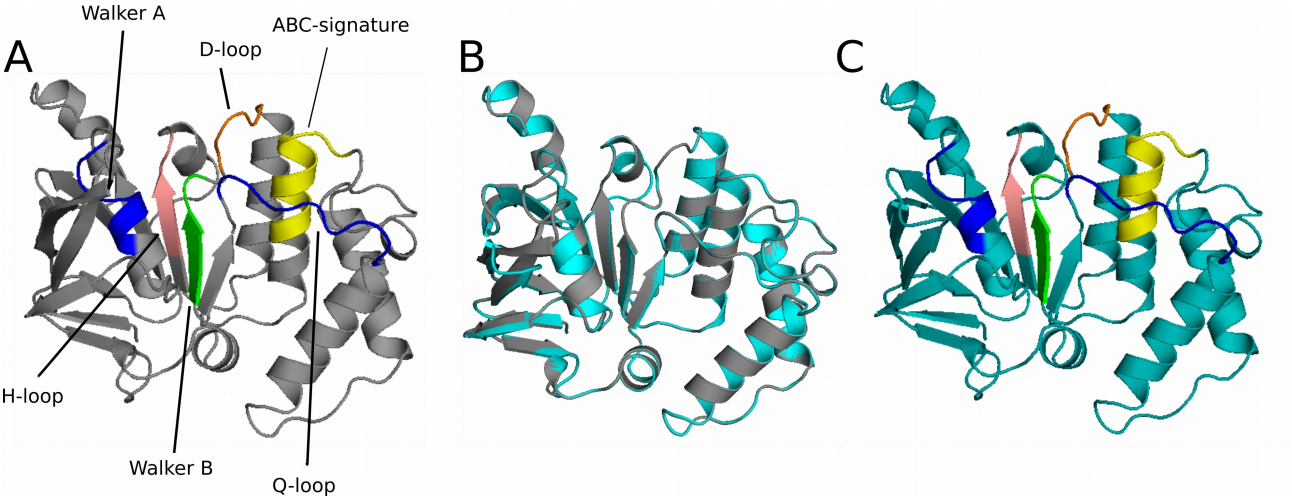

Fig. 5 – Predicted model of SufC

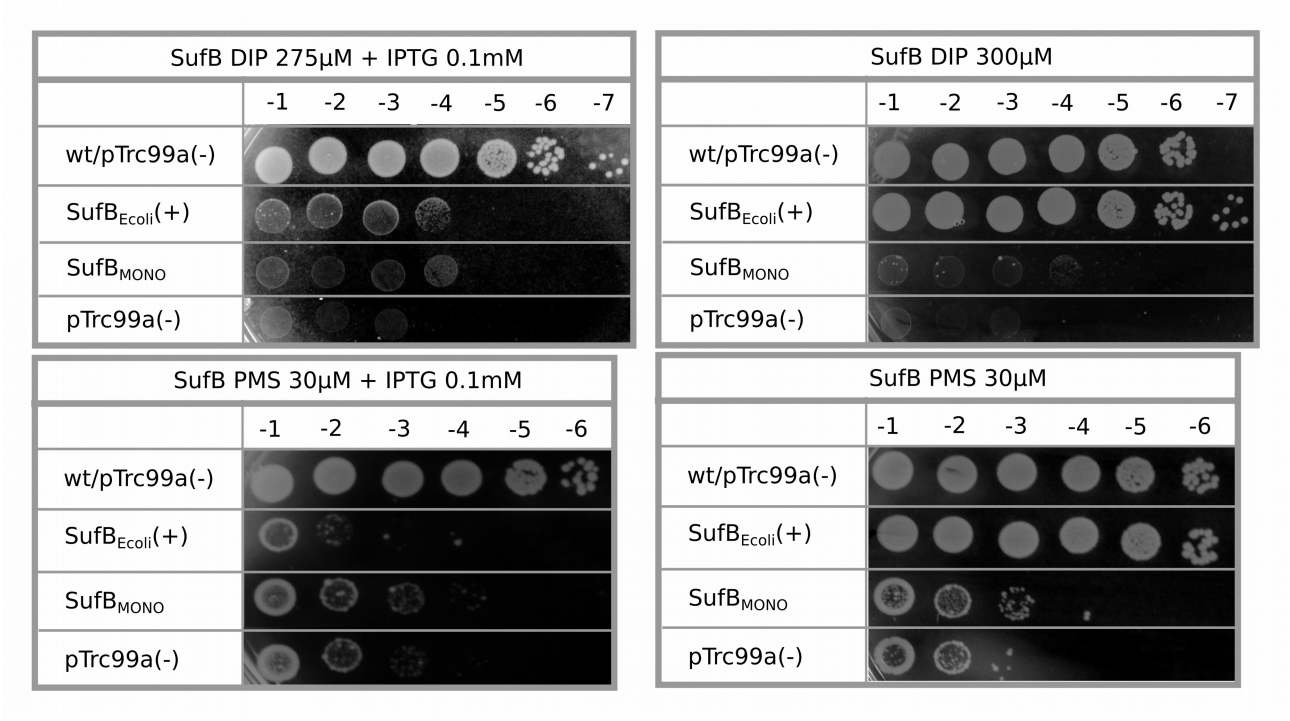

Fig. 6 – Complementation of SufB in E. coli

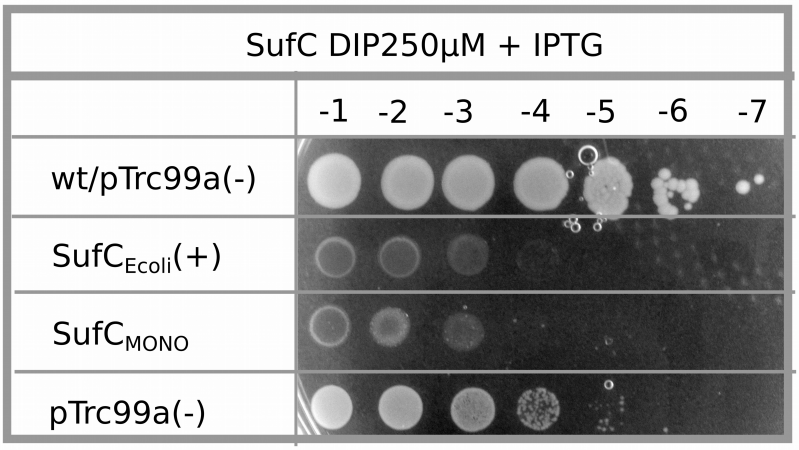

Fig. 7 – Complementation of SufC in E. coli

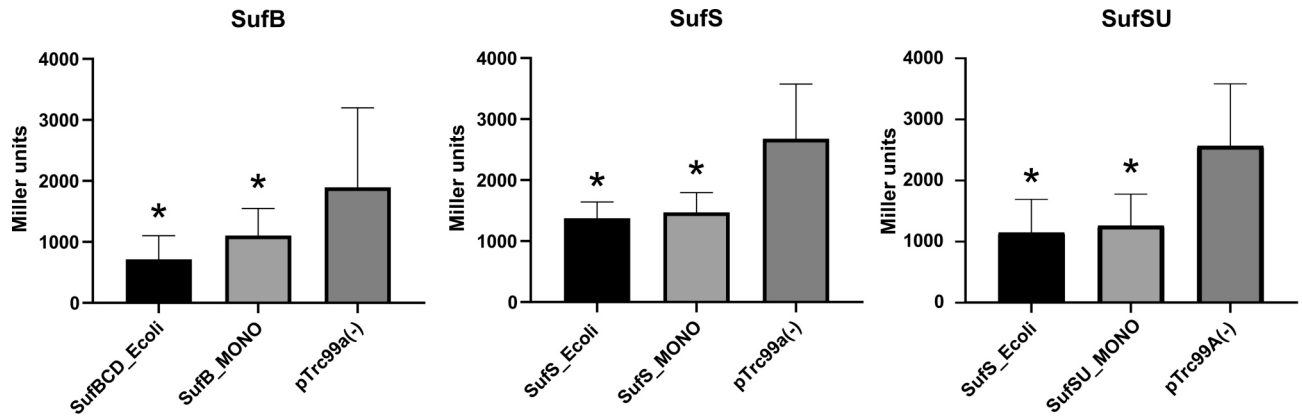

Fig. 8 – Measurement of Fe-S cluster assembly in double mutant strains of E. coli

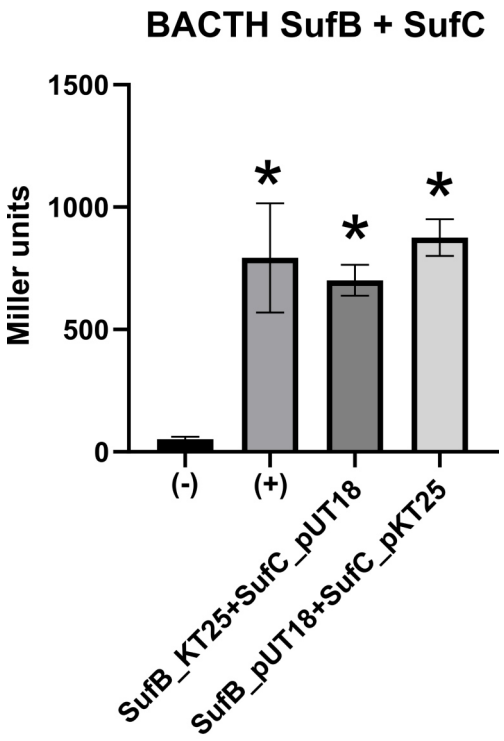

Fig. 9 – BACTH assay showing an interaction between SufB and SufC